NUCLEAR ENGINEERING

MASSACHUSETTS INSTITUTE
OF TECHNOLOGY

A CORE RELOAD PATTERN AND COMPOSITION OPTIMIZATION METHODOLOGY FOR PRESSURIZED WATER REACTORS

by

I.L. SAUER and M.J. DRISCOLL

MITNE-266 March 1985

MITNE-266

A CORE RELOAD PATTERN AND COMPOSITION OPTIMIZATION METHODOLOGY FOR PRESSURIZED WATER REACTORS

by

I.L. SAUER and M.J. DRISCOLL

MITNE-266 March 1985

A CORE RELOAD PATTERN AND COMPOSITION OPTIMIZATION METHODOLOGY FOR PRESSURIZED WATER REACTORS

by

Ildo Luis Sauer

and

Michael John Driscoll

March 1985

Department of Nuclear Engineering

Massachusetts Institute of Technology

Cambridge, Massachusetts 02139

A CORE RELOAD PATTERN AND COMPOSITION OPTIMIZATION METHODOLOGY FOR PRESSURIZED WATER REACTORS

by

Ildo Luis Sauer

and

Michael John Driscoll

ABSTRACT

The primary objective of this research was the development of a comprehensive, rapid and conceptually simple methodology for PWR core reload pattern and fuel composition optimization, capable of systematic incorporation of constraints, in which cycle burnup is defined as the optimality criterion.

A coarse mesh nodal method for PWR core analysis was formulated by coupling the one-and-one-half-group diffusion theory model for spatial power calculations with the linear reactivity versus burnup model (LRM) for depletion calculations. The accuracy and suitability of this model was determined through comparisons of its results with those of state-of-the-art core analysis methods.

The simplicity of the LRM-based core model allowed the direct analytical computation of the derivatives necessary in the steepest-gradient type optimization methods applied in the present work, and its versatility permitted use of the analytical and computational methods for a variety of applications, ranging from core reload pattern searches to burnable poison (BP) and composition optimization. Algorithms for identification of unconstrained maximum-burnup core reload patterns and for optimal BP allocation were successfully implemented and tested, and the basis for systematic incorporation of constraints on power peaking was developed. The potential application of the methodology to fuel composition optimization was also examined.

Most of the methodological developments have been embodied in the LRM-NODAL code which was programmed in the course of this research. From the numerical and analytical results it was found that the optimal core configurations are arranged such as to produce power histories and profiles in which the most reactive assemblies are at their highest allowable power at EOC (thus maximizing their importance) and where the converse applies to the least reactive; these preferred profiles also produce relatively higher leakage at BOC, evolving to the lowest possible leakage at EOC, but always consistent with the maximization of the core reactivity importance.

ACKNOWLEDGMENTS

The work presented in this report has been performed primarily by the principal author, Ildo Luis Sauer, who has submitted substantially the same report in partial fulfillment of the requirements for the Ph.D. degree in Nuclear Engineering at MIT. Thanks are due Professor D. D. Lanning who served as thesis reader.

The principal author was supported during the course of this work by PRONUCLEAR administered by the COMISSÃO NACIONAL DE ENERGIA NUCLEAR of BRAZIL. Funds for report preparation were provided under a research grant from Westinghouse Electric Corporation. Typing of this report was ably handled by Vicki Law and Sandy Congleton.

TABLE OF CONTENTS

TABLE OF CONTENTS (Continued)

TABLE OF CONTENTS (Continued)

TABLE OF CONTENTS (Continued)

TABLE OF CONTENTS (Continued)

LIST OF FIGURES

LIST OF FIGURES (Continued)

LIST OF FIGURES (Continued)

LIST OF TABLES

LIST OF TABLES (Continued)

CHAPTER 1

INTRODUCTION

1.1 Foreword

Currently, Light Water Reactors (LWRs) account for more than three-quarters of the nuclear power plants operable, under construction or on order worldwide, with the Pressurized Water Reactor (PWR) comprising over two-thirds of all LWRs. The operation of these reactors over their useful lifetime will, in the next several decades, make an impressive contribution to energy production. Moreover, if the efforts currently underway on an international basis to implement the changes and innovations necessary to improve the viability of nuclear fission as a major energy source are successful, PWR-based technology is likely to retain a significant role well into the next century (M-1). Thus, under any plausible circumstances regarding expansion of nuclear generating capacity, the efficient operation and fuel management of PWRs is of utmost importance.

The effort undertaken in the present research addresses a central question in in-core fuel management, namely the optimization of PWR core reload pattern and fuel composition. While the applications here are restricted to state-of-the-art low-enriched uranium fueled PWRs over a single burnup cycle, most of the methodology should be readily extendable to several cycles in sequence and to other reactor types.

1.2 Background

The core reload design process encompasses a complex set of decisions, spread over a period of time, with the final goal of specifying a core capable of producing a demand-imposed target cycle energy, at the minimum cost, with appropriate margins to assure that given acceptable fuel design limits are not exceeded during any condition of normal operation, including the effects of anticipated operational occurrences. These margins are detailed in a reactor's final safety analysis report (FSAR).

Usually, based on an energy demand forecast and consistent with the system optimization goals, the plant's target cycle burnup is defined in advance ($\sim$1.5 years) such as to allow time for the necessary fuel cycle transactions: ore procurement, UF_6 conversion, enrichment, and fabrication. Assembly design, material/service purchase transactions and their optimization, as may be seen in Table 1.1, proceed interactively. Based on target burnup and the expected state of the old fuel, the characteristics of the core are specified: enrichment of the fresh fuel, reload pattern, and, if required, burnable poison (BP) loading. In general, optimization of system energy costs leads to a preference for long cycles (to maximize the capacity factor), which, in turn, normally requires the use of BPs to suppress excessive power peaking and to ensure an acceptable (slightly negative) moderator temperature coefficient of reactivity at the beginning of cycle (BOC). Once the cycle length (and anticipated

TABLE 1.1

Typical Core Reload Planning and Scheduling:
Time Frame Prior to BOC

Months

1) Specification of Energy Requirements: 17

Basis: Expected demand for the unit according to system optimization

2) Specification of Uranium Ore and Enrichment: 14

Basis: a) Energy requirements

b) Expected state of old batches

3) Specification of Fabrication (hence, BP loading): 8

4) Fuel Cycle Design Analysis:

a) Select Reload Pattern

b) Perform Transient and Safety Analysis (FSAR):

b.1) If design conforms with FSAR's "core exposure window": keep analysis for regulatory agency inspection.

b.2) If not: Submit analysis for regulatory agency review (at least).....3

5) Flexibility for Contingencies (e.g. new or old fuel damage)

Re-evaluation of design and safety analysis.....2

capacity factor) has been fixed the only component of the energy cost left to optimize is the fuel cycle cost. Fuel cycle cost optimization essentially corresponds to definition of the fuel composition and core arrangement such as to minimize the sum of ore, enrichment and fabrication costs. After the enrichment has been irrevocably specified, fuel cycle cost optimization becomes equivalent to finding a reload pattern that maximizes the cycle burnup capability.

However, an overriding concern at any stage of the design, is the assurance that it meets safety limits and margins. For steady state operation design margins may be translated into limits on the core's enthalpy rise hot channel factor, which in a two-dimensional model corresponds to the radial power peaking factor. State-of-the-art core analysis methods, in the form of sophisticated computer codes, are available and used industry-wide for detailed reload licensing calculations, to evaluate and ensure realization of the required margins. However, due to the cost and complexity of these analyses, it is highly desirable that a candidate reload core, before being submitted to these full scope licensing calculations, meet optimal or near-optimal conditions regarding the assembly arrangement pattern and composition. In addition to the need in the normal core reload design process, the capability to generate acceptable candidate reload patterns becomes even more important under circumstances requiring fast evaluation of alternative designs, such as forced outage due to fuel failures, accidental assembly damage during reload handling, or unplanned extended coastdown.

1.2.1 Previous Reload Optimization Work

In spite of significant efforts devoted to the problem, no standard methods, with industry-wide acceptance and an adequate compromise between simplicity and accuracy, are in general use to generate acceptable candidate core reload patterns meeting realistic optimality criteria. The most widespread approach is trial and error, aided by "rules of thumb" derived from experience and insight.

Table 1.2 provides a succinct review of some of the most relevant work dedicated to optimization and automation of the reload design process. Approaches explored include heuristic methods, direct searches, mathematical programming (linear, dynamic, quadratic and integer), variational methods, optimal control theory, perturbation methods, and combinations thereof. Optimization goals also vary: maximization of burnup or excess reactivity; minimization of power peaking, ore consumption, cycle costs, etc.

1.2.2 Linear Reactivity Model Work at MIT

The Advanced Linear Reactivity Model (ALRM), (where the well known linearity of assembly reactivity as a function of burnup is combined with prescriptions relating power density to reactivity, and these, in turn, used to compute the system reactivity) has been developed and used at MIT to perform batch-size multi-cycle analyses of fuel management strategies, with substantial success. A full account

TABLE 1.2

Summary of Relevant Core Reload Optimization Work

Author(s) and Reference		Approach						Objective			
		Linear Programming	Dynamic Programming	Variational Methods/Optimal Control Theory	Perturbation Theory	Direct Search	Heuristic Methods	Maximize Burnup	Maximize Reactivity	Minimize Power Peaking	Minimize Costs or Fuel Required
Rieck	[R-1]					x					x
Izenson	[I-1]		x							x	
Downar	[D-2]					x		x			
Goertzel	[G-1]			x							x
Wall and Fenech	[W-1]		x								x
Melice	[M-2]			x					x		
Fagan and Sesonske	[F-1]		x								x
Naft and Sesonske	[N-1]					x				x	
Suzuki and Kiyose	[S-2]	x									x
Sauar	[S-3]	x									x
Wade and Terney	[W-2]			x				x		x	
Hoshino	[H-1]						x	x			
Goldschmidt	[G-2]			x							x
Motoda, Herczeg, Sesonske	[M-3]	x				x					x
Ciechanowiecz	[C-1]			x				x			
Stout and Robinson	[S-4]		x							x	
Chitkara and Weisman	[C-2]					x					x
Mingle	[M-4]	x			x						x
Motoda and Yokomizo	[M-5]	x				x				x	
Terney and Williamson	[T-1]			x						x	
Lin, Zolotar, Weisman	[L-1]					x					x
Ho and Sesonske	[H-2]					x				x	
Ho and Rohach	[H-3]				x					x	
Huang and Levine	[H-4]			x					x		
Colletti, Levine, Lewis	[C-3]			x					x		
Chang and Levine	[C-4]			x							x
Ahn and Levine	[A-3]			x				x			
Suzuki and Kiyose	[S-8]			x				x			

of the methodology, and application to fuel management is in preparation [D-1]. Hence, here only the most relevant aspects of this work, where it provides important background to the methodology being used and extended in this research, will be reviewed.

Sefcik [S-1], on purely empirical grounds, concluded, by analyzing core power maps, that the power of a group of assemblies (usually a batch), f_i, and its reactivity ρ_i, could be related by

$$f_i \propto \left(\frac{1}{1 - \rho_i}\right)^{\theta} \tag{1.1}$$

where

θ is an empirical constant.

Loh [L-2], using a modified one group theory, showed that a better relation would be

$$f_i = \frac{\bar{f}\ (1 - \bar{\rho}_j)}{1 - \theta\, \rho_i} \approx f\ (1 + \theta\ \rho_i) \tag{1.2}$$

where

$\bar{f}_j$ is the average power for an aggregation of surrounding assemblies,

$\bar{f}$ is the core-average assembly power, and

$\bar{\rho}_j$ is the average reactivity of the aggregation.

Furthermore, Loh pointed out the similarities between his prescription and FLARE-type nodal expressions.

Kamal [K-1], extended Loh's approach to a cylindricized representation of an assembly and its surroundings, and developed another similar prescription:

$$f_i = \frac{\overline{f}_j \, (1 - \theta_j \, \overline{\rho}_j)}{1 - \theta_i \rho_i} \tag{1.3}$$

where

θ_j and θ_i are constants, depending on the ratio of the assembly cross sectional area to the neutron migration area.

All the authors just cited used the same relation to compute the system reactivity, ρ_s :

$$\rho_s = \sum_{i=1}^{n-m} f_i \, \rho_i + \sum_{i=1}^{m} f_i(\rho_i - \alpha) \tag{1.4}$$

where

n is the number of assemblies,

m is the number of peripheral assemblies, and

α is an empirical constant relating the core radial leakage and peripheral power fraction (leakage reactivity decrement).

Subsequent work built upon the results of these initial investigations. Izenson [I-1] used Kamal's prescription in an automated PWR reload design optimization method, where the optimality goal was the minimization of the radial power peaking factor. Downar [D-2] used Loh's prescriptions, in work performed concurrently with the present research, to develop an integrated method for mid-range in-core PWR

core design. Montaldo-Volachec [M-6] correlated linear reactivity model parameters for a wide range of PWR lattices and uranium enrichments. Malik [M-1] extended these correlations to plutonium-based fuels. Kamal [K-2] and Malik et al. [M-7] worked on PWR axial power shape optimization.

1.3 Research Objectives and Organization of the Report

The primary objective of the research reported here has been the development of a methodology for PWR core reload pattern and fuel composition optimization. Cycle burnup is defined as the optimality criterion, and efforts are concentrated on developing an ALRM-based methodology, having an adequate compromise between simplicity and accuracy, able to identify and generate core configurations and compositions meeting this condition under restrictions on power peaking, assembly placement and burnable poison loading.

Ease of computation and transparency of approach are highly desirable features in iterative design optimization models; and simplification, whenever possible without altering the essential nature of the problem, has often been the key to success in complex optimization tasks. Consistent with these arguments, the evaluation and extension of the Advanced Linear Reactivity Model of PWR core behavior constituted an important subsidiary goal in this work.

The research efforts are reported as follows:

- In Chapter Two a succinct review of state-of-the-art methods for core analysis and the foundations of the core physics methods and models used throughout this work are presented.
- In Chapter Three, an ALRM-based coarse-mesh nodal method is developed by analytical means. Beneficial empirical adjustments and corrections are discussed, and the accuracy of the method tested against state-of-the-art results.
- The optimization methodology is presented in Chapter Four, in conjunction with some applications.
- In Chapter Five, the research is summarized and the main conclusions and recommendations for future work are discussed.
- Finally, subsidiary derivations and analyses in support of developments in the main text, along with a listing of the computer code embodying most of the methodology, are presented in appendices.

CHAPTER 2

REACTOR PHYSICS METHODS AND MODELS

2.1 Introduction

Reactor physics calculations provide the basic information for in-core fuel management analysis. The major objective of these neutronic calculations is the prediction of core parameters such as reactivity, reaction rates (hence, power densities and burnup) and isotopic compositions. The level of accuracy required and thus the sophistication of the analysis methods to be used is problem specific. Well developed and very accurate neutronic computer codes are available to perform detailed analysis of LWR cores. One such example is EPRI's Advanced Recycle Methodology Program (ARMP) package of core analysis codes. However, the high cost and complexity associated with the use of these programs for multi-variable optimization studies, particularly when the general degree of uncertainty inherent to the problem being modeled (e.g. scoping or preliminary optimization studies) is much larger than the accuracy provided, clearly points to the need to develop simpler and more cost efficient models based on analytical and empirical methods.

In this chapter, a general overview of state-of-the-art licensing-level methods is provided, with emphasis on the codes used to to generate supporting results for the present research. Then, analytical

models and approximations, constituting the foundations for a PWR core analysis method, compatible with the requirements of the optimization procedures developed in this research, are discussed.

2.2 State-of-the-Art Nuclear Analysis Methods

The Boltzman neutron transport equation is the fundamental relation for nuclear reactor analysis [H-5]. It is a conservation equation for the angular neutron density as a function of position, direction of motion and neutron energy, describing the interaction of neutrons with their environment. However, for real-life situations, its solution is either too costly or impractical, and lower order approximations, with degree of accuracy compatible with the requirements of each specific situation, are used in reactor analysis. For most applications the main workhorse is the neutron diffusion approximation. In general, a further assumption of separability of space, time and spectrum effects is also necessary. Under this assumption, the core is divided into regions having similar characteristics, for which few-group constants are generated in independent spatially-simplified computations, and then used in few-group spatial calculations. In addition, continuous core depletion effects are evaluated in discrete steps.

Analysis procedures, described in standard fuel management and reactor physics texts (e.g. [S-5], [H-5], [G-3]) are problem dependent, and their details are, for the most part, beyond the scope of this report. Nevertheless, a succinct description of some state-of-the-art

computer codes is relevant due to their use in current core licensing analyses, and especially where they were used to provide supporting results and calculations for the present work. Figure 2.1 shows a typical sequence of calculations for PWR licensing analyses, identifying several such programs.

2.2.1 Spectrum Calculations

The LEOPARD code [B-1] has been extensively used ([G-4], [C-5], [S-1], [L-2], [K-1], [M-6]) and benchmarked ([C-5], [G-4]) at MIT by previous researchers, and its methodology is well documented. Despite having been superseded in rigor and complexity by newer programs, it is still one of the most widely used neutronic codes in the nuclear industry. In an evaluation against newer codes (LASER and EPRI-CELL) it was shown to be in better agreement with experimental results, albeit for rather simple lattice configurations [L-3].

LEOPARD is a zero-dimensional spectrum dependent depletion program used to compute neutron multiplication factors and few-group cross-sections as a function of burnup for square or hexagonal lattices, represented by unit fuel cells or supercells (cell plus extra region). The unit cell consists of fuel, gap, cladding and moderator, and the extra-region represents fuel assembly water holes, control rod sheaths, spacer grids and inter-assembly water gaps. The microscopic cross-section library for the MIT version (EPRI-LEOPARD) is derived from the ENDF/B-IV data set. The calculation at epithermal energies is done using the

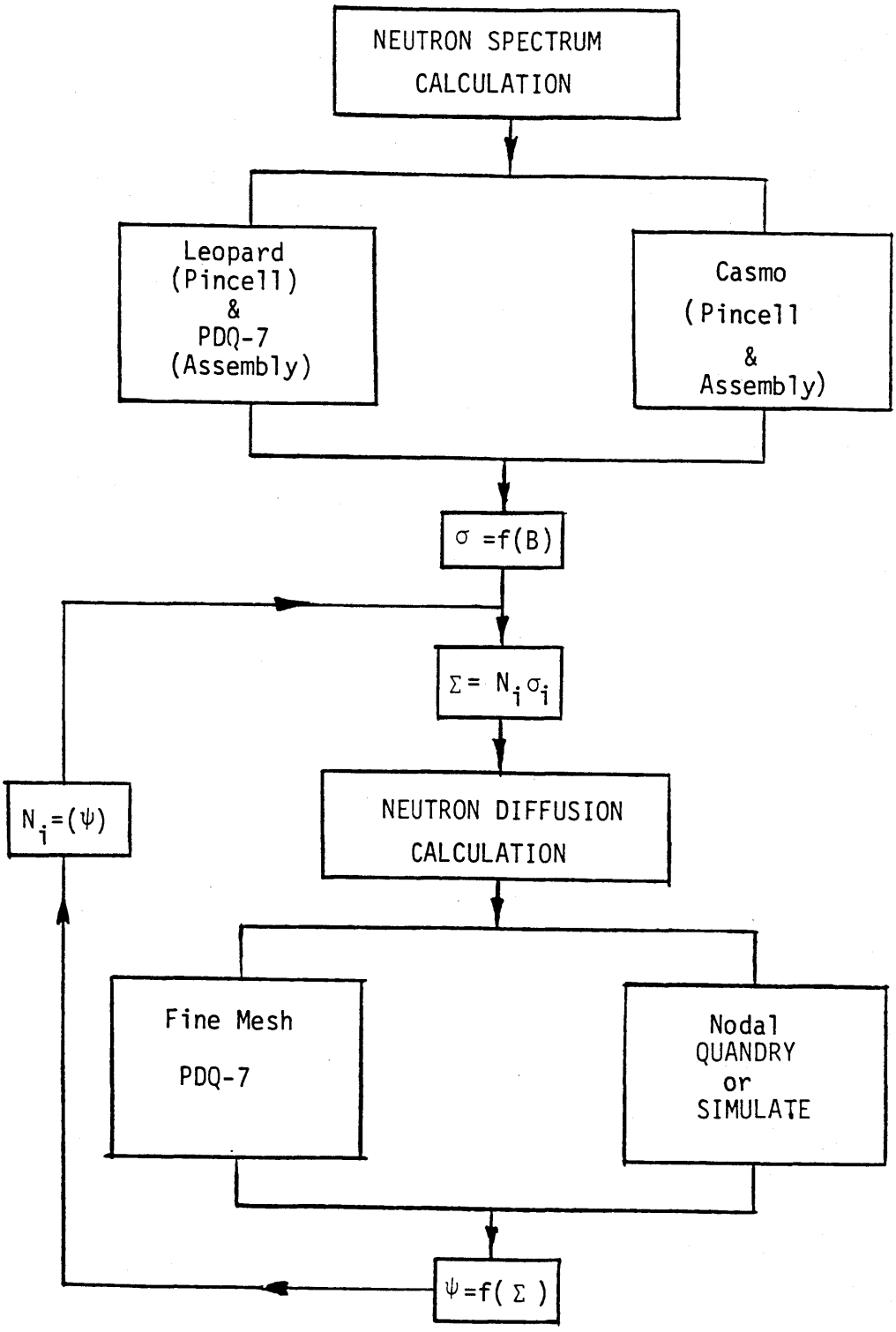

Fig. 2.1 Representative Sequence of Calculations for PWR Licensing Analysis

MUFT [B-2] sub-program while SOFOCATE, using the Wigner-Wilkins treatment, handles the thermal calculations [A-2]. Thermal disadvantage and fast advantage factors, and an iteratively adjusted resonance self-shielding factor, are used to correct for cell heterogeneity.

CASMO [E-1] has also been used and described at MIT [D-2]. It is a recent multigroup two-dimensional transport theory code for burnup calculations of BWR and PWR assemblies or cells. The program handles a geometry consisting of cylindrical fuel rods of varying composition in a square array, and is capable of treating fuel rods loaded with gadolinium, burnable absorber rods, cluster control rods, water gaps and other realistic assembly features. CASMO generates few-group cross-sections and reaction rates for any region of the assembly, as a function of burnup.

DIT [J-1] is a Combustion Engineering code, with similar capabilities to those of CASMO, also employing transport and collision probability methods. CASMO and DIT, in turn have much in common with their precursor WIMS; reference [S-5] describes their common methodology in considerable detail.

2.2.2 Spatial Calculations

Spatial calculations are performed, for the most part, using fine-mesh finite difference schemes or by coarse-mesh finite-element or nodal techniques.

PDQ-7 [C-6] is a widely used production code that has been previously used for PWR core analysis at MIT ([S-1], [L-2], [K-1]). It solves diffusion-depletion problems in up to three spatial dimensions, with a maximum of five neutron energy groups, in rectangular, spherical, cylindrical or hexagonal geometries. The program discretizes the energy variable and finite-differences (central) the spatial part of the diffusion equation, and can perform eigenvalue, boundary-value, adjoint and fixed-source calculations.

The so-called coarse mesh computational methods are efficient techniques to perform two or three dimensional reactor calculations. The reactor is represented by large (typically quarter or full assembly) homogenized regions. Representative of this category are: the two-group analytical nodal method QUANDRY [S-6], developed at MIT; and the modified one group theory (sometimes empirically-adjusted) schemes, such as FLARE [D-7], TRILUX and SIMULATE [V-1], much in use currently for fuel management purposes.

2.3 Foundations for an Optimization-Oriented Core Analysis Method

As has already been stressed, depending on the problem at hand, an adequate compromise between solution accuracy and efficiency has to be established. Speed and ease of computation are extremely important in iterative optimization schemes. Furthermore, uncertainties inherent to the overall system modeling and decision process do not warrant the

complexity and cost associated with using licensing-level codes for optimization and screening purposes. In this section, key components of the nuclear analysis method developed and used in the present research are introduced. Then, some intrinsic assumptions and limitations, as well as simplifications and approximations are discussed.

2.3.1 A Modified One Group Model

A modified one group theory method, known as the "one-and-one-half" group model, can be derived from the two-group diffusion equations ([H-5], [G-3], [S-5]):

fast group:

$$-\nabla \cdot D_1 \nabla \Phi_1 + \Sigma_{a1} \Phi_1 + \Sigma_{12} \Phi_1 - \frac{1}{\lambda} (\nu\Sigma_{f1}\Phi_1 + \nu\Sigma_{f2}\Phi_2) = 0 \quad (2.1)$$

thermal group:

$$-\nabla \cdot D_2 \nabla \Phi_2 + \Sigma_{a2}\Phi_2 - \Sigma_{12}\Phi_1 = 0 \quad (2.2)$$

where λ is the neutron multiplication factor (eigenvalue), ν the average number of neutrons released per fission, Σ_{12} the macroscopic downscattering cross section, and with 1 and 2 standing for fast and thermal groups, respectively, the remaining constants are:

D = diffusion coefficient;

Σ_a = macroscopic absorption cross section;

Σ_f = macroscopic fission cross section.

The essential approximation of the one-and-one-half group model is that thermal neutrons are absorbed at the point of removal from the fast group, or, equivalently, that thermal leakage is neglected (i.e.: $\nabla^2\Phi_2 = 0$). Thermal leakage is an order of magnitude smaller than fast leakage in LWRs (and, furthermore, the approximation may be later partially relaxed, as discussed in section 3.2.5.1). Then Eq. (2.2) becomes:

$$\Sigma_{a2}\,\Phi_2 = \Sigma_{i2}\,\Phi_1 \tag{2.3}$$

Substituting Φ_2 from this expression in Eq. (2.1), and assuming D_1 constant over the reactor, gives

$$-D_1\nabla^2\Phi_1 + \Sigma_{a1}\,\Phi_1 + \Sigma_{12}\Phi_1 - \frac{1}{\lambda}\left(\nu\Sigma_{f1} + \nu\Sigma_{f2}\,\frac{\Sigma_{12}}{\Sigma_{a2}}\right)\Phi_1 = 0 \tag{2.4}$$

Defining the migration area (also referred to as Fermi age, τ, in the literature), as:

$$M^2 = D_1/(\Sigma_{a1} + \Sigma_{12}) \tag{2.5}$$

and recalling that the local two-group infinite medium neutron multiplication factor is:

$$k_\infty = \left(\nu\,\Sigma_{f1} + \nu\Sigma_{f2}\,\frac{\Sigma_{12}}{\Sigma_{a2}}\right) \Big/ \,(\Sigma_{a1} + \Sigma_{12}), \tag{2.6}$$

Eq. (2.4) may be re-arranged as:

$$\nabla^2\Phi_1 + \left(\frac{k_\infty}{\lambda} - 1\right)\,\frac{1}{M^2}\,\Phi_1 = 0 \tag{2.7}$$

Furthermore, defining the local reactivity,

$$\rho = 1 - 1/k_\infty \quad , \tag{2.8}$$

and a modified eigenvalue, called here the "system (static) reactivity" (in a similar fashion to the "adiabatic" approximation),

$$\rho_s = 1 - 1/\lambda \quad , \tag{2.9}$$

an equivalent expression for Eq. (2.7) is obtained, namely:

$$\nabla^2\Phi_1 + \frac{(\rho - \rho_s)}{(1 - \rho)} \frac{1}{M^2} \Phi_1 = 0 \tag{2.10}$$

For a critical reactor (i.e.: $\lambda = 1$, $\rho_s = 0$) Eqs. (2.7) and (2.10) become

$$\nabla^2\Phi_1 + \frac{\rho}{(1 - \rho)} \frac{1}{M^2} \Phi_1 = 0 \tag{2.11}$$

or, equivalently,

$$\nabla^2 \Phi_1 + (k_\infty - 1) \frac{1}{M^2} \Phi_1 = 0 \tag{2.12}$$

Recognizing that the local thermal power density can be written as:

$$q''' = \kappa \Sigma_{f1} \Phi_1 + \kappa \Sigma_{f2} \Phi_2 \tag{2.13}$$

where κ is the energy released per fission, and, with the aid of Eqs. (2.3), (2.6) and (2.5), Eq. (2.13) can be re-written as:

$$q''' = \frac{\kappa}{\nu} \frac{D_1}{M^2} k_\infty \Phi_1 \tag{2.14}$$

The fast flux and local thermal power density, using Eq. (2.8), may be related by:

$$\Phi_1 = q''' \frac{\nu}{\kappa} \frac{M^2}{D_1} (1 - \rho) \tag{2.15}$$

An equivalent relation holds after integration over the volume of the node:

$$\int_V \Phi_1 \, dv = \frac{\nu}{\kappa} \frac{M^2}{D_1} (1 - \rho). \, f_i \, . \, Q \, / n \tag{2.16}$$

where f_i is the normalized nodal power fraction:

$$f_i = \frac{1}{Q} \int_v q'''dv = q'''\frac{v}{Q} \quad n \tag{2.17}$$

in which Q is the core thermal power, v is the volume of the node (in this work taken to be an assembly), and n is the number of nodes in the core.

2.3.2 System Reactivity Balance and Eigenvalue

It is important to emphasize that, according to Eq. (2.9), the system reactivity is a modified eigenvalue determining the core criticality and thus the null reactivity limited end of cycle (EOC). Furthermore, the calculational procedures developed in the next chapter to solve the one-and-one-half group model, are based on Eq. (2.11), which requires ρ_s to be always zero. This condition is satisfied by performing a reactivity balance, and determining a reduction in the local reactivities (simulating the soluble boron poisoning process in real life core operation).

Equation (2.10) may be re-arranged and integrated over the core volume, V, to yield

$$\rho_s = \frac{\int_V \frac{\rho}{1-\rho} \frac{D_1}{M^2} \Phi_1 \, dv + \int_V \nabla \cdot D_1 \nabla \Phi_1 \, dv}{\int_V \frac{1}{1-\rho} \frac{D_1}{M^2} \Phi_1 \, dv} \tag{2.18}$$

Since there are no internal flux discontinuities, application of the Divergence Theorem to the last term in the numerator leads to the following equivalence:

$$\int_V \nabla \cdot D_1 \nabla \Phi_1 \, dv = \int_S \underline{dA} \cdot D_1 \nabla \Phi_1 \tag{2.19}$$

where S is the outer surface of the core. This term corresponds to the loss of neutrons due to leakage out of the core. For a core with n nodes, of which m are on the periphery, defining J_i as the leakage rate out of peripheral node i, and with the help of Eq. (2.16), ρ_S becomes:

$$\rho_S = \frac{\sum_{i=1}^{n} \rho_i \, f_i \, \frac{\nu}{\kappa} i \; - \; \sum_{i=1}^{n} J_i}{\sum_{i=1}^{n} f_i \; \frac{\nu}{\kappa_i}} \tag{2.20}$$

Defining a normalized neutron source as

$$S_i = \frac{f_i \; \frac{\nu}{\kappa_i}}{\sum_{i=1}^{n} f_i \; \frac{\nu}{\kappa_i}} \tag{2.21}$$

and a "leakage reactivity",

$$\rho_L = \frac{\sum_{i=1}^{m} J_i}{\sum_{i=1}^{n} f_i \frac{\nu}{\kappa_i}} = - \frac{\int_S \underline{dA} \cdot D_1 \nabla \Phi_1}{\int_V \frac{1}{1-\rho} \frac{D_1}{M^2} \Phi_1 \, dV} , \tag{2.22}$$

ρ_S may be written as,

$$\rho_S = \sum_{i=1}^{n} S_i \; \rho_i - \rho_L \tag{2.23}$$

From this reactivity balance, the requirement of setting $\rho_s=0$ may be fulfilled by reducing the local nodal reactivities by ρ_s. Or, in an even closer approximation to reality, the quantity ρ_{sp},corresponding to the dissolved boron reactivity required for criticality, may be calculated with the aid of the local-spectrum-dependent relative boron worth factors, W_i,as:

$$\rho_{SP} = \frac{\sum_{i=1}^{n} S_i \rho_i - \rho_L}{\sum_{i=1}^{n} S_i W_i} \quad , \tag{2.24}$$

and the necessary local reactivity reduction,$\Delta\rho_i$, in each node is given by:

$$\Delta\rho_i = \rho_{SP} \cdot W_i \tag{2.25}$$

The leakage calculation is detailed in the next chapter, as part of the coarse mesh nodal method. However, in view of the results of this section, it is important to stress that ρ_S represents a modified eigenvalue, which is set to zero in an iterative numerical solution scheme. Therefore the perturbation approach (which implies what amounts to source square weighting), proposed in ref. (D-2) to perform a steady-state reactivity balance, is not conceptually appropriate. Otherwise, it is interesting to note that Eq. (2.11) is self-adjoint, and the flux can be also interpreted as the local importance.

2.3.3 The Linear Reactivity Model (LRM)

The linearity as a function of burnup of both the unpoisoned reactivity and the reactivity attributable to "well designed" burnable poisons for PWR fuel assemblies has been exploited to develop simple

and surprisingly accurate models to perform various fuel management tasks [L-2]. In the core model being developed in the present research this feature will be fully used and play a key role due to the simplicity it allows in the description of the otherwise rather complex phenomena of fuel and burnable poison depletion.

2.3.3.1 LRM for Unpoisoned Fuel Assemblies

It is a well established fact that the unpoisoned reactivity of an assembly, ρ, defined by Eq. (2.8), varies linearly with burnup [K-2], [S-1], [L-2], [M-6], [M-7], even though all of the reasons and compensatory mechanisms that cause this behavior have not yet been fully explained. This variation may be represented mathematically as:

$$\rho = \rho_0 - A\,B \tag{2.26}$$

where

ρ_0 = extrapolated Beginning-of-Life (BOL) reactivity

B = assembly burnup, MWD/kg

A = slope of the linear curve-fit of ρ versus B, kg/MWD.

The intercept ρ_0, determined by extrapolation, corresponds to the value after saturating fission products (xenon, samarium) have come to equilibrium. (Therefore, at BOC, the LRM may not provide an accurate description of the core state).

A remarkable fact is that the linearity holds for the entire burnup span of practical interest for LWR uranium fuel, over a wide range of enrichments and all fuel-to-moderator volume ratios (V_F/V_M).

Figure 2.2 displays plots of reactivity as a function of burnup for a representative PWR lattice and enrichments from 2.0 w/o to 5 w/o. Furthermore, besides enriched uranium, the linearity holds for other fertile/fissile combinations, with the exception of Th/Pu.

Montaldo-Volachec [M-6], using LEOPARD results, developed correlations for the parameters ρ_o, ρ_o/A and A for uranium LWR fuels with enrichments spanning the range from 2.5 w/o to 4.5 w/o and V_F/V_M from 0.5 to 1.0. Malik [M-1] subsequently extended this methodology to plutonium/uranium lattices. Montaldo-Volachec's results for the standard Maine Yankee lattice ($V_F/V_M \approx 0.60393$) are:

$$\rho_o = 0.357936 - 0.404919/X_p \tag{2.27}$$

$$A = 13.7304 - 1.52734.X_p, \ 10^{-3} \text{ kg/MWD} \tag{2.28}$$

where X_p is the U-235 enrichment, w/o.

It should be noted that LEOPARD results are sensitive to the length of the burnup steps employed. For example, for runs using steps of 1 and 5 MWD/kg, after 35 MWD/kg the computed reactivity in the latter case exceeded that of the former by 0.01. Reference [R-2] indicates that steps of 2 MWD/kg are adequate for most purposes.

2.3.3.2 Burnable Poison Modeling

Following the lead of Loh [L-2], here an idealized model for burnable poisons will be adopted: that is, a poison material is postulated which provides a required initial negative reactivity at BOC

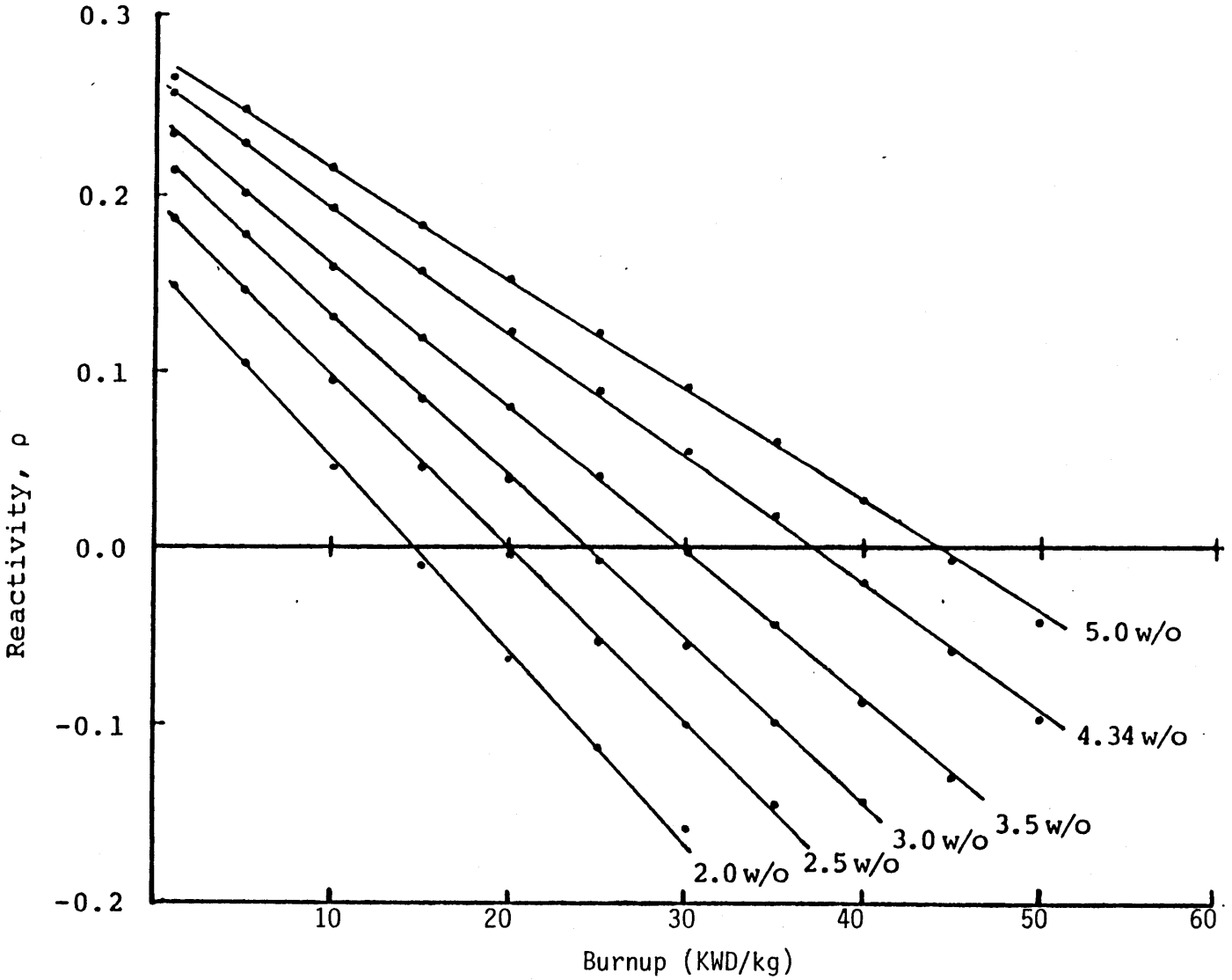

Fig. 2.2 Reactivity as a Function of Burnup for a Representative PWR Lattice

and then burns out at a uniform rate over the cycle, leaving a small residual at EOC. Besides the ease of modeling, such burnable poison behavior is desirable for other reasons. Uniformity of depletion and EOC burn-out are, in general required to avoid excessive power peaking; and usually the maximum cycle burnup, an optimization goal, is associated with power histories that require the burn-out point to coincide with the EOC. Furthermore, this modeling is not physically unrealistic, since actual burnable poisons can be designed that approximate very well this ideal behavior: in fact, a black cylindrical absorber depleting in "ash-layer" fashion can be shown to exhibit linearity in a formally exact manner [H-6].

Figure 2.3 displays a generic ρ versus burnup trace for an assembly with "ideal" burnable poison. Figure 2.4 is the plot of CASMO-computed reactivity traces as a function of burnup for two Maine Yankee, 3 w/o U-235 enriched, assemblies; one of which contains eight B_4C shims. The boron-based burnable poisons' characteristic non-linear "tail" is evident close to the burn-out point. In the neutronically blacker gadolinia burnable poisons, linearity persists until burn-out, even though higher residual reactivity results, mostly due to transmutation of the even-A gadolinium isotopes present.

The (somewhat over simplified) ash-layer model [H-6] may be used to demonstrate the feasibility of matching any desired initial hold-down reactivity and depletion (linear) slope combination, by appropriately choosing the number and the loading of poison pins in the assembly [D-1]. Roughly speaking, the initial hold-down

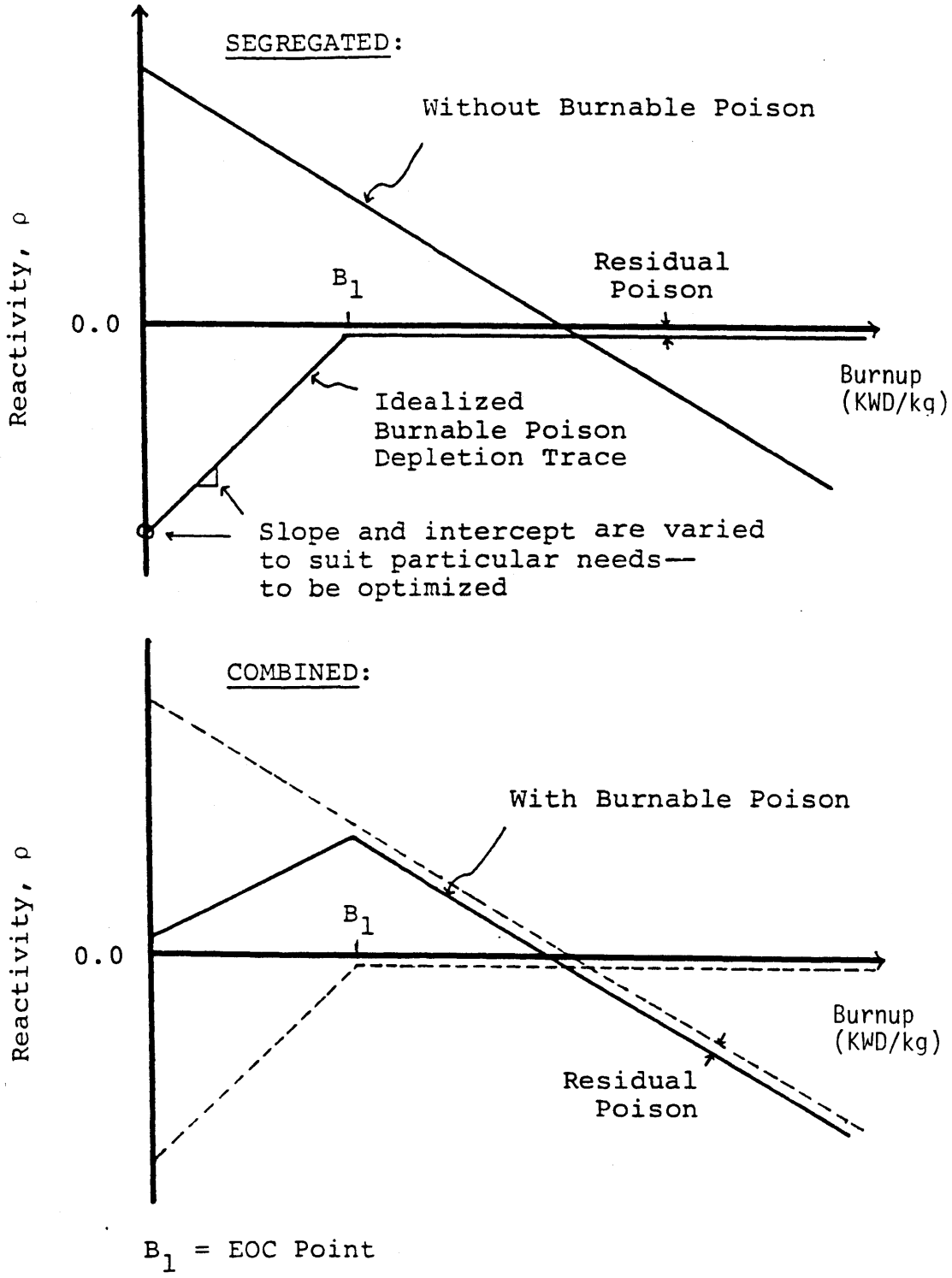

Fig. 2.3 Generic ρ versus Burnup Trace for Assembly with Burnable Poison

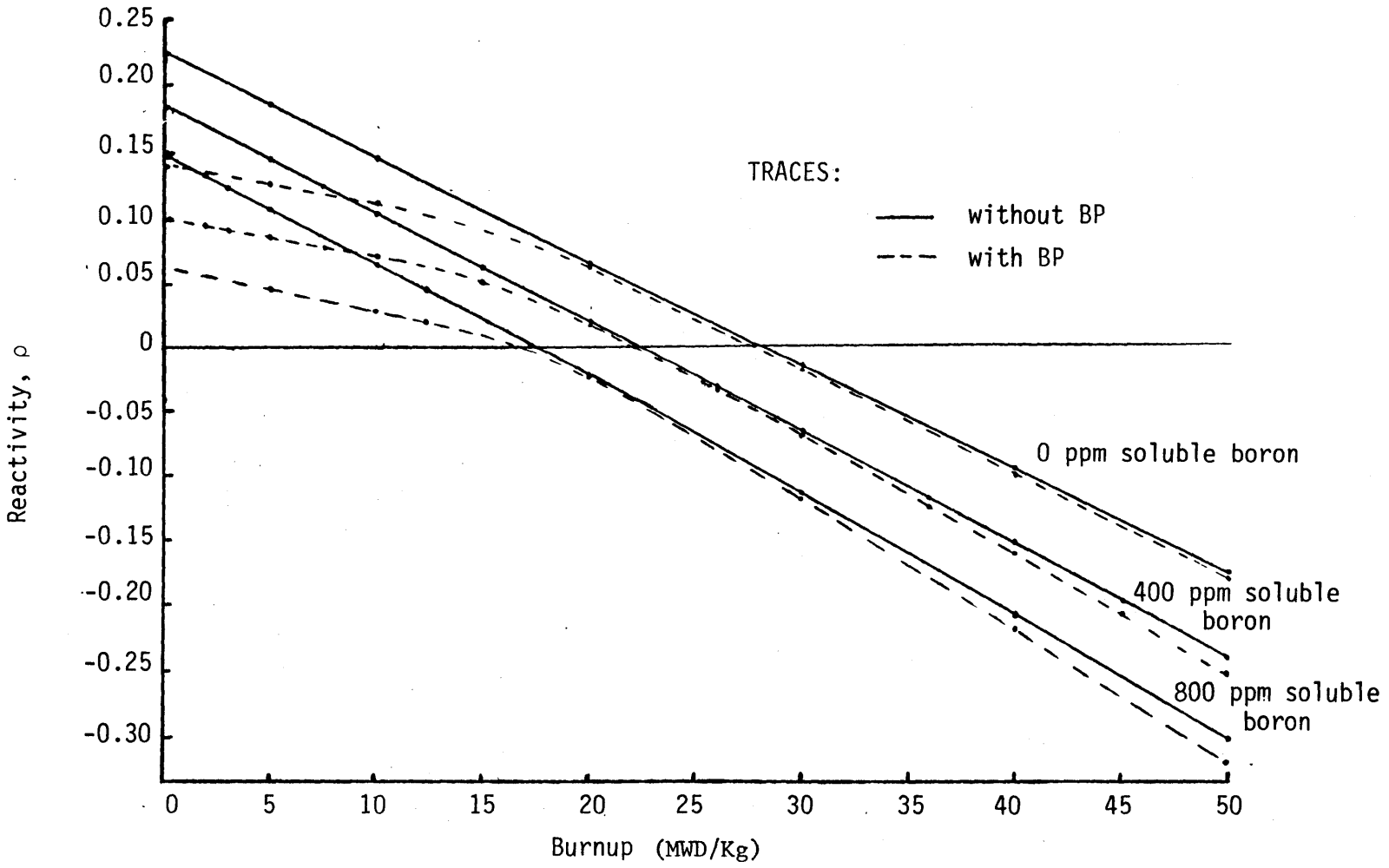

Fig. 2.4 Reactivity as a Function of Burnup for B_4C Poisoned and BP-free Assemblies (3% U-235, Maine Yankee lattice)

is related to the number of poison pins and the slope is related to the poison loading in each pin.

2.3.4 Evaluation of Simplifications, Approximations and Assumptions

The basic relations for PWR core modeling, consisting of Eqs. (2.11), (2.15), (2.23), and the linear reactivity model equation, Eq. (2.26), have now been derived or justified. Consistent with the goal of developing a methodology with an adequate compromise between accuracy and simplicity, some simplifications in the solution of the equations will next be evaluated. Aspects regarding the adequacy of the linear reactivity model will also be discussed. Then the basis will exist for proceeding to solve the equations, and further develop the model in the next chapter.

2.3.4.1 Power and Flux Relationship

A detailed parametric analysis of the factor $\left[\frac{\nu}{\kappa}\ \frac{M^2}{D_1}\right]$, which according to Eqs. (2.15) and (2.16) relates thermal power and flux, is presented in Appendix A. As a result of several compensatory effects, LEOPARD predicts that this factor remains quasi-invariant as a function of burnup and local reactivity for typical PWR lattices and compositions, at around 0.50 neutron · cm/MeV. CASMO predicts a slight dependence on local reactivity (or burnup state), which can be linearized to yield:

$$\left[\frac{\nu}{\kappa}\ \frac{M^2}{D_1}\right] \approx C_1\ (1 - C_2\ \rho),\ \text{neut.cm/MeV} \qquad (2.29)$$

where, for example, for the Maine Yankee lattice, at 3% U-235, with $R^2 = 0.9335$,

$$C_1 = 0.4919$$

$$C_2 = 0.1450$$

Since ρ varies between roughly ± 0.2, the corresponding variation in $\left[\frac{\nu}{\kappa}\ \frac{M^2}{D_1}\right]$ can be seen to be rather small. Moreover, if the degree of realism is increased to include power/temperature feedback effects and a more detailed (nuclide-by-nuclide) computation of capture gamma energy, the variation of $\left[\frac{\nu}{\kappa}\ \frac{M^2}{D_1}\right]$ with burnup (hence reactivity) would be decreased and more linear in the CASMO results.

This parametric invariance (or linear dependence on local reactivity) is a fortunate finding, which can be taken advantage of in the core modeling. By solving Eq. (2.11) and incorporating this simple flux versus power relationship, expressions may be developed to yield directly the nodal power.

2.3.4.2 Power Weighting of Reactivity

Power, instead of source-weighting of local reactivities to perform the system reactivity balance (i.e., eigen value calculation), has been used previously [S-1], [L-2], [K-1], under the assumption that the variation of κ/ν with burnup was negligible. Here, in view of the results of Appendix A, the numerical error of this approximation is evaluated for selected, extreme, but simplified, cases of leakage-free cores composed of three uniform batches, having hypothetical

power fractions of 1.4, 1.0 and 0.6. Results and data are shown in Table 2.1. These results indicate that the consequences of the approximation are not severe. Since the power weighting consistently slightly over estimates the system reactivity, it should contribute to a bias on the high side in cycle length (burnup) calculations. The errors in nodal power fraction calculations, due to the approximation are completely negligible.

Hence, Eq. (2.24) may be approximated by:

$$\rho_S = \left(\sum_{i=1}^{n} f_i \rho_i - \rho_L \right) \Big/ \sum_{i=1}^{n} f_i \qquad (2.30)$$

2.3.4.3 Spectral Ambiguity

The LEOPARD program, when computing the few-group cross sections and the reactivity as a function of burnup, uses an infinite medium spectrum and enforces criticality by adjusting the buckling. In a reactor, where local criticality is maintained by a combination of buckling (i.e.: leakage to and from neighboring assemblies) and by addition of control absorber, the LEOPARD-convention is not reproduced exactly, and consequently the actual local reactivity may differ from that predicted by the linear reactivity model. Another situation where spectral changes may induce significant local effects, arises at the interface of nodes with differing compositions. These effects are especially pronounced at the core periphery (reflector) where corrective measures are required.

TABLE 2.1

Power* Versus Source Weighting: Eigenvalue Difference for Selected Cases

Batch Burnup (MWD/kg)	0	10	15	20	30	40	Results		
ρ	0.223	0.131	0.084	0.038	-0.055	-0.147	ρ_S Source-Weighted [Eq. (2.23)]	ρ_S Power-Weighted [Eq. (2.30)]	Difference ρ_S Power - ρ_S Source
κ/ν (MeV/neutron)	79.6	77.5	76.7	76.1	75.0	74.4			
Case (Points Used)	X	X		X			0.15406	0.15533	0.00127
		X		X	X		0.06187	0.06280	0.00093
	X		X		X		0.11850	0.12106	0.00256
	X			X		X	0.08341	0.08733	0.00392

*For assumed power fractions of 1.4, 1.0 and 0.6

These "spectral ambiguity" effects are most severe at the BOC, when more soluble poison is required. Because boron suppresses preferentially the thermal flux, whereas in adjusting the buckling fast leakage dominates, the spectral mismatch becomes most pronounced when more boron is present. In the poison-free condition, at EOC, reactivities should be well predicted by the LEOPARD-based linear reactivity model.

One way to reduce these spectral effects is to use the cycle-average boron concentration in the LEOPARD calculation, thus hardening the spectrum for which the cross sections are computed, and then later excluding the boron cross-sections from the reactivities. Moreover, the spectral ambiguity effects arising from changes in the ambient spectrum due to the presence of soluble poison can be mitigated by applying properly defined weighting factors to the local poison-related reactivity reduction (W_i of Eq. (2.25)), such as to incorporate only the net effects. The mismatch at interfaces of differing media may be partially included in differential thermal leakage corrections such as that proposed by Becker [B-3].

More detailed discussions of this subject are documented in references [D-1] and [S-5]. In general (except where noted), refinements related to these fine points will not be justified in the present work: the resulting errors are generally inconsequential.

2.3.4.4 Superposition of Reactivity

In addition to spectral ambiguity, another aspect associated with modeling of soluble boron as a control poison is the validity of the superposition of local reactivities.

The local reactivity, defined by Eq. (2.8) may be written as:

$$\rho = \frac{(\nu\Sigma_{f1}\Phi_1 + \nu\Sigma_{f2}\Phi_2) - (\Sigma_{a1}\Phi_1 + \Sigma_{a2}\Phi_2)}{(\nu\Sigma_{f1}\Phi_1 + \nu\Sigma_{f2}\Phi_2)} \quad , \tag{2.31}$$

which suggests the representation of absorber addition, such as soluble boron, as a reduction, $\Delta\rho$, in the local reactivity. However, due to the spatial variation of the spectrum throughout the core, the same amount of absorber will yield different local $\Delta\rho_i$. This additional effect may be corrected for by associating local relative weighting factors, W_i, as shown in Eq. (2.25), which correspond to normalized relative boron worths.

It should be pointed out that in the case of burnable poison modeling, as described in section 2.3.3.2, the spectral effects are accounted for implicitly. The local BP reactivity decrement, as a function of burnup, is given by the difference between the unpoisoned and poisoned traces, each of which incorporates the appropriate spectral effects.

2.4 Chapter Summary

In this chapter the state-of-the-art computer codes used to provide results and supporting data for the present research, namely LEOPARD, CASMO, DIT and PDQ-7, have been briefly described. Then, the basic relations providing the foundation for an optimization-oriented core analysis method have been derived or justified. Inherent assumptions and approximations, as well as possible simplification have been discussed and evaluated.

CHAPTER 3

A COARSE MESH NODAL METHOD

3.1 Introduction

Nodal methods [H-5] [G-3] [S-5] provide an efficient and accurate means of analysis whenever a reactor may be represented by regularly repeating, internally-homogenized regions - nodes - as is the case for PWRs, whose array of geometrically similar assemblies normally constitute such a configuration. In the previous chapter, a consistent set of relations capable of describing core behavior, on an assembly level, have been derived, along with suitable approximations and simplifications. Specifically, Eq. (2.11) constitutes the basis for spatial diffusion calculations, coupled with the use of Eq. (2.24) for eigenvalue determination (or equivalently, system reactivity balance computation); and the linear reactivity model has been shown to provide a simplified and accurate description of the local reactivity as a function of burnup. Although approximate, as pointed out previously, those prescriptions provide the basis for the coarse mesh nodal method to be formulated in this chapter. In PWR fuel management, the axial behavior is, normally, rather predictable, hence a two-dimensional representation of the core suffices for most applications, as, for instance, in the present research.

In what follows it is assumed that methods are available to the user (e.g. LEOPARD) to determine average node (assembly) characteristics (local reactivity as a function of burnup). Refer to Appendix B for supplementary details in support of the analysis in this chapter; in particular Fig. B.1 is a one-quarter core representation of the Maine Yankee Reactor, showing the nodal coordinate system used in Appendix B and in this chapter.

3.2 Derivation of the Nodal Equations

In Appendix B a detailed analytical solution of the "one-and-one-half" group theory equation has been developed. The main assumptions made were: the continuity of fluxes and currents at the nodal interfaces; the invariance of the fast group diffusion coefficient throughout the fueled nodes; and furthermore, the criticality of the core (i.e., ρ_s=0), as required to validate Eq. (2.11). Starting with these analytical solutions, the nodal flux and power expressions will be obtained in the subsections which follow.

3.2.1 Interior Nodes

For an interior node, the solutions for the flux integrated over the node, in the X- and Y-directions are reproduced in Table 3.1,

TABLE 3.1

Analytical Solution for Interior Node Integrated Flux

X-direction:

$$\frac{\Phi_{ij}\alpha_{ij}^2}{2} = \tag{3.1}$$

$$\frac{\Phi_{i-1,j}\alpha_{i-1,j}\,\mathrm{csch}(\alpha_{i-1,j}\,h)\left[\frac{\tanh(\alpha_{ij}\,h/2)}{\alpha_{ij}}+\frac{\tanh(\alpha_{i+1,j}\,h/2)}{\alpha_{i+1,j}}\right]+\Phi_{i+1,j}\alpha_{i+1,j}\,\mathrm{csch}(\alpha_{i+1,j}\,h)\left[\frac{\tanh(\alpha_{ij}\,h/2)}{\alpha_{ij}}+\frac{\tanh(\alpha_{i-1,j}\,h/2)}{\alpha_{i-1,j}}\right]}{\left[\frac{\coth(\alpha_{ij}\,h/2)}{\alpha_{ij}}+\frac{\tanh(\alpha_{i-1,j}\,h/2)}{\alpha_{i-1,j}}\right]\left[\frac{\tanh(\alpha_{ij}\,h/2)}{\alpha ij}+\frac{\tanh(\alpha_{i+1,j}\,h/2)}{\alpha_{i+1,j}}\right]+\left[\frac{\coth(\alpha_{ij}\,h/2)}{\alpha_{ij}}+\frac{\tanh(\alpha_{i+1,j}\,h/2)}{\alpha_{i+1,j}}\right]\left[\frac{\tanh(\alpha_{ij}\,h/2)}{\alpha_{ij}}+\frac{\tanh(\alpha_{i-1,j}\,h/2)}{\alpha_{i-1,j}}\right]}$$

Y-direction:

$$\frac{\Phi_{ij}\beta_{ij}^2}{2} = \tag{3.2}$$

$$\frac{\Phi_{i,j+1}\beta_{i,j+1}\,\mathrm{csch}(\beta_{i,j+1}\,h)\left[\frac{\tanh(\beta_{ij}\,h/2)}{\beta_{ij}}+\frac{\tanh(\beta_{ij-1}\,h/2)}{\beta_{ij-1}}\right]+\Phi_{i,j-1}\beta_{i,j-1}\,\mathrm{csch}(\beta_{i,j-1}\,h)\left[\frac{\tanh(\beta_{ij}\,h/2)}{\beta_{ij}}+\frac{\tanh(\beta_{i,j+1}\,h/2)}{\beta_{i,j+1}}\right]}{\left[\frac{\coth(\beta_{ij}\,h/2)}{\beta_{ij}}+\frac{\tanh(\beta_{i,j+1}\,h/2)}{\beta_{i,j+1}}\right]\left[\frac{\tanh(\beta_{ij}\,h/2)}{\beta_{ij}}+\frac{\tanh(\beta_{ij-1}\,h/2)}{\beta_{ij-1}}\right]+\left[\frac{\coth(\beta_{ij}\,h/2)}{\beta_{ij}}+\frac{\tanh(\beta_{ij-1}\,h/2)}{\beta_{ij-1}}\right]\left[\frac{\tanh(\beta_{ij}\,h/2)}{\beta_{ij}}+\frac{\tanh(\beta_{i,j+1}\,h/2)}{\beta_{i,j+1}}\right]}$$

Subject to: $B_{ij}^2 = \alpha_{ij}^2 + \beta_{ij}^2$ (3.3)

as Eqs. (3.1) and (3.2), respectively. Both equations are subject to the condition expressed by Eq. (3.3)

$$B_{ij}^2 = \alpha_{ij}^2 + \beta_{ij}^2 = - \frac{\rho_{ij}}{(1-\rho_{ij})\, M_{ij}^2} \tag{3.3}$$

Expansion of the hyperbolic functions provides the approximation necessary to the derivation of the simplified nodal expressions. For a generic Xh variable the following expansions hold within the limits stated [D-3]:

$$\operatorname{csch}(Xh) \approx \frac{1}{Xh} - \frac{Xh}{6} + \frac{7}{360}(Xh)^3 - \ldots \approx \frac{1}{Xh}\left(1 - \frac{X^2h^2}{6}\right) + \ldots, [(Xh)^2 < \pi^2] \tag{3.4}$$

$$\coth\left(\frac{Xh}{2}\right) \approx \frac{2}{Xh} + \frac{Xh}{6} - \frac{(Xh)^3}{45} + \ldots \approx \frac{2}{Xh}\left(1 + \frac{X^2h^2}{12}\right) - \ldots, \left[\left(\frac{Xh}{2}\right)^2 < \pi^2\right] \tag{3.5}$$

$$\tanh\left(\frac{Xh}{2}\right) \approx \frac{Xh}{2} - \frac{(Xh)^3}{12} + \ldots \approx \frac{Xh}{2} - \ldots, \left[\left(\frac{Xh}{2}\right)^2 < \pi^2\right] \tag{3.6}$$

Any degree of accuracy (within the limits stated) is possible, depending on the number of terms of the expansions that are retained. Here the objective is to obtain an approximation appropriate for $h \lesssim 20$ cm; $M^2 \approx$ 50-55 cm^2; and a broad range of reactivities, i.e.: $|\rho| \leq 0.25$. Several approximations have been tested against full-scope one-dimensional analytical benchmarks (using the corresponding trigonometric functions instead of their hyperbolic counterparts,

where appropriate). The approximation judged to have the best compromise between simplicity and accuracy was to neglect terms of third and higher orders in the expansions. The relative error in nodal power was always less than 3% for realistic cases; and higher only for clusters of assemblies all of which have very high or very low reactivity. As expected, a reduction in h (e.g. using quarter-assembly nodes) produced very good accuracy, even for those extreme cases.

Neglecting all terms that are of third and higher order in the expansions (hence, retaining second order accuracy), Eqs. (3.1) and (3.2) yield respectively:

$$\Phi_{ij} \approx \frac{\Phi_{i-1,j}\left(1 - \frac{\alpha^2_{i-1,j}\, h^2}{6}\right) + \Phi_{i+1,j}\left(1 - \frac{\alpha^2_{i+1,j}\, h^2}{6}\right)}{2\left(1 + \frac{\alpha^2_{ij}\, h^2}{3}\right)} \tag{3.7}$$

and

$$\Phi_{ij} \approx \frac{\Phi_{ij-1}\left(1 - \frac{\beta^2_{ij-1}\, h^2}{6}\right) + \Phi_{ij+1}\left(1 - \frac{\beta^2_{ij+1}\, h^2}{2}\right)}{2\left(1 + \frac{\beta^2_{ij}\, h^2}{3}\right)} \tag{3.8}$$

Equations (3.7), (3.8) and (3.3) may be solved for Φ_{ij}, to give:

$$\Phi_{ij} = \frac{\sum_{\substack{k=i-1 \\ k\neq i}}^{i+1} \Phi_{kj}\left(1 - \frac{\alpha_{kj}^2 h^2}{6}\right) + \sum_{\substack{l=j-1 \\ l\neq j}}^{j+1} \Phi_{il}\left(1 - \frac{\beta_{il}^2 h^2}{6}\right)}{4\left(1 + \frac{\beta_{ij}^2 h^2}{6}\right)} \tag{3.9}$$

Note that estimates for the directional apportionment of the nodal bucklings, α^2 and β^2, could also be obtained by the addition of an extra loop in the Gauss-Seidel iterative solution process. Due to Eq. (3.3) only the ratio between α^2 and β^2 is needed, and this relation may be computed by estimating α_{ij}^{*2} and β_{ij}^{*2} from Eqs. (3.7) and (3.8) as follows:

$$\alpha_{ij}^{*2} \approx \frac{3}{h^2}\left[\frac{\sum_{\substack{k=i-1 \\ k\neq i}}^{i+1} \Phi_{kj}\left(1 - \frac{\alpha_{kj}^2 h^2}{6}\right)}{2\,\Phi_{ij}} - 1\right] \tag{3.10}$$

and

$$\beta_{ij}^{*} \approx \frac{3}{h^2}\left[\frac{\sum_{\substack{k=j-1 \\ k\neq j}}^{j+1} \Phi_{ik}\left(1 - \frac{\beta_{ik}^2 h^2}{6}\right)}{2\,\Phi_{ij}} - 1\right] \tag{3.11}$$

At each iteration the ratios provided by $\alpha_{ij}^{*2}/\beta_{ij}^{*2}$, together with Eq. (3.3) could allow the computation of the directional apportionments of the nodal bucklings. However, due to the small numerical impact of the αs and βs in the numerator of Eq. (3.9), and to avoid the extra calculational requirements, another simplification, called here

the "isobuckling" approximation was used in the present work: it consists simply in using:

$$\alpha_{ij}^2 = \frac{B_{ij}^2}{2} \tag{3.12}$$

and,

$$\beta_{ij}^2 = \frac{B_{ij}^2}{2} \tag{3.13}$$

The power and flux relationship, provided by Eq. (2.16), may be used in Eq. (3.9) to obtain, with the aid of Eqs. (3.12) and (3.13), and after simplification:

$$f_{ij}\left[\frac{\nu}{\kappa}\frac{M^2}{D_1}\right] = \frac{\sum_{\substack{k=i-1 \\ k\neq 1}}^{i+1} f_{kj}\left[\frac{\nu}{\kappa}\frac{M^2}{D_1}\right]_{kj}\left\{1-\left(1-\frac{h^2}{12\,M_{kj}^2}\right)\rho_{kj}\right\} + \sum_{\substack{l=j-1 \\ l\neq j}}^{j+1} f_{il}\left[\frac{\nu}{\kappa}\frac{M^2}{D_1}\right]_{il}\left\{1-\left(1-\frac{h^2}{12M_{il}^2}\right)\rho_{il}\right\}}{4\left\{1-\left(1+\frac{h^2}{6\,M_{ij}^2}\right)\rho_{ij}\right\}} \tag{3.14}$$

Using Eq. (2.29) for the factor $\frac{\nu}{\kappa}\frac{M^2}{D_1}$, and defining,

$$\theta = 1 + \frac{h^2}{6\,M^2} + C_2 \tag{3.15}$$

and

$$\theta_s = 1 - \frac{h^2}{12\,M^2} - C_2 \tag{3.16}$$

where, for LEOPARD results, in Eq. (2.29), $C_2 \approx 0$, the nodal power expression becomes:

$$f_{ij} = \frac{\sum_{\substack{k=i-1 \\ k\neq i}}^{i+1} f_{kj}\,(1-\theta_s\rho_{kj}) + \sum_{\substack{l=j-1 \\ l\neq j}}^{j+1} f_{il}\,(1-\theta_s\rho_{il})}{4\,(1-\theta_{ij})} \tag{3.17}$$

The slight dependence of M^2 on local reactivity is assumed to be incorporated in θ, to first order.

3.3.2 Radial Leakage Calculation

Knowledge of the radial leakage simplifies the derivation of the expressions for the powers of the peripheral nodes. Therefore, the prescription for its computation will be derived first.

Equations (B.40) and (B.41), giving the net currents out of a peripheral node, in the X- and Y-directions, after minor re-arrangements, become:

$$J_{xij} = -\frac{D_{ij}\Phi_{ij}\alpha_{ij}^2}{2}\left[1 - \frac{\dfrac{\coth(\alpha_{ij}\,h/2)}{\alpha_{ij}} + \dfrac{E\,D_{ij}}{D_rB_r}\tanh(B_rh_r)}{\dfrac{\tanh(\alpha_{ij}\,h/2)}{\alpha_{ij}} + \dfrac{E\,D_{ij}}{D_rB_r}\tanh(B_rh_r)}\right] \tag{3.18}$$

and

$$J_{yij} = -\frac{D_{ij}\Phi_{ij}\beta_{ij}^2}{2}\left[1 - \frac{\dfrac{\coth(\beta_{ij}\,h/2)}{\beta_{ij}} + \dfrac{E\,D_{ij}}{D_rB_r}\tanh(B_rh_r)}{\dfrac{\tanh(\beta_{ij}\,h/2)}{\beta_{ij}} + \dfrac{E\,D_{ij}}{D_rB_r}\tanh(B_rh_r)}\right] \tag{3.19}$$

or, defining the terms in brackets as complementary non-leakage probabilities $(1-N_{LPX})$ and $(1-N_{LPY})$:

$$J_{xij} = - \frac{D_{ij} \Phi_{ij} \beta_{ij}^2}{2} \left[1 - N_{LPX}\right] \tag{3.20}$$

and

$$J_{yij} = - \frac{D_{ij} \Phi_{ij} \beta_{ij}^2}{2} \left[1 - N_{LPY}\right] \quad , \tag{3.21}$$

(where N_{LPX} and N_{LPY} are of interest in the peripheral nodal power expression derivations).

Making use of the "infinite reflector" approximation (since $\tanh (B_r h_r) \approx 1$, for $B_r h_r > 2$, as for PWRs), using the expansions for hyperbolic functions given by Eqs. (3.5) and (3.6), neglecting the terms of third and higher orders, and after simplification, Eqs. (3.18) and (3.19) become:

$$J_{xij} = \frac{2D_{ij}\Phi_{ij}}{h^2} \left[\frac{1 - \frac{\alpha_{ij} h^2}{6}}{1 + \frac{2ED_{ij}}{D_r B_r h}} \right] \tag{3.22}$$

and

$$J_{yij} = \frac{2D_{ij}\Phi_{ij}}{h^2} \left[\frac{1 - \frac{\beta_{ij}^2 h^2}{6}}{1 + \frac{2ED_{ij}}{D_r B_r h}} \right] \tag{3.23}$$

Defining the ratio of neutron leakage rate in the X- and Y-directions to production rate of the the peripheral assemblies as "leakage reactivities" ρ_{LXij} and ρ_{LYij}, these expressions become,

$$\rho_{LXij} = \frac{J_{Xij}}{\left(\frac{\nu}{\kappa}\right) f_{ij}} \tag{3.24}$$

and

$$\rho_{LYij} = \frac{J_{Yij}}{\left(\frac{\nu}{\kappa}\right) f_{ij}} \tag{3.25}$$

and, using Eq. (2.16) for Φ_{ij}, and Eqs. (3.22) and (3.23) for J_{Xij} and J_{Yij},

$$\rho_{LXij} = \frac{2 M_{ij}^2 (1 - \rho_{ij})}{h^2} \left[\frac{1 - \frac{\alpha_{ij}^2 h^2}{6}}{1 + \frac{2ED_{ij}}{D_r B_r h}} \right] \tag{3.26}$$

and

$$\rho_{LYij} = \frac{2 M_{ij}^2 (1 - \rho_{ij})}{h^2} \left[\frac{1 - \frac{\beta_{ij}^2 h^2}{6}}{1 + \frac{2ED_{ij}}{D_r B_r h}} \right] \tag{3.27}$$

For an assembly with only one reflector interface, either Eq. (2.26) or (2.27) is applicable. For an assembly with two reflector interfaces, $\rho_{Lij} = \rho_{LXij} + \rho_{LYij}$, becomes

$$\rho_{Lij} = \frac{4 M_{ij}^2 (1 - \rho_{ij})}{h^2} \left[\frac{1 - \frac{B_{ij}^2 h^2}{12}}{1 + \frac{2 E D_{ij}}{D_r B_r h}} \right] \tag{3.28}$$

or, equivalently, after using Eq. (3.3) and simplifying:

$$\rho_{Lij} = \frac{4 M_{ij}^2}{h^2} \left[\frac{1 - \left(1 - \frac{h^2}{12 M_{ij}^2}\right) \rho_{ij}}{1 + \frac{2 E D_{ij}}{D_r B_r}} \right] \tag{3.29}$$

For the cases of interest here, with h $\approx$ 20 cm, $M^2 \approx$ 50 cm^2, the slight dependence of ρ_L on ρ_{ij} may be neglected (or included in the nodal coupling coefficient θp: note that $(1-h^2/12\ M_{ij}^2)=\theta s)$); then an approximation for ρ_L becomes:

$$\rho_{Lij} \cong \frac{4\ M_{ij}^2}{h^2} \left[\frac{1}{1 + \frac{2\ E\ D_{ij}}{D_r B_r h}} \right] \tag{3.30}$$

A similar result is obtained, by applying this same approximation, for assemblies having one reflector interface:

$$\rho_{LXij} = \rho_{LYij} = \frac{2\ M_{ij}^2}{h^2} \left[\frac{1}{1 + \frac{2\ E\ D_{ij}}{D_r B_r h}} \right] \tag{3.32}$$

Note that, in any event, the factor $2\ E\ D_{ij}/D_r B_r h$ is empirically adjustable, and thus able to account for required corrections and, as shown in Eq. (B-36), has a direct relation with conventional albedo-type boundary conditions.

As noted by Khalil [K-5], the albedos are functions of the soluble boron content of the reflector. A linear dependence is appropriate, and may be included in the expression for ρ_L without causing undue additional complexity. Hence, ρ_L may be written as:

$$\rho_{Lij} = N_r \frac{2\ M_{ij}^2}{h^2 \left(1 + \frac{2\ E\ D_{ij}}{D_r B_r h} \right)} \quad (1 + k_L\ \rho_{SP}) \tag{3.32}$$

where,

ρ_{SP} = soluble poison reactivity penalty, and

k_L = coefficient accounting for the dependence of ρ_L on soluble boron reactivity.

As an illustration, considering typical Maine Yankee core albedos of 0.582 at EOC (0 ppm boron), 0.538 at MOC (~400 ppm boron) and 0.495 at BOC (~800 ppm boron), a value of $k_L \approx 1.5$ would result.

Hence, due to this and other effects (e.g. thermal back-leakage, etc.) the empirical adjustment of the leakage constant, if possible on an individual peripheral node basis (as in the case of albedos), is clearly necessary, and this fact has been implicitly acknowledged through the inclusion of the parameter E in its formulation.

3.2.3 Peripheral Nodes

First the quantities N_{LPX} and N_{LPY} will be derived as a function of the "leakage reactivities". Re-arrangement of Eqs. (3.20) and (3.21), with the aid of Eqs. (3.24), (3.25) and (2.16) yields, after some algebra:

$$N_{LPX} = \frac{2\,\rho_{LXij}}{M_{ij}^2(1 - \rho_{ij})\,\alpha_{ij}^2} + 1 \qquad (3.29)$$

and

$$N_{LPY} = \frac{2\,\rho_{LYij}}{M_{ij}^2(1 - \rho_{ij})\,\beta_{ij}^2} + 1 \qquad (3.30)$$

Equations (B.33) and (B.34), re-written in Table 3.2, as Eqs. (3.31) and (3.32), are the solutions in the X- and Y-directions for the integrated flux of a peripheral node, under the restriction expressed by Eq. (3.3).

The first factor of the second term in the denominators of Eqs. (3.31) and (3.32) may be identified, respectively, as N_{LPX} and N_{LPY}, defined by Eqs. (3.29) and (3.30). Using this fact and, again, expanding the hyperbolic functions in series, as given by Eqs. (3.4), (3.5) and (3.6), and neglecting all terms of third and higher orders, after some simplifications, the following expressions result:

$$\Phi_{ij} = \frac{\Phi_{i-1,j}\left(1 - \frac{\alpha_{i-1,j}\, h^2}{6}\right)}{1 + \frac{5\,\alpha_{ij}^2\, h^2}{6} + \frac{h^2}{M_{ij}^2\,(1 - \rho_{ij})}\,\rho_{LXij}} \quad , \qquad (3.31)$$

and

$$\Phi_{ij} = \frac{\Phi_{ij+1}\left(1 - \frac{\beta_{ij+1}\, h^2}{6}\right)}{1 + \frac{5\,\beta_{ij}^2\, h^2}{6} + \frac{h^2}{M_{ij}^2\,(1 - \rho_{ij})}\,\rho_{LYij}} \quad , \qquad (3.32)$$

subject to Eq. (3.3) (i.e.: $\alpha_{ij}^2 + \beta_{ij}^2 = B_{ij}^2$).

For assemblies with two reflector interfaces, Eqs. (3.31), (3.32) and (3.3) may be solved for Φ_{ij} (as well as for the directional apportionment of the buckling, if desired as in Eqs. (3.10) and (3.11)), in the same fashion as for the interior nodes. The result for Φ_{ij} becomes:

TABLE 3.2

Analytical Solution for Peripheral Node Integrated Flux

X-direction:

$$\frac{\Phi_{ij}\alpha_{ij}^2}{2} = \frac{\Phi_{i-1,j}\,\alpha_{i-1,j}\,\mathrm{csch}(\alpha_{i-1,j}\,h)}{\left[\frac{\coth(\alpha_{ij}\,h/2)}{\alpha_{ij}} + \frac{\tanh(\alpha_{i-1,j}\,h/2)}{\alpha_{i-1,j}}\right] + \frac{\left[\frac{\coth(\alpha_{ij}\,h/2)}{\alpha_{ij}} + \frac{ED_{ij}}{D_rB_r}\tanh(B_rh_r)\right]}{\left[\frac{\tanh(\alpha_{ij}\,h/2)}{\alpha_{ij}} + \frac{ED_{ij}}{D_rB_r}\tanh(h_rB_r)\right]}\left[\frac{\tanh(\alpha_{ij}\,h/2)}{\alpha_{ij}} + \frac{\tanh(\alpha_{i-1,j}\,h/2)}{\alpha_{i-1,j}}\right]} \qquad (3.31)$$

Y-direction:

$$\frac{\Phi_{ij}\beta_{ij}^2}{2} = \frac{\Phi_{i,j+1}\,\beta_{i,j+1}\,\mathrm{csch}(\beta_{i,j+1}\,h)}{\left[\frac{\coth(\beta_{ij}\,h/2)}{\beta_{ij}} + \frac{\tanh(\beta_{i,j+1}\,h/2)}{\beta_{i,j+1}}\right]\frac{\left[\frac{\coth(\beta_{ij}\,h/2)}{\beta_{ij}} + \frac{ED_{ij}}{D_rB_r}\tanh(B_rh_r)\right]}{\left[\frac{\tanh(\beta_{ij}\,h/2)}{\beta_{ij}} + \frac{ED_{ij}}{D_rB_r}\tanh(B_rh_r)\right]}\left[\frac{\tanh(\beta_{ij}\,h/2)}{\beta_{ij}} + \frac{\tanh(\beta_{i,j+1}\,h/2)}{\beta_{i,j+1}}\right]} \qquad (3.32)$$

Subject to: $B_{ij}^2 = \alpha_{ij}^2 + \beta_{ij}^2$ (3.3)

$$\Phi_{ij} = \frac{\Phi_{i-1,j}\left(1 - \frac{\alpha_{i-1,j}\, h^2}{6}\right) + \Phi_{ij+1}\left(1 - \frac{\beta_{ij+1}\, h^2}{6}\right)}{2\left[1 + \frac{5}{12} B_{ij}^2 h^2 + \frac{h^2}{2 M_{ij}^2 (1-\rho_{ij})} \rho_L\right]} \qquad (3.33)$$

The corresponding nodal power equation, using the isobuckling approximation and Eq. (2.29) for the factor $\frac{\nu}{\kappa}\frac{M^2}{D_1}$, becomes

$$f_{ij} = \frac{f_{i-1,j}\left[1 - \left(1 - \frac{h^2}{12 M_{ij}^2} - C_2\right)\rho_{i-1,j}\right] + f_{ij+1}\left[1 - \left(1 - \frac{h^2}{12 M_{ij+1}^2} - C_2\right)\rho_{ij+1}\right]}{2\left[1 - \left(1 + \frac{5}{12}\frac{h^2}{M_{ij}^2} + C_2\right)\rho_{ij} + \frac{h^2}{2 M_{ij}^2}\rho_L\right]} \qquad (3.34)$$

For the cases of one and one-half reflector interfaces, expressions with similar functional form may be obtained by recognizing the fact that the denominators in Eqs. (3.31), (3.32), (3.7) and (3.8) are numerically similar for the range of interest in the present work. The results for these cases are included in Table 3.3, which summarizes the nodal power equations for all cases, as well as the expressions for leakage calculation. However, for simplicity, since the nodes of interest are always coupled only to the interfacing nodes regardless of the order of the coordinates, the double subscript "ij" has been dropped. From now on, in general, the subscripts "i" and "j" or "s" will be used to designate the node of interest and its interfacing nodes, respectively. The coupling coefficients, other constants and data of interest, as well as numerical estimates are summarized

TABLE 3.3

Summary of the Nodal Power and Leakage Equations

Interior Nodes:

$$f_i = \frac{\sum_{j=1}^{4} f_j(1 - \theta_s \rho_j)}{4(1 - \theta\rho_i)} \tag{3.35}$$

Peripheral Nodes:

$$f_i = \frac{\sum_{j=1}^{N_p} f_j(1 - \theta_s\rho_j)}{N_p(1 - \theta_p\rho_i + \theta_L\rho_{Li})} \tag{3.36}$$

Leakage Reactivity:

$$\rho_{Li} = N_r \cdot \frac{2 M_i^2}{h^2\left(1 + \frac{2 E D_i}{D_r B_r h}\right)} \cdot (1 + k_L \rho_{sp}) \tag{3.37}$$

where:

N_p = number of fuel/fuel interfaces on assembly i;

$N_r = 4\text{-}N_p$ = number of fuel/reflector interfaces on assembly i;

and, the coupling coefficients, other constants and numerical estimates are summarized in Table 3.4.

(Note change in notation from double (ij) to single (i) subscripts.)

in Table 3.4. It should be noted, as a point of interest, that the coupling coefficients are inter-related; hence θ_s, θ_L and the θ_ps may all be written as a function of θ.

3.2.4 Relation to Previous Results

The results derived for interior nodes are in good agreement with those obtained by Kamal [K-1] using a cylindricized representation of an assembly and its surroundings; differences exist however for the peripheral nodes. Also, with appropriate choice of terms in the expansion of the hyperbolic functions of Eqs. (3.1) and (3.2), a lower order approximation, similar to that proposed by Loh [L-2] and employed by Downar [D-2], may be obtained; after solving for Φ_i, with the aid of Eq. (3.3) one obtains:

$$\Phi_i = \frac{\sum_{j=1}^{4} \Phi_j}{4\left[1 + \frac{B_i h^2}{8}\right]} \tag{3.38}$$

The corresponding nodal power equation can be derived using Eqs. (2.16) and (2.29). After simplification the result becomes:

$$f_i = \frac{\frac{1}{4}\sum_{j=1}^{4} f_j(1 - \rho_j)}{1 - \left(1 + \frac{h^2}{8 M_i^2}\right)\rho_i} \tag{3.39}$$

The numerator is merely an arithmetic average over the surroundings, hence the result is similar to that of Loh [L-2], reproduced in Eq. (1.2).

TABLE 3.4

Summary of Coupling Coefficients, Leakage Constants and Numerical Estimates

INTERIOR:

$$\theta = 1 + \frac{h^2}{6\,M^2} + \gamma_1 = 2.234$$

$$\theta_s = 1 - \frac{h^2}{12\,M^2} + \gamma_2 = 0.383$$

PERIPHERY:

Case: Number of Reflector Interfaces (N_r)	θ_p	Numerical Estimate	θ_L	Numerical Estimate	ρ_{Li} Eq. (3.37)	ρ_{Li}^* Eq. (3.37)
2	$1 + \frac{5\,h^2}{12\,M^2} + \gamma_3$	4.086	$\frac{h^2}{2\,M^2}$	3.704	0.26	0.2622
1	$1 + \frac{h^2}{4\,M^2} + \gamma_4$	2.852	$\frac{h^2}{3\,M^2}$	2.469	0.13	0.1311
1/2	$1 + \frac{17\,h^2}{84\,M^2} + \gamma_5$	2.500	$\frac{h^2}{3.5\,M^2}$	2.116	0.065	0.0655

ASSUMPTIONS:

1) Empirical corrections: $\gamma_1 = \ldots = \gamma_5 = 0$.

2) $M^2 = 54\ cm^2$; $h = 20$ cm; $\rho_{sp} = 0$ (EOC).

3) ρ_{Li} was computed using: $D_i = 1.4$ cm; $D_r = 2.25$ cm; $1/B_r = 8$ cm and $E \approx 2.2$ (Appendix C).

4) ρ_{Li}^* was computed using: Eq. (B.36) to calculate $E/D_rB_r = 0.1321$ (for Maine Yankee's EOC albedo, $\beta^* = 0.583$); and $D_i = 1.4$.

An interesting point is the good agreement between the value predicted by Eq. (3.39) for the coupling coefficient ($1 + h^2/8\ M^2 \approx 1.9$, for $h = 20$ cm $M^2 \approx 55\ cm^2$) and that obtained empirically by prior investigators [L-2], [K-1] from empirical fits to state-of-the-art core maps (1.42 to 1.81).

3.2.5 Incorporation of Corrections and Empirical Adjustments

Besides providing a simple and reasonably accurate core model (as will be shown later in this chapter), a major merit of the relations derived so far is the capability of their functional form to incorporate corrections due to inherent analytical deficiencies as well as to accommodate empirical adjustments. In fact, empirically adjustable parameters have been the key to the successful use of the FLARE/TRILUX-type of fuel management codes.

In the previous sections, two adjustments, both related to the conventional albedo, namely the factors E (for peripheral thermal back-leakage, baffle transmission, etc.) and k_L (to account for the dependence of the leakage on the soluble boron content of the reflector) have been introduced. In this section other corrections will be suggested and possible compensatory adjustments indicated.

3.2.5.1 Differential Thermal Leakage

One of the assumptions in deriving the one-and-one-half group model, was the inconsequential magnitude of thermal leakage, implemented by setting $\nabla^2 \Phi_2 = 0$ (or alternatively $D_2 = 0$) in Eq. (2.2). For peripheral nodes the factor E, to account for thermal back-leakage of neutrons from the reflectors, has already been discussed in the preceeding sections and in appendices B and C. Appendix C presents a derivation along the lines proposed by Becker [B-3], to account partially for the differential thermal leakage [D-1]. It was shown that the readjustment of the coupling coefficient θ (or θ_p) is sufficient to incorporate first order effects between adjacent assemblies. Then, generically, a new coefficient θ^* may be defined as:

$$\theta^* = \theta + \left(\frac{\gamma h^2}{M^2}\right)\left(\frac{\Sigma_{12} L_i^2}{L_i + L_j}\right) + \ldots \qquad (3.40)$$

where, γ = 1/6 for interior nodes, 5/12 for twice-reflected nodes, etc., and L_i, L_s = thermal diffusion lengths for assembly "i" and surroundings "j" ($\sim$ 2 cm).

3.2.5.2 Power Related Feedback

In Appendix A power feedback effects on the fast group parameter D_1/M^2 have been examined. Here the objective is to evaluate the effects on the assembly reactivity status, which is also affected by the power level. An increase in power leads to increases in moderator and fuel

temperature, both of which slightly reduce the local reactivity due to the negative moderator temperature coefficient and the Doppler reactivity coefficient of the fuel. Higher power density also corresponds to higher concentrations of saturating fission products leading to a further slight reduction in local reactivity. The first order incorporation of these feedback effects, as demonstrated in Appendix C, will not necessarily affect the power level; core-average power level is fixed by demand: it is differential local changes in power shape that are of concern here. In any event, a first order correction for feedback can be incorporated if the coupling coefficient is adjusted to match results of more sophisticated calculations that explicitly consider the coupling between neutronic and thermal hydraulic effects. Hence, as shown in Appendix C, the new coupling coefficient, θ^*, would satisfy the relation

$$\theta^* = \theta + \left(\frac{1}{f_i}\frac{\partial f_i}{\partial \rho_i}\right) \tag{3.41}$$

3.2.5.3 Axial Leakage

For PWR assemblies, with initially uniform axial enrichment, the axial power shape (hence, local burnup) behavior usually follows a characteristic pattern as burnup progresses, starting with a close-to-cosine shape at BOL and ending almost flat at EOL. Leakage, as in the radial case already derived, depends strongly on local power (thus

also local reactivity) close to the reflector interfaces (as well as on the soluble poison content of the core and its reflector). Knowledge of the evolution of an equivalent axial (2-dimensional) buckling as a function of burnup allows one to account for the related leakage effects in a two-dimensional (X,Y) model as a decrement, ρ_{LZ}, in the assembly's reactivity. Numerical results show a close-to-directly-proportional dependence (increase) of ρ_{LZ} as a function of assembly burnup. Typical values of the reactivity decrement, ρ_{LZ}, for the Maine Yankee core are: 0.0048 at BOL; 0.0105 at 20 MWD/kg, and 0.0157 at 40 MWD/kg. The error incurred by neglecting the change in axial leakage (or indeed the leakage itself) is inconsequential for present purposes, since it has an only minor effect on the radial power distribution, and consistently biases the absolute value of the cycle burnup towards the high side.

In general, however, the incorporation of this correction is readily feasible given the availability of an appropriate correlation for ρ_{LZ} as a function of burnup. One simple scheme to account for the axial leakage is to include a BOL reactivity decrement and slightly increase the reactivity versus burnup slope, A, to allow for the differential increase in axial leakage with burnup.

3.2.5.4 Differential Boron Worth

As discussed in section 2.3.4.4, the net local reactivity decrement due to the control poison (soluble boron) is dependent on

the local spectrum. An illustration of the effect is provided in Fig. (2.4), by the differing slopes of ρ as a function of burnup for the cases of different soluble boron content in the assemblies (0, 400 and 800 ppm). As suggested in Eqs. (2.24) and (2.25) the effect may be accounted for by using weighting factors which are functions of local burnup and burnable poison content, for any given initial enrichment. Even though provision is made in the computer program developed in the course of the present research to allow for such weighting factors, normally they have been set to unity, since the resulting error is minor, given the objectives of this work.

3.3 The Solution Strategy

The equations and relations of Tables (3.3) and (3.4), together with the system reactivity balance equation and the applicable corrections as discussed in section 3.2.5, constitute the basis for the spatial power distribution calculation. In the present work a standard Gauss-Seidel iterative procedure has been used to solve these equations simultaneously. It may be noted that, in Table 3.3 the equations are cast in a form suitable for such an iterative scheme (instead of the conventional matrix formalism).

Figure 3.1 shows the calculational procedure used in the method, which is embodied in a microcomputer program, as documented in

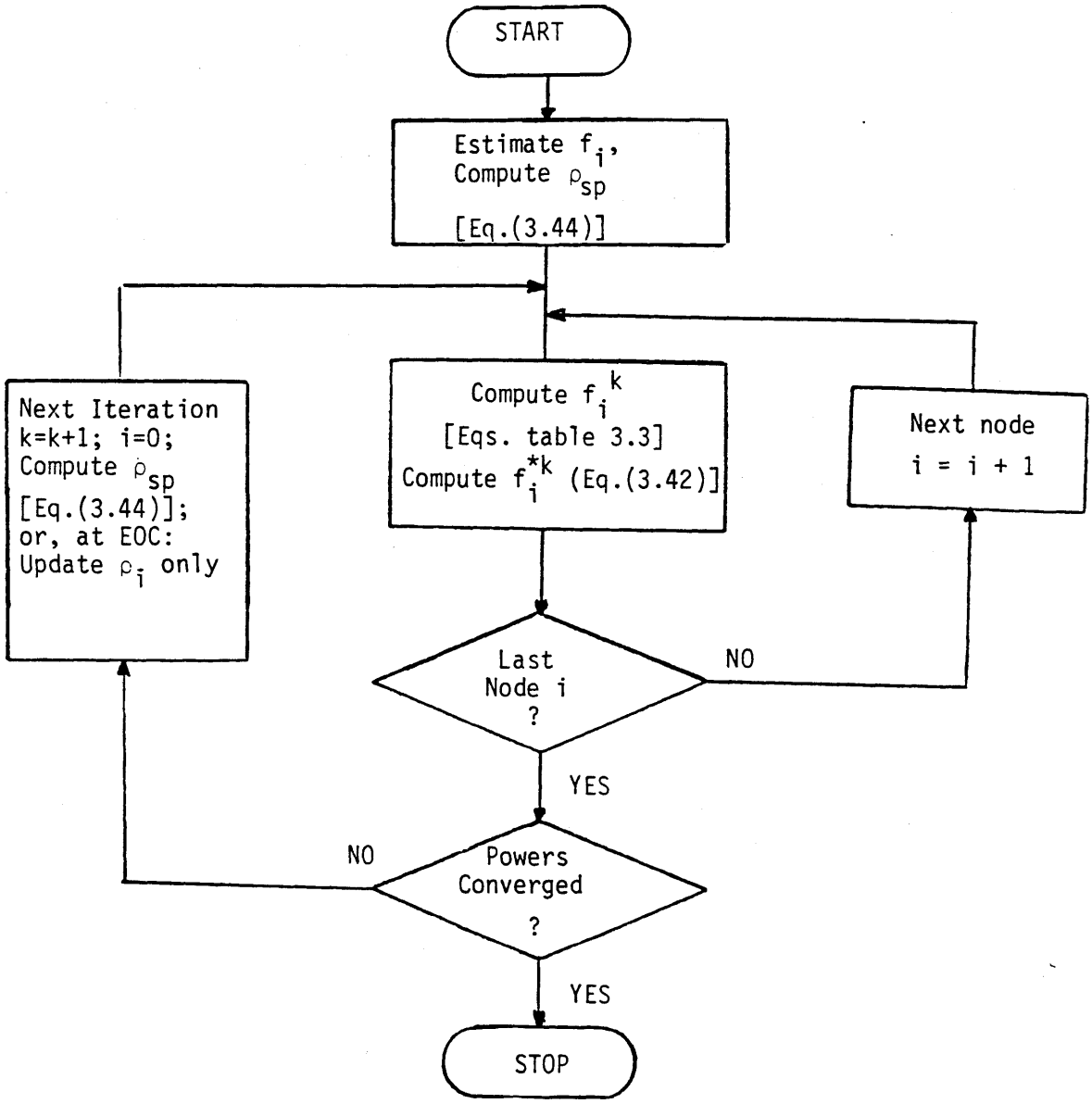

Fig. 3.1 Flowchart of Power Distribution Calculation

Appendix D. The power distribution calculation process is initialized by setting all nodal power fractions to unity. If better estimates are available (from a previous burnup step, for example) then these are used. Then, ρ_{sp} is calculated using Eq. (2.30), and the iteration loops are started. Normally the process converges monotonically, and a simple relaxation method has been implemented to take advantage of this characteristic and accelerate the convergence. At each inner iteration, k, the power fraction, f_i^k is recomputed as f_i^{*k}:

$$f_i^{*k} = \frac{f_i^k}{1 - A_c(f_i^k - f_i^{*k-1})} \tag{3.42}$$

where A_c is an empirical factor, found to lie between 0.4 and 0.66 for best results. This simple artifice allowed a reduction in the number of iterations required to achieve a given accuracy by a factor close to 2. The local reactivity, ρ_i, to be used in the appropriate equations of Table 3.3 is given by:

$$\rho_i = \rho_{oi} - A_i B_i - \rho_{boi} + S_{bi} B_i - \rho_{sp} W_i \tag{3.43}$$

where:

ρ_{boi} = initial BP reactivity decrement

S_{bi} = slope of BP reactivity decrement as a function of burnup.

The outer loop recomputes the critical boron reactivity, ρ_{sp}, each time after all nodal powers have been updated. Convergence for ρ_{sp} is very fast and a value close to the final one is achieved in the first few iterations. Power-, instead of source-weighting is used to compute

ρ_{sp}, consistent with the approximation evaluated in section 2.3.4.3. Hence, using Eqs. (2.22), (2.24), (3.24) and (3.25), ρ_{sp} is given by:

$$\rho_{sp} = \frac{\sum_{i=1}^{n} f_i \rho_i - \sum_{i=1}^{m} f_i \rho_{Li}}{\sum f_i W_i} \qquad (3.44)$$

where:

$$\rho_i = \rho_{oi} - A_i B_i + \rho_{Boi} + S_{bi} B_i$$

For the EOC nodal power calculation the process is the same, except that the soluble boron reactivity, ρ_{sp}, is zero. Instead of ρ_{sp} computation, as will be seen later, the local reactivities are recomputed according to the nodal and cycle burnups, such as to maintain the core's criticality.

A rigorous convergence criterion would require that all computed nodal power values in a given iteration be close to those of the previous iteration by less than some small margin δ. Experience, however, has shown that this condition can, for problems of present interest, be translated into specification of the number of iterations to be carried out (approximately 20, when the initial power fractions are set to unity); hence this option has been adopted in the computer program.

3.4 Burnup Calculation

Reactivity (as formulated in the LRM), may be regarded as a local state function, in the sense that it is able to provide, in a very simple fashion, an accurate description of the assembly status as a function of burnup. In this section, computational methods to describe the core state as a function of its burnup, will be formulated using the LRM. Three methods, here demoninated "synthesis", "integrated" and "step-wise depletion", have been developed and incorporated in the computer program.

3.4.1 Synthesis Method

For normal operational circumstances the end of cycle, and thus the cycle burnup, is determined by the null reactivity limit. The LRM may be used to evaluate this condition and compute the cycle burnup. The reactivity balance is provided by Eq. (3.44). At EOC, $\rho_{sp} = 0$ and, as postulated in section 2.3.3.2, defining r as the residual BP reactivity fraction,

$$\rho_{boi} - S_{bi} B_i = r\rho_{boi} \tag{3.45}$$

Then Eq. (3.43) becomes, using the superscript e to denote EOC:

$$\frac{\sum_{i=1}^{n} f_i^e (\rho_{oi} - A_i B_i - r\rho_{boi}) - \sum_{i=1}^{n} f_i^e \rho_{Li}}{\sum f_i^e W_i} = 0 \tag{3.46}$$

Recognizing that the B_i, the assembly burnups, may be written as a function of cycle-average power fraction, f_{ai}, as:

$$B_i = B_c \, f_{ai} \quad , \tag{3.47}$$

the expression for the cycle burnup becomes:

$$B_c = \frac{\sum_{i=1}^{n} f_i^e \, (\rho_{oi} - r\rho_{boi}) - \sum_{i-1}^{m} f_i^e \, \rho_{Li}}{\sum_{i=1}^{n} A_i \, f_i^e \, f_{ai}} \tag{3.48}$$

The only unknowns in this equation are the cycle-average power fractions, f_{ai} . In analogy to the conventional flux synthesis method, a means may be devised to compute these quantities from the BOC and EOE power fractions (f_i^b, f_i^e) by the appropriate choice of mixing coefficients; i.e.:

$$f_{ai} = f_i^b \cdot V_i^b + f_i^e \cdot V_i^e \tag{3.49}$$

If the required weighting coefficients (importances) were known (e.g. from experience, or variational methods, etc.) this technique would yield the exact answer. Experience gained in the course of the present work shows that for "well-behaved" (i.e. realistic) cores composed of assemblies having linear BP and reactivity traces as functions of burnup, the power fraction, f_i, to a good approximation, also varies linearly with burnup. Hence 0.5 is a natural choice for the mixing coefficients.

Figure 3.2 displays the flowchart of the computational process using this approximation. A standard BOC power distribution calculation

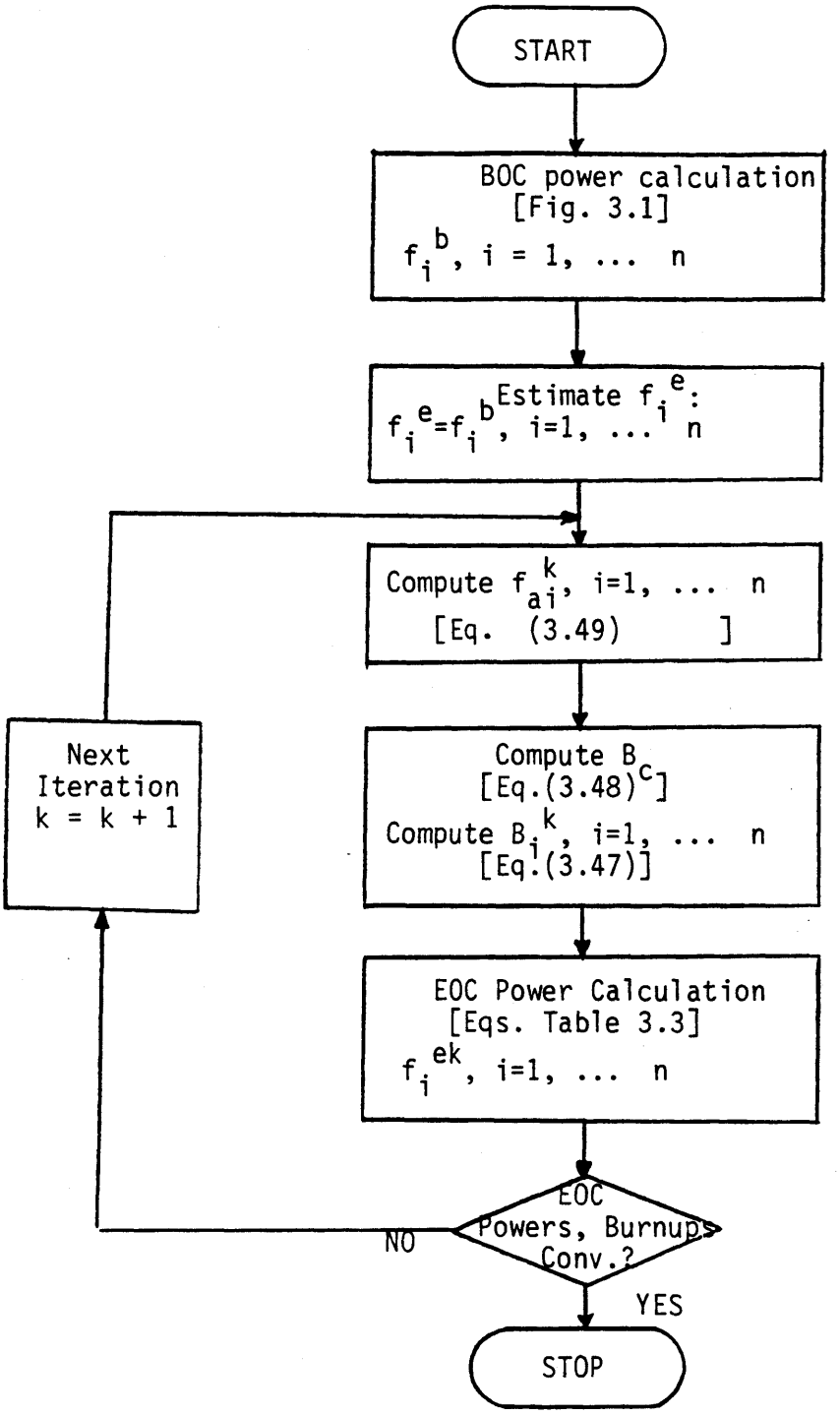

Fig. 3.2 Flowchart for Synthesis Method

is performed, and then EOC power distribution, cycle and assembly burnup calculations are carried out in tandem until convergence is achieved (usually, about 20 iterations are required at BOC and EOC).

Non-negligible errors can be associated with the method, due to nonlinearities in the power fraction as a function of burnup, as can arise when there is a significant power difference between the various regions of the core, or when exceptionally reactive assemblies are present. In the latter case the usual consequence is that an over-prediction of burnup of the highly reactive assemblies results (with a corresponding underprediction for the least reactive ones). In general the results were fairly accurate for realistic core loading patterns (that is, core maps not having excessive power tilting or local assembly overpower). The real usefulness of this method in the present research is related to its compatibility with the optimization scheme formulated in the next chapter.

3.4.2 Integrated Method

Integration of the nodal power equations over the cycle yields a set of relations that permits the computation of the nodal burnups in a fashion similar to the way power is calculated at a fixed point in time. As in the synthesis method, however, an assumption is also required: this time regarding the computation of the nodal integrated soluble boron reactivity decrement, as will be shown later.

The interior nodal equation may be re-written as an integral over the cycle as:

$$\int_0^{B_c} f_i \left\{1 - \theta(\rho_{oi} - A_i B_i - \rho_{boi} + S_{bi} B_i - W_i \rho_{sp})\right\} dBc =$$

$$\frac{1}{4} \sum_{j=1}^{n} \int_0^{B_c} f_j \left\{1 - \theta_s(\rho_{oj} - A_j B_j - \rho_{bj} + S_{bj} B_j - W_j \rho_{sp})\right\} dBc \quad (3.50)$$

where i indicates the reference node of concern, and j designates the nodes which share interfaces with the reference node. Recognizing that f_i dBc = dBi, all the integrations are well defined, except that of the local reactivity decrement due to the soluble control poison, which may be written out as:

$$[\rho_{sp}] = \int_0^{B_c} W_i \rho_{sp} (B_c) f_i \, dBc \quad (3.51)$$

Assumptions regarding the behavior of the integrand with respect to cycle burnup are required. Linearity of both ρ_{sp} W_i and f_i as functions of cycle burnup appears to be the simplest choice, one which is also not too unrealistic, considering that burnable poison and assembly reactivities are approximately linear with burnup and that core-average soluble poison concentrations, as actually measured on operating PWRs, decrease very nearly linearly with core average burnup. Under this assumption, a quadratic equation for the local burnup results after integration and re-arrangement. Realizing that only

positive values are physically acceptable, the solution for the local burnup becomes:

$$B_i = \frac{-\left\{1 - \theta\left[\rho_{oi} - \rho_{boi}(1+r)/2 - \rho_{spo}/3\right]\right\}}{\theta A_i} + \frac{\left[\left\{1 - \theta\left[\rho_{oi} - \rho_{boi}(1+r)/2 - \rho_{spo}/3\right]\right\}^2 + Z\right]^{1/2}}{\theta A_i} \tag{3.52}$$

where ρ_{spo} is the BOC ρ_{sp}, and

$$Z = 2\theta A_i \left\{ \frac{1}{N_p} \sum_{j=1}^{N_p} \frac{\theta_s B_j^2 A_j}{2} + \frac{1}{N_p} \sum_{j=1}^{N_p} \left\{1 - \theta_s\left[\rho_{oj} - \rho_{boj}(1+r)/2 - \rho_{spo}/3\right]\right\} + \frac{B_c}{6}\left(\theta f_i^b + \frac{1}{N_p}\sum_{j=1}^{N_p} \theta f_j^b\right)\right\} \tag{3.53}$$

An entirely analogous result may be obtained for the peripheral nodes:

$$B_i = \frac{-\left\{1 - \theta_p\left[\rho_{oi} - \rho_{boi}(1+r)/2 - \rho_{spo}/3\right] + \theta_L \rho_{Li}\right\}}{\theta_p A_i} + \frac{\left[\left\{1 - \theta_p\left[\rho_{oi} - \rho_{boi}(1+r)/2 - \rho_{spo}/3\right] + \theta_L\rho_{Li}\right\}^2 + Z_p\right]^{1/2}}{\theta_p A_i} \tag{3.54}$$

where ρ_{Li} has been assumed constant, and Z_p is obtained by substituting θ_p for θ in Eq. (3.53).

The core cycle average burnup is given by:

$$B_c = \frac{1}{n} \sum_{i=1}^{n} B_i \qquad (3.55)$$

The flowchart for the computations is shown in Fig. 3.3.

The results in this case, as opposed to the synthesis method, have been found to underpredict the burnup of very reactive assemblies (and overpredict that of those with low reactivity). This is due to the error introduced by linearizing the power fractions as a function of burnup in Eq. (3.51). Better results would probably be obtained if the control poison reactivity were calculated by integrating the system reactivity balance equation over the cycle, and if the linearity of the power fractions with burnup was related explicitly to the EOC power fractions (in Eq. (3.53)), instead of those at BOC, and also if the null reactivity condition were explicitly verified.

3.4.3 Step-wise Depletion Method

In principle, step-wise depletion can be made as accurate as desired, by appropriately choosing the burnup step length, ΔB. Figure 3.4 displays the computational flowchart formulated for this method. After ΔB has been specified, the process begins with a BOC power calculation. Equation (3.48) is used to test if enough reactivity is available for a full burnup step. Depletion step s is executed using an average power fraction, computed as:

$$f_{ai} = (f_i^{s-1} + f_i^s) / 2 \qquad (3.56)$$

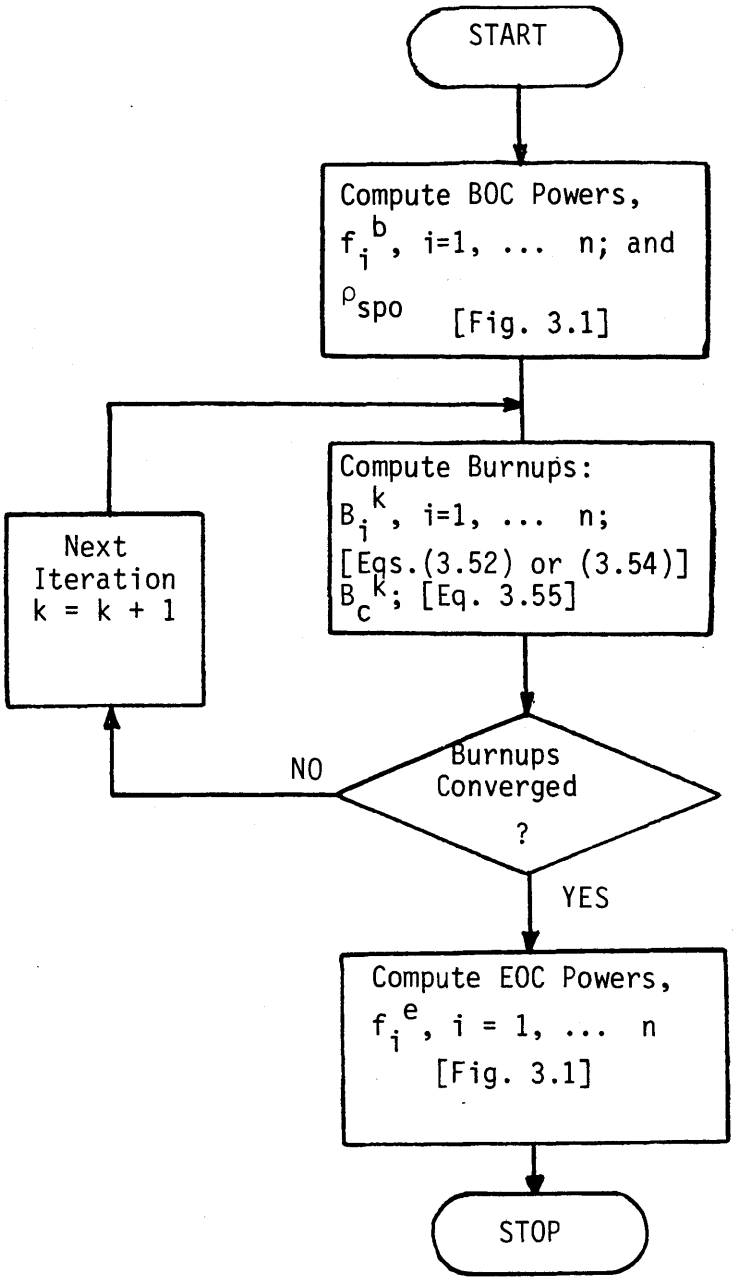

Fig. 3.3 Computational Flowchart for Integrated Burnup Method

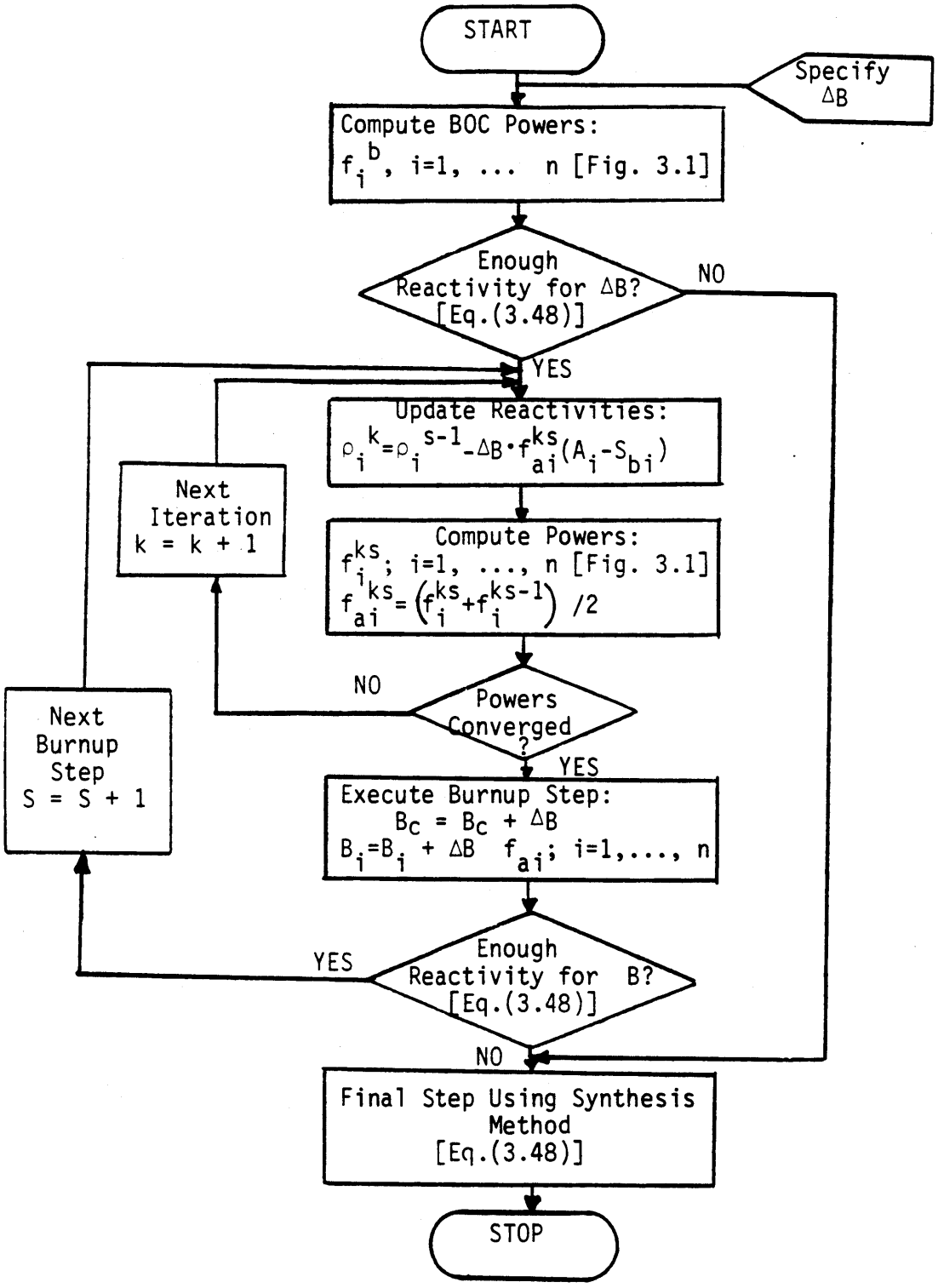

Fig. 3.4 Computational Flowchart for Step-wise Depletion Method

and the local burnup is calculated as

$$\Delta B_i = \Delta B \cdot f_{ai} \tag{3.57}$$

after the power calculation has converged for that step. At each inner iteration for power calculation, the local reactivities are updated. When not enough reactivity is available for a full step, the final step length is computed using Eq. (3.48), in the same way as in the synthesis method (with the previous step considered as the BOC calculation in the flowchart of Fig. 3.2).

The step-wise depletion method was preferred in this research for core burnup calculations due to its accuracy, flexibility and relatively high speed. Its speed results from the fact that the power fractions from one step are used as initial estimates for the next step, and therefore fewer iterations are required until convergence. Typically 15 iterations are used at BOC and 5 to 8 for the remaining steps prior to EOC. The use of several intermediate steps between BOC and EOC makes it only a little slower than the other methods (which cover the interval in a single step), but this is compensated by the flexibility and accuracy gained. Its accuracy, as compared to state-of-the-art results is discussed in the next section.

3.5 Accuracy: A Comparison with State-of-the-art Results

The accuracy of the three methods* just described has been tested against licensing-quality calculations for the Maine Yankee reactor core. Here selected results from the step-wise depletion method are compared to LEOPARD/PDQ-7 calculations for the Maine Yankee cycle 6 core [H-8]. The core loading and BOC fuel characteristics are shown in Fig. 3.5. From this information the input data for the LRM-Nodal program have been computed and are reproduced in Table 3.5. It should be noted that these data are independent best estimate values generated by the author using EPRI-LEOPARD (MIT's version) correlations (and CASMO results for BP related information). The analytically estimated coupling coefficients and leakage constants, displayed in Table 3.4, without empirical adjustments to optimize the match between MIT and Yankee results, have been used in the calculations.

Before comparing the results, the different definitions used for assembly average power have to be clarified: Yankee's LEOPARD/PDQ-7 results represent power per unit of fuel mass (or equivalently, average pin powers in the assembly). The LRM-Nodal results are power per unit of volume. Hence an inconsistency exists (consistent underprediction by LRM-Nodal), since the burnable-poisoned assemblies have fewer fuel pins (and consequently less mass, in kg, as follows: E-16: 353.4; I-0: 388.7; I-4: 379.9; J-0 and K-0: 381.1; J-4 and K-4: 372.5; J-8 and K-8: 363.8). As shown in Figs. 3.6 through 3.10, the

(*) For relative merits of each method, see sections 3.4.1, 3.4.2 and 3.4.3

	1	2	3	4	5	6	7	8	9
1	E16 4 17,697	J0 5 7,612	I4 6 25,332	J0 7 7,612	I0 8 22,223	J8 9 13,913	I0 10 22,223	K8 3 -	K0 1 -
2	J0 5 7,612	I0 11 19,936	J0 12 10,193	I4 13 25,830	J0 14 8,743	I4 15 24,432	K8 3 -	I0 16 23,980	K0 1 -
3	J4 6 25,332	J0 12 10,193	I4 17 23,552	J0 18 12,394	I0 19 19,337	J0 20 7,343	J8 21 12,098	K0 1 -	
4	J0 7 7,612	I4 13 25,830	J0 18 12,394	J4 22 13,411	J0 23 9,930	I0 24 20,678	I0 25 20,364	K0 1 -	
5	I0 8 22,223	J0 14 8,743	I0 19 19,337	J0 23 9,930	I0 26 18,920	J8 27 14,488	K8 3 -	K0 1 -	
6	J8 9 13,913	I4 15 24,432	J0 20 7,343	I0 24 20,678	J8 27 14,488	K4 2 -	K0 1 -		
7	I0 10 22,223	K8 3 -	J8 21 12,098	I0 25 20,364	K8 3 -	K0 1 -			
8	K8 3 -	I0 16 23,980	K0 1 -	K0 1 -	K0 1 -				
9	K0 1 -	K0 1 -							

.....Fuel/Shim Type (see Note) and Fuel Type Number (Table 3.5)
.....Burnup at BOC KWD/kg

Note: a) Initial Enrichments:
E = 2.52 w/o; I = 3.03 w/o;
J = 3.0 w/o; K = 3.0 w/o;

b) Number of B_4C shim rods:

given by number in alphanumeric code (e.g. K-8 indicates 8 shim rods).

Fig. 3.5 Maine Yankee Cycle 6 Core Loading and Fuel Characteristics at BOC

TABLE 3.5

Quarter-Core BOC Estimated Data for Maine Yankee Cycle 6

Assembly Type Number	Number of Assemblies	BOC Reactivity, ρ_o	Slope, A (kg/KWD)	BP Reactivity Decrement, ρ_{bo}	BP Slope, S_b (kg/KWD)
1	12	0.221973	9.0538E-06	0	0
2	1	0.221973	9.0538E-06	0.045	2.8125E-06
3	5	0.221973	9.0538E-06	0.080	5.0E-06
20	2	0.155491	9.0538E-06	0	0
5	1	0.153055	9.0538E-06	0	0
7	1	0.153055	9.0538E-06	0	0
14	2	0.142816	9.0538E-06	0	0
23	2	0.132068	9.0538E-06	0	0
12	2	0.129688	9.0538E-06	0	0
21	2	0.11244	9.0538E-06	0	0
18	2	0.10976	9.0538E-06	0	0
22	1	0.100552	9.0538E-06	0	0
9	1	0.0960075	9.0538E-06	0	0
27	2	0.0908015	9.0538E-06	0	0
26	1	0.0520786	9.10256E-06	0	0
19	2	0.0482828	9.10226E-06	0	0
11	1	0.0428304	9.10256E-06	0	0
25	2	0.0389345	9.10256E-06	0	0
24	2	0.0360762	9.10256E-06	0	0
4	1	0.0223811	9.8815E-06	0	0
8	1	0.0220128	9.10256E-06	0	0
10	1	0.0220128	9.10256E-06	0	0
17	1	0.0099155	9.10256E-06	0	0
15	2	0.00190525	9.0538E-06	0	0
16	2	-0.0061966	9.10256E-06	0	0
6	1	-0.0062870	9.10256E-06	0	0
13	2	-0.0108201	9.10256E-06	0	0

	1	2	3	4	5	6	7	8	9
1	E16 4 1.0431 1.050 0.6	J0 5 1.1882 1.230 3.5	I4 6 0.9530 0.9311 -2.3	J0 7 1.1329 1.137 0.36	I0 8 0.9698 0.9606 -0.9	J8 9 1.0391 1.000 -3.7	I0 10 0.9169 0.9293 1.3	K8 3 1.0124 1.007 -0.5	K0 1 0.7454 0.8396 12.6
2	J0 5 1.1819 1.230 4.1	I0 11 1.0248 1.042 1.6	J0 12 1.0986 1.098 -0.05	I4 13 0.9424 0.9123 -3.2	J0 14 1.1584 1.151 -0.6	I4 15 0.9863 0.9415 -4.0	K8 3 1.1512 1.144 -0.6	I0 16 0.8316 0.8124 -2.3	K0 1 0.5860 0.6440 9.9
3	I4 6 0.9479 0.9313 -1.7	J0 12 1.0950 1.098 0.3	I4 17 0.9683 0.9394 -3.0	J0 18 1.1300 1.111 -1.7	I0 19 1.132 1.078 -4.7	J0 20 1.2575* 1.253 * -0.3	J8 21 1.1554 1.163 0.6	K0 1 1.0385 1.159 11.6	
4	J0 7 1.1320 1.138 0.5	I4 13 0.9428 0.9122 -3.2	J0 18 1.1303 1.112 -1.6	J4 22 1.2226 1.186 3.0	J0 23 1.2518 1.211 -3.2	I0 24 1.0439 0.9869 -5.4	I0 25 0.9429 0.9116 -3.3	K0 1 0.8663 0.9607 10.9	
5	I0 8 0.9712 0.9618 -1.0	J0 14 1.1607 1.151 -0.8	I0 19 1.1157 1.078 -3.4	J0 23 1.2550 1.210 -3.6	I0 26 1.0953 1.030 -5.9	J8 27 1.0854 1.017 -6.3	K8 3 0.9845 0.9506 -3.4	K0 1 0.6015 0.6707 11.5	
6	J8 9 1.0413 1.003 -3.7	I4 15 0.9891 0.9468 -4.2	J0 20 1.2619* 1.256* -0.5	I0 24 1.0483 0.9870 -5.8	J8 27 1.0883 1.022 -6.1	K4 2 1.1017 1.075 -2.4	K0 1 0.7093 0.7184 1.3		
7	I0 10 0.9190 0.9315 1.4	K8 3 1.1544 1.146 -0.7	J8 21 1.1596 1.165 0.5	I0 25 0.9467 0.9109 -3.8	K8 3 0.9871 0.9544 -3.3	K0 1 0.7102 0.7168 0.9			
8	K8 3 1.0146 1.009 -0.5	J0 16 0.8334 0.8138 -2.3	K0 1 1.0415 1.163 11.6	K0 1 0.8690 0.9615 10.6	K0 1 0.6031 0.6747 11.8				
9	K0 1 0.7469 0.8409 12.6	K0 1 0.5873 0.6422 9.3							

.....Fuel Type: Maine Yankee/Table 3.5
.....LEOPARD/PDQ-7 (F_1)
.....LRM-NODAL (F_2)
.....% Error = 100 (F_2 - F_1)/F_1

* Indicates Peakers

Fig. 3.6 Assembly Power Comparison at 1 MWD/kg

	1	2	3	4	5	6	7	8	9
1	E16 4 0.9698 0.9989 3.0	J0 5 1.1053 1.164 5.3	I4 6 0.8981 0.894 -.5	J0 7 1.0796 1.097 1.6	I0 8 0.9454 0.9447 -0.1	J8 9 1.0464 0.9967 -4.7	I0 10 0.9606 0.9516 -0.9	K8 3 1.0792 1.049 -2.8	K0 1 0.7963 0.8764 10.1
2	J0 5 1.0998 1.165 3.8	I0 11 0.9887 0.991 1.0	J0 12 1.0352 1.052 1.6	I4 13 0.9014 0.8903 -1.2	J0 14 1.1238 1.125 0.1	I4 15 0.9864 0.9518 -3.5	K8 3 1.1975 1.175 -1.9	I0 16 0.8740 0.8449 -3.3	K0 1 0.6226 0.6637 6.6
3	I4 6 0.8936 0.8976 0.4	J0 12 1.0320 1.052 1.9	I4 17 0.9200 0.9101 -1.1	J0 18 1.0801 1.075 -0.5	I0 19 1.0792 1.055 -2.2	J0 20 1.2453* 1.236* -0.7	J8 21 1.1833 1.172 -0.9	K0 1 1.0786 1.178 9.2	
4	J0 7 1.0785 1.098 1.8	I4 13 0.9012 0.8897 -1.3	J0 18 1.0802 1.076 -0.4	J4 22 1.1758 1.158 -2.3	J0 23 1.2167 1.187 -2.5	I0 24 1.0407 0.9895 -4.9	I0 25 0.9648 0.9227 -4.3	K0 1 0.8994 0.9847 9.4	
5	I0 8 0.9462 0.9461 -0.001	J0 14 1.1255 1.124 -0.13	I0 19 1.0811 1.056 -2.3	J0 23 1.2194 1.184 -2.9	I0 26 1.0840 1.026 -5.3	J8 27 1.1011 1.029 -6.5	K8 3 1.0258 0.9849 -4.0	K0 1 0.6298 0.6924 9.9	
6	J8 9 1.0478 0.993 -4.6	I4 15 0.9883 0.9505 -3.8	J0 20 1.2487* 1.238* -0.8	I0 24 1.0444 0.9895 -5.2	J8 27 1.1035 1.031 -6.5	K4 2 1.1378 1.113 -2.2	K0 1 0.7395 0.7428 0.4		
7	I0 10 0.9518 0.9542 0.2	K8 3 1.1996 1.174 -2.1	J8 21 1.1866 1.174 -1.1	I0 25 0.9679 0.9239 -4.5	K8 3 1.0279 0.9878 -3.9	K0 1 0.7402 0.7428 0.3			
8	K8 3 1.0810 1.051 -2.7	J0 16 0.8750 0.8451 -3.4	K0 1 1.0816 1.177 8.8	K0 1 0.9013 0.9868 9.5	K0 1 0.6311 0.6938 9.9				
9	K0 1 0.7971 0.8786 10.2	K0 1 0.6234 0.6695 7.4							

.....Fuel Type: Maine Yankee/Table 3.5
.....LEOPARD/PDQ-7 (F_1)
.....LRM-NODAL (F_2)
.....% Error = 100 (F_2 - F_1)/F_1

*Indicates Peakers

Fig. 3.7 Assembly Power Comparison at 2 MWD/kg

	1	2	3	4	5	6	7	8	9
1	E16 4 0.9149 0.9286 1.5	J0 5 1.0396 1.086 4.4	I4 6 0.8565 0.8502 -0.7	J0 7 1.0333 1.049 1.5	I0 8 0.9254 0.9180 -0.8	J8 9 1.0591 0.9965 -5.9	I0 10 0.9934 0.9851 -0.8	K8 3 1.1646 1.126 -3.3	K0 1 0.8542 0.9326 9.1
2	J0 5 1.0348 1.086 4.9	I0 11 0.9082 0.9380 3.3	J0 12 0.9834 0.9975 1.4	I4 13 0.8672 0.8531 -1.6	J0 14 1.0878 1.089 0.1	I4 15 0.9875 0.9469 -4.1	K8 3 1.2546* 1.223* -2.5	I0 16 0.9213 0.8835 -4.1	K0 1 0.6642 0.7058 6.2
3	I4 6 0.8526 0.8502 -0.2	J0 12 0.9807 0.9974 1.7	I4 17 0.8793 0.8671 -1.4	J0 18 1.0287 1.028 -0.07	I0 19 1.0383 1.017 -2.0	J0 20 1.2201 1.210 -0.8	J8 21 1.2032 1.176 -2.3	K0 1 1.1105 1.195 7.6	
4	J0 7 1.0322 1.049 1.6	I4 13 0.8672 0.8524 -1.7	J0 18 1.0286 1.028 -0.06	J4 22 1.1185 1.105 -1.2	J0 23 1.1665 1.147 -1.7	I0 24 1.0285 0.9820 -4.5	I0 25 0.9811 0.9424 -3.9	K0 1 0.9249 1.007 8.8	
5	I0 8 0.9256 0.9190 -0.7	J0 14 1.0886 1.087 -0.1	I0 19 1.0394 1.018 -2.0	J0 23 1.1684 1.145 -2.0	I0 26 1.0614 1.014 -4.4	J8 27 1.1080 1.048 -5.4	K8 3 1.0701 1.044 -2.4	K0 1 0.6599 0.7320 10.9	
6	J8 9 1.0594 0.9984 -5.7	I4 15 0.9885 0.9450 -4.4	J0 20 1.2222 1.211 -0.9	I0 24 1.0312 0.9815 -4.8	J8 27 1.1098 1.050 -5.4	K4 2 1.1691 1.162 -0.6	K0 1 0.7698 0.7898 2.6		
7	I0 10 0.9936 0.9868 -0.7	K8 3 1.2554* 1.221* -2.7	J8 21 1.2054 1.177 -2.3	I0 25 0.9830 0.9426 -4.1	K8 3 1.0713 1.047 -2.3	K0 1 0.7702 0.7888 2.4			
8	K8 3 1.1645 1.127 -3.2	J0 16 0.9213 0.8829 -4.1	K0 1 1.1112 1.193 7.4	K0 1 0.9258 1.008 8.8	K0 1 0.6605 0.7332 11.0				
9	K0 1 0.8545 0.9340 9.3	K0 1 0.6641 0.7097 6.8							

.....Fuel Type: Maine Yankee/Table 3.5
.....LEOPARD/PDQ-7 (F_1)
.....LRM-NODAL (F_2)
.....% Error = 100 (F_2 - F_1)/F_1

*Indicates Peakers

Fig. 3.8 Assembly Power Comparison at 4 MWD/kg

	1	2	3	4	5	6	7	8	9
1	E16 4 0.9232 0.8900 -3.6	J0 5 1.0422 1.042 -0.01	I4 6 0.8625 0.8249 -4.4	J0 7 1.0298 1.018 -1.1	I0 8 0.9253 0.9006 -2.6	J8 9 1.0672 0.9951 -6.7	I0 10 1.0156 1.009 -0.6	K8 3 1.2086 1.186 -1.9	K0 1 0.8746 0.9696 10.8
2	J0 5 1.0380 1.042 0.4	I0 11 0.9139 0.9052 -0.9	J0 12 0.9842 0.9663 -1.8	I4 13 0.8670 0.8315 -4.1	J0 14 1.0755 1.062 -1.3	I4 15 0.9885 0.9429 -4.6	K8 3 1.2836* 1.262* -1.7	I0 16 0.9379 0.9103 -2.9	K0 1 0.6779 0.7340 8.2
3	I4 6 0.8590 0.8248 -4.0	J0 12 0.9817 0.9662 -1.1	I4 17 0.8788 0.8419 -4.2	J0 18 1.0137 0.9958 -1.7	I0 19 1.0187 0.9890 -2.9	J0 20 1.1958 1.183 -1.1	J8 21 1.1941 1.170 -2.0	K0 1 1.1030 1.1955 8.4	
4	J0 7 1.0288 1.019 -0.9	I4 13 0.8670 0.8307 -4.2	J0 18 1.0135 0.9962 -1.7	J4 22 1.0909 1.066 -2.3	J0 23 1.1349 1.115 -1.7	I0 24 1.0148 0.9731 -4.1	I0 25 0.9785 0.9527 -2.6	K0 1 0.9222 1.017 10.3	
5	I0 8 0.9253 0.915 -1.1	J0 14 1.0761 1.061 -1.4	I0 19 1.0195 0.9897 -2.9	J0 23 1.1364 1.113 -2.1	I0 26 1.0432 1.002 -3.9	J8 27 1.1016 1.059 -3.8	K8 3 1.0917 1.094 0.2	K0 1 0.6716 0.7612 13.3	
6	J8 9 1.0672 0.9966 -6.6	I4 15 0.9891 0.9408 -4.8	J0 20 1.1972 1.184 -1.1	I0 24 1.0170 0.9725 -4.4	J8 27 1.1030 1.061 -3.8	K4 2 1.1776 1.200 1.9	K0 1 0.7818 0.8265 5.7		
7	I0 10 1.0155 1.011 -0.4	K8 3 1.2840* 1.259* -1.9	J8 21 1.1959 1.171 -2.1	I0 25 0.9799 0.9524 -2.8	K8 3 1.0926 1.096 0.3	K0 1 0.7820 0.8250 5.5			
8	K8 3 1.2081 1.187 -1.7	J0 16 0.9376 0.9091 -3.0	K0 1 1.1033 1.193 8.1	K0 1 0.9226 1.018 10.3	K0 1 0.6719 0.7621 13.4				
9	K0 1 0.8741 0.9705 11.0	K0 1 0.6777 0.7372 8.7							

.....Fuel Type: Maine Yankee/Table 3.5
.....LEOPARD/PDQ-7 (F_1)
.....LRM-NODAL (F_2)
.....% Error = 100 (F_2 - F_1)/F_1

*Indicates Peakers

Fig. 3.9 Assembly Power Comparisons at 6 MWD/kg

	1	2	3	4	5	6	7	8	9
1	E16 4 0.9076 0.8677 -4.4	J0 5 1.0223 1.016 -0.6	I4 6 0.8530 0.8112 -4.5	J0 7 1.0146 0.9992 -1.5	I0 8 0.9196 0.8886 -3.3	J8 9 1.0714 0.9931 -7.3	I0 10 1.0425 1.028 -1.4	K8 3 1.2645 1.236 -2.2	K0 1 0.8980 0.9938 10.6
2	J0 5 1.0186 1.016 -.3	I0 11 0.9014 0.8869 -1.6	J0 12 0.9894 0.9481 -4.1	I4 13 0.8576 0.8183 -4.6	J0 14 1.0592 1.043 -1.5	I4 15 0.9894 0.9395 -5.0	K8 3 1.3207* 1.294* -2.0	I0 16 0.9604 0.9292 -3.2	K0 1 0.6941 0.7535 8.5
3	I4 6 0.8499 0.8112 -4.5	J0 12 0.9672 0.9481 -2.0	I4 17 0.8675 0.8269 -4.6	J0 18 0.9930 0.9728 -2.0	I0 19 0.9989 0.9663 -3.3	J0 20 1.175 1.159 -1.4	J8 21 1.1865 1.161 -2.1	K0 1 1.1006 1.187 7.8	
4	J0 7 1.0136 0.9994 -1.4	I4 13 0.8576 0.8176 -4.7	J0 18 0.9927 0.9731 -2.0	J4 22 1.0617 1.037 -2.3	J0 23 1.1068 1.088 -1.7	I0 24 1.0048 0.9641 -4.0	I0 25 0.9806 0.9582 -2.3	K0 1 0.9236 1.020 10.4	
5	I0 8 0.9193 0.8895 -3.2	J0 14 1.0596 1.041 -1.7	I0 19 0.9994 0.9670 -0.06	J0 23 1.1080 1.086 0.6	I0 26 1.0288 0.9915 -0.4	J8 27 1.0993 1.065 -3.1	K8 3 1.1226 1.139 1.4	K0 1 0.6869 0.7842 14.0	
6	J8 9 1.0711 0.9946 -7.1	I4 15 0.9896 0.9374 -5.2	J0 20 1.1759 1.160 -1.4	I0 24 1.0066 0.9634 -4.3	J8 27 1.1003 1.068 -2.9	K4 2 1.1946 1.230 2.9	K0 1 0.7988 0.8561 7.1		
7	I0 10 1.0421 1.029 -1.3	K8 3 1.3207* 1.292* -2.2	J8 21 1.1876 1.161 -2.2	I0 25 0.9815 0.9577 -2.4	K8 3 1.1231 1.140 1.5	K0 1 0.7989 0.8545 6.9			
8	K8 3 1.2638 1.236 -2.2	J0 16 0.9598 0.9279 -3.3	K0 1 1.1004 1.185 7.7	K0 1 0.9236 1.020 10.4	K0 1 0.6870 0.7848 14.2				
9	K0 1 0.8979 0.9945 10.7	K0 1 0.6937 0.7565 9.0							

.....Fuel Type: Maine Yankee/Table 3.5
.....LEOPARD/PDQ-7 (F_1)
.....LRM-NODAL (F_2)
.....% Error = 100 (F_2 - F_1)/F_1

*Indicates Peakers

Fig. 3.10 Assembly Power Comparison at 8 MWD/kg

LRM-Nodal program has generated core power maps having the following general characteristics when compared to Yankee's reference licensing calculations:

- For interior assemblies there is good agreement; only in a few assemblies is the error in excess of 5%. Moreover, most of the larger "errors" are due to the aforementioned difference in computational conventions: if the corrections for the mass differences (about 4% for J-8 assemblies and 2% for J-4 assemblies) are considered, the agreement is even better, and the maximum real error is well below 5%;
- For the periphery, the LRM-Nodal program always overpredicts the power, thus confirming the expectation that empirical adjustment of the peripheral constants is advisable, as is common practice for nodal codes of this kind;
- The program consistently identified the assemblies having the highest power (i.e. "peakers"), an important feature for its intended applications.

In addition to the inherent simplicity of the model and the already stressed fact that no empirical adjustment of coefficients has been made, the major sources of inaccuracy (hence, potential improvements) may be related to:

- the absence of a correction for differential boron worth;
- the omission of residual BP reactivity for the old fuel assemblies;

- the omission of a differential thermal leakage correction;
- neither axial leakage nor its variation with burnup have been taken into consideration;
- the isobuckling approximation has been used;
- and, most importantly, the LRM parameters used to represent the core have been generated independently, and are therefore not necessarily completely compatible with those used to generate the reference PDQ-7 core maps.

The value for the cycle burnup predicted by the LRM-Nodal program of 9,539.14 KWD/kg is lower than the full-power EOC burnup (without coastdown) actually achieved during Maine Yankee's cycle 6, of about 10,700 KWD/kg. Factors that explain this discrepancy are:

- the parameters of Fig. 3.5 and Table 3.5 were computed assuming a core exposure of 11,000 KWD/MT for cycle 5, but the actual cycle 5 length was 10,796 KWD/kg [D-4];
- the high residual BP reactivity still present at the EOC predicted by the LRM-Nodal program;
- and, most importantly, apart from the use of unadjusted leakage constants, the computation of the reactivity versus burnup slopes, A (kg/KWD),at MIT using slightly different input data (cell parameters) and burnup steps than at Yankee, with different LEOPARD program and cross-section library versions; (A test computation using an arbitrary reduction of about 10% in the values of A yielded a cycle burnup matching almost exactly the reference value logged by Maine Yankee).

The results shown (average absolute error in interior assembly powers of approximately 3%) may be regarded as well within the range of acceptability for iterative core reload optimization and preliminary scoping studies, for which the present methodology is intended. The discrepancy between the absolute values of the cycle burnups is irrelevant, since only relative differences between core arrangements are of interest here. Moreover, a slight adjustment in the slopes, A, of the reactivity versus burnup curves introduces an adequate correction, if required. (It is noteworthy that a state-of-the-art core analysis system (CASMO/SIMULATE) incurs an uncertainty in cycle length prediction of $\pm$ 200 KW/kg [D-4].)

Even though, as will be seen in the next chapter, the larger than average discrepancies between the peripheral powers (average absolute error of approximately 8%) does not affect the usefulness of the program for core loading pattern optimization purposes, as an illustration of the improvements available to future users, empirical adjustments have been used to generate the results shown in Fig. 3.11. These results correspond to a cycle burnup of 1 MWD/Kg, hence they should be compared to those of Fig. 3.6. As can be seen a significant reduction in the discrepancies is possible through empirical adjustment of the leakage constants (ρ_{Li}, which is equivalent to adjusting albedo in other nodal methods). The average absolute error in the peripheral assembly powers is reduced to approximately 5% (from the unadjusted value of $\sim$8%); furthermore, no attempt has been made to continue with systematic adjustment to minimize some measure of the error. Further improvement

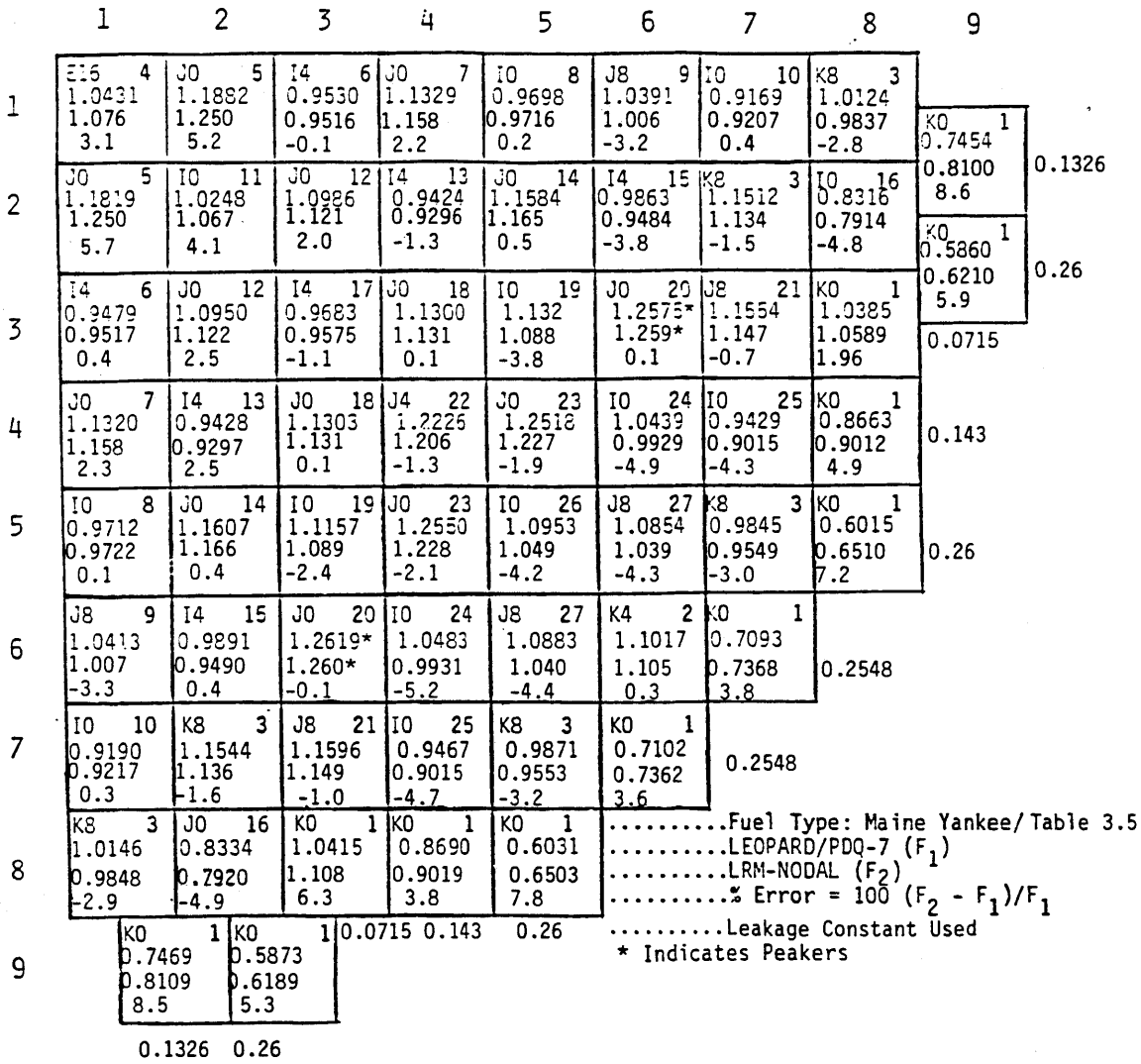

Fig. 3.11 Assembly Power Comparison at 1 MWD/kg, Using Adjusted Leakage Parameters

may also be achieved by adjusting the peripheral coupling coefficients, θ_p. It should also be noted that the interior assembly errors remain about the same as before.

The power fraction comparisons of Figs. 3.6 through 3.10 cover virtually the entire cycle length. No comparison has been shown at precisely zero burnup, since the LRM does not account for transient xenon and samarium, as discussed in section 2.3.3.

3.6 Chapter Summary

In this chapter nodal power equations have been derived from the firm foundation provided by a two-dimensional analytical solution of the one-and-one-half group equation (as documented in Appendix B). Possible corrections to make up for analytical and modeling deficiencies have been discussed. Finally, a core burnup calculation capability has been developed from the nodal power equations and the linear reactivity model (as embodied in the microcomputer code LRM-NODAL - see Appendix D), and evaluated against state-of-the-art results. The overall suitability of the model for its intended use, loading pattern and reload composition optimization - the subject of the next chapter, is inferred on the basis of this comparison (which was preceded by numerous other test runs on these and other core maps in the course of method and program development).

CHAPTER 4

OPTIMIZATION METHODOLOGY

4.1 Introduction

The theory and practice of optimization have experienced a rapid development over the last several decades, particularly after the advent of electronic computers, which allowed the combination of the well-established methods of differential calculus and the calculus of variations with mathematical programming techniques.

Linear Programming techniques (e.g. the simplex method, introduced in the 1940s [D-5], [G-7]), have been, and still continue to be, widely used in almost all fields. Nonlinear optimization methods came into prominence with the extension of the classical Lagrange multiplier method to problems with inequality constraints by Kuhn and Tucker in 1951. Techniques to solve the problem of the optimal control of dynamical systems became available with the advent of dynamic programming (Bellman, 1957) and the introduction of the maximum principle by Pontryagin (1958). Despite being formally different, both are closely related to the calculus of variations and to each other. Direct search methods, involving evaluation and comparison

of functions, and gradient methods, requiring the evaluation of the function and its derivatives, have both been used, and are still undergoing development, to solve general (constrained) nonlinear optimization problems. Significant progress has also been achieved in discrete optimization, for example through integer programming techniques and graph theory. Table 1.2 surveys the variety of approaches employed in core reload optimization work: as can be seen almost all methods referred to in this paragraph have been applied to this problem.

The choice of the best optimization technique is not obvious. One fundamental consideration is the nature of the mathematical model describing the problem; but, even so, for any case alternative methods may be formulated, with varying degrees of accuracy and efficiency. The objective, in general, is the development of efficient, reliable and accurate algorithms. In this chapter an optimization methodology is pursued, exploiting the potentials of analytical simplicity and transparency provided by the core model formulated in this research. Evaluations and applications will be carried out as allowed by the computational facility used in the research: a TRS-8, Model III, 48 K bytes microcomputer. Far from being exhaustive, the developments and, especially, the applications described here should be regarded as the first step toward formulation of a systematic and consistent methodology for automated optimization of core reload patterns and compositions, taking advantage of the

inherently favorable features, for optimization purposes, of the LRM-based core model and the auxiliary routines developed in this chapter.

In the next section the optimality criterion will be discussed. Then, in the remainder of the chapter, the approaches explored in this research, along with some applications, will be presented.

4.2 Optimality Criterion

Usually the optimality criterion is expressed as an objective function or functional, and, in the case of a generalized (constrained) problem, the constraints are expressed as equality or/and inequality functions.

In this work, for all applications, the objective is the maximization of the cycle burnup, and the ability to incorporate constraints an overriding concern. In the algorithms that will be formulated, only restrictions on power peaking have been explicitly considered, even though extensions to intra-assembly power peaking limits and assembly burnup restrictions, as well as others, are feasible.

The mathematical representation of the objective function and the constraints will be formulated in the following sections, during the development of the theoretical basis, and the routines and algorithms supporting and embodying the optimization method.

4.3 The Optimization Method

As will be illustrated later, the optimal solution (for the core configuration, BP loading and composition) is essentially determined by the EOC core condition, thus depending on the BOC configuration and the power history leading from BOC to EOC, which in turn is dependent on the criticality control strategy. Hence, strictly speaking, this constitutes a problem of the optimal control of a dynamical system, suitable for the application of optimal control theory (Pontryagin's maximum principle) or dynamic programming formalisms. However, due to the BP model (as well as soluble boron control system characteristics) adopted in this research, once the BOC configuration (assembly arrangement) and composition (fuel enrichment and BP loading) are determined a unique burnup history, hence EOC condition is also defined. For this reason, the entire optimization problem reduces to the search for the maximum cycle burnup as a function of BOC configuration and composition.

According to the classical theory for unconstrained optima (e.g. refs. [B-4] and [W-3]) given a function $f(x)$, where $x = (x_1 \ldots x_n)$,

for which all the first partial derivatives, $\frac{\partial f}{\partial x_i}$, i=1,...,n, exist at all points, a necessary condition for a maximum of f(x) is that,

$$\frac{\partial f}{\partial x_i} = \frac{\partial f}{\partial x_2} = \ldots \quad \frac{\partial f}{\partial x_n} = 0 \tag{4.1}$$

A sufficient condition for a point satisfying these equations to be a maximum is that all of the second partial derivatives, $\frac{\partial^2 f}{\partial x_j \, \partial x_k}$ (j, k=1, ..., n) exist at all points and that $D_i < 0$ for i=1, ..., n, where

$$D_i = \begin{vmatrix} \frac{\partial^2 f}{\partial x_1^2} & \frac{\partial^2 f}{\partial x_1 \, x_2} & \ldots & \frac{\partial^2 f}{\partial x_1 \, \partial x_i} \\ \vdots & & & \\ \frac{\partial^2 f}{\partial x_i \, \partial x_1} & & & \frac{\partial^2 f}{\partial x_i^2} \end{vmatrix} \tag{4.2}$$

i.e. all the principal minors of the matrix of second partial derivatives must be negative.

For constrained optima the classical theoretical approach is the method of Lagrangian multipliers, which states that, with certain qualifications, the maximum of a function f(x), subject to equality constraints,

$$c_j(x_1, \ldots, x_n) = b_j \quad \text{for } j = 1, 2, \ldots, s \tag{4.3}$$

is found to be the stationary points of the Lagrangian form

$$\Phi(x, \lambda) = f(x) + \sum_{j=1}^{s} \lambda_j \, c_j \, (x) \tag{4.4}$$

where $\lambda = (\lambda_1, \ldots, \lambda_s)$ are the Lagrange multipliers.

Inequality constraints may be transformed into equalities by introducing appropriate slack variables. The solution, when the first partial derivatives of f(x) and c(x) exist, is equivalent to finding an unconstrained solution for x and λ of the set of equations:

$$c_j(x_1, \ldots, x_n) - b_j = 0 \quad \text{for } j = 1, 2, \ldots, s \tag{4.5}$$

and

$$\frac{\partial f}{\partial x_i} + \sum_{j=1}^{s} \lambda_j \frac{\partial c_j}{\partial x_j} = 0 \quad \text{for } i - 1, 2, \ldots, n \tag{4.6}$$

The important contribution of Kuhn-Tucker [K-6] was to extend this classical method to incorporate inequality constraints in a direct manner, deriving the necessary conditions for local optima (and, for certain special cases, necessary and sufficient conditions for a global optimum) for the general constrained nonlinear problem. In essence, when suitable conditions are placed on the function f(x) and the m inequality constraints $g_i(x) \geq 0$ of the Lagrangian form

$$\Phi(x,\lambda) = f(x) + \sum_{i-1}^{m} \lambda_i \, g_i \, (x) \quad , \tag{4.7}$$

the constrained extremum of f(x) corresponds to a saddle point of $\Phi(x,\lambda)$. In this formulation, equality constraints may be treated as a pair of inequalities.

With few exceptions (as for example, the quadratic programming schemes), nonlinear methods are accessible only to numerical solution approaches. A wide range of general schemes, with varying degrees of efficiency, are available (as described, for example in references

[W-3], [W-4], [B-4], [A-1]) to perform such tasks. Usually, however, the goals of efficiency and accuracy are better served with the development of methods tailored to the specific features of the particular nonlinear problem at hand. The demonstration or verification of the fulfilment of the necessary and sufficient conditions for the existence of the global optimum for complex problems (such as the one at hand) is normally either impractical or too costly. In such cases usually one attempts to demonstrate the satisfaction (or quasi-satisfaction) of the necessary condition (that the first derivatives are zero) and, when local optima may occur, tries to distinguish these from the global optimum by carrying out searches starting at different initial conditions.

In the following sections the basis for the optimizing algorithms will be developed, exploring the features of the core model, in which similar equations and routines, with minor modifications, may be used to represent changes in local reactivity, corresponding to assembly shuffles, to changes in enrichment or to the addition of BPs. Furthermore, the partial derivatives computed by such routines, beyond indicating closeness to optimality, are a fundamental constituent of the gradient method which will be formulated, as well as other approaches such as the sensitivity theory approach, which is also explored here.

4.3.1 A Gradient Method

The basic reason for using the gradient direction in an iterative search for optima may be explained using the classical Lagrange multiplier method. At any point x the direction of the gradient is the direction whose components are proportional to the first partial derivatives of the objective function at the point in question. To first order approximation, the change in the objective function due to small perturbations in the components $(\delta x_1, \ldots, \delta x_n)$, will be given by

$$df = \sum_{j=1}^{n} \frac{\partial f}{\partial x_j} \delta x_j \tag{4.8}$$

where the derivatives are evaluated at the current point $x=(x_1,\ldots,x_n)$. The greatest change in the objective function due to a perturbation $\Delta = \left[\sum_{j=1}^{n} \delta x_j^2 \right]^{\frac{1}{2}}$ from the current point x may be evaluated using the Lagrangian form

$$\Phi(x,\lambda) = df + \lambda\left(\sum_{j=1}^{n} \delta x_j^2 - \Delta^2\right) \tag{4.9}$$

or

$$\Phi(x,\lambda) = \sum_{j=1}^{n} \frac{\partial f}{\partial x_j} \delta x_j + \lambda\left(\sum_{j=1}^{n} \delta x_j^2 - \Delta^2\right) \tag{4.10}$$

Differentiating with respect to δx_j, and requiring it to vanish, Eq. (4.10) yields:

$$\frac{\partial f}{\partial x_j} + 2\,\lambda\,\delta x_j = 0,\ j=1,\ 2,\ \ldots,\ n \tag{4.11}$$

Equation (4.11) may be re-arranged to become:

$$\frac{\delta x_1}{\frac{\partial f}{\partial x_1}} = \frac{\delta x_2}{\frac{\partial f}{\partial x_2}} = \ldots = \frac{\delta x_n}{\frac{\partial f}{\partial x_n}} \tag{4.12}$$

Hence, the greatest change in the function f(x) occurs when the δx_i are chosen to be proportional to the corresponding $\frac{\partial f}{\partial x_i}$.

The derivatives can be obtained either analytically or numerically (using some finite difference scheme). Experience, however, has shown that, with few exceptions, numerical differentiation leads to inferior results [B-4]. Therefore, in the following sections, a direct analytical approach to compute the derivatives, taking into account the specific features of the core model and of the optimization problem, will be formulated.

4.3.2 The Computation of the Derivatives

Two methods to compute the conventional partial derivative of the objective function (and of the constraints), based on the synthesis and integrated schemes for burnup calculations, described in Chapter 3, have been developed. The derivatives of the nodal powers and of the system reactivity will be formulated first, because they are constituents of the objective function derivative. Moreover, they will play an important role in the development of the algorithms to incorporate power peaking restrictions and to optimize compositions.

As a point of interest it is noted that an alternative method to compute the derivatives, similar to that developed to compute sensitivity coefficients, (e.g. at ORNL by Oblow, Williams, Weisbin, [O-1], [O-2], [W-5], [W-6], [L-4]) is worth pursuing. In this approach through an appropriate adjoint formulation, which is independent of the "forward" problem solution, the partial derivatives may be computed directly from the adjoint results and from the "forward" solution. Hence, for each parameter in a given configuration, only one adjoint solution has to be computed and may be stored for future use. This approach has not been fully pursued in the present work, in part because of limited data storage capacity of the computer system used. However in section 4.3.3 another aspect of the sensitivity theory approach, namely, the use of the logarithmic derivatives will be explored.

4.3.2.1 Nodal Power Derivative Calculations

The nodal power equations of Table 3.3 may be re-written as follows:

for interior nodes:

$$f_i = \frac{\frac{1}{N_p} \sum_{j=1}^{N_p} f_j \left[1-\theta_s(\rho_{oj} - A_j B_j + \rho_{boj} - S_{bj} B_j - \rho_{sp} W_j)\right]}{1 - \theta(\rho_{oi} - A_i B_i - \rho_{boi} + S_{bi} B_i - \rho_{sp} W_i)} \qquad (4.13)$$

and for peripheral nodes:

$$f_i = \frac{\frac{1}{N_p} \sum f_j[1-\theta_s(\rho_{oj} - A_j B_j + \rho_{boj} - S_{bj} B_j - \rho_{sp} W_j)]}{1 - \theta_p (\rho_{oi} - A_i B_i - \rho_{boi} + S_{boi} B_i - \rho_{sp} W_i) + \theta_L \rho_{Li}}$$

where, according to Eq. (3.44) (4.14)

$$\rho_{sp} = \frac{\sum_{i=1}^{n} f_i(\rho_{oi} - A_i B_i - \rho_{boi} + S_{bi} B_i) - \sum_{i=1}^{m} f_i \rho_{Li}}{\sum_{i=1}^{n} f_i W_i} \qquad (4.15)$$

and subject to the normalization condition adopted in this work:

$$\sum_{i=1}^{n} f_i = n \qquad (4.16)$$

where n is the number of assemblies.

Even though the derivatives could be taken generically in the prescriptions above, the cases of interest in this work are only the BOC and the EOC conditions.

4.3.2.1.1 BOC Nodal Power Derivative Calculation

At BOC the nodal burnups (B_i) are zero. Then, assuming that all W_i are equal to 1.0, taking the derivative of f_i with respect to a generic ρ_x (which may represent either ρ_{oi} or ρ_{boi}), after defining the "source terms" (origins of the change or first order perturbation, Γ_k,

$$\Gamma_k = \frac{d}{d\rho_x} (\rho_{ok} - \rho_{bok} + S_{bk} B_k) \qquad (4.17)$$

the results become:

for interior nodes:

$$\frac{\partial f_i}{\partial \rho_x} = \frac{\partial f_i \left(\Gamma_i + \frac{\partial \rho_{sp}}{\partial \rho_x}\right) - \frac{\theta_s}{N_p} \sum_{j=1}^{N_p} f_j \left(\Gamma_j - \frac{\partial \rho_{sp}}{\partial \rho_x}\right)}{1 - \theta(\rho_{oi} - \rho_{boi} - \rho_{sp})}$$

$$+ \frac{\frac{1}{N_p} \sum_{j=1}^{N_p} [1 - \theta_s(\rho_{oi} - \rho_{boi} - \rho_{sp})] \frac{\partial f_j}{\partial \rho_x}}{1 - \theta(\rho_{oi} - \rho_{boi} - \rho_{sp})} \qquad (4.18)$$

and, for peripheral nodes, ignoring the negligible value of $d\rho_{Li}/d\rho_x$:

$$\frac{\partial f_i}{\partial \rho_x} = \frac{\theta_p f_i \left(\Gamma_i - \frac{\partial \rho_{sp}}{\partial \rho_x}\right) - \frac{\theta_s}{N_p} \sum_{i=1}^{N_p} f_j \left(\Gamma_j - \frac{\partial \rho_{sp}}{\partial \rho_x}\right)}{1 - \theta_p (\rho_{oi} - \rho_{boi} - \rho_{sp}) + \theta_L \rho_{Li}}$$

$$+ \frac{\frac{1}{N_p} \sum_{i=1}^{N_p} [1 - \theta_s(\rho_{oi} - \rho_{boi} - \rho_{sp})] \frac{\partial f_j}{\partial \rho_x}}{1 - \theta_p (\rho_{oi} - \rho_{boi} - \rho_{sp}) + \theta_L \rho_{Li}} \qquad (4.19)$$

subject to the normalization condition

$$\sum_{j=1}^{n} \frac{\partial f_j}{\partial \rho_x} = 0 \qquad (4.20)$$

and where,

$$\frac{\partial \rho_{sp}}{\partial \rho_x} = \frac{1}{\sum_{j=1}^{n} f_j W_i} \left\{ f_x \Gamma_x + \sum_{j=1}^{n} (\rho_{oj} - \rho_{boj}) \frac{\partial f_j}{\partial \rho_x} - \sum_{j=1}^{m} \rho_{Lj} \frac{\partial f_j}{\partial \rho_x} \right\} \qquad (4.21)$$

where the term $\rho_{sp} \sum_{j=1}^{n} \left(W_j \frac{\partial f_j}{\partial \rho_x} + f_j \frac{dW_j}{d\rho_x} \right)$ has been ignored due to the normalization condition of Eq. (4.20) and the negligible variation of the W_is.

The terms Γ_k constitute the source of the "perturbation" (or change) being evaluated, and have to be specified according to the case being analyzed. In the case of only one assembly being "perturbed" (or equivalently, for computation of the power derivatives due to a change in the reactivity of only one assembly), designated assembly k, the term exists only when x=k, and becomes:

$$\Gamma_k = \begin{cases} 1 \text{ for a change in } \rho_{ok} \\ \\ -1 \text{ for a change in } \rho_{bok}. \end{cases} \tag{4.22}$$

Hence, for the assembly k, for example, the terms involving $\theta f_i \Gamma_i$ in Eqs. (4.18) or (4.19) would become,

$$\theta f_k \Gamma_k = \begin{cases} \theta f_k \text{ for a change in } \rho_{ok} \\ \\ -\theta f_k \text{ for a change in } \rho_{bok}, \end{cases} \tag{4.23}$$

and would be zero for all other assemblies.

Similarly, the terms involving $\frac{\theta_s}{N_p} \sum_{j=1}^{N_p} f_j \Gamma_j$ would become, for the assemblies having interfaces with assembly k:

$$\frac{\theta_s}{N_p} \sum_{j=1}^{N_p} f_j \Gamma_j = \begin{cases} \frac{\theta_s}{N_p} f_j \text{ for a change in } \rho_{ok} \\ \\ -\frac{\theta_s}{N_p} f_j \text{ for a change in } \rho_{bok}, \end{cases} \tag{4.24}$$

and would be zero for all other assemblies (those lacking interfaces with the assembly k). The case above is appropriate for describing the first order effect of the addition or subtraction of reactivity

(ρ_o or ρ_{bo}) in a node. Physically, a change in ρ_o may correspond to a change in the assembly's enrichment or to the replacement of an assembly by another; a change in ρ_{bo} corresponds to the addition (or subtraction) of burnable poison in the assembly. For example, the first order effects of the exchange of fuel assemblies may be evaluated by computing the corresponding derivatives.

The preceding mathematical development has been applied in the LRM-NODAL program; what follows in this section is a generalization of these ideas which provides valuable further insight into the nature of the optimization process, and may prove useful in extension of the the present work.

A more general case results when constraints on the reactivities are considered, as for example, the conservation of the reactivities over a certain number of assemblies or over the entire core. This more general case may be used as an artifice to evaluate, for example, the differential effects (or marginal effects) on cycle burnup, power peaking or assembly burnup distribution, of the relocation of one differential unit (or appropriately weighted differential unit) of reactivity within a given pool of assemblies. The resulting array of derivatives can be translated into changes in design variables such as enrichment or burnable poison content, by resorting to equations relating reactivity to these variables. This evaluation may be carried out by appropriately defining the source terms Γ, to be used in

Eqs. (4.18), (4.19) and (4.21). Weighting may be introduced to impose the conservation of costs, natural uranium or even particular isotopes (e.g. U-235) associated with the redistribution of the reactivities over the pool of assemblies considered. To compute these weights it should be noted that assembly reactivity is related to enrichment, as given, for example, by Eq. (2.27), and that the ratio of natural uranium to enriched fuel F/P is given by

$$\frac{F}{P} = \frac{X_P - X_W}{X_F - X_W} \quad , \tag{4.25}$$

where X_p is the fuel enrichment, X_F is the natural uranium enrichment and X_W is the enrichment plant tails assay. Hence, natural uranium requirements are related to enrichment and to reactivity via Eqs. (4.25) and (2.27), and fuel costs, in turn, are directly related to enrichment and natural uranium requirements. (As shown by Malik [M-1], separative work requirements are also, to a very good approximation, a linear function of enrichment, hence, reactivity). Once the appropriate weighting functions are selected, the Lagrange multiplier method can be used to determine the optimal source terms for the problem being analyzed. Here only the case of conservation of volume-weighted reactivity with uniform relocation (i.e. equal increments transferred from each member of the pool), will be detailed. It is required that

$$\frac{d\rho_{oi}}{d\rho_x} = \frac{d}{d\rho_x} \sum_{j=1}^{N_x} \lambda_j \rho_{oj} \quad , \tag{4.26}$$

where N_x is the number of assemblies from which reactivity is to be relocated. Since one differential unit of reactivity is being relocated,

Eq. (4.26) becomes:

$$1 = \sum_{j=1}^{N_x} \lambda_j \frac{d\rho_{oj}}{d\rho_x} \quad , \tag{4.27}$$

Hence, for uniform relocation, the source terms become:

$$\Gamma_j = - \frac{1}{N_x} \quad , \quad j = 1, \ldots , N_x \ , \tag{4.28}$$

and $$\Gamma_i = 1 \ , \tag{4.29}$$

for the assembly to which the marginal unit is being transferred.

The discussion on how to incorporate the source terms in Eq. (4.18) and (4.19), previously presented and illustrated through Eqs. (4.22), (4.23) and (4.24) applies individually to each new source term Γ_j (of course, with appropriate values considered for each case). These new source terms will affect the system reactivity derivative, which will become:

$$\frac{\partial \rho_{sp}}{\partial \rho_x} = \frac{1}{\sum_{j=1}^{n} f_i \, W_i} \left\{ \sum_{j=1}^{N_x} f_j \Gamma_j + \sum_{j=1}^{n} (\rho_{oj} - \rho_{boj}) \frac{\partial f_j}{\partial \rho_x} - \sum_{j=1}^{n} \rho_{Lj} \frac{\partial f_j}{\partial \rho_x} \right\} \tag{4.30}$$

For the special case where N_x=n (i.e.: the whole core is the pool), Eq. (4.30) becomes:

$$\frac{\partial \rho_{sp}}{\partial \rho_x} = \frac{1}{\sum_{j=1}^{n} f_j \, W_i} \left\{ f_i - 1 + \sum_{j=1}^{n} (\rho_{oi} - \rho_{boj}) \frac{\partial f_j}{\partial \rho_x} - \sum_{j=1}^{m} \rho_{Lj} \frac{\partial f_j}{\partial \rho_x} \right\} \tag{4.31}$$

Once the appropriate source terms have been defined, the solution of the system of equations is straightforward, paralleling that of the standard power distribution calculation, as shown in the flowchart of Fig. 4.1. To accelerate convergence, the node-to-node sweeping in the Gauss-Seidel iterative procedure is in a spiral pattern so as to update successively the values at the nodes equidistant from the perturbed node. As in the power calculation, since convergence proceeds monotonically, a relaxation scheme has been implemented. At each iteration, k, the value $\frac{\partial f_i^k}{\partial \rho_x}$, is recomputed as:

$$\frac{\partial f_i^{*k}}{\partial \rho_x} = \frac{\partial f_i^k}{\partial \rho_x} \left[1 + A_p \left(\frac{\partial f_i^k}{\partial \rho_x} - \frac{\partial f_i^{*k-1}}{\partial \rho_x} \right) \right] \tag{4.32}$$

where A_p is an empirical factor, found to lie between 0.3 and 0.5 for best results.

4.3.2.1.2 EOC Nodal Power Derivative Calculation

The major difference between EOC and BOC power derivative computations arises from the fact that at EOC ρ_{sp} is zero, and the burnups B_i, are not (as opposed to BOC, where ρ_{sp} is finite and assembly cycle burnup increments are zero). Additionally, as postulated in section 2.3.2.2, at EOC, $\rho_{boi} - S_{bi} B_i$ becomes $r\rho_{boi}$, where r represents the residual BP reactivity fraction. The burnup derivatives, B_i, have to be computed independently or iteratively, in tandem with the power derivatives (as will be shown later).

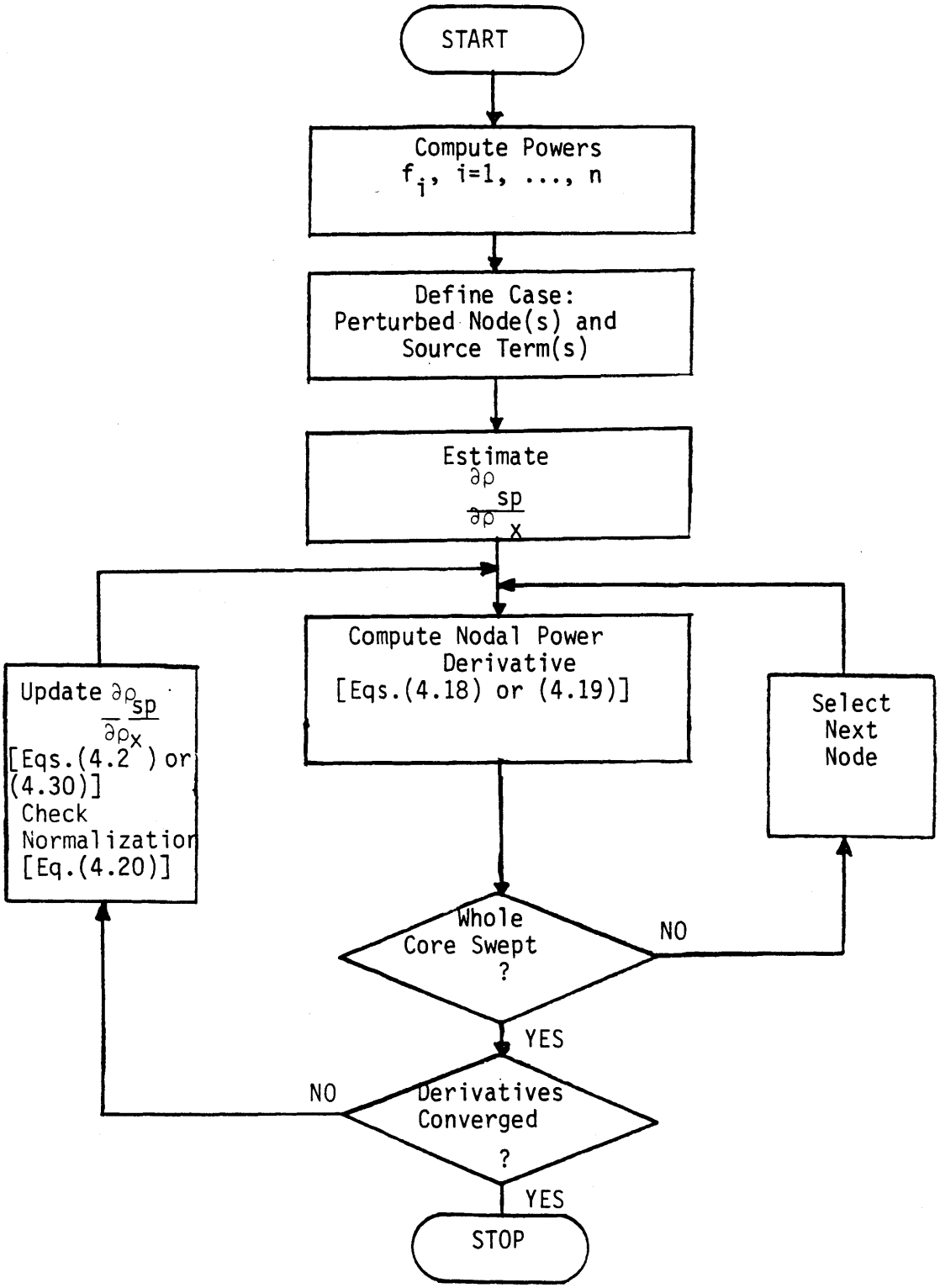

Fig. 4.1 Flowchart for Nodal Power Derivative Calculation at BOC

Assuming, for the moment, that the burnup derivatives are available, Eqs. (4.13) and (4.14) may be differentiated directly to yield:

for interior nodes:

$$\frac{\partial f_i}{\partial \rho_x} = \frac{\theta f_i \left[\Gamma_i - \frac{\partial}{\partial \rho_x}(A_i B_i)\right] - \frac{\theta_s}{N_p}\sum_{j=1}^{N_p} f_j\left[\Gamma_j - \frac{\partial}{\partial \rho_x}(A_i B_i)\right]}{1 - \theta(\rho_{oi} - r\rho_{boi} - A_i B_i)} + \frac{\frac{1}{N_p}\sum_{j=1}^{N_p}\left\{1 - \theta_s\left[\Gamma_j - \frac{\partial}{\partial \rho_x}(A_i B_i)\right]\right\}\frac{\partial f_i}{\partial \rho_x}}{1 - \theta(\rho_{oi} - r\rho_{boi} - A_i B_i)} \tag{4.33}$$

and for the peripheral nodes, again neglecting $d\rho_{Li}/d_x$:

$$\frac{\partial f_i}{\partial \rho_x} = \frac{\theta_p f_i \left[\Gamma_i - \frac{\partial}{\partial \rho_x}(A_i B_i)\right] - \frac{\theta_s}{N_p}\sum_{j=1}^{N_p} f_j\left[\Gamma_j - \frac{\partial}{\partial \rho_x}(A_i B_i)\right]}{1 - \theta_p(\rho_{oi} - r\rho_{boi} - A_i B_i) + \theta_L \rho_{Li}} + \frac{\frac{1}{N_p}\sum_{j=1}^{N_p}\left\{1 - \theta_s\left[\Gamma_j - \frac{\partial}{\partial \rho_x}(A_j B_j)\right]\right\}\frac{\partial f_j}{\partial \rho_x}}{1 - \theta_p(\rho_{oi} - r\rho_{boi} - A_i B_i) + \theta_L \rho_{Li}} \tag{4.34}$$

the above being subject to the normalization condition:

$$\sum_{j=1}^{n} \frac{\partial f_i}{\partial \rho_x} = 0 \tag{4.35}$$

The criticality condition at EOC is assured through the burnup derivatives, as will be seen later. The discussion regarding the source terms at BOC remains valid for EOC, except that for evaluation of BP changes the term:

$$\Gamma_i = \frac{d}{d\rho_x}(\rho_{oi} - r\rho_{boi}) = -r \tag{4.36}$$

instead of -1, which applies at the BOC.

The solution strategy is analogous to that at BOC. The flowchart of Fig. 4.2 shows the computational sequence to evaluate the EOC power derivatives together with the cycle and assembly burnup derivatives in the synthesis approach (see section 4.3.1.2.1). The sweeping sequence in the iterative procedure and the relaxation artifice are the same as applied at BOC.

4.3.2.2 Burnup Derivatives

Two methods to compute the burnup derivatives, based respectively on the synthesis and integrated approaches developed in the previous chapter, have been explored. The synthesis approach has been implemented in the optimization routines of the LRM-Nodal program since it is faster and requires less computer memory. However the integrated approach appears to be potentially more accurate, and hence may deserve further consideration.

4.3.2.2.1 Synthesis Approach

The synthesis method to compute cycle and assembly burnups, described in section 3.4.1, may be extended to calculate the burnup derivatives. The equation for cycle burnup, B_c, derived for the null EOC reactivity conditions, was shown to be:

$$B_c = \frac{\sum_{i=1}^{n} f_i^e(\rho_{oi} - r\rho_{boi}) - \sum_{i=1}^{m} f_i^e \rho_{Li}}{\sum_{i=1}^{n} A_i f_i^e f_{ai}} , \qquad (4.37)$$

where, using the mixing coefficients, V_i:

$$f_{ai} = f_i^b V_i^b + f_i^e V_i^e \tag{4.38}$$

and assembly burnup is given by:

$$B_i = B_c \ f_{ai} \tag{4.39}$$

Since the cycle burnup, B_c, and the assembly burnups, B_{is}, are provided by the core depletion computation (in this work, by the step-wise method formulated in section 3.4.3), the f_{ai}s may be calculated, exactly, as:

$$f_{ai} = \frac{B_i}{B_c} \quad , \tag{4.40}$$

and the synthesis approximation of Eq. (4.38) is only partially needed to compute the assembly burnup derivatives:

$$\frac{\partial B_i}{\partial \rho_x} = f_{ai} \frac{\partial B_c}{\partial \rho_x} + B_c \left(\frac{\partial f_i^b}{\partial \rho_x} V_i^b + \frac{\partial f_i^e}{\partial \rho_x} V_i^e \right) \tag{4.41}$$

It may be shown under the assumption that the fractional change of power, $\frac{\partial f_i}{\partial \rho_x} f_i$, varies linearly with burnup from BOC to EOC, that the mixing coefficients, V_i, are both equal to 0.5. With this assumption, taking the derivative of Eq. (4.37), and after some simplifications, the expressions for $\frac{\partial B_c}{\partial \rho_x}$ and $\frac{\partial B_i}{\partial \rho_x}$ become:

$$\frac{\partial B_c}{\partial \rho_x} = \frac{\sum_{j=1}^{n} f_j^e \Gamma_j + \sum_{j=1}^{n} \left[\rho_{oj} - r\rho_{boj} - A_j \left(B_j + \frac{B_c}{2} f_j^e \right) \right] \frac{\partial f_j^e}{\partial \rho_x} - \sum_{j=1}^{m} \rho_{Lj} \frac{\partial f_j^e}{\partial \rho_x}}{\sum_{j=1}^{n} A_j f_j^e f_{aj}}$$

$$- \frac{B_c \sum_{j=1}^{n} \left(\frac{A_j f_j^e}{2} \frac{\partial f_j^b}{\partial \rho_x} + f_{aj} f_j^e \frac{dA_j}{d\rho_x} \right)}{\sum_{j=1}^{n} A_j f_j^e f_{aj}} \tag{4.42}$$

and

$$\frac{\partial B_i}{\partial \rho_x} = f_{ai}\left(\frac{\partial B_c}{\partial \rho_x}\right) + \frac{B_c}{2}\left(\frac{\partial f_i^{\,b}}{\partial \rho_x} + \frac{\partial f_i^{\,e}}{\partial \rho_x}\right) \tag{4.43}$$

where the superscripts b and e denote BOC and EOC, respectively.

According to Eq. (2.28), for a fixed lattice design the value of A_i varies only slightly with the initial enrichment (thus with ρ_o), and hence this variation has been neglected in the present work, because the initial assembly enrichments are all similar. With this consideration the last term in Eq. (4.42) may be neglected. Recalling the discussion presented previously regarding the source terms Γ_k, and with Eq. (4.43) providing the assembly burnup derivatives to be used in Eqs. (4.33) and (4.34), a consistent set of relations to compute the necessary partial derivatives of the objective function $\frac{\partial B_c}{\partial \rho_x}$, of the assembly burnups, and of the BOC and EOC nodal power derivatives are now available.

The computational flowchart to solve this set of equations is displayed in Fig. 4.2. The computational sequence is very similar to that described for BOC power derivative computation. The spiral-pattern order for updating the nodal derivatives as well as the relaxation artifice used to accelerate convergence are the same as applied at BOC.

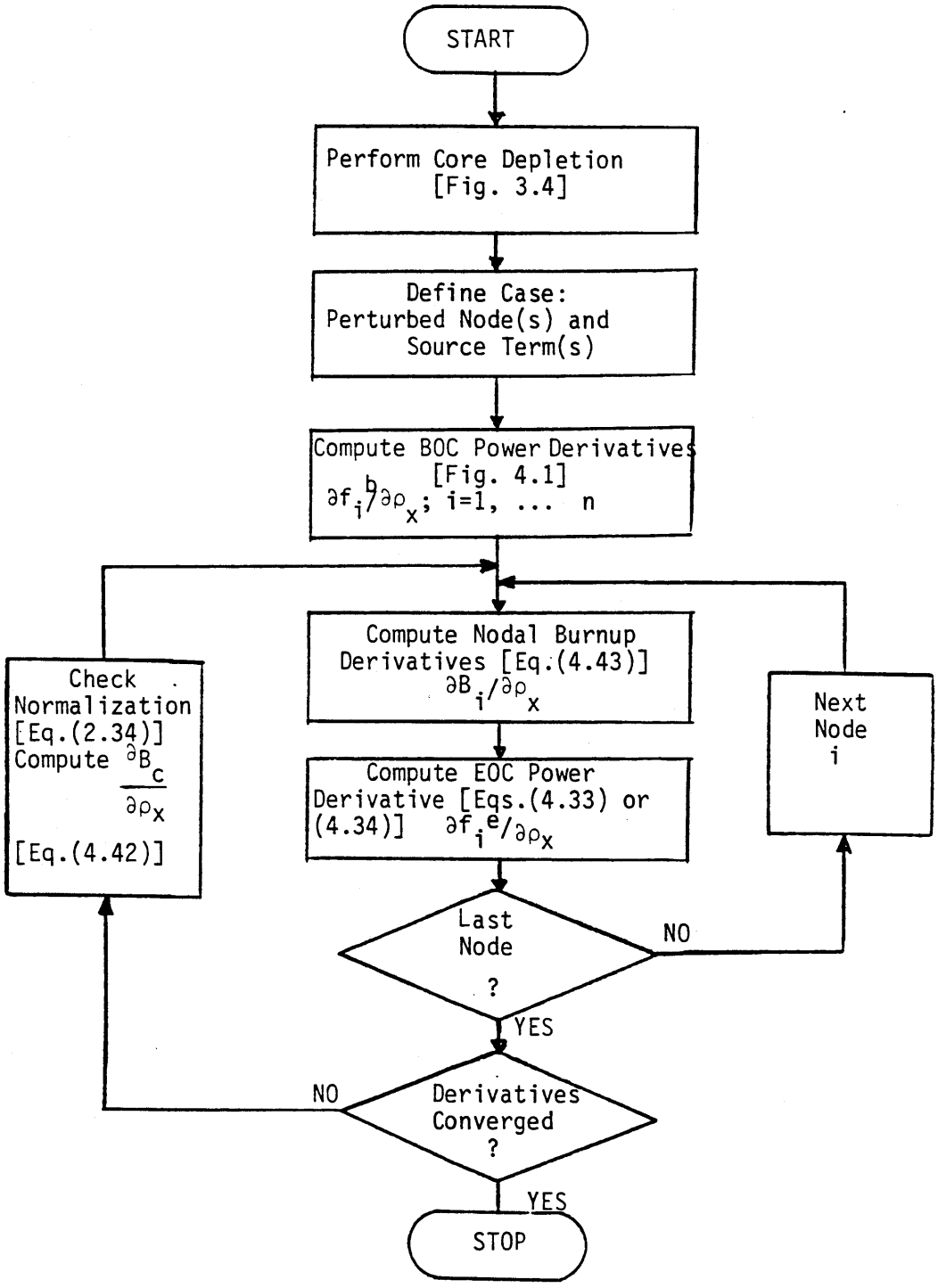

Fig. 4.2 Flowchart to Compute the Derivatives of Cycle and Assembly Burnups and of EOC Nodal Powers, using the Synthesis Method

4.3.2.2.2 Integrated Approach

In a similar fashion as in the synthesis method, the integrated approach may be extended to obtain a set of equations to compute the cycle and assembly burnup derivatives. In fact, Eqs. (3.52), (3.54) and (3.55) may be differentiated directly to yield expressions for the assembly and cycle burnup derivatives. The approach has not been implemented in the optimization procedures of the LRM-NODAL program, due to excessive memory requirements and increased running times for the microcomputer used. However the method may be worth further consideration, in future work, due to its potential for improved accuracy, when compared to the synthesis approach, especially if the improvements described in section 3.4.2 are included. Furthermore, correction factors to partially compensate for the main approximation of the method (i.e. the assumptions of linearity of the nodal power fractions and the soluble boron reactivity with core average burnup) may be computed from a numerical integration of Eq. (3.51) during the step-wise depletion procedures.

4.3.3 Sensitivity Theory Approach

The sensitivity-based methodology has been developed to estimate reactor performance parameters and associated uncertainties, using differential and integral information (e.g. Weisbin et al. in [L-4]). The methodology has been successful in several applications, such as

radiation transport, reactor thermal-hydraulics, reactor physics and fuel cycle analyses [O-1], [O-2], [W-5], [W-6]. One essential and powerful part of the approach, regarding the computation of partial derivatives, has been briefly referred to in section 4.3.2. For the present interest, another aspect will be explored, namely the use of the logarithmic derivative $\frac{d \ln P}{d \ln \alpha} \equiv \frac{d P/P}{d \alpha/\alpha}$, which represents the sensitivity of the response P to the parameter α, and constitutes the fractional change in the response due to a fractional change in parameter α. Use of the logarithmic derivative, instead of the conventional partial derivative allows one to account for the fact that the partial derivative at a given point is dependent on the amount of reactivity already allocated at the point in question. In other words, a common normalization scale is sought for the derivatives. This is important to partially overcome the limitation of the conventional partial derivative in the gradient method, which inherently is only able to account for the effects of small perturbations around the current point (or to the extent that linearity is valid). This consideration is especially relevant in assembly shuffling routines, where the perturbations are not always small.

Then, specializing to the case of cycle burnup, which is the objective function, the sensitivity coefficient becomes:

$$S_{BC} = \frac{d \ln B_c}{d \ln \rho} = \frac{\partial B_c/B_c}{\partial \rho/\rho} \tag{4.44}$$

Since ρ may assume the value of zero, to avoid singularities a change in variable is in order. The natural choice appears to be the neutron multiplication factor $k = 1/(1 - \rho)$ (which is also obtained mathematically as $k = \sum_{x=0}^{\infty} \rho^x$). Then S_{BC} becomes:

$$S_{BC} = \frac{d \ln B_c}{d \ln k} = \frac{\partial B_c}{\partial k} \cdot \frac{k}{B_c} = \frac{\partial B_c}{\partial \rho} \cdot \frac{\partial \rho}{\partial k} \cdot \frac{k}{B_c} \tag{4.45}$$

or,

$$S_{BC} = \frac{\partial B_c}{\partial \rho} \frac{1}{kB_c} = \frac{\partial B_c}{\partial \rho} \frac{(1-\rho)}{B_c} \tag{4.46}$$

The fractional change $\Delta B_c/B_c$, due to a change $\delta\rho^*$ in the local reactivity may be evaluated:

$$\frac{\Delta B_c}{B_c} = S_{BC} \cdot \frac{\delta\rho^*}{1 - (\rho + \delta^*)} \tag{4.47}$$

or, after some simplification, ΔB_c becomes:

$$\Delta B_c = \frac{\partial B_c}{\partial \rho} \frac{(1 - \rho)}{(1 - \rho - \delta\rho^*)} \cdot \delta\rho^* \tag{4.48}$$

Defining $\rho^* = \rho + \delta\rho^*$, Eq. (4.48) becomes:

$$\Delta B_c = \frac{\partial B_c}{\partial \rho} \frac{(1 - \rho)}{(1 - \rho^*)} (\rho^* - \rho) \tag{4.49}$$

or,

$$\Delta B_c = \frac{\partial B_c}{\partial \rho} (1 - \rho) \left[\frac{1 - \rho}{1 - \rho^*} - 1\right] \tag{4.50}$$

The main purpose of using the sensitivity approach (with the logarithmic derivative) is to provide an improved method to predict

the best set of shuffles, or in other words, an improved gradient direction that maximizes the gain in the cycle burnup. For a given core configuration, with n assemblies, according to Eq. (4.50) the change in B_c will be given by:

$$\Delta B_c = \sum_{j=1}^{n} \frac{\partial B_c}{\partial \rho_j} (1 - \rho_j) \left[\frac{(1 - \rho_j)}{(1 - \rho_j^*)} - 1 \right] \tag{4.51}$$

where ρ_j is the current reactivity at position j, and the ρ_j^* are to be chosen from among the n assemblies making up the core. The maximum gain in ΔB_c will be obtained by matching the rankings of the ρ_{js}^* and $\frac{\partial B_c}{\partial \rho}(1 - \rho_j)^2$, as may be seen by inspection.

This approach has been tested in the reload pattern algorithms described in section 4.4.1, and it has been successful in improving the objective function at a faster rate (i.e., in less iterations) than where using the conventional partial derivative. However, one disadvantage associated with its use is that it sometimes leads to an overprediction of the gain in the objective function, which ultimately results in an instability in convergence.

A remedy to this situation may be obtained by recognizing that Eq. (4.51) may be approximated by:

$$\Delta B_c \cong \sum_{j=1}^{n} \frac{\partial B_c}{\partial \rho_j} (1 - \rho_j) (\rho_j^* - \rho_j) \tag{4.52}$$

As before, the maximum gain in B_c is obtained by matching the rankings of ρ_j^* and the coefficient $\frac{\partial B_c}{\partial \rho_j} (1 - \rho_j)$. Equation (4.52) provides an

intermediate option between use of the full sensitivity coefficient and the conventional partial derivative in the gradient method. In the computer program LRM-NODAL, all three options are available to the user by appropriate specification of the exponent g (as 0, 1, or 2) in the coefficient $\frac{\partial B_c}{\partial \rho} (1 - \rho)^g$. Further evaluations need to be carried out to determine the best option for the various applications to which the present work can be put. It is also noteworthy that the logarithmic derivative approach, applied here to the cycle burnup, may also be extended to the nodal power and assembly burnup derivatives.

4.3.4 A Direct Search Method

An analysis of the objective function, B_c, as expressed by Eq. (4.37), and of its derivative, given by Eq. (4.42), indicates the important role of the EOC power fraction distribution in the determination of the optimality condition. Numerical examples have confirmed the strong correlation between the partial derivative $\frac{\partial B_c}{\partial \rho_j}$ and f_j^e for a given node j. This was to be expected because of the power weighting of reactivity, and the fact that B_c is determined by the system null reactivity limit. This situation may be exploited in a direct search method, where the EOC power fractions are to be used to determine the best changes in the core configuration, playing a role similar to that of the cycle burnup derivative in the gradient method.

The denominator in Eq. (4.42) usually does not vary much in magnitude for different assembly arrangements of the core. Then,

the aim becomes to maximize the numerator of Eq. (4.42). Defining,

$$N_b = \sum_{j=1}^{n} f_j^e \, (\rho_{oi} - r\rho_{boi}) - \sum_{j=1}^{m} f_j^e \, \rho_{Lj} \quad , \tag{4.53}$$

a scheme may be devised to maximize N_b by recognizing that this may be accomplished by matching the rankings of the $f_j^e \, (1 - \rho_{Lj})$ and ρ_{oj}. Hence, an "importance factor" may be defined as:

$$P_j = f_j^e \, (1 - \rho_{Lj}) \, (1 - \rho_{oj}) \quad , \tag{4.54}$$

expressing the EOC "importance" $f_j^e(1 - \rho_{Lj})$ per unit of initial (BOC) reactivity. Then an iterative search may be carried out to maximize N_b: in successive depletions shuffle the assemblies such as to match the ranking of P_j and of the reactivity of the assembly to be placed in position j. Convergence will be achieved when no further shuffles meeting this criterion are possible.

This method is available in the LRM-NODAL program as an optional preliminary search technique in the shuffling routine used to maximize the cycle burnup. The main advantage of the method is its speed, when compared to the full-fledged gradient method (requiring about a factor of 20 less time per iteration). The main shortcoming, besides being less rigorous, is the difficulty of systematically incorporating constraints. This, however may be overcome with programming techniques that take advantage of practical restrictions derived from experience, such as those used by Izenson [I-1].

4.4 Applications and Optimization Algorithms

In this section the use and application of the methods and their embodying routines in the algorithms formulated to perform specific optimization tasks will be described and discussed. For reload pattern optimization, first the algorithm to search for the assembly arrangement yielding the unconstrained maximum cycle burnup will be presented; then the optimization of burnable poison loading will be dealt with; following which the incorporation of constraints will be examined. For composition optimization two cases will be discussed. To demonstrate the capability and adequacy of the methodology the results of the application of various algorithms to the Maine Yankee Cycle 6 core are presented and discussed.

4.4.1 Unconstrained Reload Pattern Optimization Algorithm

For a typical PWR core, with around 200 fuel assemblies, even using quarter- or eighth-core symmetry, the number of possible core configurations becomes astronomical ($200! \approx 10^{375}$, $25! \approx 10^{25}$) so that an exhaustive search is impractical, and efficient programming techniques have to be used to search for the optimal or near optimal arrangement(s). Moreover, strictly speaking, the optimal arrangement of fuel assemblies in the core constitutes a discrete optimization problem, suitable for integer programming methods. The fundamental problem in the iterative optimization process is to define which

transformations in the core configuration should be performed such as to yield the maximum gain in the objective function. The gradient method as discussed in section 4.3.1 (or its extensions examined in section 4.3.3) is able to provide this answer, as long as the discreteness of the variables may be successively relaxed and the linearization around each current point remains valid. (Such successive linearization schemes for nonlinear optimization problems have been also referred to as the Method of Approximation Programming [G-6].) With this assumption stated, the algorithm may be formulated. Convergence of the steepest ascent methods, with certain qualifications, is assured by theorems available in the literature [W-3].

First the flowchart for the direct search method, discussed in section 4.3.4 will be presented, since it is available as a preliminary search option in the gradient based method. Figure 4.3 shows the sequence of computations. Successive depletions are carried out in tandem with shuffles, until the rankings of reactivities and of the P_i, given by Eq. (4.54) match. The flowchart for the gradient method(s) is shown in Fig. 4.4. The most important aspects of the algorithm, as incorporated in the LRM-NODAL program are:

- the initial pattern may be defined by the user or from a library;
- assemblies may be restricted to remain in defined positions in the core;
- an option is available to use either the conventional partial derivative or the modified logarithmic derivative, as discussed in section 4.3.3;

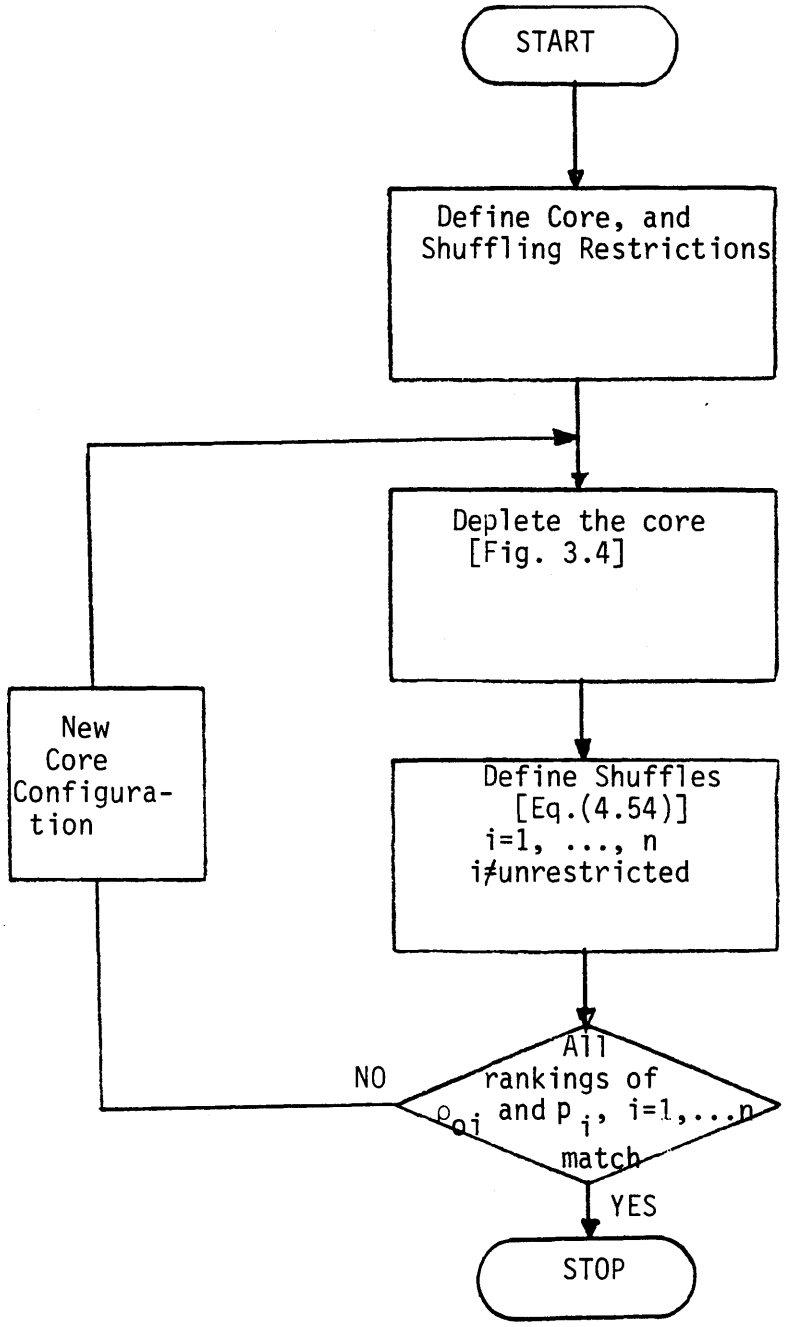

Fig. 4.3 Flowchart for Direct Search Method

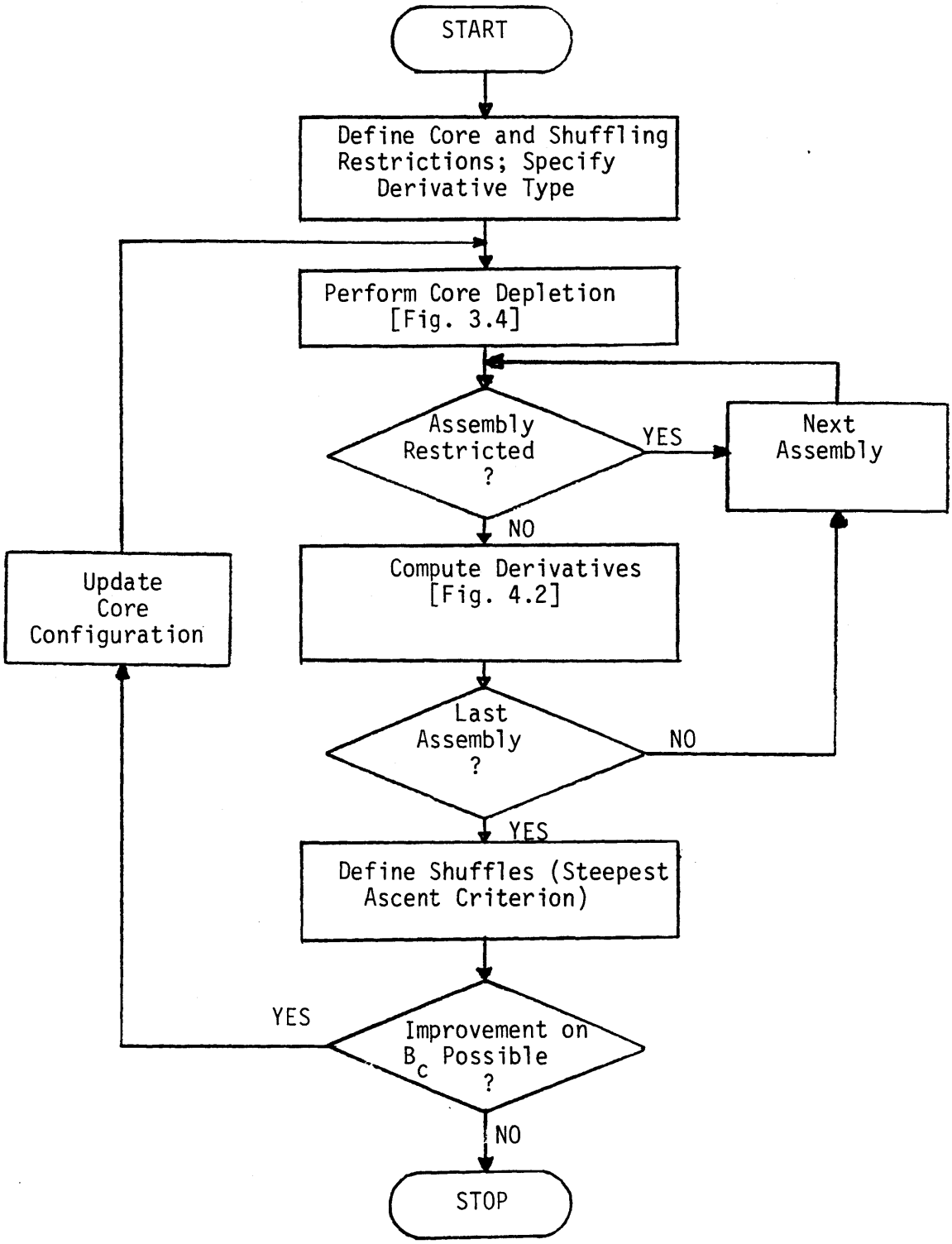

Fig. 4.4 Unconstrained Maximum Burnup Search Algorithm

- a preliminary optimization using the direct search method (Flowchart of Fig. (4.3)), is optional;
- convergence is achieved when no improvement may be found; i.e., the rankings of all assembly reactivities and corresponding derivatives of the objective function match. This criterion, as will be discussed later, may be replaced by another, based on the objective function improvement in a series of successive iterations.

One of the more controversial aspects of this method, even though consistent with the steepest gradient approach theory developed in section 4.3.1, is the over-relaxation resulting from the fact that all unrestricted assemblies may be moved at each iteration. The derivatives of the objective function that determine the assembly moves depend on the surroundings; so that if these are modified, the derivatives will also change. Even though this has not caused any convergence problems in the cases studied in the present effort, improvements may be achieved if only selective changes are permitted - for example, limiting the number of transformations in a given region or by requiring a certain minimum improvement in the objective function. The stability observed in the convergence process in the current method may be associated with the fact that the peripheral assemblies (typically one-fourth of the entire assemblies in a large PWR) are correctly assigned in the initial iterations,thus confining further maps to an option space bound by a successively smaller range of options in core configurations and changes in the objective function.

As an example, the algorithm just described is next applied to search for improvements in the Maine Yankee Cycle 6 core burnup. The fuel assembly data are the same as presented in Table 3.5, except that BPs have been removed (to avoid the bias that would arise from the associated extraneous power history effects). The initial core configuration is the same as in Fig. 3.5. The function of this example is merely to demonstrate the capability of the method to converge to optimal or near-optimal configurations, when all assemblies are unrestricted (i.e., they are completely free to be moved at each and every iteration).

Figure 4.5 summarizes the iterative process, giving the cycle burnup and the number of assemblies moved at each iteration. As can be seen the preliminary direct search converged after 11 iterations yielding a cycle burnup of 12,813.3 KWD/kg, and generating the assembly arrangement shown in Fig. 4.6. Then, the gradient method using the conventional (partial derivative) iterative process was started, requiring 12 iterations to achieve a configuration in which it could no longer identify possible improvements, and yielding a cycle burnup of 12,743.9 KWD/kg. An explanation is required for the reduction in the nominal B_c of 87.40 KWD/kg in the final values for the direct and gradient searches. Since no restrictions have been placed on any assembly, the odd, low-reactivity assembly in the center of the core has been changed. Exchange of this assembly is equivalent to replacing three assemblies of the type being moved into the center by three of the type being taken out, due to the fact that quarter-core symmetry was

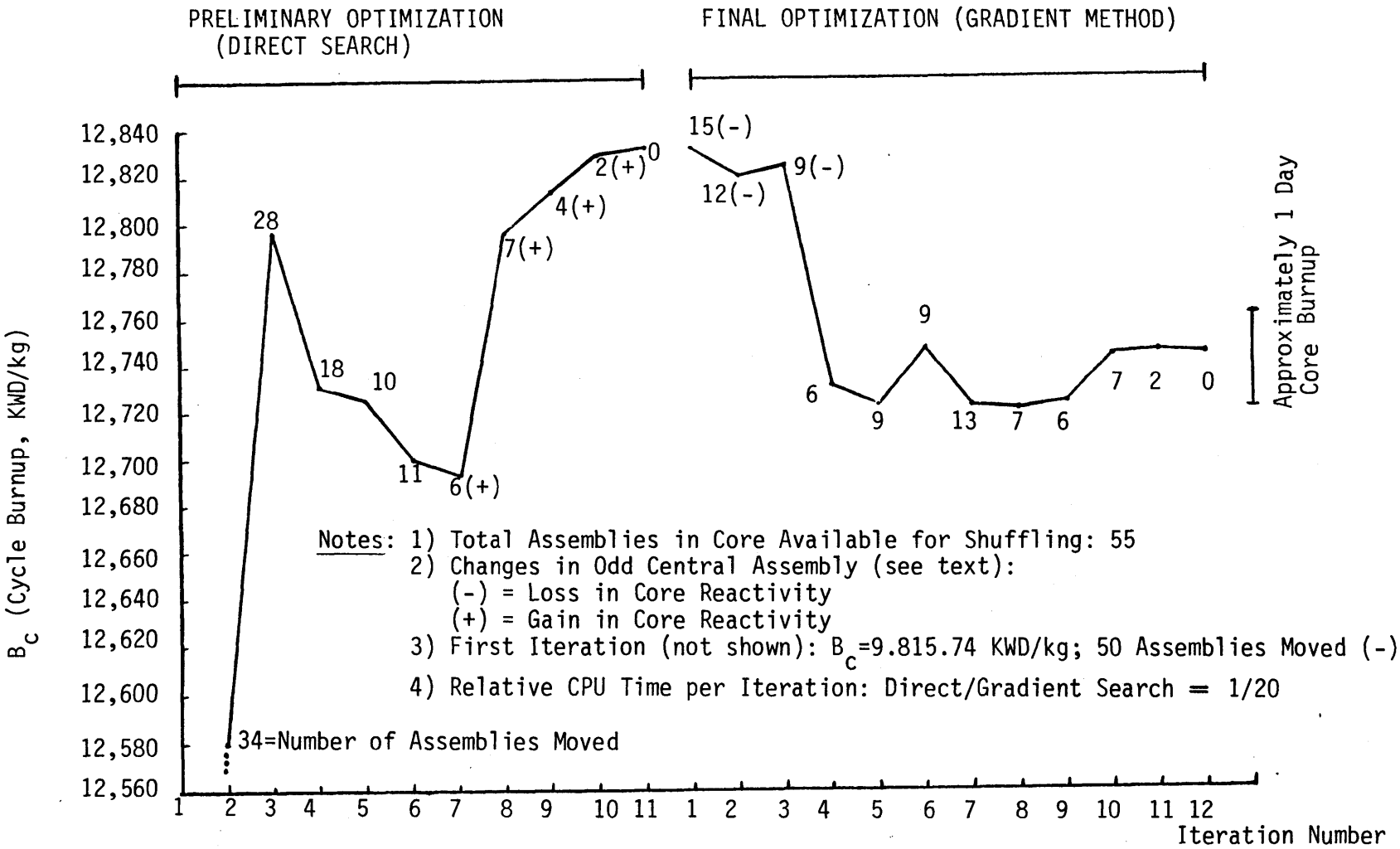

Fig. 4.5 Road Map of Convergence Progress for Burnup Maximization Algorithm

	1	2	3	4	5	6	7	8	9
1	0.129688 6	0.132068 5	0.142816 4	0.153055 3	0.221973 1	0.0221973 1	0.11244 7	0.048282 13	0.001905 20
2	0.132068 5	0.132068 5	0.153055 3	0.221973 1	0.221973 1	0.221973 1	0.10976 8	0.389345 15	-0.010820 23
3	0.143816 4	0.142816 4	0.155491 2	0.221973 1	0.221973 1	0.221973 1	0.090801 11	0.223811 17	
4	0.153055 3	0.15491 2	0.221973 1	0.221973 1	0.221973 1	0.129688 6	0.530786 12	0.220128 18	
5	0.221973 1	0.221973 1	0.221973 1	0.221973 1	0.221973 1	0.0960071 10	0.036076 16	-0.00628 22	
6	0.221973 1	0.221973 1	0.221973 1	0.221973 1	0.10976 8	0.048282 13	-0.00619 21		
7	0.11244 7	0.11244 7	0.100552 9	0.908015 11	0.038934 15	0.001905 20			
8	0.042828 13	0.042834 14	0.036762 16	0.0220128 18	-0.00619 21	..... ρ_{oi} ..... Ranking of ρ_{oi}			
9	0.009915 19	-0.01082 23							

Fig. 4.6 Assembly Arrangement Generated by the Preliminary Direct Search Method

imposed upon the analysis. Hence, moving the original assembly elsewhere represents a net loss of reactivity in three other assemblies of (0.221973 - 0.129688) = 0.092285, which corresponds to a loss of about 130 KWD/kg of cycle burnup. Figure 4.7 shows the final core configuration. It may be noted that the configurations of Figs. 4.6 and 4.7 are consistent with the results reported in ref. [A-3], for optimal core reload arrangements.

The use of the logarithmic derivative in the gradient method (sensitivity approach) led to similar values for the objective function, but with slightly larger oscillations between iterations.

A notable observation is that both the direct search method and the gradient method lead to similar cycle burnups, with values differing by less than the uncertainty range in the calculational method. This indicates that, in principle, all the approaches examined are able, for practical situations, to answer the fundamental question in reload pattern optimization: that is, to indicate which are the best exchanges to be pursued. Another important aspect regards oscillations in the value of the objective function during the process. This behavior was to be expected due to inherent approximations made in the course of the gradient approach (i.e., the successive linearizations around the current configuration). Furthermore, the small oscillations in B_c encompass a wide variety of configurations, indicating that a great number of near-optimal configurations exist, and it may not be worthwhile, even

	1	2	3	4	5	6	7	8	9
1	0.221973 1 3067.6	0.221973 1 2854.6	0.221973 1 2586.9	0.14281 4 1989.3	0.129688 6 1863.6	0.221973 1 2400.6	0.221973 1 2603.0	0.048282 13 1125.8	-0.00619 21 271.8
2	0.221973 1 2854.6	0.221973 1 2639.8	0.155491 2 2179.4	0.129688 6 1864.3	0.11244 7 1820.8	0.221973 1 2471.9	0.155491 2 2155.3	0.042830 14 958.4	-0.010820 23 181.8
3	0.221973 1 2586.9	0.221973 1 2472.6	0.153055 3 2061.6	0.13068 5 1894.8	0.221973 1 2308.0	0.221973 1 2533.5	0.090801 11 1632.7	0.022381 17 659.3	
4	0.142816 4 1989.3	0.11244 7 1831.0	0.132068 5 1894.3	0.142816 4 1985.0	0.221973 1 2463.2	0.221973 1 2549.1	0.05207 12 1239.1	0.022128 18 434.8	
5	0.129688 6 1863.6	0.10926 8 1791.0	0.153055 3 2061.8	0.221973 1 2496.1	0.221973 1 2588.8	0.096007 10 1683.4	0.03607 16 792.3	-0.00628 22 209.2	
6	0.221973 1 2400.5	0.221973 1 2440.7	0.221973 1 2536.0	0.221973 1 2616.0	0.10976 8 1777.8	0.038934 15 900.3	0.001905 20 280.9		
7	0.221973 1 2603.0	0.221973 1 2526.3	0.100552 9 1761.8	0.090815 11 1458.6	0.389345 15 846.3	0.001905 20 289.0			
8	0.048282 13 1125.8	0.42828 13 1043.2	0.360762 16 748.4	0.022012 18 479.4	-0.00699 21 224.8	..... ρ_{oi} ..... ρ_{oi} ..... $\frac{\partial B_c}{\partial \rho_{oi}}$	Ranking		
9	0.009915 19 311.6	-0.01082 23 199.0							

Fig. 4.7 Final Assembly Arrangement Generated by the Conventional Gradient Method

if adequate methods were available, to search for the absolute maximum burnup achievable. As a consequence, attainment of the region of small oscillations in B_c may be used as a criterion to stop the search.

Another important conclusion from the analysis of these results is that all optimal and near-optimal assembly configurations violate acceptable power peaking constraints for practical cores. The optimal configuration yields a core where the most reactive assemblies are located in regions having the highest power at EOC. This confirms the expectations drawn from a qualitative analysis of Eq. (4.37), in which the reactivity is power weighted, and the EOC is determined by the null reactivity limit. In other words, high reactivity assemblies should be at their highest power and low reactivity assemblies at their lowest power. This general observation also conforms with the well-known burnup benefits and power peaking detriments of low-leakage fuel management schemes - which are generally described in terms similar to these above: i.e., putting low reactivity assemblies in (inherently low power) peripheral positions. Furthermore, these results are consistent with those reported in ref. [H-4], as well as with those of Suzuki and Kiyose [S-2], [S-8], who state that: "At an optimal EOC state it is necessary to have all control rods withdrawn from the entire core and have the worst power distribution within thermal design limits."

In view of these results the need to incorporate power limit constraints cannot be overstated. This will be discussed in section

4.4.3. In as much as it relates to convergence of the algorithm, the incorporation of constraints on power limits (upper, and even lower) or on assembly position, will be beneficial by reducing the degrees of freedom of the system. It is also anticipated that satisfaction of the constraints will dominate the final states of the optimizing process, thus rendering unimportant the slight oscillations in the value of the objective function noted here. Another observation is that, for well-behaved cores, the peripheral assemblies may be placed by inspection: i.e., as can be seen from the results, to each peripheral assembly location a ranking may be assigned which would allow direct placement of the assemblies according to their reactivities. Further experience may allow similar assignments for the core interior. Such information would, at the very least, be useful in the generation of the initial loading patterns to be submitted to the optimization.

4.4.2 Burnable Poison Optimization Algorithm

The primary objective of the use of BPs is to suppress excessive power peaking and to ensure an overall negative moderator temperature coefficient of reactivity at BOC. In addition, depending on the residual reactivity, the BPs may be used to optimize cycle burnup by shaping the assemblies' power histories such as to yield an optimal EOC core configuration. Both objectives, that of supressing excessive power peaking and power history shaping to optimize the core average burnup, are combined in the algorithm described here, which is

diagrammed in the computational flowchart of Fig. 4.8, and incorporated in the LRM-NODAL program.

The main features of the algorithm may be summarized as follows:

- Restrictions on BP concentration in each assembly may be input - these will never be exceeded;
- Absolute priority is given to poisoning the assemblies that exceed the allowable power peaking limits according to the following criteria:
  a) if power fractions at BOC and EOC exceed the limits, the assemblies in question are poisoned such that both exceed the limits by the same increment (hence, if the limits are the same, the BOC and EOC power fractions will be equal);
  b) otherwise, poisoning is carried out such as to suppress the excess power fraction (i.e., reduce it to a specified limit) and. if possible. in addition, such as to maximize B_c;
- Except for the cases above (peakers), the burnable poison is allocated according to the steepest gradient method; i.e., in proportion to the local derivative, up to the maximum allowed. The total amount to be allocated at

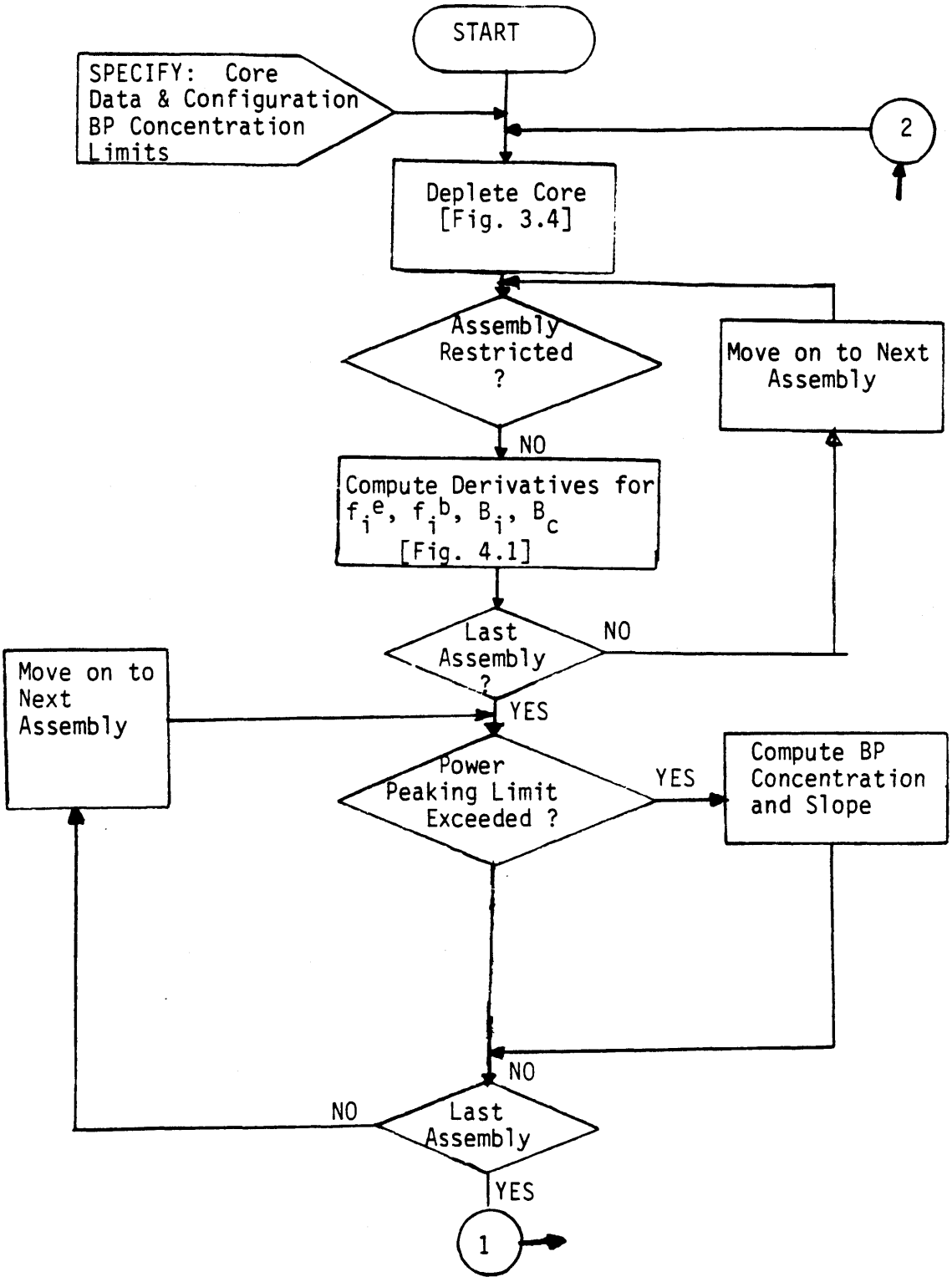

Fig. 4.8 Search Algorithm for Optimal Burnable Poison Allocation

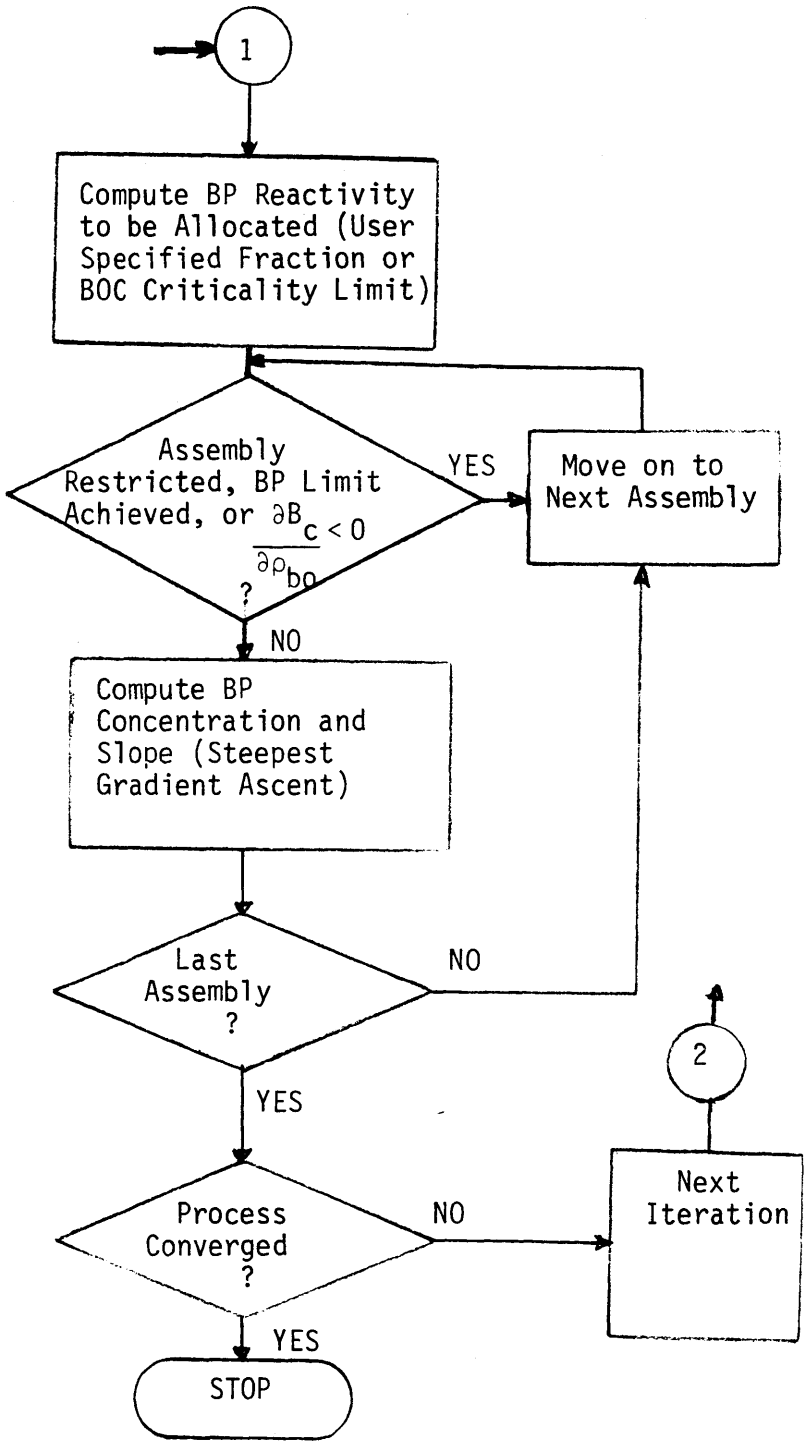

Fig. 4.8 (Continued) Search Algorithm for Optimal Burnable Poison Allocation

each iteration may be user defined, or be defined as a fraction of the estimated total BP loading required to keep the overall core critical at BOC;

- Convergence is achieved when:
  a) all $\left|\frac{\partial B_c}{\partial \rho_{bi}}\right| \leq E$, where E is a tolerance limit; or,

  b) all assemblies have achieved: the BP concentrations required to depress their power to the specified limits; or their maximum allowed BP concentration; or, otherwise, when the maximum core BP loading has been allocated.

As an illustration, this algorithm has been applied to the Maine Yankee Cycle 6 core. Fig. 4.9 displays the results for the BP-free core depletion. Only seven assemblies have been allowed to be poisoned and their BP concentration limits are shown also on Fig. 4.9. An assembly power peaking constraint of 1.3 at EOC and BOC was imposed. The residual BP reactivity fraction, r, was specified as 0.0025. Figure 4.10 shows the BOC and EOC power distributions, as well as the BP concentrations allocated. Additionally, the computed slopes, S_b, and the derivatives, $\frac{\partial B_c}{\partial \rho_{bo}}$, for the assemblies in question are shown.

As can be seen, all assemblies are within the convergence range of the 1.3 power peaking limit, and as required by the algorithm, the powers of assembly (7,2) at BOC and EOC have been equalized, and nearly the same happened with assembly (2,7). The important conclusions from these results are:

(a) After poisoning, the cycle burnup increased to 9,858.11 KWD/Kg

	1	2	3	4	5	6	7	8	9
1	E16 4 - 0.6272 0.9833	J0 5 - 0.7391 1.1503	I4 6 - 0.6013 0.9019	J0 7 - 0.8077 1.0762	I0 8 - 0.7991 0.9161	J8 9 - 1.0066 0.9823	I0 10 - 1.1792 0.98806	K8 3 0.3 1.4948 1.2265	K0 1 - 1.0096 0.9298
2	J0 5 - 0.7345 1.1496	I0 11 - 0.6482 0.9927	J0 12 - 0.7113 1.0486	I4 13 - 0.6711 0.8711	J0 14 - 0.9615 1.0666	I4 15 - 0.9762 0.9192	K8 3 0.3 1.5945 1.2722	I0 16 - 1.02932 0.8775	K0 1 - 0.7192 0.7130
3	I4 6 - 0.6012 0.9013	J0 12 - 0.7106 1.0502	I4 17 - 0.6504 0.9000	J0 18 - 0.8350 1.0277	I0 19 - 0.9122 0.9835	J0 20 - 1.2143 1.1343	J8 21 - 1.2948 1.1036	K0 1 - 1.2859 1.1039	
4	J0 7 - 0.8075 1.0750	I4 13 - 0.6709 0.8717	J0 18 - 0.8360 1.0252	J4 22 - 0.9625 1.0639	J0 23 - 1.0604 1.0914	I0 24 - 0.9806 0.9415	I0 25 - 1.0015 0.9325	K0 1 - 1.0977 0.9654	
5	I0 8 - 0.7986 0.9152	J0 14 - 0.9588 1.0683	I0 19 - 0.9121 0.9833	J0 23 - 1.0599 1.0941	I0 26 - 1.0025 0.9859	J8 27 - 1.1361 1.0506	K8 3 0.3 1.3157 1.1746	K0 1 - 0.7717 0.7697	
6	J8 9 - 1.0053 0.9807	I4 15 - 0.9741 0.9194	J0 20 - 1.2129 1.1315	I0 24 - 0.9805 0.9409	J8 27 - 1.1327 1.0495	K4 2 0.3 1.4007 1.2128	K0 1 - 0.8882 0.8406		
7	I0 10 - 1.1779 0.9875	K8 3 - 1.5884 1.2722	J8 21 - 1.2920 1.1031	I0 25 - 1.0030 0.9308	K8 3 0.3 1.3142 1.1723	K0 1 - 0.8904 0.8377			
8	K8 3 0.3 1.4926 1.2145	J0 16 - 1.0259 0.8761	K0 1 - 1.2771 1.1051	K0 1 - 1.0470 0.9642	K0 1 - 0.7681 0.7703				
9	K0 1 - 1.0074 0.9262	K0 1 - 0.7278 0.7096	-- BP Concentration Limit -- BOC Power Fraction -- EOC Power Fraction						

B_c = 9815.74 KWD/Kg

Fig. 4.9 Maine Yankee Cycle 6 BP-free Core Depletion Results

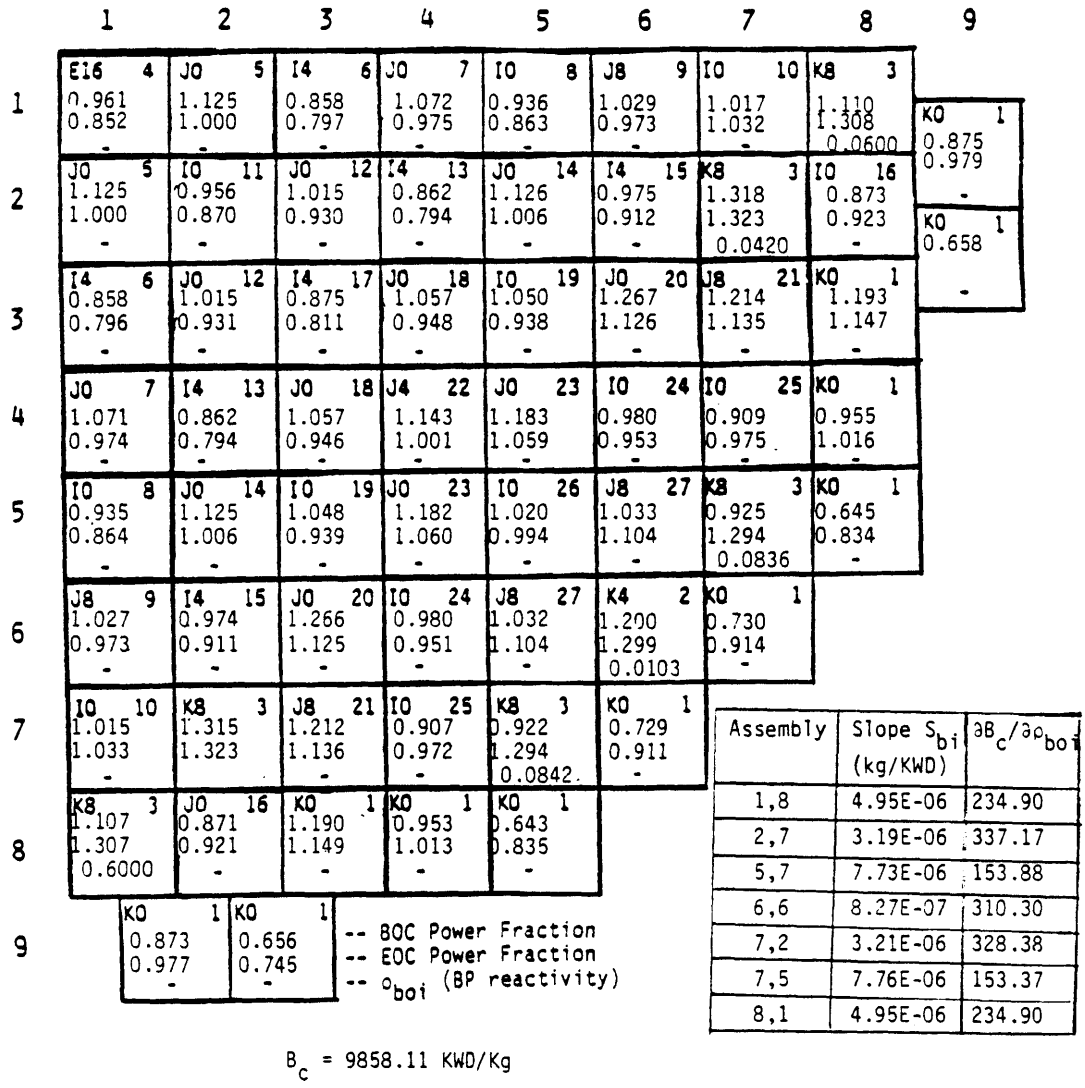

Assembly	Slope S_{bi} (kg/KWD)	$\partial B_c/\partial \rho_{boi}$
1,8	4.95E-06	234.90
2,7	3.19E-06	337.17
5,7	7.73E-06	153.88
6,6	8.27E-07	310.30
7,2	3.21E-06	328.38
7,5	7.76E-06	153.37
8,1	4.95E-06	234.90

B_c = 9858.11 KWD/Kg

Fig. 4.10 Maine Yankee Cycle 6 Core Results after Optimal BP Allocation

(from 9,815.74 KWD/Kg); (b) The EOC powers for the poisoned assemblies are close to their maximum allowable value (within the fairly loose convergence tolerance); (c) For these assemblies all the derivatives of the objective function, $\frac{\partial B_c}{\partial \rho_{boi}}$, are positive, indicating that more BP allocation in these assemblies would further increase the cycle burnup. These results are consistent with the basic principle of maximization of EOC reactivity importance (in a sense, "saving" reactivity for the EOC when its importance is higher). Moreover, these results are consistent with those reported by Suzuki and Kiyose [S-8], and, along with those of the previous algorithm, contradict the assumption made in Ref. [D-2], that a constant power shape held over the duration of the burnup cycle results in the highest achievable energy production from the core.

Regarding the methodology, it is appropriate to note that the successive linearizations intrinsic to the gradient approach and to the projection of derivatives may result in convergence problems when BP reactivity allocation steps are too large. Specifically, when only a few assemblies are to be poisoned, the procedure of allocating BP fractions such as to achieve core criticality by BP control only should not be used. This inconvenience is easily avoided by specifying appropriate ΔBP allocation fractions in the iterative optimization process.

4.4.3 Incorporation of Constraints

The results from the application of the previous algorithms show that their optimal patterns clearly violate normally acceptable power peaking constraints. Hence, these algorithms, in spite of providing valuable insight into the nature of optimal core configurations, are of little practical use without a concurrent ability to account for power (or other, such as assembly burnup) constraints. The master algorithm described in this section uses the same routines and methods previously developed to search for configurations satisfying power peaking constraints, as shown in Fig. 4.11

The main innovation consists of the use of the computed derivatives to evaluate, through projection, the effects of assembly moves (prioritized to improve the objective function) and thus avoid potential violations of constraints. Furthermore, when, due to inaccuracies inherent in the linearization of the projections, violations do occur, the derivatives may be used in a backwards search for a feasible configuration having a minimum loss in the objective function.

The priorities in core transformations (i.e. assembly moves) are to be defined based on the potential gains (or losses), projected by the derivatives of the objective function with respect to variables of assembly reactivity (ρ_{oi}) and burnable poison reactivity decrement (ρ_{boi}), but without potential violation of constraints. Thus two arrays of

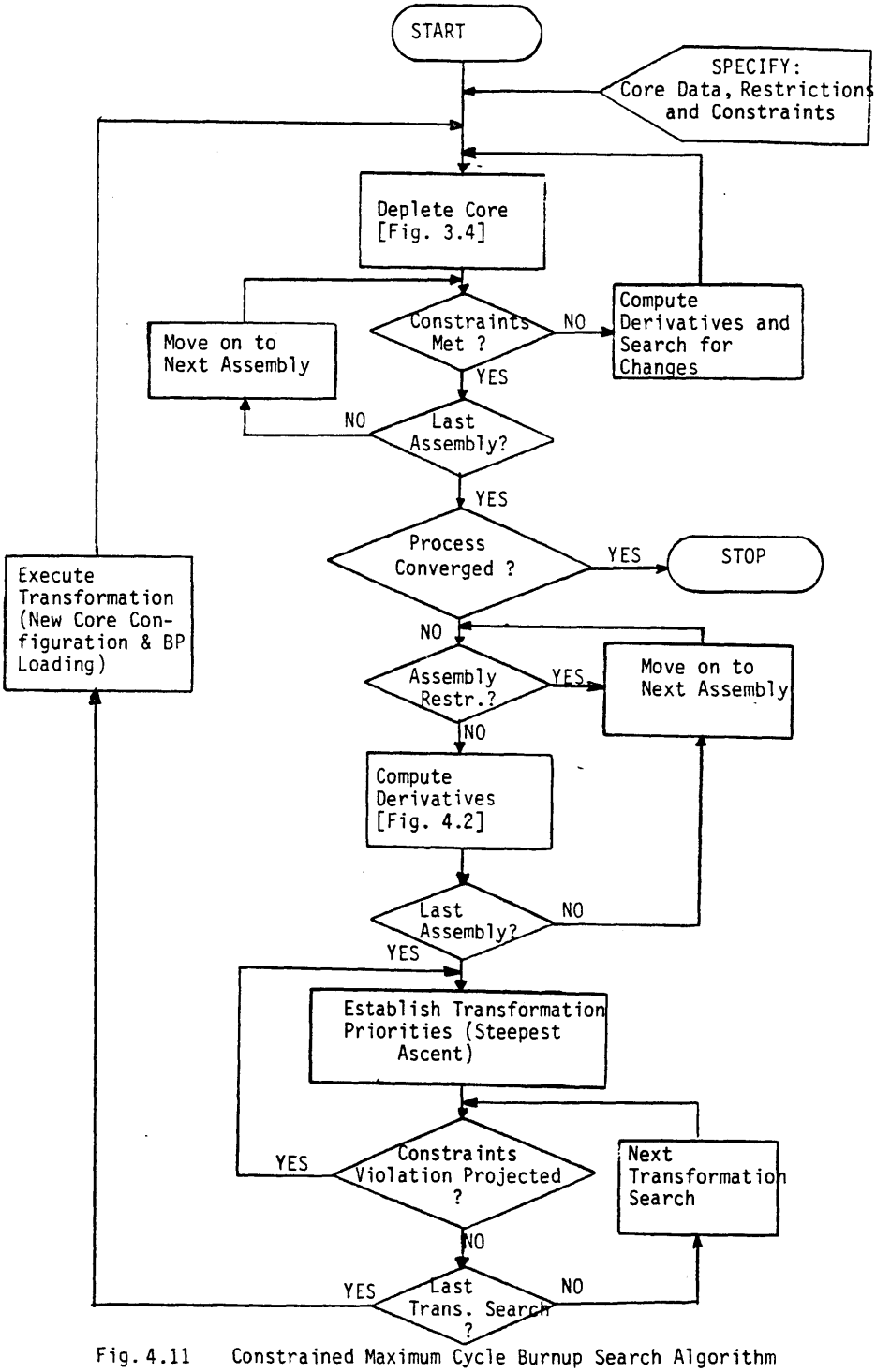

Fig. 4.11 Constrained Maximum Cycle Burnup Search Algorithm

derivatives are required at each iteration. A possible simplification may arise if the effects of BP loading can be decoupled from those of assembly arrangement in the search for optimality; i.e., if the unpoisoned optimal core arrangements still remain optimal after being burnable-poisoned to the optimal limits (or are poisoned only to suppress excessive power peaking).

If, as expected, the decoupling of both effects is possible, the derivatives with respect to ρ_{bo} will be required only to assess if potential power peaking violations may be overcome (or dealt with) through burnable poisoning. After the priorities have been defined, the transformations are executed, i.e., the assemblies are shuffled and the BP allocated. Then the core is depleted and checked for satisfaction of all constraints. If constraints are violated, optimal changes are searched for (i.e., additional poisoning or if necessary, assembly exchanges) and executed in tandem with core depletions, until a feasible configuration is found.

The optimization process is considered to converged when no worthwhile transformations (i.e., those resulting in a minimum threshold gain in B_c) can be found, and all constraints are met.

The algorithm has not been fully implemented and evaluated in the present work for two main reasons: insufficient memory (by a factor of about 10) in the particular microcomputer for which the necessary

routines were written (TRS-80 Model III, 48K); and, an impractically long running time (days) that would be required to perform the calculations. The additional efforts necessary to transport the software embodying the routines to a larger and faster computer were not judged warranted, since the major research objectives, development and demonstration of an adequate core model and a systematic optimization methodology have been satisfactorily achieved. Moreover, confidence in the accuracy and reliability of the algorithm described herein is based on the fact that the individual constituent routines have been tested (as demonstrated by the examples previously presented), and, also because similar methods (i.e., the "Hemstitching" method of Roberts and Lyers [R-3] and the Gradient Projection Method [R-4]) have been successfully used for complex nonlinear problems [B-4] [W-3]. In particular, it should be noted that the Gradient Projection Method appears to be well suited for problems such as the one at hand, where the active constraints play an important role in the optimal condition. In this method the current solution is assumed to lie on one or more constraint boundaries, and the basic idea is to search in a direction in which the objective function improves, but which is tangential to the boundaries of the active constraints.

It is recommended, however, that transfer of the software to a larger computer and full implementation of the algorithm be undertaken as the starting point for future work. (Projections are that within two years megabyte capacity minicomputers an order of magnitude faster than the one used here will become available).

4.4.4 Application to Composition Optimization

In this section the application of the gradient methods and routines to tailor design compositions of assemblies (and cores) will be briefly discussed. Two simple approaches will be considered, called here "forward" and "backward" methods.

4.4.4.1 Forward Method

Suppose that the positions to be occupied by the assemblies to be designed, as well as the compositions and arrangement of the remainder of the assemblies are given. The objective then is to design assemblies such that the marginal benefit (the partial derivative of the objective function) for an incremental unit to be allocated (cost, ore commitment, etc., represented by the appropriately weighted "reactivity units") is the same in all locations. Thus, starting with an initial guess, the incremental "reactivity units" may be allocated at each iteration strictly proportional to the derivatives at each location, as prescribed by the steepest gradient theory. If the total amount of resources (represented in "reactivity units") is constrained, then the source terms discussed in the latter part of section 4.3.2.1.1 should be used, and the process will converge when all derivatives are zero. The approach just described could be coupled to a reload pattern algorithm to form an iterative method to tailor-design optimal reload batches.

4.4.4.2 Backward Method

The LRM provides another possible approach to optimization of compositions. The average cycle burnup may be written as:

$$B_c = \frac{1}{n} \sum_{i=1}^{n} B_i = \frac{1}{n} \sum_{i=1}^{n} \frac{\rho_{oi} - \rho_i^e}{A_i} \tag{4.55}$$

where, ρ_i^e is the assembly reactivity at EOC. Since, for a given core, the ρ_{oi}/A_i are fixed, the optimization goal is equivalent to minimizing the sum:

$$Y = \sum_{i=1}^{n} \frac{\rho_i^e}{A_i} \approx \sum_{i=1}^{n} \rho_i^e \tag{4.56}$$

The Bellman Optimality Principle* [D-5] may be invoked to argue that, if expression (4.56) is minimized at EOC, the core obtained by a "backwards depletion" will be optimal.

A steepest descent approach may be used to minimize Eq. (4.56), subject to the condition that the core be just critical. The algorithm of Fig. 4.1 provides the derivatives necessary at each iteration, through $\frac{\partial \rho_{sp}}{\partial \rho_i}$. A simple iterative procedure may be used (assuming

---

*The Bellman Optimality Principle is as follows: "An optimal sequence of decisions in a multistage decision process problem has the property that whatever the initial stage, state and decisions are, the remaining decisions must constitute an optimal sequence of decisions for the remaining problem, with the stage and the state resulting from the first decision considered as initial conditions."

that the slopes of the reactivity versus burnup curves, A_is, do not vary substantially):

1) Guess an initial composition;
2) Perform a power calculation [Fig. 3.1];
3) Make $\rho_i = \rho_i - \rho_{sp}$, for i = 1, ..., n;
4) Compute $\frac{\partial \rho_{sp}}{\partial \rho_i}$, for i = 1, ..., n [Fig. 4.1];
5) Make $\rho_i = \rho_i + \Delta \cdot \frac{\partial \rho_{sp}}{\partial \rho_i}$, for i = 1, ..., n;
6) Repeat steps 2 to 5 until

$$\frac{\partial \rho_{sp}}{\partial \rho_1} = \ldots = \frac{\partial \rho_{sp}}{\partial \rho_n} \quad ;$$

In step 5, Δ is an arbitrarily chosen increment, which should be reduced as the process converges.

It is anticipated that the optimal configuration(s) resulting from this process will not meet practical power peaking limitations. Hence the practical use of its results may be as a "yardstick for optimality", and beyond this, the method may be useful as part of a comprehensive iterative algorithm for core reload batch optimization.

4.5 Chapter Summary and Conclusions

In the present chapter, after a brief survey of optimization methods, the theoretical basis for the gradient approach used in this work has

been presented. The relations and routines required by this method have been developed and implemented. Improvements of the conventional gradient method, for shuffling purposes, by using the logarithmic derivative, as well as possible simplifications through direct search methods, have been analyzed and implemented.

The gradient approach has been shown to be successful when used to search for core configurations having improved cycle burnup, and to optimize the burnable poison loading. The basis for incorporating power peaking constraints in the methodology has also been developed, along with possible applications for composition optimization.

From the numerical and analytical results obtained it is concluded that optimal reload patterns for PWR cores depend essentially on the EOC configuration resulting from an appropriate BOC arrangement of the assemblies and their power history. For realistic cores this condition always implies that the most reactive assemblies will be at their maximum allowable power at EOC, and vice-versa for the least reactive ones; in achieving this, the reactivity of the most reactive assemblies is, in a certain measure, saved, thus maximizing their importance at EOC.

CHAPTER 5

SUMMARY, CONCLUSIONS AND RECOMMENDATIONS

5.1 Introduction

Pressurized Water Reactors (PWRs) account, currently, for more than half of the nuclear power plants operable, under construction or on order worldwide; and, moreover, PWR-based technology is likely to retain a significant role well into the next century. Thus the efficient operation and fuel management of PWRs is of substantial importance, a factor which motivated dedication of the present research to developing a methodology for PWR core reload pattern and composition optimization.

The core reload design process encompasses a complex set of decisions, having the goal of specifying a core capable of producing a demand-imposed target cycle energy, at the minimum cost, with appropriate margins to assure that design limits (detailed in the reactor's FSAR), are not exceeded. For steady state operation these design limits may be translated into constraints on the radial power peaking factor in a two-dimensional analysis. The goal of minimizing overall system costs, after the cycle length has been approximately fixed, corresponds to minimizing the fuel cycle costs; and this, in turn, after the reload assembly enrichment(s) have been specified, to finding an acceptable reload pattern that maximizes

the core average cycle burnup, Bc. Thus accurate computation of global and local power histories and burnup have long been the goal of reactor core designers.

Standard, sophisticated LWR core analysis methods having the above capability (such as EPRI's ARMP package) are available to perform licensing calculations, and are in use industry-wide. However, due to the complexity and the high cost of such analysis it is desirable that candidate core reload configurations be as close to optimal as possible before they are submitted to full-scope analysis. Significant prior efforts, resorting to a variety of methodologies and optimality goals, as summarized in table 5.1, have been dedicated to optimization and automation of the core reload preliminary design process. However, no standard methods, having industry-wide acceptance and an adequate compromise between simplicity and accuracy are in general use. The most widespread approach is still trial and error aided by "rules of thumb" derived from experience and insight.

In view of the above circumstances the primary objective of the research summarized here has been the development of a methodology for PWR core reload pattern and fuel composition optimization, where cycle burnup, Bc, is defined as the optimality criterion, and where the capability for a systematic incorporation of restrictions on power peaking, assembly placement and burnable poison (BP) concentration, constituted a central concern. Furthermore, ease of computation, transparency of approach, and simplification, whenever possible (without distortion of the essential features of the problem) have often been the key to success in complex optimization tasks. Therefore, due to the previous success, and the po-

TABLE 5.1

Summary of Relevant Core Reload Optimization Work

Author(s) and Reference		Approach						Objective			
		Linear Programming	Dynamic Programming	Variational Methods/Optimal Control Theory	Perturbation Theory	Direct Search	Heuristic Methods	Maximize Burnup	Maximize Reactivity	Minimize Power Peaking	Minimize Costs or Fuel Required
Rieck	[R-1]					x					x
Izenson	[I-1]		x							x	
Downar	[D-2]					x		x			
Goertzel	[G-1]			x							x
Wall and Fenech	[W-1]		x								x
Melice	[M-2]			x					x		
Fagan and Sesonske	[F-1]		x								x
Naft and Sesonske	[N-1]					x				x	
Suzuki and Kiyose	[S-2]	x									x
Sauar	[S-3]	x									x
Wade and Terney	[W-2]			x				x		x	
Hoshino	[H-1]						x	x			
Goldschmidt	[G-2]			x							x
Motoda, Herczeg, Sesonske	[M-3]	x				x					x
Ciechanowiecz	[C-1]			x				x			
Stout and Robinson	[S-4]		x							x	
Chitkara and Weisman	[C-2]					x					x
Mingle	[M-4]	x			x						x
Motoda and Yokomizo	[M-5]	x				x				x	
Terney and Williamson	[T-1]			x						x	
Lin, Zolotar, Weisman	[L-1]					x					x
Ho and Sesonske	[H-2]					x				x	
Ho and Rohach	[H-3]				x					x	
Huang and Levine	[H-4]			x					x		
Colletti, Levine, Lewis	[C-3]			x					x		
Chang and Levine	[C-4]			x							x
Ahn and Levine	[A-3]			x				x			
Suzuki and Kiyose	[S-8]			x				x			
This work				x		x		x			

tential for improvement, of MIT's Advanced Linear Reactivity Model of PWR core behavior [S-1], [L-2], [K-1], [D-1], its evaluation for, and extension to the tasks at hand, constituted an important subsidiary goal in the present work.

5.2 Methodology Development

The use of sophisticated state-of-the-art licensing-level methods for preliminary scoping studies and optimization procedures is not warranted, if not due to their high complexity and computational costs, then because the degree of accuracy provided is much greater than the inherent uncertainties in the problem being modeled. Hence more cost-efficient and simpler methods, based on analytical and empirical models are called for. In this section, the methodology development efforts to fulfill this need for speed and simplicity will be summarized. First, the main features of the PWR core model which has been formulated will be described. Then, its extension to the optimization process will be summarized.

5.2.1 A Coarse Mesh Nodal Method

The basis for the PWR core model developed in the present work was provided by the modified one group diffusion theory model (also known as the one-and-one-half-group model) applied to spatial calculations, coupled with the empirically-well-established fact of the linearity of PWR assembly reactivity [S-1], [K-1], [L-2], [M-6] and burnable poison (BP) reactivity decrement [L-2] as a function of burnup, for core depletion calculations.

Each assembly was assumed to be represented by one square node of width h. Throughout this work, even though a compact matrix formalism could have been used, a formulation of the equations suitable for direct use in the Gauss-Seidel type iteration process was preferred.

5.2.1.1. Nodal Power Calculation

The one-and-one-half group equation is derived from the two-group diffusion equations [H-5], by neglecting the thermal leakage, which is an order of magnitude smaller than the fast leakage:

$$-\nabla \cdot D_1 \nabla \Phi_1 + (\Sigma_{a1} + \Sigma_{12})\Phi_1 - \frac{1}{\lambda}(\nu\Sigma_{f1} + \nu\Sigma_{f2}\frac{\Sigma_{12}}{\Sigma_{a2}})\Phi_1 = 0 \quad (5.1)$$

After defining the migration area, M^2, as:

$$M^2 = D_1/(\Sigma_{a1} + \Sigma_{12}) \quad (5.2)$$

the local reactivity as:

$$\rho = 1 - 1/k_\infty \quad , \quad (5.3)$$

where:

$$k_\infty = (\nu\Sigma_{f1} + \nu\Sigma_{f2}\frac{\Sigma_{12}}{\Sigma_{a2}})/(\Sigma_{a1} + \Sigma_{12}), \quad (5.4)$$

and the system reactivity,or the modified eigenvalue

$$\rho_S = 1 - 1/\lambda, \tag{5.5}$$

Eq. (5.1) may be written as:

$$\nabla \cdot D_1 \nabla \Phi_1 + \frac{(\rho - \rho_s)}{(1 - \rho)} \frac{D_1}{M^2} \Phi_1 = 0 \tag{5.6}$$

The local thermal power density is given by

$$q''' = \frac{\kappa}{\nu} \frac{D_1}{M^2} k_\infty \Phi_1. \tag{5.7}$$

After defining the normalized nodal power fraction, f_i, and after integration over the nodal volume, Eq. (5.7) yields, for the integrated nodal flux, Φ_i:

$$\Phi_i = \frac{\nu}{\kappa} \frac{M^2}{D_1} (1-\rho) f_i Q \tag{5.8}$$

where Q is the core thermal power.

Integration of Eq. (5.6) over the core, and use of Eq. (5.8), yields a system reactivity balance, which enables the computation of the modified eigenvalue ρ_S:

$$\rho_S = \frac{\sum_{i=1}^{n} f_i \frac{\nu}{\kappa} \rho_i}{\sum_{i=1}^{n} f_i \frac{\nu}{\kappa}} - \rho_L \quad , \tag{5.9}$$

where the "system leakage reactivity" ρ_L, is given by:

$$\rho_L = - \frac{\int_S \underline{dA} \cdot D_1 \nabla \Phi_1}{\sum_{i=1}^{n} f_i \frac{\nu}{\kappa}} = \frac{\sum_{i=1}^{m} J_i}{\sum_{i=1}^{n} f_i \frac{\nu}{\kappa}} \tag{5.10}$$

and, S designates the core outer surface, n is the number of total assemblies, and J_i is the net current out of each of the m peripheral assemblies. Evaluation of the paramatric behavior of κ/ν as a function of burnup, and the numerical analysis of its impact on Eq. (5.9) validated the approximation, used by previous researchers, of power-instead of source-weighting the reactivity in Eq. (5.9); hence:

$$\rho_S = \frac{\sum_{i=1}^{n} f_i \rho_i}{\sum_{i=1}^{n} f_i} - \rho_L \tag{5.12}$$

Furthermore, use of local normalized relative soluble boron worth weighting factors, accounting for spatially-varying spectral effects, allows the direct computation of the soluble boron reactivity, ρ_{sp}, required for core criticality (i.e.: ρ_S = o or λ = 1):

$$\rho_{SP} = \frac{\sum_{i=1}^{n} f_i \rho_i}{\sum_{i=1}^{n} f_i} - \rho_L \qquad (5.12)$$

For a critical core, Eq. (5.6) becomes:

$$\nabla^2\Phi_1 + \frac{\rho}{1-\rho}\frac{1}{M^2}\Phi_1 = \nabla^2\Phi_1 - B^2\Phi_1 = 0 \qquad (5.13)$$

This equation, Eq. (5.13), was solved analytically in two dimensions, to provide a firm basis for the nodal equations. The main assumptions made were: continuity of fluxes and net neutron currents at nodal interfaces (on an integrated basis for the orthogonal direction) and constant fast group diffusion coefficient over the core interior. For the peripheral nodes a correction factor, E, was incorporated to account for thermal back-leakage from the reflector region, and other effects requiring empirical adjustment to achieve adequately accurate results. The analytical solutions for the integrated nodal fluxes are shown in tables 5.2 and 5.3 for interior and peripheral nodes, respectively, whereas table 5.4 shows the equations for the net currents out of peripheral nodes.

Expansion of the hyperbolic functions in the analytical solutions, and the neglect of third and higher order terms in these expansions, was shown to provide adequate approximations for the integrated nodal fluxes and leakages. A further important simplification resulted from the para-

TABLE 5.2

Analytical Solution for Interior Node Integrated Flux

X-direction:

$$\frac{\Phi_{ij}\alpha_{ij}^2}{2} = \tag{5.14}$$

$$\frac{\Phi_{i-1,j}\alpha_{i-1,j}\,\mathrm{csch}(\alpha_{i-1,j}\,h)\left[\frac{\tanh(\alpha_{ij}\,h/2)}{\alpha_{ij}}+\frac{\tanh(\alpha_{i+1,j}\,h/2)}{\alpha_{i+1,j}}\right]+\Phi_{i+1,j}\alpha_{i+1,j}\,\mathrm{csch}(\alpha_{i+1,j}\,h)\left[\frac{\tanh(\alpha_{ij}\,h/2)}{\alpha_{ij}}+\frac{\tanh(\alpha_{i-1,j}\,h/2)}{\alpha_{i-1,j}}\right]}{\left[\frac{\coth(\alpha_{ij}\,h/2)}{\alpha_{ij}}+\frac{\tanh(\alpha_{i-1,j}\,h/2)}{\alpha_{i-1,j}}\right]\left[\frac{\tanh(\alpha_{ij}\,h/2)}{\alpha ij}+\frac{\tanh(\alpha_{i+1,j}\,h/2)}{\alpha_{i+1,j}}\right]+\left[\frac{\coth(\alpha_{ij}\,h/2)}{\alpha_{ij}}+\frac{\tanh(\alpha_{i+1,j}\,h/2)}{\alpha_{i+1,j}}\right]\left[\frac{\tanh(\alpha_{ij}\,h/2)}{\alpha_{ij}}+\frac{\tanh(\alpha_{i-1,j}\,h/2)}{\alpha_{i-1,j}}\right]}$$

Y-direction:

$$\frac{\Phi_{ij}\beta_{ij}^2}{2} = \tag{5.15}$$

$$\frac{\Phi_{i,j+1}\beta_{i,j+1}\,\mathrm{csch}(\beta_{i,j+1}\,h)\left[\frac{\tanh(\beta_{ij}\,h/2)}{\beta_{ij}}+\frac{\tanh(\beta_{i,j-1}\,h/2)}{\beta_{i,j-1}}\right]+\Phi_{i,j-1}\beta_{i,j-1}\,\mathrm{csch}(\beta_{i,j-1}\,h)\left[\frac{\tanh(\beta_{ij}\,h/2)}{\beta_{ij}}+\frac{\tanh(\beta_{i,j+1}\,h/2)}{\beta_{i,j+1}}\right]}{\left[\frac{\coth(\beta_{ij}\,h/2)}{\beta_{ij}}+\frac{\tanh(\beta_{i,j+1}\,h/2)}{\beta_{i,j+1}}\right]\left[\frac{\tanh(\beta_{ij}\,h/2)}{\beta_{ij}}+\frac{\tanh(\beta_{i,j-1}\,h/2)}{\beta_{i,j-1}}\right]+\left[\frac{\coth(\beta_{ij}\,h/2)}{\beta_{ij}}+\frac{\tanh(\beta_{i,j-1}\,h/2)}{\beta_{i,j-1}}\right]\left[\frac{\tanh(\beta_{ij}\,h/2)}{\beta_{ij}}+\frac{\tanh(\beta_{i,j+1}\,h/2)}{\beta_{i,j+1}}\right]}$$

Subject to: $B_{ij}^2 = \alpha_{ij}^2 + \beta_{ij}^2$ (5.16)

TABLE 5.3

Analytical Solution for Peripheral Node Integrated Flux

X-direction:

$$\frac{\Phi_{ij}\alpha_{ij}^2}{2} = \frac{\Phi_{i-1,j}\,\alpha_{i-1,j}\,\mathrm{csch}(\alpha_{i-1,j}\,h)}{\left[\frac{\coth(\alpha_{ij}\,h/2)}{\alpha_{ij}} + \frac{\tanh(\alpha_{i-1,j}\,h/2)}{\alpha_{i-1,j}}\right] + \frac{\left[\frac{\coth(\alpha_{ij}\,h/2)}{\alpha_{ij}} + \frac{ED_{ij}}{D_rB_r}\tanh(B_rh_r)\right]}{\left[\frac{\tanh(\alpha_{ij}\,h/2)}{\alpha_{ij}} + \frac{ED_{ij}}{D_rB_r}\tanh(h_rB_r)\right]}\left[\frac{\tanh(\alpha_{ij}\,h/2)}{\alpha_{ij}} + \frac{\tanh(\alpha_{i-1,j}\,h/2)}{\alpha_{i-1,j}}\right]} \qquad (5.17)$$

Y-direction:

$$\frac{\Phi_{ij}\beta_{ij}^2}{2} = \frac{\Phi_{ij+1}\,\beta_{ij+1}\,\mathrm{csch}(\beta_{ij+1}\,h)}{\left[\frac{\coth(\beta_{ij}\,h/2)}{\beta_{ij}} + \frac{\tanh(\beta_{ij+1}\,h/2)}{\beta_{ij+1}}\right]\frac{\left[\frac{\coth(\beta_{ij}\,h/2)}{\beta_{ij}} + \frac{ED_{ij}}{D_rB_r}\tanh(B_rh_r)\right]}{\left[\frac{\tanh(\beta_{ij}\,h/2)}{\beta_{ij}} + \frac{ED_{ij}}{D_rB_r}\tanh(B_rh_r)\right]}\left[\frac{\tanh(\beta_{ij}\,h/2)}{\beta_{ij}} + \frac{\tanh(\beta_{ij+1}\,h/2)}{\beta_{ij+1}}\right]} \qquad (5.18)$$

Subject to: $B_{ij}^2 = \alpha_{ij}^2 + \beta_{ij}^2$ (5.16)

TABLE 5.4

Analytical Solutions for the Net Neutron Currents Out of the Peripheral Nodes

$$J_{xij} = -\frac{D_{ij}\Phi_{ij}\alpha_{ij}^2}{2}\left[1 - \frac{\frac{\coth(\alpha_{ij}\, h/2)}{\alpha_{ij}} + \frac{E\, D_{ij}}{D_r B_r}\tanh(B_r h_r)}{\frac{\tanh(\alpha_{ij}\, h/2)}{\alpha_{ij}} + \frac{E\, D_{ij}}{D_r B_r}\tanh(B_r h_r)}\right] \tag{5.19}$$

and

$$J_{yij} = -\frac{D_{ij}\Phi_{ij}\beta_{ij}^2}{2}\left[1 - \frac{\frac{\coth(\beta_{ij}\, h/2)}{\beta_{ij}} + \frac{E\, D_{ij}}{D_r B_r}\tanh(B_r h_r)}{\frac{\tanh(\beta_{ij}\, h/2)}{\beta_{ij}} + \frac{E\, D_{ij}}{D_r B_r}\tanh(B_r h_r)}\right] \tag{5.20}$$

metric analysis, as a function of assembly burnup, of the factor $[\frac{\nu}{\kappa}\frac{M^2}{D_1}]$ relating integrated nodal fluxes and nodal powers. This factor was shown to be essentially invariant for LEOPARD results and only slightly (and nearly linearly) dependent on local reactivity for CASMO and DIT results; both dependencies are amenable to direct incorporation in the nodal equations. The resulting nodal power equations are summarized in Table 5.5, along with the prescription for leakage reactivity calculation, and the corresponding coupling coefficients and leakage constants are given in Table 5.6

5.2.1.2 Burnup Calculation

The linearity as a function of burnup of both the unpoisoned reactivity and reactivity decrement attributable to BPs has been used because of its accuracy and simplicity, to describe the otherwise complex phenomena of assembly fuel and burnable poison depletion. Thus the fuel assembly reactivity is represented simply by:

$$\rho_i = \rho_{oi} - A_i B_i \quad . \qquad (5.25)$$

Following ref. [L-2], the BP was modelled as an ideal material providing a required negative reactivity at BOC, burning out uniformly over the cycle, and then leaving a small residual fraction, r, at EOC. Such BP behavior, besides being desirable for power suppression and for attainment of optimality goals, is not unrealistic, as shown in Fig. 5.1, which illustrates

TABLE 5.5

Summary of the Nodal Power and Leakage Equations

Interior Nodes:

$$f_i = \frac{\sum_{j=1}^{4} f_j(1 - \theta_s \rho_j)}{4(1 - \theta\rho_i)} \tag{5.21}$$

Peripheral Nodes:

$$f_i = \frac{\sum_{j=1}^{N_p} f_j(1 - \theta_s\rho_j)}{N_p(1 - \theta_p\rho_i + \theta_L\rho_{Li})} \tag{5.22}$$

Leakage Reactivity:

Peripheral Assembly:

$$\rho_{Li} = N_r \cdot \frac{2 M_i^2}{h^2\left(1 + \frac{2 E D_i}{D_r B_r h}\right)} \cdot (1 + k_L \rho_{sp}) \tag{5.23}$$

System:

$$\rho_L = \sum_{i=1}^{m} f_i \rho_{Li} \Big/ \sum_{i=1}^{n} f_i \tag{5.24}$$

where:

N_p = number of fuel/fuel interfaces on assembly i;

$N_r = 4\text{-}N_p$ = number of fuel/reflector interfaces on assembly i;

and, the coupling coefficients, other constants and numerical estimates are summarized in Table 3.4.

TABLE 5.6

Summary of Coupling Coefficients, Leakage Constants and Numerical Estimates

INTERIOR:

$$\theta = 1 + \frac{h^2}{6\,M^2} + \gamma_1 = 2.234$$

$$\theta_s = 1 - \frac{h^2}{12\,M^2} + \gamma_2 = 0.383$$

PERIPHERY:

Case: Number of Reflector Interfaces (N_r)	θ_p	Numerical Estimate	θ_L	Numerical Estimate	ρ_{Li} Eq. (3.37)	ρ_{Li}^* Eq. (3.37)
2	$1 + \frac{5\,h^2}{12\,M^2} + \gamma_3$	4.086	$\frac{h^2}{2\,M^2}$	3.704	0.26	0.2622
1	$1 + \frac{h^2}{4\,M^2} + \gamma_4$	2.852	$\frac{h^2}{3\,M^2}$	2.469	0.13	0.1311
1/2	$1 + \frac{17\,h^2}{84\,M^2} + \gamma_5$	2.500	$\frac{h^2}{3.5\,M^2}$	2.116	0.065	0.0655

ASSUMPTIONS:

1) Empirical corrections: $\gamma_1 = \ldots = \gamma_5 = 0$.

2) $M^2 = 54\ cm^2$; $h = 20$ cm; $\rho_{sp} = 0$ (EOC).

3) ρ_{Li} was computed using: $D_i = 1.4$ cm; $D_r = 2.25$ cm; $1/B_r = 8$ cm and $E \approx 2.2$ (Appendix C).

4) ρ_{Li}^* was computed using: Eq. (B.36) to calculate $E/D_rB_r = 0.1321$ (for Maine Yankee's EOC albedo, $\beta^* = 0.583$); and $D_i = 1.4$.

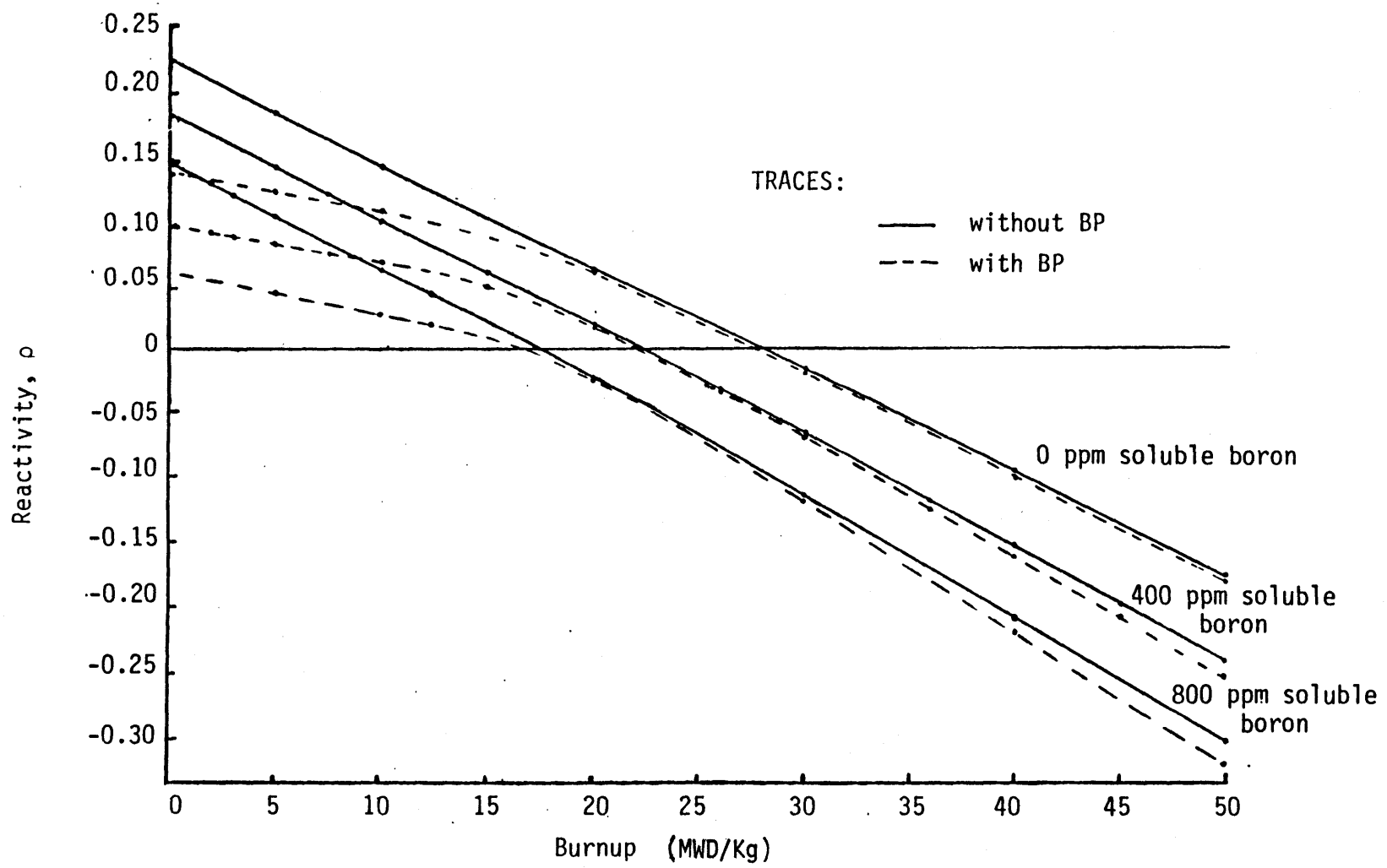

Fig. 5.1 Reactivity as a Function of Burnup for B_4C Poisoned and BP-free Assemblies (3% U-235, Maine Yankee lattice)

both the poisoned and unpoisoned reactivity traces for B_4C BP in a Maine Yankee assembly, generated by the CASMO program. Furthermore, gadolinia - based poisons maintain linearity up to the burnout point, and, roughly speaking, any BOC BP reactivity decrement and slope may be obtained by appropriately selecting the number of shim pins per assembly and their poison loading. Hence, the BP model is represented by:

$$\rho_{bi} = \begin{cases} \rho_{boi} - S_{bi} B_i & , 0 \leq Bi \leq Bi(EOC) \\ r\rho_{boi} & , Bi \geq Bi(EOC) \end{cases} \qquad (5.26)$$

Three core depletion computation methods - synthesis, integrated and step-wise - have been developed and evaluated. The stepwise approach was preferred in this work (due to its flexibility and adequate compromise between speed and accuracy); it essentially consists in performing successive nodal power calculations and core depletions in steps of length ΔB, until achieving the EOC null reactivity condition. A general computational flowchart of the power and burnup calculation method is diagrammed in Fig. 5.2 The same general logical structure is embodied in the LRM-NODAL program written to permit application and evaluation of the analytic methods developed in the course of this research.

5.2.1.3 Accuracy: A Comparison with LEOPARD/PDQ-7 Results

The suitability of the LRM-NODAL core model for its intended applications was determined by comparison of its results with state-of-the-art LEOPARD/PDQ-7 licensing-level calculations for the Maine-Yankee Reactor

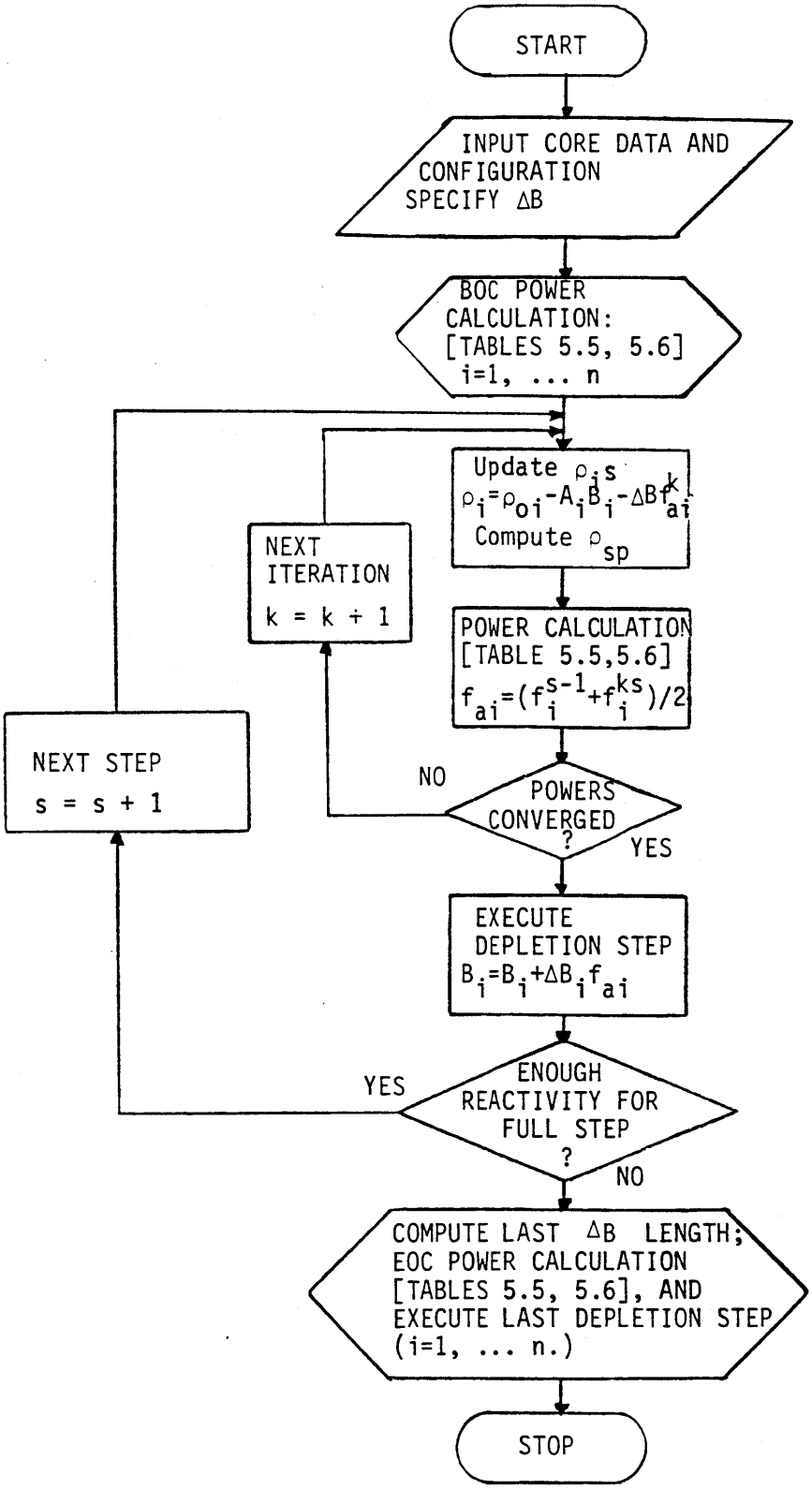

Fig. 5.2 Flowchart for the LRM-NODAL Core Model Computation

core. Figures 5.3 and 5.4 show typical comparisons for the assembly average power fractions, for Maine Yankee cycle 6 core at a cycle burnup of 1 MWD/kg. For the LRM-NODAL code two results are shown: one using unadjusted, analytically estimated coupling and leakage coefficients (Fig. 5.3); and the other using empirically-adjusted peripheral constants (Fig. 5.4), thus mimicking the procedure commonly followed with albedos in other nodal codes, to which these constants are related. In evaluating these comparisons, a difference in conventions should be noted: Maine Yankee PDQ-7 results are average assembly pin powers whereas the LRM-NODAL results are average assembly powers; hence due to the replacement of fuel pins by BP rods (whose number is given in the alphanumeric assembly code, e.g. 8 in J8, 4 in I4, etc.) the LRM nodal powers should be about 4% and 2% lower for assemblies containing 8 and 4 BP pins, respectively.

- good agreement exists for interior assemblies: maximum real errors typically less than 5% and an average error of about 3%;
- for the periphery, the LRM-NODAL program always overpredicted the assembly powers when using unadjusted constants, but a considerable improvement was achieved (maximum errors less than 9 %) when empirically adjusted constants were used;
- the program consistently identified assemblies having the highest powers (the "peakers");
- for the cycle burnup, disagreements existed, mainly due to differences in the data used to independently estimate the parameters to

	1	2	3	4	5	6	7	8	9
1	E16 4 1.0431 1.050 0.6	J0 5 1.1882 1.230 3.5	I4 6 0.9530 0.9311 -2.3	J0 7 1.1329 1.137 0.36	I0 8 0.9698 0.9606 -0.9	J8 9 1.0391 1.000 -3.7	I0 10 0.9169 0.9293 1.3	K8 3 1.0124 1.007 -0.5	K0 1 0.7454 0.8396 12.6
2	J0 5 1.1819 1.230 4.1	I0 11 1.0248 1.042 1.6	J0 12 1.0986 1.098 -0.05	I4 13 0.9424 0.9123 -3.2	J0 14 1.1584 1.151 -0.6	I4 15 0.9863 0.9415 -4.0	K8 3 1.1512 1.144 -0.6	I0 16 0.8316 0.8124 -2.3	K0 1 0.5860 0.6440 9.9
3	I4 6 0.9479 0.9313 -1.7	J0 12 1.0950 1.098 0.3	I4 17 0.9683 0.9394 -3.0	J0 18 1.1300 1.111 -1.7	I0 19 1.132 1.078 -4.7	J0 20 1.2575* 1.253 * -0.3	J8 21 1.1554 1.163 0.6	K0 1 1.0385 1.159 11.6	
4	J0 7 1.1320 1.138 0.5	I4 13 0.9428 0.9122 -3.2	J0 18 1.1303 1.112 -1.6	J4 22 1.2226 1.186 -3.0	J0 23 1.2518 1.211 -3.2	I0 24 1.0439 0.9869 -5.4	I0 25 0.9429 0.9116 -3.3	K0 1 0.8663 0.9607 10.9	
5	I0 8 0.9712 0.9618 -1.0	J0 14 1.1607 1.151 -0.8	I0 19 1.1157 1.078 -3.4	J0 23 1.2550 1.210 -3.6	I0 26 1.0953 1.030 -5.9	J8 27 1.0854 1.017 -6.3	K8 3 0.9845 0.9506 -3.4	K0 1 0.6015 0.6707 11.5	
6	J8 9 1.0413 1.003 -3.7	I4 15 0.9891 0.9468 -4.2	J0 20 1.2619* 1.256* -0.5	I0 24 1.0483 0.9870 -5.8	J8 27 1.0883 1.022 -6.1	K4 2 1.1017 1.075 -2.4	K0 1 0.7093 0.7184 1.3		
7	I0 10 0.9190 0.9315 1.4	K8 3 1.1544 1.146 -0.7	J8 21 1.1596 1.165 0.5	I0 25 0.9467 0.9109 -3.8	K8 3 0.9871 0.9544 -3.3	K0 1 0.7102 0.7168 0.9			
8	K8 3 1.0146 1.009 -0.5	J0 16 0.8334 0.8138 -2.3	K0 1 1.0415 1.163 11.6	K0 1 0.8690 0.9615 10.6	K0 1 0.6031 0.6747 11.8				
9	K0 1 0.7469 0.8409 12.6	K0 1 0.5873 0.6422 9.3							

.....Fuel Type: Maine Yankee/Table 3.5
.....LEOPARD/PDQ-7 (F_1)
.....LRM-NODAL (F_2)
.....% Error = 100 (F_2 - F_1)/F_1

* Indicates Peakers

Fig. 5.3 Assembly Power Comparison at 1 MWD/kg Using Analytically Estimated Parameters

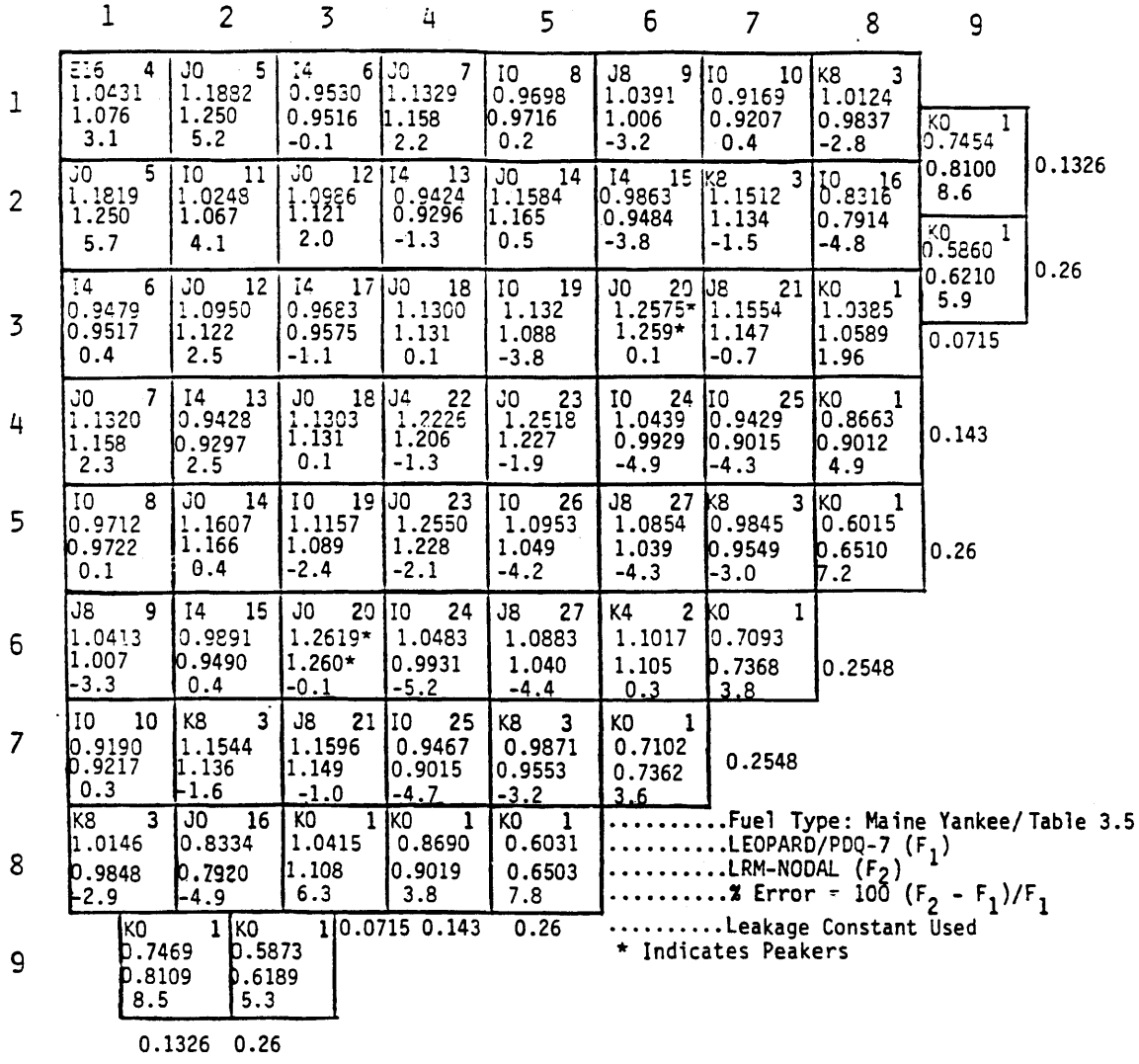

Fig. 5.4 Assembly Power Comparison at 1 MWD/kg, Using Adjusted Leakage Parameters

describe the Maine Yankee core in the LRM-NODAL program, a feature that may be easily overcome through consistent computation of the LRM parameters, especially the slopes, A, and the BP related data.

In view of the errors reported above, it is worth noting that the state-of-the-art licensing-level core analysis systems LEOPARD/PDQ-7 and CASMO/SIMULATE exhibit disagreements of up to 4.3% in assembly average powers, and uncertainties of ±200 KWD/Kg in cycle length predictions [D-4].

Finally, several corrections to overcome analytical and modeling deficiencies in the LRM-NODAL methodology, such as the incorporation of axial leakage, differential thermal leakage and power related feedback effects, through simple adjustment of coupling coefficients or LRM parameters, or the use of differential soluble boron worth weighting factors, provided by appropriate correlations, have been shown to be possible, thus indicating that even better accuracy may be achieved.

5.2.2 Optimization Methodology

It was an important concern in the formulation of the optimization method to take advantage of the simplicity and versatility of the LRM-based core model, i.e. the fact that a change in the basic variable, assembly "reactivity", may be used to represent changes in enrichment, BP concentration or exchange of the assembly itself, which allows the multiple use of the model's analytical developments and computational routines for diverse objectives, such as optimal core reload pattern searches and BP loading and composition optimization.

The optimal core configuration (i.e. assembly arrangement and composition), is essentially determined by the EOC core condition (assembly power and reactivity distributions). As a result of the characteristics of the burnable and soluble poison models adopted in this work, the EOC condition is uniquely defined once the BOC core configuration is determined. Hence, the otherwise complex problems of optimal control of a dynamical system and discrete optimization of core pattern selection, are transformed into a search for the BOC loading pattern and composition (BP loading, when the assembly reactivities are given), that yields the maximum cycle burnup, Bc.

5.2.2.1 Optimization Approaches

The main theoretical foundation for the optimization technique used in the present work relies on the well known steepest gradient approach. Using the Lagrange multiplier method it may be shown that the greatest change in a multivariable function f(x), due to a perturbation $\Delta = [\sum_{i=1}^{n} \delta x_i^2]^{\frac{1}{2}}$ around its current position $X = (x_1, x_2, \ldots, x_n)$ is given by choosing the individual perturbations δx_i, i=1,..., n, proportional to the first partial derivatives, (i.e. the change should follow the gradient direction). Hence the maximum improvement is given by making:

$$\frac{\delta x_i}{\frac{\partial f}{\partial x_i}} = \cdots = \frac{\delta x_i}{\frac{\partial f}{\partial x_i}} \cdots = \frac{\delta x_n}{\frac{\partial f}{\partial x_n}} \qquad (5.27)$$

In order to partially overcome the limitation that the conventional gradient direction search strictly holds for small perturbations only, or as long as linearization around the current position remains valid, the use of the logarithmic derivative (as is done in the sensitivity theory approach [0-1], [0-2]) instead of the conventional partial derivative was investigated and made available as an option in the optimization routines; which was especially useful for the assembly shuffling procedures, where the perturbations are not always small.

The necessary partial derivatives were computed by direct analytic differentiation of the objective function, B_c, of the nodal power equations (at the BOC and EOC conditions) and of the assembly burnup equations, with respect to a generic ρ_x (representing either ρ_o or ρ_{bo}). The cycle average burnup, Bc, given by application of the EOC null reactivity limit is:

$$B_c = \frac{\sum_{j=1}^{n} f_j^e (\rho_{oj} - r\rho_{boj}) - \sum_{j=1}^{n} f_j \rho_{Lj}}{\sum_{j=1}^{n} A_j f_j^e f_{aj}} \qquad (5.28)$$

The equations used to compute the partial derivatives are reproduced in Table 5.7, and the solution scheme is similar to the conventional power and burnup calculation process.

Recognition of the important role of the EOC power fractions in Eqs. (5.28) and (5.36) in the determination of the optimal EOC core condition, as confirmed by the numerical results, led to the formulation of a direct search method for the maximum B_c configuration. In this method, the EOC power fractions are used essentially in the same

TABLE 5.7

Equations for the Calculation of Derivatives Used in Core Reload Optimization Routines

Nodal Power Derivatives:

BOC:

Interior Nodes:

$$\frac{\partial f_i}{\partial \rho_x} = \frac{\frac{\partial f_i}{\partial \rho_x}\left(\Gamma_i + \frac{\partial \rho_{sp}}{\partial \rho_x}\right) - \frac{\theta_s}{N_p}\sum_{j=1}^{N_p} f_j\left(\Gamma_j - \frac{\partial \rho_{sp}}{\partial \rho_x}\right) + \frac{1}{N_p}\sum_{j=1}^{N_p}\left[1 - \theta_s(\rho_{oi} - \rho_{boi} - \rho_{sp})\right]\frac{\partial f_j}{\partial \rho_x}}{1 - \theta(\rho_{oi} - \rho_{boi} - \rho_{sp})} \qquad (5.29)$$

Peripheral Nodes:

$$\frac{\partial f_i}{\partial \rho_x} = \frac{\theta_p f_i\left(\Gamma_i - \frac{\partial \rho_{sp}}{\partial \rho_x}\right) - \frac{\theta_s}{N_p}\sum_{i=1}^{N_p} f_j\left(\Gamma_j - \frac{\partial \rho_{sp}}{\partial \rho_x}\right) + \frac{1}{N_p}\sum_{i=1}^{N_p}\left[1 - \theta_s(\rho_{oi} - \rho_{boi} - \rho_{sp})\right]\frac{\partial f_j}{\partial \rho_x}}{1 - \theta_p(\rho_{oi} - \rho_{boi} - \rho_{sp}) + \theta_L \rho_{Li}} \qquad (5.30)$$

where,

$$\frac{\partial \rho_{sp}}{\partial \rho_x} = \frac{1}{\sum_{j=1}^{n} f_j W_i}\left\{f_x \Gamma_x + \sum_{j=1}^{n}(\rho_{oj} - \rho_{boj})\frac{\partial f_j}{\partial \rho_x} - \sum_{j=1}^{m} \rho_{Lj}\frac{\partial f_j}{\partial \rho_x}\right\} \qquad (5.31)$$

and,

$$\Gamma_k = \frac{d}{d\rho_x}\left(\rho_{ok} - \rho_{bok} + S_{bk} B_k\right) \qquad (5.32)$$

subject to the normalization condition:

$$\sum_{j=1}^{n}\frac{\partial f_j}{\partial \rho_x} = 0 \qquad (5.33)$$

TABLE 5.7 (Continued)

Equations for the Calculation of Derivatives Used in Core Reload Optimization Routines

EOC:

Interior Nodes:

$$\frac{\partial f_i}{\partial \rho_x} = \frac{\theta_p f_i \left[\Gamma_i - \frac{\partial}{\partial \rho_x}(A_i B_i)\right] - \frac{\theta_s}{N_p}\sum_{j=1}^{N_p} f_j \left[\Gamma_j - \frac{\partial}{\partial \rho_x}(A_i B_i)\right] + \frac{1}{N_p}\sum_{j=1}^{N_p}\left\{1 - \theta_s\left[\Gamma_j - \frac{\partial}{\partial \rho_x}(A_j B_j)\right]\right\}\frac{\partial f_j}{\partial \rho_x}}{1 - \theta_p(\rho_{oi} - r\rho_{boi} - A_i B_i) + \theta_L \rho_{Li}} \tag{5.34}$$

Peripheral Nodes:

$$\frac{\partial f_i}{\partial \rho_x} = \frac{\theta f_i \left[\Gamma_i - \frac{\partial}{\partial \rho_x}(A_i B_i)\right] - \frac{\theta_s}{N_p}\sum_{j=1}^{N_p} f_j \left[\Gamma_j - \frac{\partial}{\partial \rho_x}(A_i B_i)\right] + \frac{1}{N_p}\sum_{j=1}^{N_p}\left\{1 - \theta_s\left[\Gamma_j - \frac{\partial}{\partial \rho_x}(A_i B_i)\right]\right\}\frac{\partial f_i}{\partial \rho_x}}{1 - \theta(\rho_{oi} - r\rho_{boi} - A_i B_i)} \tag{5.35}$$

Burnup Derivatives:

Cycle Burnup:

$$\frac{\partial B_c}{\partial \rho_x} = \frac{\sum_{j=1}^{n} f_j^e \Gamma_j + \sum_{j=1}^{n}\left[\rho_{oj} - r\rho_{boj} - A_j\left(B_j + \frac{B_c}{2} f_j^e\right)\right]\frac{\partial f_j^e}{\partial \rho_x} - \sum_{j=1}^{m} \rho_{Lj}\frac{\partial f_j^e}{\partial \rho_x} - B_c \sum_{j=1}^{n}\left(\frac{A_j f_j^e}{2}\frac{\partial f_j^b}{\partial \rho_x} + f_{aj} f_j^e \frac{dA_j}{d\rho_x}\right)}{\sum_{j=1}^{n} A_j f_j^e f_{aj}} \tag{5.36}$$

Assembly Burnup:

$$\frac{\partial B_i}{\partial \rho_x} = f_{ai}\left(\frac{\partial B_c}{\partial \rho_x}\right) + \frac{B_c}{2}\left(\frac{\partial f_i^b}{\partial \rho_x} + \frac{\partial f_i^e}{\partial \rho_x}\right) \tag{5.37}$$

where the superscripts b and e denote BOC and EOC, respectively.

way as are derivatives of the objective function in the gradient method; i.e., the maximum gain in the objective function is obtained by performing assembly shuffles such that the changes in reactivities are proportional to the derivatives (in the gradient method) or to $P_i = f_i^e (1 - \rho_{oi}) \cdot (1 - \rho_{Li})$ (in the direct search method). This procedure ultimately corresponds to matching the rankings of reactivities and $\frac{\partial B_c}{\partial \rho_i}$, or P_i, at each iteration of the optimization process.

5.2.2 Optimization Algorithms and Applications

Algorithms for the unconstrained maximum cycle burnup and optimal BP allocation have been fully developed and implemented in the LRM-NODAL program. The basis for the systematic incorporation of constraints on power peaking, as well as other limits such as assembly burnup, has also been developed, but not fully implemented and tested, due to speed and memory limitations of the microcomputer (TRS-80 Model III, 48K) with which the computations were carried out. The potential application of the methodology to tailor-design assembly or batch compositions has been examined and described within the framework of the steepest gradient approach.

The essential features of the maximum cycle burnup algorithm in LRM-NODAL are:

- the initial pattern may be defined by the user or input from a library of prototypic patterns;
- assemblies may be restricted to certain fixed positions in the core;

- options are available to use the direct search method for a preliminary optimization, and to select either the conventional or the logarithmic derivative in the steepest ascent search.

Figure 5.5 summarizes the step-by-step convergence of the algorithms when applied to the Maine Yankee Cycle 6 Core, and Figs. 5.6 and 5.7 show the configurations generated by the direct search and gradient methods, respectively.

The main features of the BP allocation algorithm are:

- the maximum allowable BP concentration limit in each assembly may be user defined;
- absolute priority is given to depression of excessive power fractions to within specified limits;
- the steepest gradient approach is used to allocate BP such as to optimize the burnup histories (that is, maximizing B_c) whenever possible without conflicting with the objectives above.

The results of this algorithm as applied to the Maine Yankee Cycle 6 core are shown in Fig. 5.8. Only the seven indicated assemblies have been allowed to be poisoned, and a power peaking constraint of 1.3 was imposed at BOC and EOC. As can be seen, consistent with the basic principle of maximization of EOC reactivity importance, the EOC powers of these assemblies are within the convergence tolerance of the maximum allowed; and, moreover, the derivatives, $\partial B_c/\partial \rho_{boi}$, are all positive, indicating that more BP allocation in these assemblies would further increase the cycle burnup (which for the BP-free core was 9815.74 KWD/Kg).

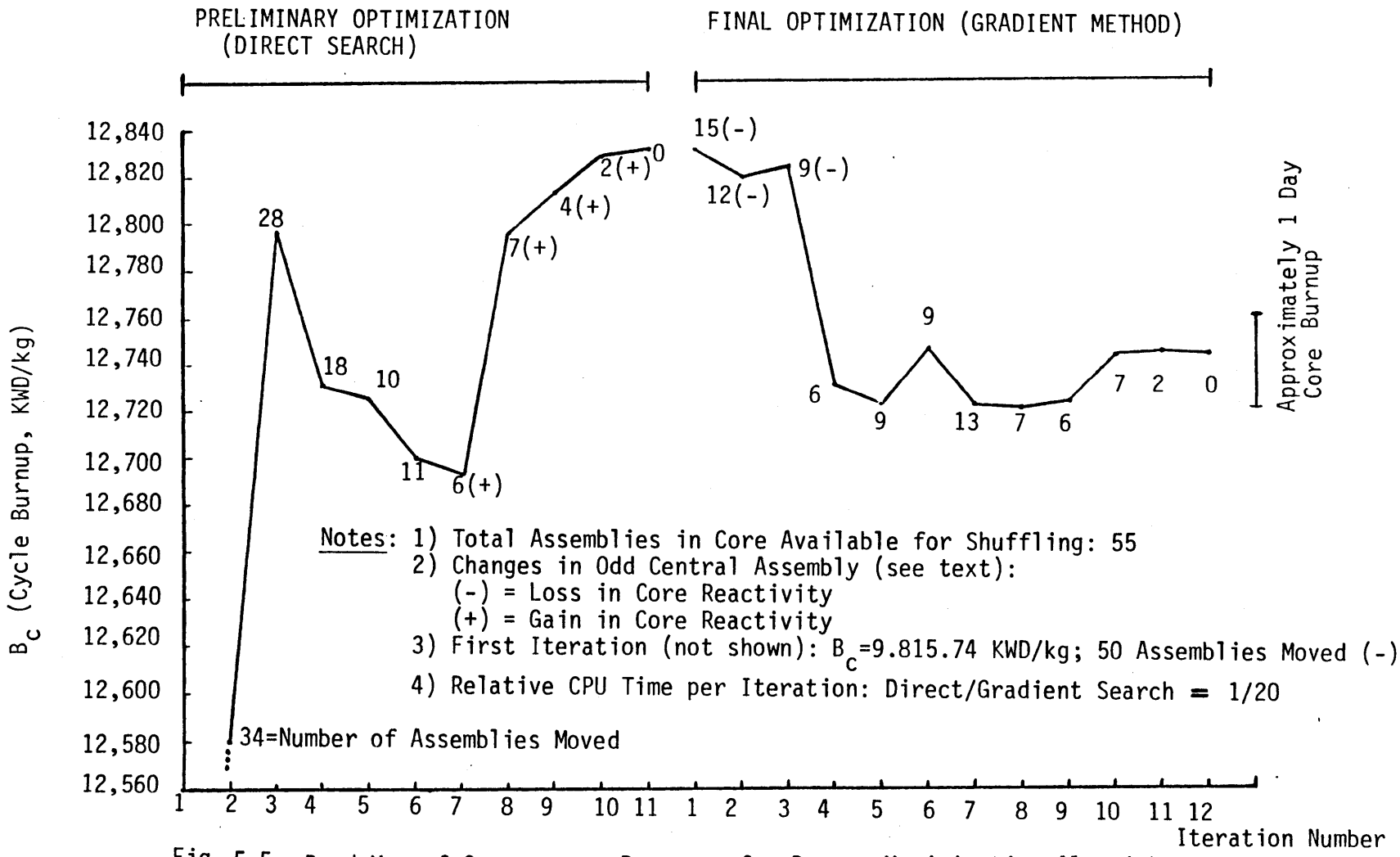

Fig. 5.5 Road Map of Convergence Progress for Burnup Maximization Algorithm

	1	2	3	4	5	6	7	8	9
1	0.129688 6	0.132068 5	0.142816 4	0.153055 3	0.221973 1	0.0221973 1	0.11244 7	0.048282 13	0.001905 20
2	0.132068 5	0.132068 5	0.153055 3	0.221973 1	0.221973 1	0.221973 1	0.10976 8	0.389345 15	-0.010820 23
3	0.143816 4	0.142816 4	0.155491 2	0.221973 1	0.221973 1	0.221973 1	0.090801 11	0.223811 17	
4	0.153055 3	0.15491 2	0.221973 1	0.221973 1	0.221973 1	0.129688 6	0.530786 12	0.220128 18	
5	0.221973 1	0.221973 1	0.221973 1	0.221973 1	0.221973 1	0.0960070 10	0.036076 16	-0.00628 22	
6	0.221973 1	0.221973 1	0.2219730 1	0.221973 1	0.10976 8	0.048282 13	-0.00619 21		
7	0.11244 7	0.11244 7	0.100552 9	0.908015 11	0.038934 15	0.001905 20			
8	0.042828 13	0.042834 14	0.036762 16	0.0220128 18	-0.00619 21	.....ρ_{oi} .....Ranking of ρ_{oi}			
9	0.009915 19	-0.01082 23							

Fig. 5.6 Assembly Arrangement Generated by the Preliminary Direct Search Method

	1	2	3	4	5	6	7	8	9
1	0.221973 1 3067.6	0.221973 1 2854.6	0.221973 1 2586.9	0.14281 4 1989.3	0.129688 6 1863.6	0.221973 1 2400.6	0.221973 1 2603.0	0.048282 13 1125.8	-0.00619 21 271.8
2	0.221973 1 2854.6	0.221973 1 2639.8	0.155491 2 2179.4	0.129688 6 1864.3	0.11244 7 1820.8	0.221973 1 2471.9	0.155491 2 2155.3	0.042830 14 958.4	-0.010820 23 181.8
3	0.221973 1 2586.9	0.221973 1 2472.6	0.153055 3 2061.6	0.13068 5 1894.8	0.221973 1 2308.0	0.221973 1 2533.5	0.090801 11 1632.7	0.022381 17 659.3	
4	0.142816 4 1989.3	0.11244 7 1831.0	0.132068 5 1894.3	0.142816 4 1985.0	0.221973 1 2463.2	0.221973 1 2549.1	0.05207 12 1239.1	0.022128 18 434.8	
5	0.129688 6 1863.6	0.10926 8 1791.0	0.153055 3 2061.8	0.221973 1 2496.1	0.221973 1 2588.8	0.096007 10 1683.4	0.03607 16 792.3	-0.00628 22 209.2	
6	0.221973 1 2400.5	0.221973 1 2440.7	0.221973 1 2536.0	0.221973 1 2616.0	0.10976 8 1777.8	0.038934 15 900.3	0.001905 20 280.9		
7	0.221973 1 2603.0	0.221973 1 2526.3	0.100552 9 1761.8	0.090815 11 1458.6	0.389345 15 846.3	0.001905 20 289.0			
8	0.048282 13 1125.8	0.42828 13 1043.2	0.360762 16 748.4	0.022012 18 479.4	-0.00699 21 224.8	$\ldots\ldots\rho_{oi}$ $\ldots\ldots\rho_{oi}$ $\ldots\ldots\ldots\frac{\partial B_c}{\partial \rho_{oi}}$	Ranking		
9	0.009915 19 311.6	-0.01082 23 199.0							

Fig. 5.7 Final Assembly Arrangement Generated by the Conventional Gradient Method

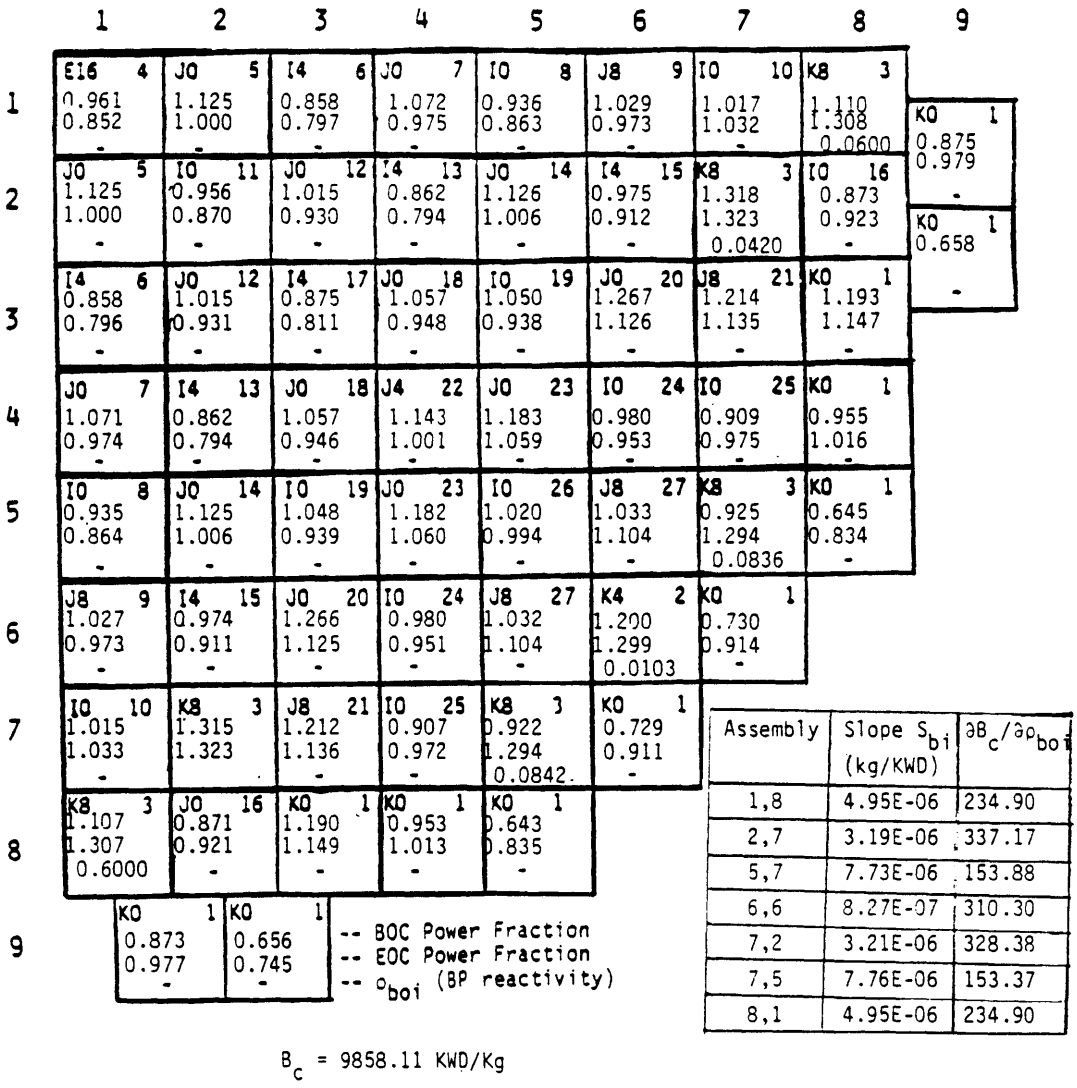

Assembly	Slope S_{bi} (kg/KWD)	$\partial B_c/\partial \rho_{boi}$
1,8	4.95E-06	234.90
2,7	3.19E-06	337.17
5,7	7.73E-06	153.88
6,6	8.27E-07	310.30
7,2	3.21E-06	328.38
7,5	7.76E-06	153.37
8,1	4.95E-06	234.90

B_c = 9858.11 KWD/Kg

Fig. 5.8 Maine Yankee Cycle 6 Core Results after Optimal BP Allocation

5.3 Conclusions

The main conclusions arrived at in the course of the present research may be summarized as follows:

A) Regarding the Methodology:

- The LRM based nodal model provides an adequate description of PWR cores for optimization-oriented applications:
- The gradient methods and the direct search approach have been shown to be successful in yielding substantially improved core burnup configurations, and are thus able to answer the fundamental question as to which assembly exchanges to pursue to maximize the gain in the objective function, B_C;
- The gradient approach, as formulated here, is able to successfully determine optimal loading assignments of an idealized burnable poison (as defined by Loh [L-2]);

B) Regarding the Results:

From the analytical and the numerical results obtained using the LRM-NODAL code, the optimal core configuration (i.e. yielding the maximum B_C) may be described as having the following characteristics:

- The most reactive assemblies are at their highest powers at the EOC (thus maximizing their importance), and the converse applies to the least reactive;
- The power histories and profiles are such as, usually, to produce relatively higher leakage at BOC, evolving to a lower leakage

at EOC (the lowest possible for typical state-of-the-art PWRs) but always consistent with the maximization of EOC core reactivity importance;

These results are consistent with the characteristics of the well-known low-leakage core loading schemes now gaining favor as PWR reload patterns, as well as with the results reported by other researchers, especially, Suzuki and Kiyose [S-8], [S-2], and Huang and Levine [H-4].

It may also be concluded that for typical state-of-the-art PWRs, a large number of core configurations yielding burnups close to the maximum achievable (or having burnups oscillating well within the range of the calculational uncertainty of the model used) do exist, and it is expected that the satisfaction of acceptable power peaking constraints will dominate the last stages of the optimization process.

5.4 Recommendations for Future Work

Based on the results obtained in the work just reported, several productive areas for its extension appear worthwhile:

- The computational routines and software should be transferred to a faster and larger (RAM) computer, to permit the full implementation and testing of the incorporation of constraints.
- The Gradient Projection Method deserves to be evaluated for use in the optimization procedures especially due to its efficiency in dealing with constrained optima;
- Improved (faster) methods to compute the derivatives required

in the algorithms $\left(\frac{\partial B_c}{\partial \rho_x}, \frac{\partial B_i}{\partial \rho_x}, \frac{\partial f_i^b}{\partial \rho_x}, \text{and } \frac{\partial f_i^e}{\partial \rho_x}\right)$ should be investigated and implemented.

- Review and improvements of the computer programming techniques should also prove beneficial in terms of computing efficiency and speed;
- For maximum utility the nodal subroutine in LRM-NODAL needs to be expanded to: allow quarter-assembly analysis, handle three-dimensional problems, relax the isobuckling approximation, and incorporate reconstruction of intra-assembly power shapes (using the analytical solutions of Appendix B);
- The addition of a three-dimensional analysis capability will allow the explicit incorporation of axial constraints, which in the present two-dimensional method can only be partially and indirectly considered (via specification of different BOC and EOC power peaking limits that account for the variation of the axial power shape with burnup);
- Relaxation of the linearity of fuel and BP reactivity traces as a function of burnup should also be considered. Specifically, with little additional effort, the capability to analyze poison burn-out before EOC may be incorporated. Such BP traces, despite not being preferred (since they do not maximize cycle burnup and tend to yield higher intra-cycle peak power) are of interest because they correspond to the behavior of some burnable poison designs in contemporary use;

- Generalized Perturbation Theory, as developed by Williams [W-5], [W-6] and others, to compute sensitivity coefficients for neutron/nuclide coupled fields, should be examined because of its potential to allow the use of state-of-the-art methods (such as QUANDRY) in optimization methods similar to the one developed in the present research;
- Use of Optimal Control Theory within the framework of the LRM-based core model should be investigated;
- The coupling of the direct search method for maximum burnup, as developed here, with dynamic programming techniques to account for power peaking and other constraints should be examined;
- And, finally, extensive applications of the methodology developed in the present work to core reload pattern and composition optimization should be carried out, to obtain valuable further insight into the nature of the optimality condition. It may even be possible, in the long run, to develop a set of purely prescriptive rules which would permit realization of a near optimum assembly array without the need to exercise a full-capability optimization program.

APPENDIX A

Analysis of the Power Versus Flux Normalization Factor $\left[\frac{\nu}{\kappa}\frac{M^2}{D_1}\right]$ and Related Parameters

Previous researchers [S-1], [L-2], [K-1], relying upon LEOPARD calculations, assumed D_1 and M^2 constant and the κ/ν variation a negligible function of burnup in the Advanced Linear Reactivity Model. However, correlations reported earlier by Rieck [R-1], also based on LEOPARD, appeared to contradict these assumptions. Therefore the investigation summarized here was carried out to clarify these issues and to guide possible simplification regarding the incorporation of the normalization factor in the nodal power expression.

A parametric analysis of the factor $\left[\frac{\nu}{\kappa}\frac{M^2}{D_1}\right]$ was performed using results from the LEOPARD, CASMO and DIT codes, for typical (state-of-the-art) low-enriched uranium-fueled PWR lattices. As a representative base case, a 3 w/o enriched uranium, standard Maine Yankee lattice, was considered, and minor variations about this configuration were examined. (Hence, the extrapolation of the conclusions to substantially different configurations and compositions is not warranted without further analysis.)

Figure A.1 shows the behavior predicted by LEOPARD and CASMO for the factor $\left[\frac{\nu}{\kappa}\frac{M^2}{D_1}\right]$ as a function of burnup and local reactivity, for the base case. The LEOPARD result may be well represented by a constant, and for CASMO a good representation is provided by a linear correlation (with coefficient of determination R^2=0.9335):

$$\left[\frac{\nu}{\kappa}\ \frac{M^2}{D_1}\right] \approx 0.4919\ (1 - 0.145\rho),\ \text{neut.cm/MeV} \qquad (A.1)$$

LEOPARD has also been used to examine several other cases, and the virtual invariance of $\left[\frac{\nu}{\kappa}\frac{M^2}{D_1}\right]$ with burnup (ranging from 0 to 40 MWD/kg) was consistently maintained. For example: for a 3 w/o enrichment, standard Maine Yankee lattice, the factor ranged from 0.498785 (at 1 MWD/kg) to 0.502152 (at 18 MWD/kg); for a very dry lattice having a cell fuel-to-moderator volume ratio of 0.75 and 4.5 w/o U-235 enrichment, the variation was only from 0.525582 (at 1 MWD/kg) to 0.521759 (at 39 MWD/kg).

The fortunate cancellation of factors, resulting in the parametric invariance predicted by LEOPARD or in the possible linearization with local reactivity as suggested by CASMO, is a welcome feature, allowing for an easy incorporation of the factor in the functional form of the nodal power expression (derived in Chapter 3). The discrepancy between LEOPARD and CASMO, however, deserves further analysis. Table A.1 indicates that the relative source of discrepancy originates almost equally from κ and D_1/M^2 ($= \Sigma_{12} + \Sigma_{a1}$), with ν having negligible influence. Thus separate evaluation of each constituent parameter will be performed.

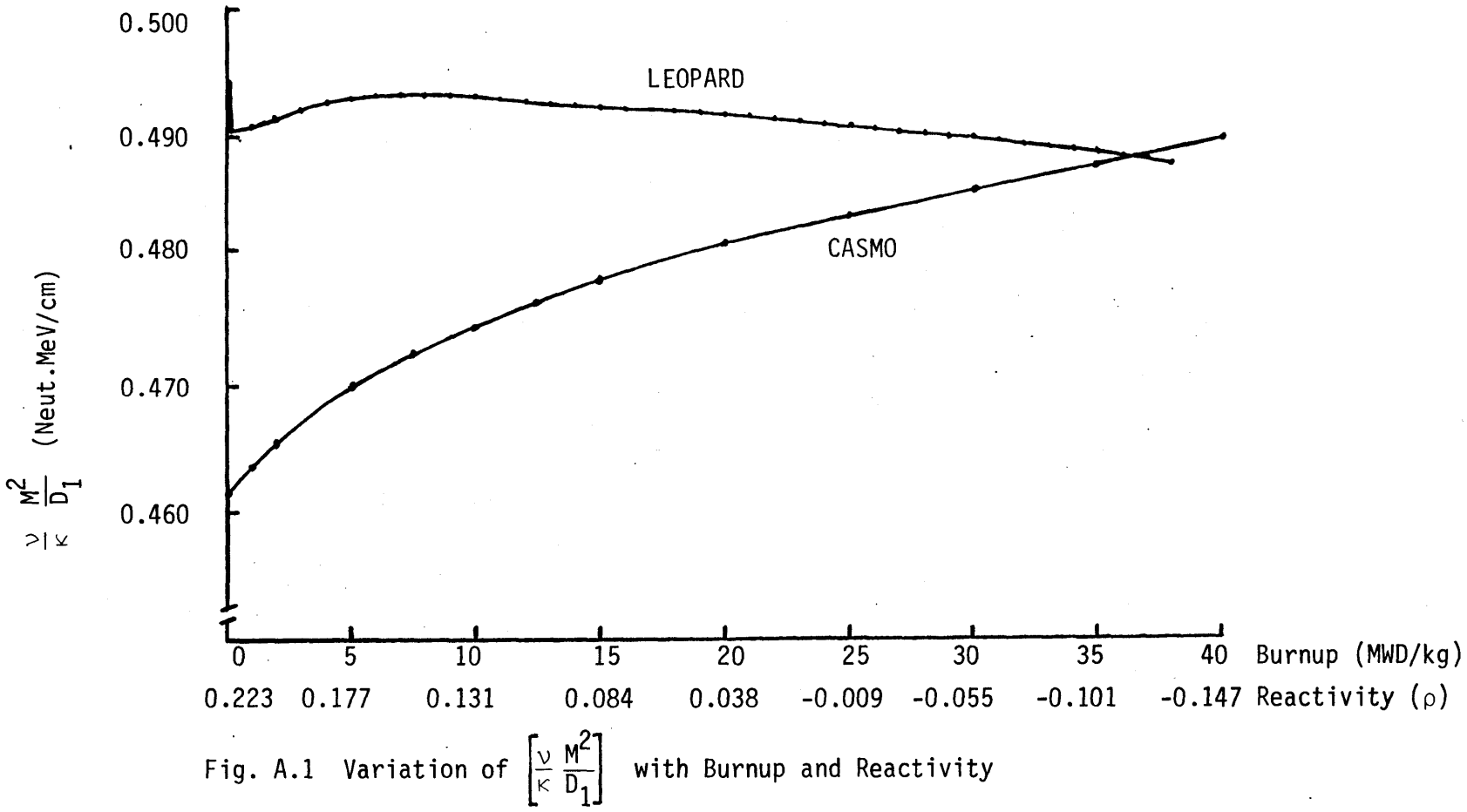

Fig. A.1 Variation of $\left[\frac{\nu}{\kappa}\frac{M^2}{D_1}\right]$ with Burnup and Reactivity

TABLE A.1

CASMO/LEOPARD Ratio for Parameters ν, κ, D_1/M^2

BURNUP (MWD/kg)	$\frac{\nu \text{ (CASMO)}}{\nu \text{ (LEOPARD)}}$	$\frac{\kappa \text{ (CASMO)}}{\kappa \text{ (LEOPARD)}}$	$\frac{D_1/M^2 \text{ (CASMO)}}{D_1/M^2 \text{ (LEOPARD)}}$
1	1.0088	1.0296	1.0259
10	1.0079	1.0212	1.0161
20	1.0062	1.0139	1.0081
35	1.0031	1.0033	0.9994

A.1 κ/ν Variation with Burnup and Reactivity

In addition to being part of the power versus flux normalization the κ/ν variation is important in the system reactivity balance (modified eigenvalue) calculation, of Eq. (2.20). Figure A.2 shows the results of CASMO, LEOPARD and DIT computations (the DIT results are for 2.9 w/o U-235). Since ν is consistently calculated by LEOPARD and CASMO, as shown in Table A.1, the difference should be explained by the computation of the energy released per fission. CASMO and DIT are in good agreement, but between these two codes and LEOPARD two differences are evident: first, the absolute value of κ/ν is always lower for LEOPARD; second, the behavior (slope) with burnup is markedly different. The explanation resides on computational methodologies and data differences, as will be discussed.

LEOPARD computes separately the energy contributions from fission and radiative captures. The energy released by capture of neutrons in the reactor materials is calculated from a detailed neutron balance, considering individually the number of neutrons captured in each material and the subsequent energy release characteristic of each material. The energy from fissions is calculated from two components: direct fission energy, and kinetic energy of the non-leaking neutrons. CASMO's simplified approach attributes to each fissioning nuclide a global amount of energy released per fission, which includes a fixed fraction due to

radiative capture. CASMO does, however, smear throughout the assembly an energy fraction due to gammas.

The different approaches regarding the radiative capture energy treatment explain the main difference in the shapes of the curves shown in Fig. A.2. To a lesser extent, the neutron kinetic energy treatment may also contribute. This conclusion is substantiated by the curve "LEOPARD without capture gammas", in the same figure. This curve, which is almost parallel to those of CASMO and DIT was calculated from LEOPARD data as follows: using the material transmutation and neutron balances, as well as the power fractions shared by each material, given by LEOPARD at each burnup step, and the data of energy released per neutron capture provided by the LEOPARD manual [B-1], the energy due to capture gammas in all materials was computed and subtracted from the original LEOPARD κ/ν curve (also plotted in Fig. A.2). The radiative capture energy fraction increases from about 2% (at BOL) to about 5% (at EOL $\sim$ 40 MWD/kg) of the total energy released per fission. The increase is mainly attributable to incremental captures in heavy isotopes (due to the buildup of plutonium isotopes and spectral changes affecting U-238 captures), as well as in the growing fission product inventory.

The observed difference in κ/ν is also due to the outdated data used in LEOPARD for energy released from fission, as well as for

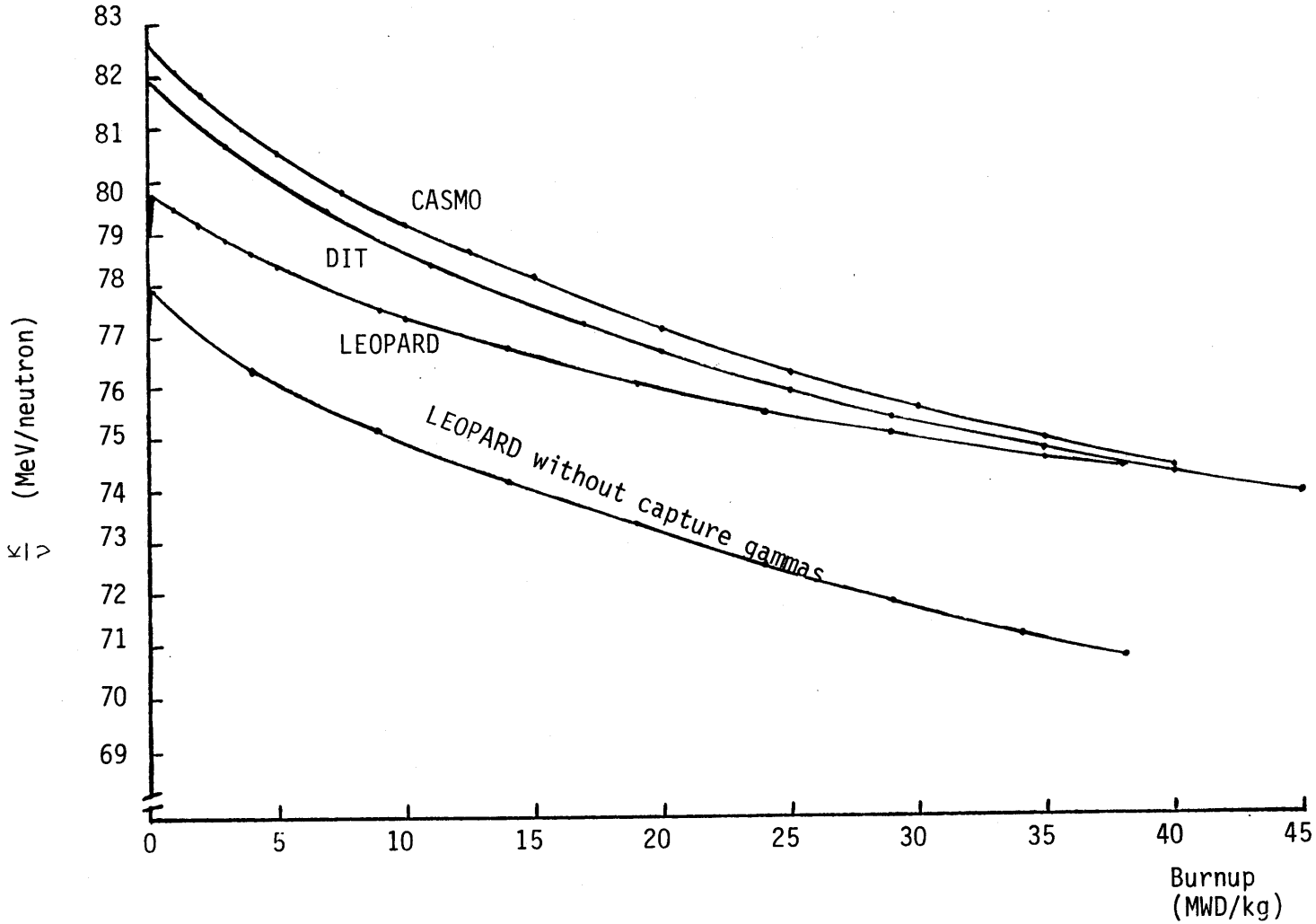

Fig. A.2 Energy Release per Fission Neutron as a Function of Burnup

some radiative captures. The program's manual [B-1] recognizes that the mean energy per fission is too low "by about 5 out of 200". Detailed compilation of state-of-the-art data is beyond the scope of the present research. References [U-1] and [S-7] provide a critical review of the energy released in nuclear fission. References [H-7], [K-3] and [K-4] report data and measurements of gamma energy released in neutron captures carried out at MIT. Table A.2 displays the values used in CASMO (for total energy released per fission event), in LEOPARD (for direct fission energy only), and the values given by reference [U-1] for the lowest estimate of direct fission energy effectively recoverable, and for the total recoverable energy from a fission event. These total energy values are the direct energy plus the energy resulting from capture of the excess (ν - 1) neutrons released per fission, computed for the EBR-II fast reactor spectrum and composition. The actual amount of effectively recoverable energy depends on the irradiation history. Typically, however, less than 0.25% of the total energy is recovered after 30 days of the originating events. The good agreement existing between CASMO and the values of Ref. [U-1] for total energy seems to indicate that in CASMO all energy from capture of excess neutrons is assigned to the assembly of origin. In a reactor the excess local neutrons leak to the periphery, into adjoining assemblies, thereby exporting some of their associated capture and kinetic energy. Table A.3 shows the energy released in radiative captures for selected elements, as given in the LEOPARD manual [B-1], and references [U-1]

TABLE A.2

Energy Released per Fission (MeV)

Nuclide	CASMO (TOTAL)	LEOPARD (DIRECT)	Unik and Gindler [U-1] (DIRECT)	(TOTAL)
U-235	202.2	189.0	192.4	201.7
U-236	202.2	189.0	-	-
U-238	199.7	186.7	191.2	203.0
Pu-239	209.1	196.0	198.4	210.6
Pu-240	209.7	196.0	196.3	210.5
Pu-241	211.0	198.0	199.4	212.0
Pu-242	211.0	198.0	197.9	212.1

TABLE A.3

Energy (MeV) Released in Radiative Captures for Selected Elements

Element	LEOPARD [B-1]	KALRA [K-1]	UNIK and GINDLER [U-1]
O	4.140	4.140	4.140
Fe	7.790	7.770	-
B-10	2.880	-	-
U-235	6.430	6.540	5.670
U-238	4.062	4.800	5.670
Pu-240	5.710	5.240	-
Pu-241	6.060	-	-
Pu-242	5.500	-	-
Xe-135	4.000	-	-
Sm-149	7.980	-	-
Other Fission Products	4.000	-	-

and [K-4], the last two for fast neutron spectra. The numbers for U-238 indicate that a non-negligible difference may exist and contribute to the overall deficiency in LEOPARD's predicted value.

From this data and analysis some conclusions, not all related directly to the main focus of this research, may be drawn:

- The κ/ν results from LEOPARD appear to represent in a better fashion the physical phenomena (on a relative basis, at least), even though giving absolute values which are too low;
- These lower values may cause an underprediction of the achievable burnup from a given amount of transmutations;
- The incorporation of a method, similar to that of LEOPARD, to calculate in detail the contributions of radiative neutron captures in the advanced codes CASMO and DIT, may result in a small power peaking margin gain, due to the relative shifting of gamma energy to older (less reactive) fuel. It appears that gamma smearing (transport) would not affect this expectation, since, despite increasing fractionally with burnup the total gamma energy would still be lower in the old fuel because of the reduced power fraction. Accurate analysis of the gamma energy transport, deposition and heating is beyond the scope of the present research. Such a study, for fast reactors, has been carried out at MIT by Kalra [K-4].

A.2 D_1/M^2, D_1 and M^2 Variation with Burnup

The parameter D_1/M^2 is actually the sum of $\Sigma_{a1} + \Sigma_{12}$, as may be seen from Eq. (2.5). Figure A.3 shows the variation of this parameter with burnup, for the base case. As can be seen from the plot of the individual constituents, Σ_{12} in Fig. A.4 and Σ_{a1} in Fig. A.5, the discrepancy is mainly due to the higher values given by CASMO for Σ_{12} at BOL.

The diffusion coefficient, D_1, is another quantity of interest, since according to Eq. (2.5), $M^2 = D_1/(\Sigma_{a1} + \Sigma_{12})$. In Fig. A.6, the undoubtedly unphysical peaking of D_1 given by LEOPARD (at $\sim$ 25 MWD/kg, for this case), is noticeable. Similar deflections normally appear in LEOPARD results (e.g., in Rieck's [R-1] correlations for M^2), but seem to be the result of numerical convergence problems rather than actual phenomenological behavior. For CASMO two diffusion coefficients are depicted: a) D_1 calculated from the transport cross section ($D_1 \approx 1/3\ \Sigma_{tr}$); b) fundamental mode D_1, which for epithermal energy groups reproduces the fundamental mode solution when used in homogeneous diffusion theory calculations. A typical plot of M^2, as predicted by LEOPARD, is given in Fig. A.7. The influence of the peak in D_1 may be noted, causing a "bumpy" variation of M^2 with burnup.

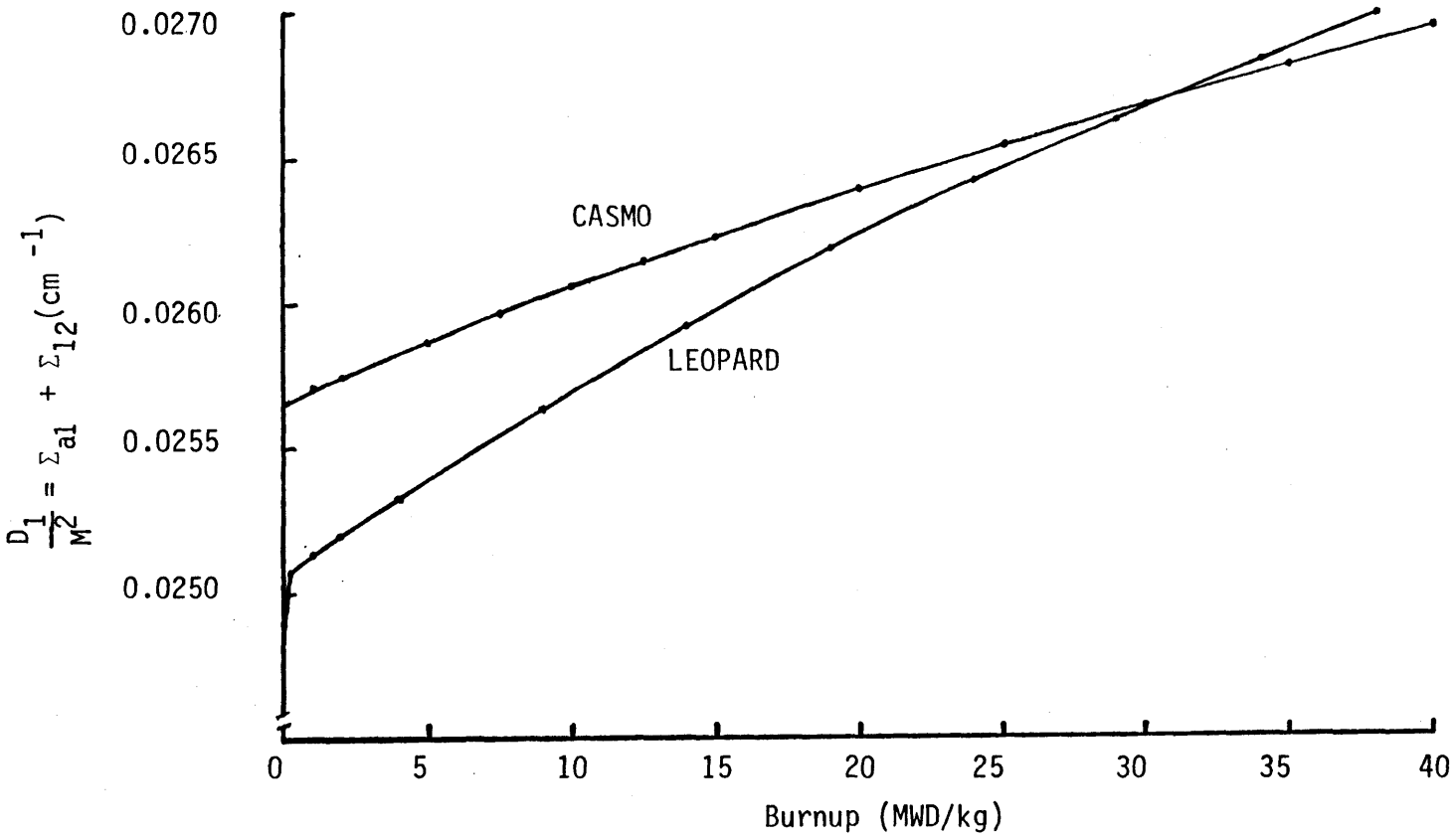

Fig. A.3 Variation of D_1/M^2 as a Function of Burnup

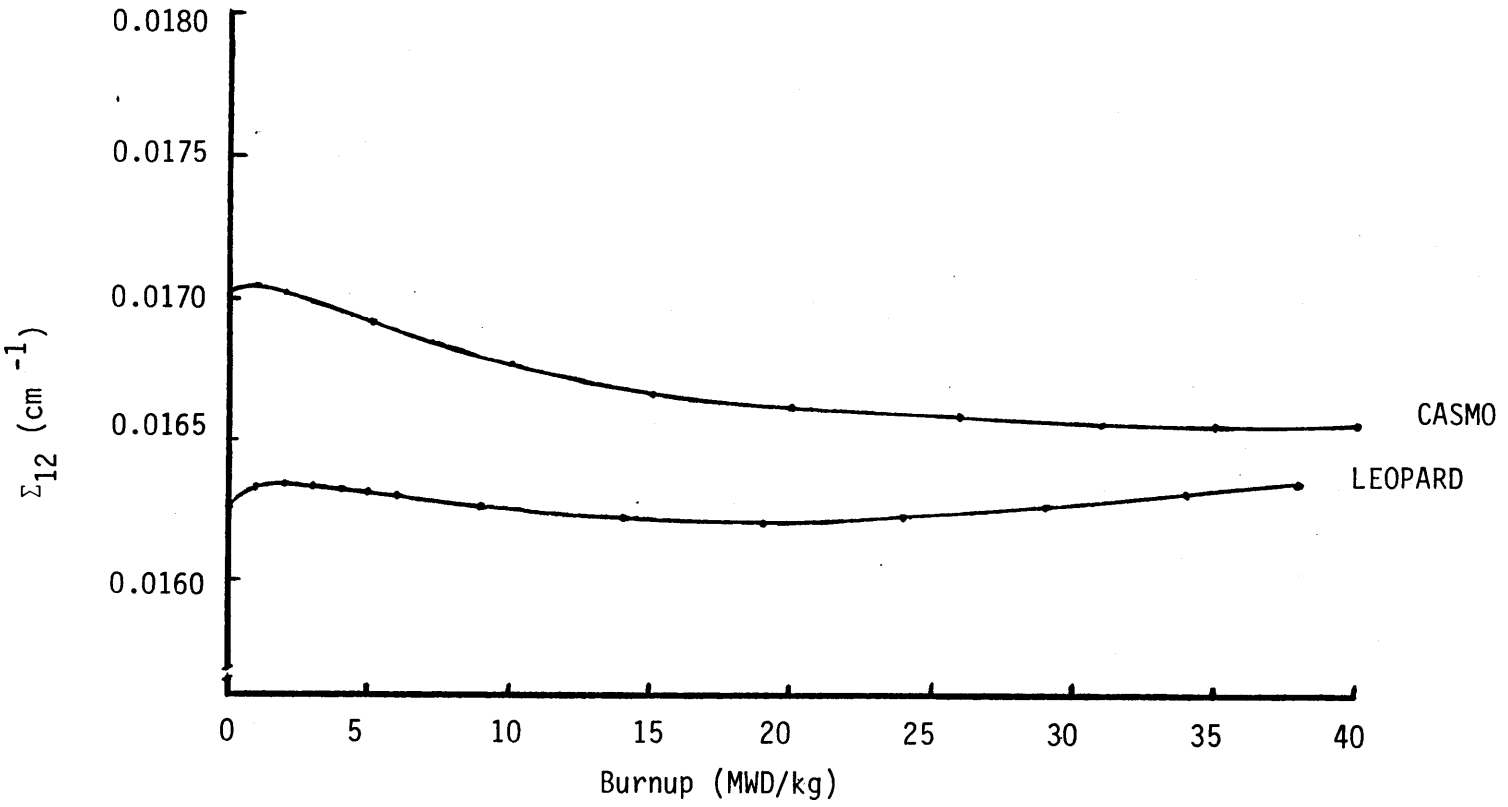

Fig. A.4 Variation of Σ_{12} as a Function of Burnup

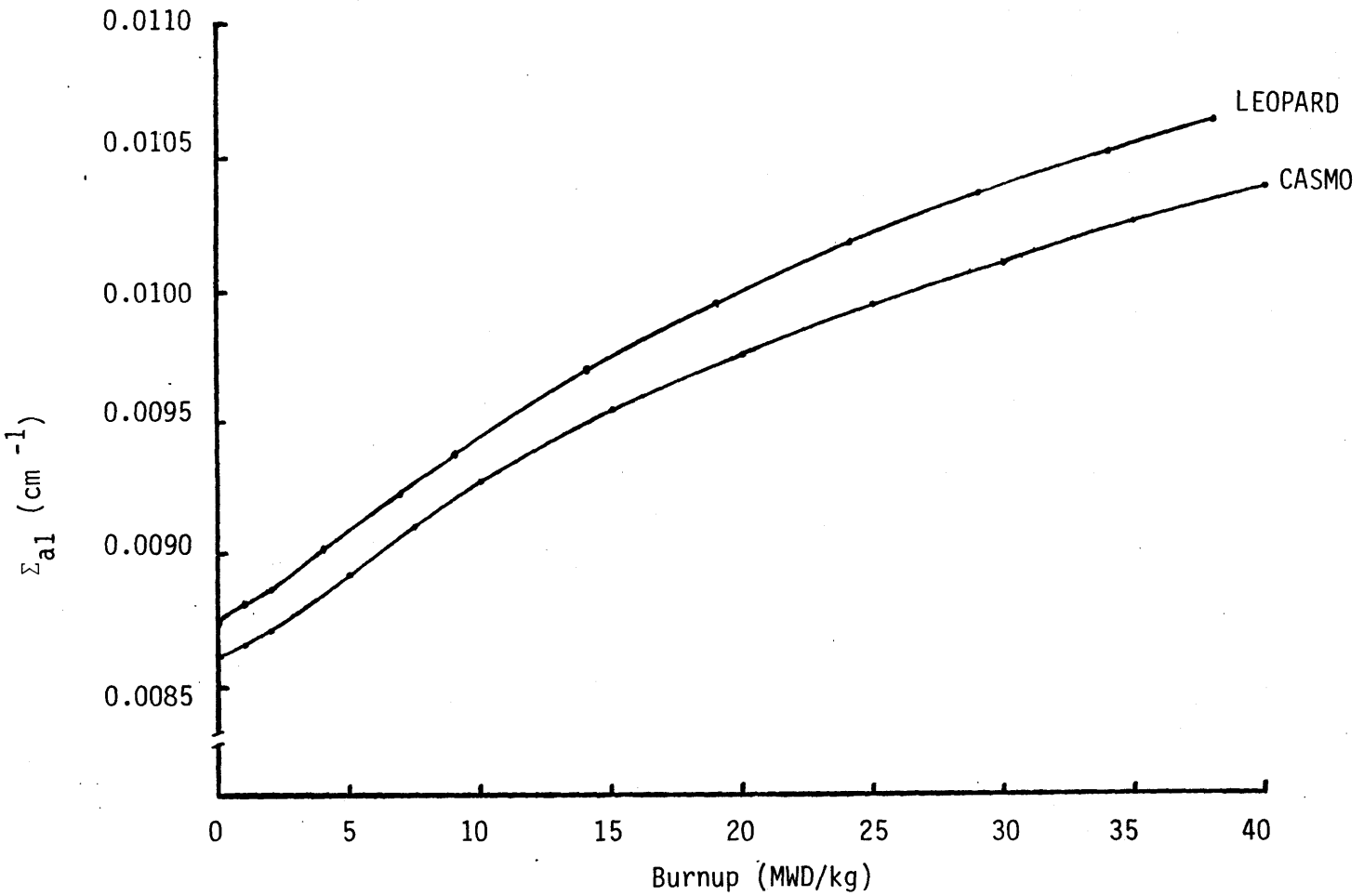

Fig. A.5 Variation of Σ_{a1} as a Function of Burnup

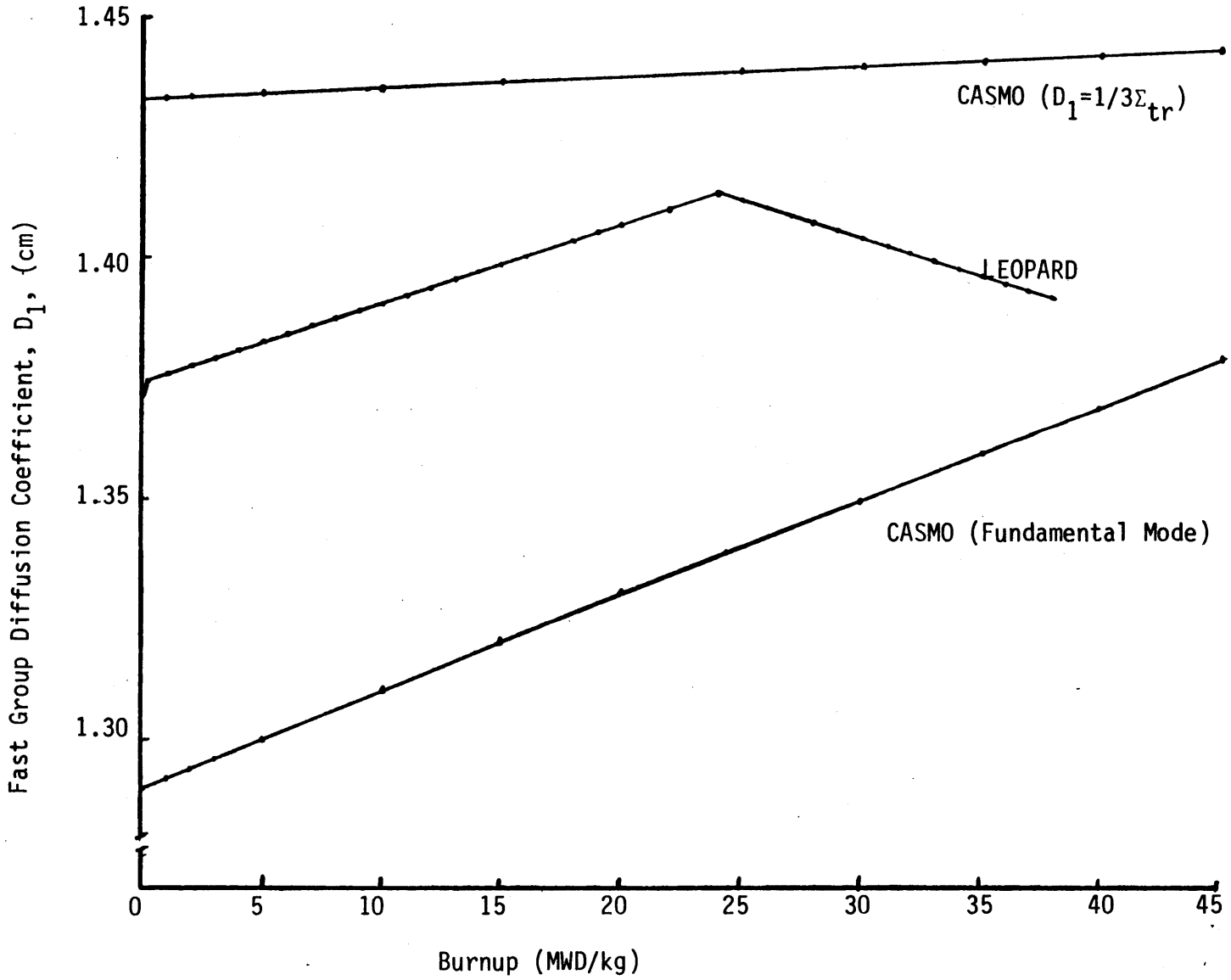

Fig. A.6 Variation of D_1 as a Function of Burnup

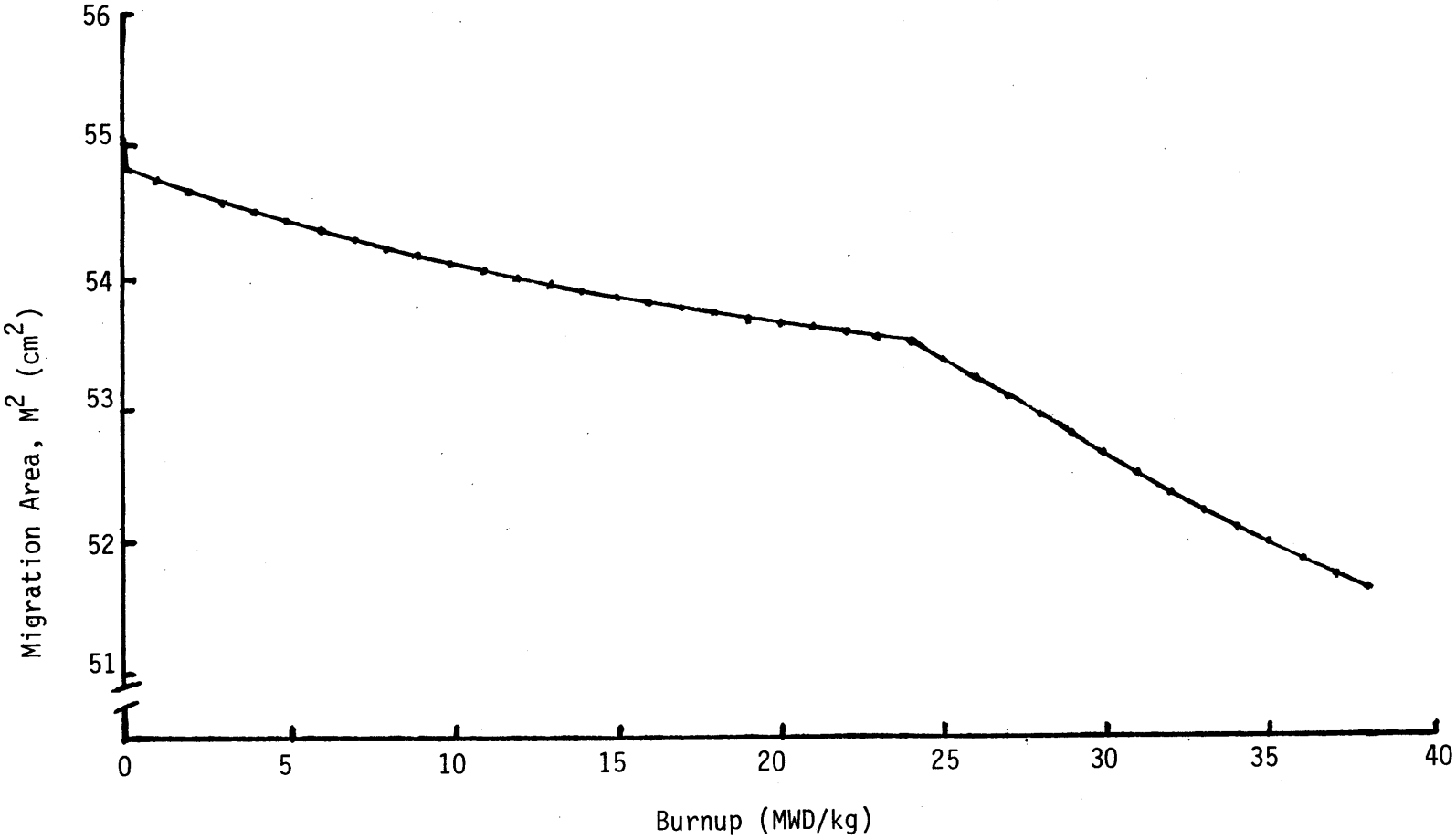

Fig. A.7 Variation of M^2 as a Function of Burnup (LEOPARD)

A.3 Power Feedback Effect on D_1/M^2

Considering the discrepancy in D_1/M^2 between LEOPARD and CASMO, and assuming that CASMO produces more accurate values, a slight net variation in the parameter $\left[\frac{\nu}{\kappa}\frac{M^2}{D_1}\right]$ with burnup would result. However, in a reactor, fresher and older fuel usually operate at different power levels, hence feedback effects may affect the parametric behavior. LEOPARD was used to explore this effect by comparing the variation of the parameter as a consequence of an increase in power (relative to an average assembly) from 1 to 1.3, and a decrease to 0.7, representing the typical range in an actual reactor. Since cross-flow is negligible in PWRs [T-2], temperature changes are proportional to the power fraction changes. Table A.4 shows the resulting input data.

Figure A.8 shows that, as expected, power feedback will reduce the actual variation of D_1/M^2 in a beneficial way, i.e., such as to mitigate the net variation of $\left[\frac{\nu}{\kappa}\ \frac{M^2}{D_1}\right]$ predicted by CASMO. The flattening is the net result of two opposed effects: a) due to the hardened spectrum, Σ_{a1} increases with power; b) due to higher temperatures Σ_{12} decreases with an increase in power, dominating the net effect.

TABLE A.4

Power Feedback Analysis Data

Power Fraction		1.0	0.7	1.3
Power Density (w/cm^3)		80.85	56.60	105.10
Temperature (°F)	Pellet	1,232	1,028	1,435
	Cladding	630	607	653
	Moderator	576	569	583

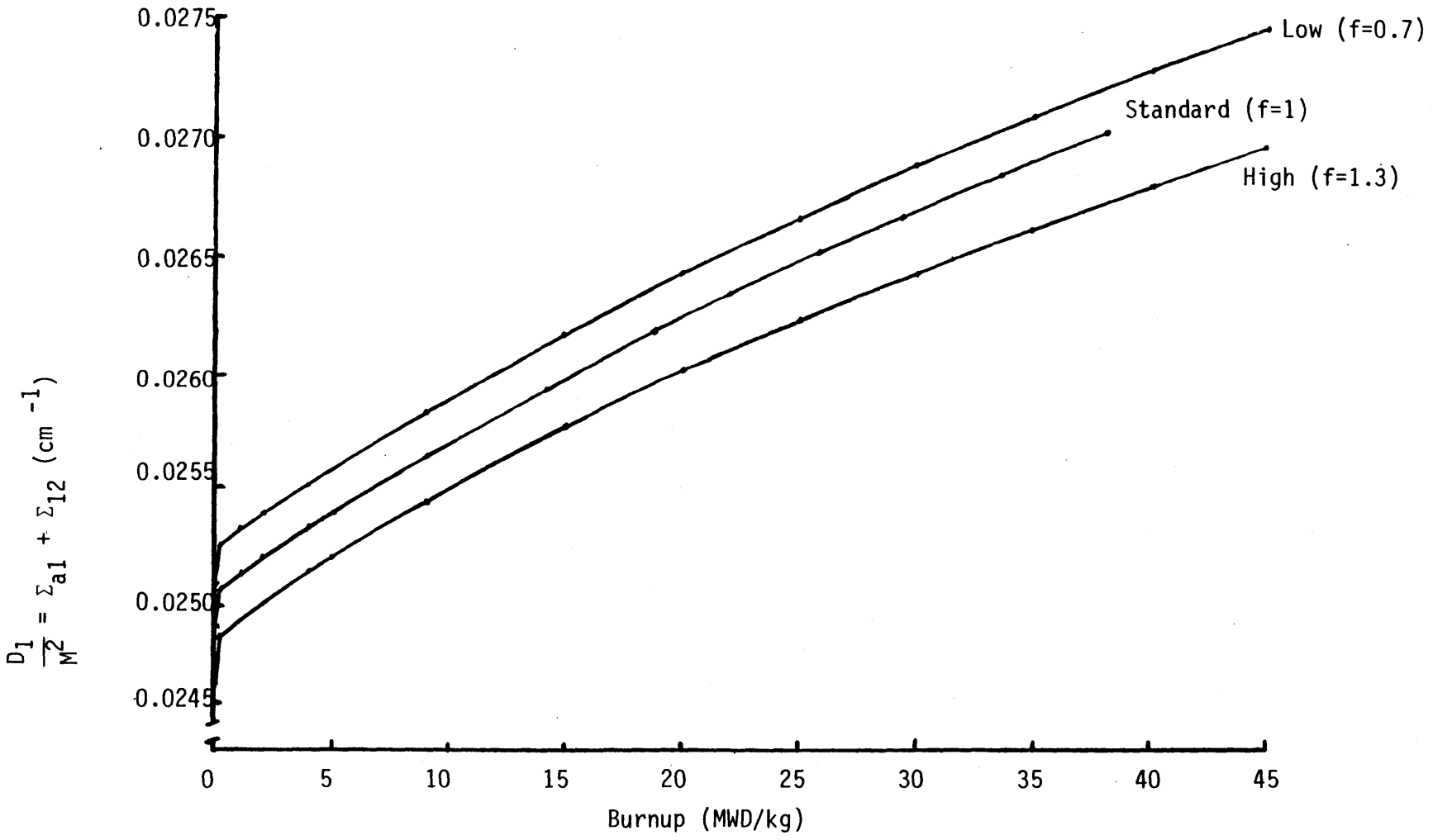

Fig. A.8 Power Feedback Effects on D_1/M^2

A.4 Conclusions

The analysis and data presented in this appendix support the conclusion that the actual dependence of the normalization factor $\left[\frac{\nu}{\kappa}\frac{M^2}{D_1}\right]$ with burnup and local reactivity, is mild and may well be represented in a linear relation, if not as a constant. This relationship is amenable for inclusion in the formalism of the nodal power expressions developed in Chapter 3. LEOPARD predicts that the parameter is quasi-invariant with burnup (and local reactivity). For CASMO a linear relation with local reactivity (Eq. (A.1)) provides a good representation. Two possible effects - a) the detailed computation of radiative neutron captures, smoothing the power deposition throughout the reactor; and b) power feedback effects on the D_1/M^2 parameter - would cause the parametric variation predicted by CASMO to be even less steep and more linear. The influence of soluble boron is not expected to affect the conclusions of this appendix, but one aspect that remains to be investigated is the influence of burnable poisons on the normalization factor $\left[\frac{\nu}{\kappa}\ \frac{M^2}{D_1}\right]$.

APPENDIX B

Two Dimensional Solution of the One-and-One-Half Group Model

In this appendix the two-dimensional version of the "one-and-one-half" group equation is solved. Each assembly is assumed to be a square node, having sides of width h. D_1 is assumed constant throughout the core. Figure B.1 shows a quarter-core representation of the Maine Yankee Reactor. Basically three different configurations of nodes and surroundings are present: a) interior nodes, surrounded by four other fueled nodes; b) peripheral nodes with two reflector interfaces; and, c) peripheral nodes with one reflector interface. Still another case, peripheral nodes with a half reflector interface are present, but here this case will be treated, approximately, by a combination of reflected and unreflected nodes. A detailed solution will be exhibited only for the first two cases, since the solution for the third configuration may then be postulated by inference.

Equation (2.12) written out for two-dimensions (for a critical reactor) becomes:

$$\nabla^2\Phi(x,y) + \frac{(k_\infty(x,y) - 1)}{M^2}\Phi(x,y) = 0 \qquad (B.1)$$

where the subscript 1 on Φ_1 has been dropped. This is an elliptic differential equation having a unique solution within a closed

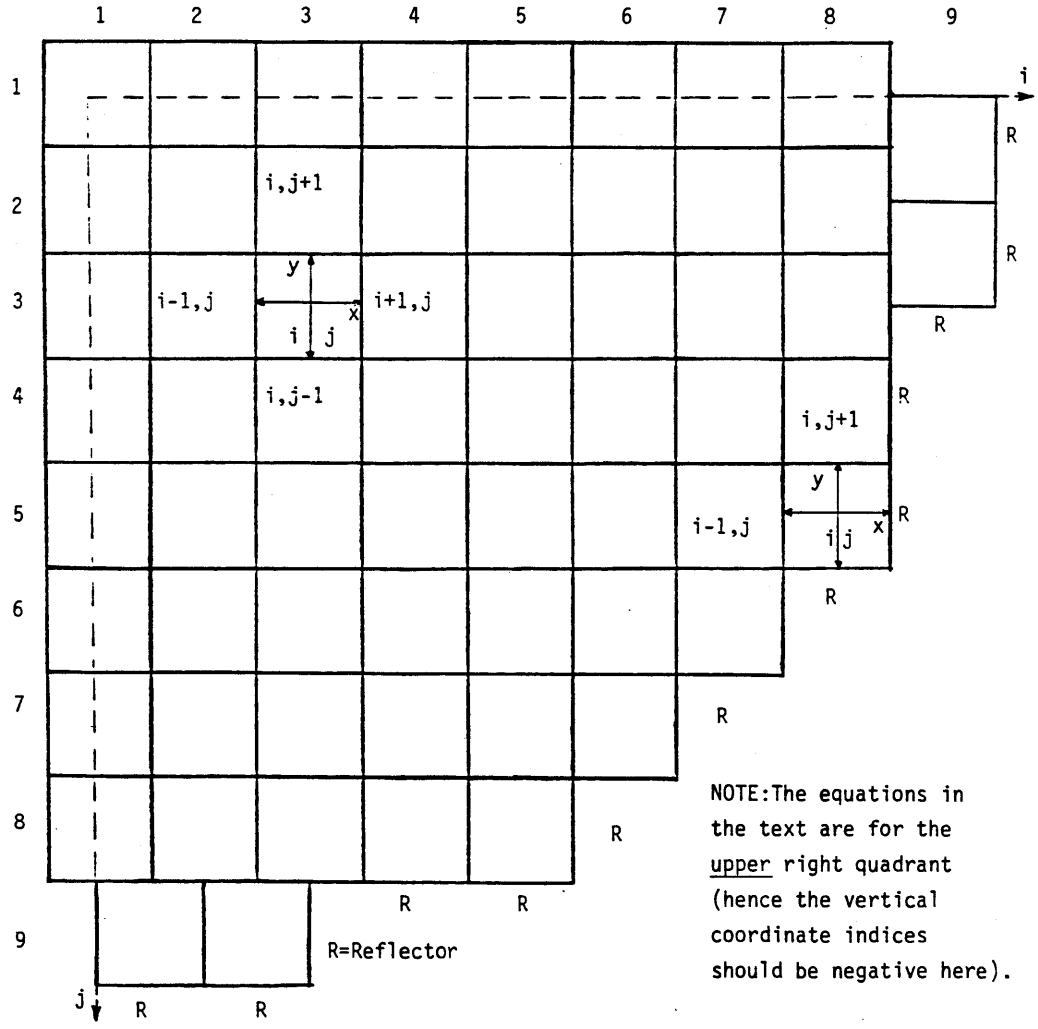

Fig. B.1 Representation of 1/4 Core of the Maine Yankee Reactor, and the Coordinate System for 2-D Nodal Solution of the 1½ Group Equation.

boundary, under conditions of the Dirichlet-Neumann type, i.e., peripheral value or slope of Φ specified. Defining

$$B_{ij}^2 = \frac{(k_{\infty ij} - 1)}{M_{ij}^2} = - \frac{\rho_{ij}}{(1 - \rho_{ij})\, M_{ij}^2} \tag{B.2}$$

and

$$B_{ij}^2 = \alpha_{ij}^2 + \beta_{ij}^2 \tag{B.3}$$

where i and j refer to the cartesian coordinates of the homogenized nodes (see Fig. B.1), and where α_{ij}^2 and β_{ij}^2 refer to the apportionment of the buckling in the X-direction and Y-direction, respectively, the solution to Eq. (B.1) is

$$\Phi(x,y) = C\, e^{\pm i(\alpha_{ij}\, x + \beta_{ij}\, y)}$$

where C is a constant to be determined from the boundary conditions, and i is the imaginary parameter, $\sqrt{-1}$.

Depending on the value of B_{ij}^2 (hence α_{ij}^2 and β_{ij}^2) under conventional strict procedures, the solution (B.4) would involve either trigonometric or hyperbolic functions. Since mathematical equivalence exists between both types of functions, here the hyperbolic will be arbitrarily preferred. Then, generically,

$$\Phi_{ij}(x,y) = [A_{ij} \cosh(\alpha_{ij}\, x) + G_{ij} \sinh(\alpha_{ij}\, x)] \cdot$$
$$\cdot [C_{ij} \cosh(\beta_{ij}\, y) + D_{ij} \sinh(\beta_{ij}\, y)] \tag{B.5}$$

The solution of the problem may be simplified (under the assumption of spatial separability), by integrating the function over the orthogonal direction, and defining:

$$\Phi_{ij}(x) = \int_{-h/2}^{h/2} \Phi_{ij}(x,y)\, dy \qquad (B.6')$$

$$= \frac{2\, C_{ij}}{\beta_{ij}} \sinh(\beta_{ij}\, h/2) \left[A_{ij} \cosh(\alpha_{ij}\, x) + G_{ij} \sinh(\alpha_{ij}\, x)\right] \qquad (B.6)$$

and,

$$\Phi_{ij}(y) = \int_{-h/2}^{h/2} \Phi_{ij}(x,y)dx \qquad (B.7')$$

$$= \frac{2\, A_{ij}}{\alpha_{ij}} \sinh(\alpha_{ij}\, h/2) \left[C_{ij} \cosh(\beta_{ij}\, y) + D_{ij} \sinh(\beta_{ij}\, x)\right] \qquad (B.7)$$

Similarly, the integrated flux of the node may be defined:

$$\Phi_{ij} = \int_{-h/2}^{h/2} \int_{-h/2}^{h/2} \Phi_{ij}(x,y)dy\, dx \qquad (B.8')$$

$$\Phi_{ij} = \left[\frac{2A_{ij}}{\alpha_{ij}} \sinh(\alpha_{ij}\, h/2)\right] \cdot \left[\frac{2C_{ij}}{\beta_{ij}} \sinh(\beta_{ij}\, h/2)\right] \qquad (B.8)$$

Now the solution may be carried out for each direction X and Y, once the boundary conditions are specified. The solution could be otained and written out in matrix formalism, where each node would be formally coupled to the surrounding ones. Here, the solution will be obtained for individual nodes under the assemption that the necessary

quantities from the surrounding nodes (Φ_{ij} and the directional apportionments of $B_{ij}^2 = \alpha_{ij}^2 + \beta_{ij}^2$) are known (as would be the case in an iterative solution procedure). The objective is to solve for Φ_{ij}, as a function of the characteristics of the node ij itself and its surroundings.

B.1 Interior Nodes

Defining, generically, the quantity,

$$b_{ij} = \frac{2C_{ij}}{\beta_{ij}} \sinh(\beta_{ij}\, h/2) \tag{B.9}$$

proceeding in the X-direction, and requiring continuity of fluxes and net neutron currents at the interfaces of the nodes, the following equations result:

for the fluxes:

$$\begin{aligned} & b_{ij}\,[A_{ij} \cosh(\alpha_{ij}\, h/2) - G_{ij} \sinh(\alpha_{ij}\, h/2)] \\ & = b_{i-1,j}\,[A_{i-1,j} \cosh(\alpha_{i-1,j}\, h/2) + G_{i-1,j} \sinh(\alpha_{i-1,j}\, h/2)] \end{aligned} \tag{B.10}$$

and

$$\begin{aligned} & b_{ij}\,[A_{ij} \cosh(\alpha_{ij}\, h/2) + G_{ij} \sinh(\alpha_{ij}\, h/2)] \\ & = b_{i+1,j}\,[A_{i+1,j} \cosh(\alpha_{i+1,j}\, h/2) - G_{i+1,j} \sinh(\alpha_{i+1,j}\, h/2)] \end{aligned} \tag{B.11}$$

for the currents:

$$D_{ij}\alpha_{ij}b_{ij}\left[G_{ij}\cosh(\alpha_{ij}\,h/2)-A_{ij}\sinh(\alpha_{ij}\,h/2)\right]$$
$$=D_{i-1,j}\alpha_{i-1,j}b_{i-1,j}\left[G_{i-1,j}\cosh(\alpha_{i-1,j}\,h/2)+A_{i-1,j}\sinh(\alpha_{i-1,j}\,h/2)\right] \tag{B.12}$$

and

$$D_{ij}\alpha_{ij}b_{ij}\left[G_{ij}\cosh(\alpha_{ij}\,h/2)+A_{ij}\sinh(\alpha_{ij}\,h/2)\right]$$
$$=D_{i+1,j}\alpha_{i+1,j}b_{i+1,j}\left[G_{i-1,j}\cosh(\alpha_{i-1,j}\,h/2)-A_{i-1,j}\sinh(\alpha_{i-1,j}\,h/2)\right] \tag{B.13}$$

Assuming as known the integrated fluxes:

$$\Phi_{i-1,j}=b_{i-1,j}\left[\frac{2A_{i-1,j}}{\alpha_{i-1,j}}\sinh(\alpha_{i-1,j}\,h/2)\right] \tag{B.14}$$

and

$$\Phi_{i+1,j}=b_{i-1,j}\left[\frac{2A_{i+1,j}}{\alpha_{i+1,j}}\sinh(\alpha_{i+1,j}\,h/2)\right] \quad , \tag{B.15}$$

then the constants $A_{i-1,j}$ and $A_{i+1,j}$ may be written as:

$$A_{i-1,j}=\frac{\Phi_{i-1,j}\cdot\alpha_{i-1,j}}{b_{i-1,j}\cdot 2\sinh(\alpha_{i-1,j}\,h/2)} \tag{B.16}$$

and

$$A_{i+1,j}=\frac{\Phi_{i+1,j}}{b_{i+1,j}}\cdot\frac{\alpha_{i+1,j}}{2\sinh(\alpha_{i+1,j}\,h/2)} \quad . \tag{B.17}$$

Since the diffusion coefficient is assumed constant, the following relations hold:

from Eqs. (B.10) and (B.16):

$$b_{i-1,j}G_{i-1,j}\sinh(\alpha_{i-1,j}\,h/2) = b_{ij}\left[A_{ij}\cosh(\alpha_{ij}\,h/2) - G_{ij}\sinh(\alpha_{ij}\,h/2)\right] - \frac{\Phi_{i-1,j}\,\alpha_{i-1,j}}{2\tanh\alpha_{i-1,j}\,h/2)} \tag{B.18}$$

from Eqs. (B.11) and (B.17):

$$b_{i+1j}G_{i+1j}\sinh(\alpha_{i+1j}\,h/2) = -b_{ij}\left[A_{ij}\cosh(\alpha_{ij}\,h/2) + G_{ij}\sinh(\alpha_{ij}\,h/2)\right] + \frac{\Phi_{i+1,j}\,\alpha_{i+1,j}}{2\tanh(\alpha_{i+1,j}\,h/2)} \tag{B.19}$$

from Eqs. (B.12) and (B.16):

$$b_{i-1,j}G_{i-1,j}\cosh(\alpha_{i-1,j}\,h/2) = \frac{b_{ij}\,\alpha_{ij}}{\alpha_{i-1,j}}\left[G_{ij}\cosh(\alpha_{ij}\,h/2) - A_{ij}\sinh(\alpha_{ij}\,h/2)\right] - \frac{\Phi_{i-1,j}\,\alpha_{i-1,j}}{2} \tag{B.20}$$

from Eqs. (B.13) and (B.17):

$$b_{i+1,j}G_{i+1,j}\cosh(\alpha_{i+1j}\,h/2) = \frac{b_{ij}\alpha_{ij}}{\alpha_{i+1,j}}\left[G_{ij}\cosh(\alpha_{ij}\,h/2) + A_{ij}\sinh(\alpha_{ij}\,h/2)\right] + \frac{\Phi_{i+1,j}\,\alpha_{i+1,j}}{2} \tag{B.21}$$

Equations (B.18) and (B.20) may be manipulated to yield:

$$A_{ij}\, b_{ij} \left[\cosh(\alpha_{ij}\, h/2) + \frac{\alpha_{ij}}{\alpha_{i-1,j}} \tanh(\alpha_{i-1,j}\, h/2) \cdot \sinh(\alpha_{ij}\, h/2)\right]$$
$$- G_{ij}\, b_{ij} \left[\sinh(\alpha_{ij}\, h/2) + \frac{\alpha_{ij}}{\alpha_{i-1,j}} \tanh(\alpha_{i-1,j}\, h/2) \cdot \cosh(\alpha_{ij}\, h/2)\right]$$
$$= - \frac{\Phi_{i-1,j}\, \alpha_{i-1,j}}{2} \left[\tanh(\alpha_{i-1,j}\, h/2) - \coth(\alpha_{i-1,j}\, h/2)\right] = \frac{\Phi_{i-1,j}\alpha_{i-1,j}}{\sinh(\alpha_{i-1,j}\, h)} \qquad \text{(B.22)}$$

Similarly Eqs. (B.19) and (B.21) may be combined to obtain:

$$A_{ij}\, b_{ij} \left[\cosh(\alpha_{ij}\, h/2) + \frac{\alpha_{ij}}{\alpha_{i+1,j}} \tanh(\alpha_{i+1,j} h/2) \cdot \sinh(\alpha_{ij}\, h/2)\right]$$
$$G_{ij}\, b_{ij} \left[\sinh(\alpha_{ij}\, h/2) + \frac{\alpha_{ij}}{\alpha_{i+1,j}} \tanh(\alpha_{i+1,j}\, h/2) \cdot \cosh(\alpha_{ij}\, h/2)\right]$$
$$= - \frac{\Phi_{i+1,j}\alpha_{i+1,j}}{2} \left[\tanh(\alpha_{i+1,j}\, h/2) - \coth(\alpha_{i+1,j}\, h/2)\right] = \frac{\Phi_{i+1,j}\alpha_{i+1,j}}{\sinh(\alpha_{i+1,j}\, h)} \qquad \text{(B.23)}$$

The objective is to solve for the integrated flux

$$\Phi_{ij} = b_{ij}\, A_{ij}\, \frac{2}{\alpha_{ij}} \sinh(\alpha_{ij}\, h/2) \quad ,$$

where the only unknown is $b_{ij}\, A_{ij}$, which can be obtained from Eqs. (B.22) and (B.23). The result for Φ_{ij}, obtained after some algebra, is reproduced in Table B.1, as Eq. (B.24).

In the Y-direction, an entirely similar development yields an analogous result for Φ_{ij}, which is also presented in Table B.1, as Eq. (B.25).

TABLE B.1

Analytical Solution for Interior Node Integrated Flux

X-direction:

$$\frac{\Phi_{ij}\alpha_{ij}^2}{2} = \tag{B.24}$$

$$\frac{\Phi_{i-1,j}\alpha_{i-1,j}\,\mathrm{csch}(\alpha_{i-1,j}\,h)\left[\frac{\tanh(\alpha_{ij}\,h/2)}{\alpha_{ij}}+\frac{\tanh(\alpha_{i+1,j}\,h/2)}{\alpha_{i+1,j}}\right]+\Phi_{i+1,j}\alpha_{i+1,j}\,\mathrm{csch}(\alpha_{i+1,j}\,h)\left[\frac{\tanh(\alpha_{ij}\,h/2)}{\alpha_{ij}}+\frac{\tanh(\alpha_{i-1,j}\,h/2)}{\alpha_{i-1,j}}\right]}{\left[\frac{\coth(\alpha_{ij}\,h/2)}{\alpha_{ij}}+\frac{\tanh(\alpha_{i-1,j}\,h/2)}{\alpha_{i-1,j}}\right]\left[\frac{\tanh(\alpha_{ij}\,h/2)}{\alpha ij}+\frac{\tanh(\alpha_{i+1,j}\,h/2)}{\alpha_{i+1,j}}\right]+\left[\frac{\coth(\alpha_{ij}\,h/2)}{\alpha_{ij}}+\frac{\tanh(\alpha_{i+1,j}\,h/2)}{\alpha_{i+1,j}}\right]\left[\frac{\tanh(\alpha_{ij}\,h/2)}{\alpha_{ij}}+\frac{\tanh(\alpha_{i-1,j}\,h/2)}{\alpha_{i-1,j}}\right]}$$

Y-direction:

$$\frac{\Phi_{ij}\beta_{ij}^2}{2} = \tag{B.25}$$

$$\frac{\Phi_{i,j+1}\beta_{i,j+1}\,\mathrm{csch}(\beta_{i,j+1}\,h)\left[\frac{\tanh(\beta_{ij}\,h/2)}{\beta_{ij}}+\frac{\tanh(\beta_{ij-1}\,h/2)}{\beta_{ij-1}}\right]+\Phi_{i,j-1}\beta_{i,j-1}\,\mathrm{csch}(\beta_{i,j-1}\,h)\left[\frac{\tanh(\beta_{ij}\,h/2)}{\beta_{ij}}+\frac{\tanh(\beta_{i,j+1}\,h/2)}{\beta_{i,j+1}}\right]}{\left[\frac{\coth(\beta_{ij}\,h/2)}{\beta_{ij}}+\frac{\tanh(\beta_{i,j+1}\,h/2)}{\beta_{i,j+1}}\right]\left[\frac{\tanh(\beta_{ij}\,h/2)}{\beta_{ij}}+\frac{\tanh(\beta_{ij-1}\,h/2)}{\beta_{ij-1}}\right]+\left[\frac{\coth(\beta_{ij}\,h/2)}{\beta_{ij}}+\frac{\tanh(\beta_{ij-1}\,h/2)}{\beta_{ij-1}}\right]\left[\frac{\tanh(\beta_{ij}\,h/2)}{\beta_{ij}}+\frac{\tanh(\beta_{i,j+1}\,h/2)}{\beta_{i,j+1}}\right]}$$

Subject to: $B_{ij}^2 = \alpha_{ij}^2 + \beta_{ij}^2$ (B.3)

Equations (B.24) and (B.25) together with Eq. (B.3) constitute the solution for an interior node, the integrated fluxes of whose surroundings (Φ_{ij-1}, Φ_{ij+1}, Φ_{i-1j} and Φ_{i+1j}) as well as the bucklings and respective directional apportionments (i.e., relative values of α^2 and β^2), are known.

B.2 Peripheral Nodes

Again solving for the X-direction, the boundary conditions at the interior (fueled) interfaces are the same as for the previous case. At the interface with the reflector, additional conditions are imposed: the flux in addition to satisfying the continuity requirement at the interface, is assumed to vanish at a distance h_r into the reflector; for the current an empirically adjustable "discontinuity" factor, E, is incorporated to account for corrections due to baffle transmission, thermal back-leakage, and other node-specific features. Furthermore, the diffusion coefficient for the reflector, D_r, may be substantially different from that of the fuel assembly. Accordingly, the equations become:

for the fluxes:

$$b_{ij}\left[A_{ij}\cosh(\alpha_{ij}\,h/2) - G_{ij}\sinh(\alpha_{ij}\,h/2)\right] = b_{i-1j}\left[A_{i-1j}\cosh(\alpha_{i-1j}\,h/2) + G_{i-1j}\sinh(\alpha_{i-1j}\,h/2)\right] \tag{B.26}$$

and

$$b_{ij}\left[A_{ij}\cosh(\alpha_{ij}\,h/2) + G_{ij}\sinh(\alpha_{ij}\,h/2)\right]$$

$$= -A_r \sinh(B_r h_r) \qquad \text{(B.27)}$$

for the currents:

$$D_{ij}b_{ij}\alpha_{ij}\left[G_{ij}\cosh(\alpha_{ij}\,h/2) - A_{ij}\cosh(\alpha_{ij}\,h/2)\right] \qquad \text{(B.28)}$$

$$= D_{i-1,j}b_{i-1,j}\alpha_{i-1,j}\left[G_{i-1,j}\cosh(\alpha_{i-1,j}\,h/2) - A_{i-1,j}\sinh(\alpha_{i-1,j}\,h/2)\right]$$

and

$$D_{ij}b_{ij}\alpha_{ij}\left[G_{ij}\cosh(\alpha_{ij}\,h/2) + A_{ij}\sinh(\alpha_{ij}\,h/2)\right]$$

$$= \frac{A_r\,D_r\,B_r}{E} \qquad \text{(B.29)}$$

where:

B_r^2 = buckling in the reflector $\approx (\Sigma_{a1}+\Sigma_{12})_r/D_r$

A_r = normalization constant (to be determined from the absolute value of the flux (or power);

and, the solution for the flux in the reflector is given by

$$\Phi_r(x) = A_r \sinh[B_r(x-h_r)] \quad .$$

The integrated flux for node i-1,j is:

$$\Phi_{i-1,j} = b_{i-1,j}\ \frac{2A_{i-1,j}}{\alpha_{i-1,j}}\ \sinh(\alpha_{i-1,j}\,h/2) \qquad \text{(B.30)}$$

Manipulation of Eqs. (B.27) and (B.29) yields:

$$b_{ij}\, A_{ij} \left[\cosh(\alpha_{ij}\, h/2) + \frac{E\, D_{ij}\alpha_{ij}}{D_r\, B_r} \tanh(B_r h_r) \cdot \sinh(\alpha_{ij}\, h/2)\right] =$$

$$- b_{ij}\, G_{ij} \left[\sinh(\alpha_{ij}\, h/2) + \frac{E\, D_{ij}\alpha_{ij}}{D_r\, B_r} \tanh(B_r h_r) \cdot \cosh(\alpha_{ij}\, h/2)\right] \tag{B.31}$$

Using Eqs. (B.26), (B.28) and (B.30) in a similar way as was done before to obtain Eq. (B.22), a formally equivalent equation results:

$$b_{ij}\, A_{ij} \left[\cosh(\alpha_{ij}\, h/2) + \frac{\alpha_{ij}}{\alpha_{i-1,j}} \tanh(\alpha_{i-1,j}\, h/2) \cdot \sinh(\alpha_{ij}\, h/2)\right]$$

$$- b_{ij}\, G_{ij} \left[\sinh(\alpha_{ij}\, h/2) + \frac{\alpha_{ij}}{\alpha_{i-1,j}} \tanh(\alpha_{i-1,j}\, h/2) \cdot \cosh(\alpha_{ij}\, h/2)\right]$$

$$= \frac{\Phi_{i-1j}\ \alpha_{i-1,j}}{\sinh\ (\alpha_{i-1,j}\ h)} \tag{B.32}$$

Again the objective is to solve for Φ_{ij}, and the unknown is $b_{ij}\, A_{ij}$, which may be obtained by combining Eqs. (B.31) and (B.32). The result is presented in Table B.2, as Eq. (B.33).

An analogous result also shown in Table B.2, as Eq. (B.34), may be obtained by similar procedures in the Y-direction.

The solution for an assembly with two reflector interfaces will be given by Eqs. (B.33), (B.34) and (B.3). For the case of one reflector interface the appropriate combination of Eq. (B.3), one out of Eqs. (B.33) or (B.34) and one out of Eqs. (B.24) or (B.25) will provide the solution, as can be seen by inspection.

TABLE B.2

Analytical Solution for Peripheral Node Integrated Flux

X-direction:

$$\frac{\Phi_{ij}\alpha_{ij}^2}{2} = \frac{\Phi_{i-1,j}\,\alpha_{i-1,j}\,\mathrm{csch}(\alpha_{i-1,j}\,h)}{\left[\frac{\coth(\alpha_{ij}\,h/2)}{\alpha_{ij}} + \frac{\tanh(\alpha_{i-1,j}\,h/2)}{\alpha_{i-1,j}}\right] + \frac{\left[\frac{\coth(\alpha_{ij}\,h/2)}{\alpha_{ij}} + \frac{ED_{ij}}{D_rB_r}\tanh(B_rh_r)\right]}{\left[\frac{\tanh(\alpha_{ij}\,h/2)}{\alpha_{ij}} + \frac{ED_{ij}}{D_rB_r}\tanh(h_rB_r)\right]}\left[\frac{\tanh(\alpha_{ij}\,h/2)}{\alpha_{ij}} + \frac{\tanh(\alpha_{i-1,j}\,h/2)}{\alpha_{i-1,j}}\right]} \qquad (B.33)$$

Y-direction:

$$\frac{\Phi_{ij}\beta_{ij}^2}{2} = \frac{\Phi_{ij+1}\,\beta_{ij+1}\,\mathrm{csch}(\beta_{ij+1}\,h)}{\left[\frac{\coth(\beta_{ij}\,h/2)}{\beta_{ij}} + \frac{\tanh(\beta_{ij+1}\,h/2)}{\beta_{ij+1}}\right]\frac{\left[\frac{\coth(\beta_{ij}\,h/2)}{\beta_{ij}} + \frac{ED_{ij}}{D_rB_r}\tanh(B_rh_r)\right]}{\left[\frac{\tanh(\beta_{ij}\,h/2)}{\beta_{ij}} + \frac{ED_{ij}}{D_rB_r}\tanh(B_rh_r)\right]}\left[\frac{\tanh(\beta_{ij}\,h/2)}{\beta_{ij}} + \frac{\tanh(\beta_{ij+1}\,h/2)}{\beta_{ij+1}}\right]} \qquad (B.34)$$

Subject to: $B_{ij}^2 = \alpha_{ij}^2 + \beta_{ij}^2$ (B.3)

The term $\frac{E\ D_{ij}}{D_r\ B_r} \tanh(B_r\ h_r)$ resulted from the boundary conditions at the reflector-node interface, requiring the flux to vanish at a distance h_r into the reflector (away from the interface). However, for values of $B_r\ h_r > 2$, which is normally the case for PWRs, $\tanh(B_r\ h_r) \approx 1$, and, hence, this "infinite reflector" approximation could have been used instead, without negative consequences.

The albedo is usually defined as the ratio of partial currents in and out of the reflector, and may be given, in terms of the reflector's properties by:

$$\beta^* = \frac{J-}{J_+} = \frac{1 - 2\ D_r B_r \coth B_r h_r}{1 + 2\ D_r B_r \coth B_r h_r} \approx \frac{1 - 2\ B_r D_r}{1 + 2\ B_r D_r} \qquad (B.35)$$

Then, once the empirically determined value for β^* is available for a given reflector, its properties, $D_r B_r$, may be inferred from Eq. (B.35):

$$2\ D_r\ B_r \approx 2\ D_r B_r \coth(B_r H_r) = \frac{1-\beta^*}{1+\beta^*} \qquad (B.36)$$

(It should be noted that this value already includes the empirical adjustment factor E, hence it actually is $E/2\ D_r B_r$).

It should be mentioned, at this point, that the intra-assembly flux shape (hence power) may be estimated from the analytical developments of this appendix. Once the solutions for the Φ_{ij}s are available, the constants A_{ij}, G_{ij}, C_{ij} and D_{ij} will have been determined, and consequently, in Eq. (B.5), the flux $\Phi_{ij}(x,y)$. Eq. (B.5) could be used to obtain an estimate of the intra-assembly peaking factor, i.e.: for reconstruction of the global intra-assembly flux shape given the set of total nodal fluxes afforded by a numerical solution.

B.3 Net Leakage Out of Peripheral Nodes

As shown in Eqs. (2.20) and (2.22), the net current out of the peripheral assemblies is an important quantity, necessary to compute the "leakage reactivity" ρ_L, used in the system reactivity balance performed in lieu of the eigenvalue calculation.

From Eq. (B.27), Jx, the net current out of the node ij, in the X-direction, is given by:

$$Jx_{ij} = -D_{ij}\alpha_{ij}b_{ij}\left[G_{ij}\cosh(\alpha_{ij}\,h/2)+A_{ij}\sinh(\alpha_{ij}\,h/2)\right] \quad (B.37)$$

From Eq. (B.8), an expression for $b_{ij}\,A_{ij}$ is:

$$b_{ij}\,A_{ij} = \frac{\Phi_{ij}\,\alpha_{ij}}{2\sinh(\alpha_{ij}\,h/2)} \quad (B.38)$$

and Eqs. (B.38) and (B.31) may be manipulated to yield for $b_{ij}\,G_{ij}$:

$$b_{ij}\,G_{ij} = -\frac{\Phi_{ij}\,\alpha_{ij}}{2\sinh(\alpha_{ij}\,h/2)} \cdot \cdot \frac{\left[\cosh(\alpha_{ij}\,h/2) + \frac{E\,D_{ij}\alpha_{ij}}{D_r B_r}\tanh(B_r h_r)\cdot\sinh(\alpha_{ij}\,h/2)\right]}{\left[\sinh(\alpha_{ij}\,h/2) + \frac{E\,D_{ij}\alpha_{ij}}{D_r B_r}\tanh(D_r h_r)\cdot\cosh(\alpha_{ij}\,h/2)\right]} \quad (B.39)$$

After some simplification Jx_{ij} becomes:

$$Jx_{ij} = -\frac{D_{ij}\Phi_{ij}\alpha_{ij}}{2}^2\left[1-\frac{\coth(\alpha_{ij}\, h/2)+\frac{E\, D_{ij}\,\alpha_{ij}}{D_r B_r}\tanh(B_r h_r)}{\tanh(\alpha_{ij}\, h/2)+\frac{E\, D_{ij}\,\alpha_{ij}}{D_r B_r}\tanh(B_r h_r)}\right] \tag{B.40}$$

In the orthogonal Y-direction an analogous result may be obtained for Jy_{ij}:

$$Jy_{ij} = -\frac{D_{ij}\Phi_{ij}\beta_{ij}}{2}^2\left[1-\frac{\coth(\beta_{ij}\, h/2)+\frac{E\, D_{ij}\,\beta_{ij}}{D_r B_r}\tanh(B_r h_r)}{\tanh(\beta_{ij}\, h/2)+\frac{E\, D_{ij}\,\beta_{ij}}{D_r B_r}\tanh(B_r h_r)}\right] \tag{B.41}$$

In this appendix some detailed analytic material has been summarized in support of the condensed presentation in the main text. The major contribution here is the establishment of a firm analytic foundation for what has been, in some applications, a more empirical approach.

APPENDIX C

Differential Thermal Leakage and Power Feedback Corrections

C.1 Introduction

It may appear remarkable that as simple a method as the modified one-group model can be as accurate as it has proven to be. Considerable work has been dedicated to improving the capabilities of nodal methods, and much of the success has come through fine tuning of the nodal model's adjustable parameters against more sophisticated computations, analytical or experimental data. In this appendix, the analyses that follow suggest how and why this can be accomplished, regarding the power-related feedback and differential thermal leakage corrections. More detailed discussion of the subject is forthcoming in Ref. [D-1].

C.2 Power-related Feedback

The reactivity status of an assembly is affected by its power level. Through the negative moderator temperature coefficient of reactivity and the Doppler reactivity coefficient of the fuel, an increase in fuel and moderator temperatures, due to an increase in

power level, leads to a slight reduction in reactivity. In addition, higher power density corresponds to a higher concentration of saturating fission products (xenon and samarium), which also reduces reactivity.

It may be shown that to first order these feedbacks will not affect the power level, as the following reasoning suggests. The perturbed and original power are related by:

$$f_i^* = f_i + \left(\frac{\partial f_i}{\partial \rho_i}\right)\Delta\rho_i + \ldots \qquad (C.1)$$

However, $\Delta\rho_i$ is proportional to the change in power level:

$$\Delta\rho_i \approx -\gamma(f_i^* - f_i) \qquad (C.2)$$

then,

$$f_i^* \approx f_i + \left(\frac{\partial f_i}{\partial \rho_i}\right)[-\gamma(f_i^* - f_i)] + \ldots \qquad (C.3)$$

which may be re-arranged to give:

$$f_i^*\left(1 + \gamma\frac{\partial f_i}{\partial \rho_i}\right) \approx f_i\left(1 + \gamma\frac{\partial f_i}{\partial \rho_i}\right) \qquad (C.4)$$

or, to first order, $f_i^* \approx f_i$.

Furthermore, neglecting the power coefficient feedback and measuring the reactivity perturbation relative to a core-average assembly which is just critical the perturbed power becomes:

$$f_i^* = f_i \left[1 + \left(\frac{1}{f_i}\frac{\partial f_i}{\partial \rho_i}\right)(\rho_i - 0) + \ldots.\right] \tag{C.5}$$

or,

$$f_i^* \approx \frac{f_i}{1 - \left(\frac{1}{f_i}\frac{\partial f_i}{\partial \rho_i}\right)\rho_i} \tag{C.6}$$

It is possible to show that, by multiplying Eq. (C.6) by the nodal power expressions of Table 3.1, to first order, the results will give the original nodal power expressions with modified coupling coefficients θ (or θp):

$$\theta^* = \theta + \left(\frac{1}{f_i}\frac{\partial f_i}{\partial \rho_i}\right) \tag{C.7}$$

Hence a first order correction can be incorporated by adjusting θ to match the results of more sophisticated calculations which explicitly consider the coupling between thermal-hydraulic and neutronic effects.

C.3 Thermal Neutron Effects

The modified one-group model and the nodal power expression of Table 3.1 have been derived under the approximation that thermal neutrons are absorbed immediately at the spot of their thermalization. However, their diffusion length, L, can be of the order of 2 cm, and as

a consequence, a non-negligible net current may result between assemblies having substantially different properties (e.g. burnups). Corrections, such as that proposed in Ref. [B-3] have been introduced into many state-of-the-art codes.

This effect will be evaluated here in the somewhat simplified slab geometry, representing two adjacent assemblies, i and j, as depicted below:

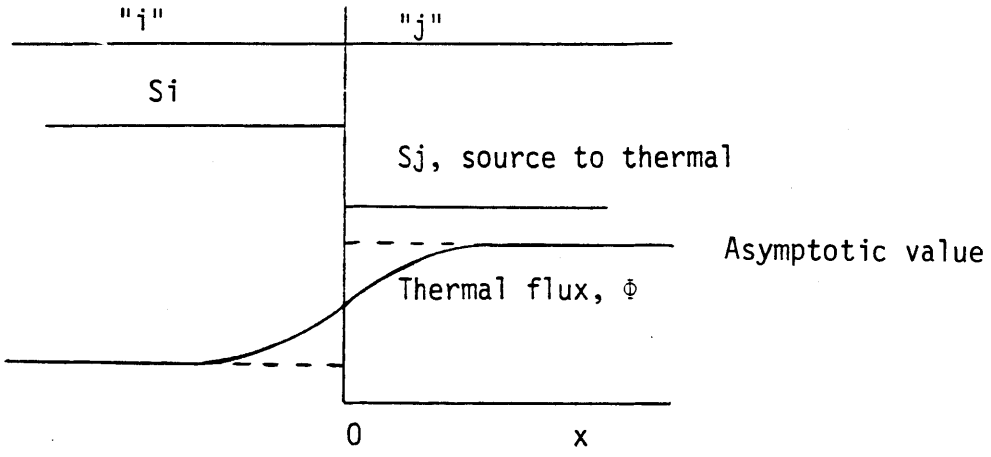

The equation for the thermal flux is:

$$-D\nabla^2\Phi + \Sigma_a\Phi = S \qquad \text{(C.8a)}$$

or

$$\frac{d^2\Phi}{dx^2} - \frac{1}{L^2}\Phi = -\frac{S}{D} \qquad \text{(C.8b)}$$

where

$S = \Sigma_{12}\Phi_1$ (thermal source)

Φ_1 = fast flux

$L^2 = D/\Sigma_a$ (thermal group constants)

Equation (C.8) has the solutions:

region "i":

$$\Phi_1 = \frac{S_i}{\Sigma_{ai}} + C_i\, e^{+X/L_i} \tag{C.9}$$

region "j":

$$\Phi_j = \frac{S_j}{\Sigma_{aj}} - C_j\, e^{-X/L_j} \tag{C.10}$$

Requiring continuity of flux, Φ, and current, J, at X=0, where $J=-D\frac{d\Phi}{dx}$, the results for C_i and C_j become, after some algebra:

$$C_i = \frac{\frac{S_j}{D_j} L_j^2 - \frac{S_i}{D_i} L_i^2}{1 + \frac{L_j}{L_i}\frac{D_i}{D_j}} \tag{C.11}$$

and

$$C_j = C_i \frac{L_j}{L_i}\frac{D_i}{D_j} \tag{C.12}$$

The net leakage into "i" is given by

$$J_i = -\frac{DC_i}{L_i} = -\frac{\left[\frac{S_j}{D_j} L_j^2 - \frac{S_i}{D_i} L_i^2\right]}{\left[\frac{L_i}{D_i} + \frac{L_j}{D_j}\right]} \tag{C.13}$$

Assuming that the thermal diffusion coefficient is the same in both regions, Eq. (C.13) reduces to:

$$J_i = -\left(\frac{S_j L_j^2 - S_i L_i^2}{L_i + L_j}\right) \tag{C.14'}$$

$$J_i = -\left(\frac{L_j^2}{L_i + L_j}\right)\Sigma_{12j}\Phi_{1j} + \left(\frac{L_i^2}{L_i + L_j}\right)\Sigma_{12i}\Phi_{1i} \tag{C.14}$$

Using Eqs. (2.11), (2.15) and (2.16), the following approximations may be established:

$$\Phi_1 \approx f(1 - \rho) \tag{C.15}$$

and

$$\nabla^2 [f(1 - \rho)] + \frac{\rho_i}{M^2} f_i = 0 \tag{C.16}$$

Then the leakage term $\nabla^2[f(1-\rho)]$ may be written as:

$$\nabla^2[f(1-\rho)] = \frac{\overline{f_s(1-\rho_s)}}{\gamma h^2} - \frac{f(1-\rho_i)}{\gamma h^2} \tag{C.17}$$

where s refers to surroundings and γ is a constant.

Using Eqs. (C.15) and (C.14), considering "j" as the surroundings, J_i becomes:

$$J_i = -\left(\frac{\Sigma_{i2s} L_s^2}{L_i + L_s}\right)\overline{f(1-\rho_s)} + \left(\frac{\Sigma_{12} L_i^2}{L_i + L_s}\right) f(1-\rho_i) \tag{C.18}$$

Define

$$\xi_s = \frac{\Sigma_{12s} L_s^2}{L_i + L_s} \tag{C.19}$$

and

$$\xi_i = \frac{\Sigma_{12i} L_i^2}{L_i + L_s} \tag{C.20}$$

Then the neutron balance equation, Eq. (C.16), can be modified to account for the thermal leakage:

$$f_s(1-\rho_s)\ (1-\xi_s) - f_i(1-\rho_i)\ (1-\xi_i) + \frac{\gamma h^2}{M^2}\rho_i\ f_i = 0 \tag{C.21}$$

The solution for f_i is:

$$f_i = \frac{\overline{f_s(1-\rho_s)}\ (1-\xi_s)}{(1-\xi_i) - \left[1 - \xi_i + \frac{\gamma h^2}{M^2}\right]\rho_i} \tag{C.22}$$

If ξ <<1 (as it is normally for PWRs),

$$f_i \quad \frac{\overline{f_s(1-\rho_s)}\ [1 - (\xi_s - \xi_i)]}{1 - \left[\frac{1 - \xi_i + \frac{\gamma h^2}{M^2}}{1 - \xi_i}\right]\rho_i} \tag{C.23}$$

Redefining

$$\theta^* = \theta + \left(\frac{\gamma h^2}{M^2}\right)\left(\frac{\Sigma_{12} L_i^2}{L_i + L_s}\right) + \ldots \tag{C.24}$$

and note that $\xi_s \approx \xi_i$, then, again it can be seen that mere adjustment of the coupling coefficient may provide a partial correction - this time for the differential thermal leakage between adjacent assemblies.

As already pointed out in Chapter 3, at the core periphery empirical corrections (in a fashion similar to the conventional albedo adjustments) are necessary to account for thermal back-leakage, core baffle transmission and other specific local details. In the peripheral nodal power

expression, provision to consider this correction was made by including the E factor. A very crude estimate of the thermal neutron return from the reflector may be obtained using an infinite medium kernel (i.e. assuming the same L in core and reflector).

The fast flux in the reflector may be approximated by:

$$\Phi_1 (x) = \Phi_1 (0)\, e^{-X/M} \tag{C.25}$$

in which case the source to thermal is $\Sigma_{12}\Phi_1$. Then the total net thermal leakage, J_{th}, into the core from the reflector may be estimated by:

$$J_{th} = \int_0^\infty \Sigma_{12}\Phi_1 (o)\, e^{-X/M} \cdot \frac{1}{2} e^{-X/L} \, dx \tag{C.26}$$

$$= \frac{\Sigma_{12}\Phi_1 (o)}{2\left(\frac{1}{M_r} + \frac{1}{L}\right)} \tag{C.27}$$

The total net fast leakage out of the core may be approximated by:

$$J_f = \int_0^\infty \Sigma_{12}\Phi_1(o)\, e^{-X/M} \cdot \frac{1}{2} e^{-X/M} \, dx \tag{C.28}$$

$$= \frac{\Sigma_{12}\Phi_1 (o)}{2\left(\frac{2}{M}\right)} \tag{C.29}$$

And the ratio of total net thermal back-leakage to the total net fast leakage out of the core may be estimated as:

$$\frac{J_{th}}{J_f} \approx \frac{4/M}{2/M + 2/L} \tag{C.30}$$

Hence, for L=3, M-8, $E=J_f/(J_f-J_{th}) \approx 2.2$

Note that this estimate does not consider the compensatory term accounting for leakage of thermalized neutrons out of the peripheral assembly into the reflector (as was done in the adjacent assemblies considered earlier). Despite the quite approximate nature of this estimate, the results presented in Table 3.4, in which the factor E/D_rB_r was computed using an empirically adjusted albedo to match Maine Yankee core maps, required that $E \approx 2.2$ (for $D_r \approx 2.25$ cm, $M=1/B_r=8$ cm, since $E/D_rB_r = 0.1321$).

APPENDIX D

The LRM-NODAL Program

D.1 Introduction

The LRM-NODAL code has been programmed in BASIC for the TRS-80 Model III, 48 K, microcomputer, for the purpose of testing and verifying most of the methodology developed during the course of the present research. The code, in its present status, requires about 34 K of memory (when the integrated depletion method subroutine is deleted) and an additional 14 K for data storage.

The main variables are described in table D.1, and are specified either in lines 0 - 100, or in the interactive initialization of the program. Interspersed remarks indicate the function of the main subroutines. The general structure of the program corresponds to the lines allocated for the following functions and subroutines:

0000 - 2000:Specification of variables;

2000 -12000:Data input and specification of core data and configuration (idealized Maine Yankee PWR);

12000-14800:Main control routine;

14800-15000:Ouput subroutine;

15000-16000:Preliminary calculations;

16000-30000:Optimization subroutines;

30000-32000:EOC power and burnup derivative calculation subroutine;

36000-37000:Step-wise depletion subroutine;

38000-39000:Synthesis depletion subroutine;

40000-45000:Power distribution calculation, with critical boron reactivity search;

45000-50000:Integrated depletion subroutine

50000-51000:EOC power distribution calculation;

51000-55000:Power calculation iteration subroutine;

55000-59000:BOC power derivative calculation subroutine;

61000-63000:Derivative calcularion iteration subroutine;

During the calculations, intermediate results are displayed on the computer screen. Hard copies are provided only for final results. Table D.2 shows a typical initialization interactive session, as (partially) hard-copied from the computer screen, and table D.3 displays a typical printout (partial) of final results.

Refinement of programming techniques will certainly improve the computational efficiency of LRM-NODAL (which is at present a research tool rather than a production program) and is therefore strongly suggested, along with transfer to a larger (RAM) and faster computer.

TABLE D.1

Main Variables Used in the LRM-NODAL Program

Variable(s)	Function	Typical Numerical Value
BS	Burnup step length	2000
NB, NO	Number of iterations for power calculation at BOC	15
ND	Number of iterations at each burnup step	7
AC, AB, AQ, AP	Relaxation factor (iterative processes)	0.5
NV, NU	Number of iterations in derivative calculations	10
TH,T1,T2,T5,TS	Coupling coefficients	(see Table 3.4)
I,J	Nodal coordinate indices	-
PR(I)	I coordinate of reflector	-
CF(I,J)	Assembly configuration type	-
Y(I,J)	Fraction of node corresponding to 1/4-core	1, 0.5, 0.25
RQ(I,J)	Leakage constant (ρ_{Li})	(see Table 3.4)
W(I,J)	Relative boron worth	1.0
R(I,J)	BOC assembly reactivity	0, 0.10, 0.20
A(I,J)	Reactivity vs burnup slope	1.0E- 05
BP(I,J)	Burnable poison reactivity	0, 0.08, 0.04
F1(I,J), F2(I,J)	BOC and EOC power fractions	1.0, 1.3, 0.7
MB, ME	Power peaking limits at BOC and EOC	1.3
B(I,J)	Assembly burnup	10,000
BC	Cycle burnup	10,000
P1(I,J), P2(I,J)	BOC and EOC power derivatives	5.0
BB(I,J), FU(I,J)	Cycle and assembly burnup derivatives	2000, 10,000
G(I,J)	BP reactivity limit	0.25

TABLE D.1 (continued)

Main Variables Used in the LRM-NODAL Program

Variable(s)	Function	Typical Numerical Value
SR(I,J)	Restriction on assembly shuffling	0 or 1
NT	Number of types of assemblies	25
H	Nodal width	
M	Migration length	7.2
SB(I,J)	BP reactivity vs. burnup slope	5.0E-06

TABLE D.2

Typical Interactive Initialization Session for the LRM-NODAL Program

```
**********************************************
 SELECT OPTIONS FOR THIS CASE :
**********************************
DATA ENTRY FORM     -     ENTER:     1 - FOR 1/4 CORE, WITH PRE-DEF
INED  PATTERN INPUT; 2 - FOR FULL CORE DATA ;  3- FOR 1/4 CORE,
WITH AUTOMATIC PATTERN GENERATION
? 1
**********************************************
**********************************************
SELECT PROBLEM OBJECTIVE :    ENTER : 1) MAXIMUM BURNUP CONFIGURA
TION AND OPT. BURNABLE POISON;  2) MAXIMUM BURNUP CONFIGURAGTION
;
 3) OPTIMAL BURNABLE POISON ;     4) DEPLETION (STEP-WISE) ;    5)
 DEPLETION  (SYNTHESIS);  6) DEPLETION (INTEGRATED METHOD);
? 4

DATA ENTRY FOR RESTRICTED ASSEMBLIES

 ENTER NUMBER OF TYPES OF FUEL TO BE PLACED DIRECTLY AND RE
STRIC
TED? 0

 DATA ENTRY FOR QUARTER CORE

 ENTER DATA FOR A TOTAL OF  55   ASSEMBLIES.

 ENTER NUMBER OF TYPES OF ASSEMBLIES - ENTER 0 TO READ DATA
 FROM
 TAPE? 27

ENTER DATA FOR FUEL TYPE: 1

REACTIVITY AND NUMBER OF ASSEMBLIES? .221973,12

 ENTER SLOPE (A)  AND INITIAL BP REACTIVITY? 9.0538E-6,0

ENTER DATA FOR FUEL TYPE: 2

REACTIVITY AND NUMBER OF ASSEMBLIES? .221973,1

 ENTER SLOPE (A)  AND INITIAL BP REACTIVITY? 9.0538E-6,.045

BP SLOPE - PRESS  ENTER  FOR  ADJUSTABLE BP SLOPE? 2.8125E-
6
```

TABLE D.2 (continued)

Typical Interactive Initialization Session for the LRM-NODAL Program

```
ENTER DATA FOR FUEL TYPE: 3
REACTIVITY AND NUMBER OF ASSEMBLIES? .221973,5
 ENTER SLOPE (A)  AND INITIAL BP REACTIVITY? 9.0538E-6,.08
BP SLOPE - PRESS  ENTER  FOR  ADJUSTABLE BP SLOPE? 5.0E-6
ENTER DATA FOR FUEL TYPE: 4
... etc.

ENTER 1 TO STORE DATA IN TAPE? 0
 ENTER 1 TO READ DATA FROM TAPE? 0
ENTER 1 TO STORE PATTERN DATA ON TAPE? 0
 ENTER TYPE OF ASSEMBLY AT : 1  , 1
? 4
 ENTER TYPE OF ASSEMBLY AT : 1  , 2
? 5
 ENTER TYPE OF ASSEMBLY AT : 1  , 3
? 6
 ENTER TYPE OF ASSEMBLY AT : 1  , 4
? 7
 ... etc.

RESTRICTIONS ON BP LOADING PER LOCATION
ENTER RESTRICTED POSITION: I,J - ENTER 0 TWICE TO EXIT? 0
?? 0
```

TABLE D.3

Typical Printout of the Final Results of the LRM-NODAL Code

	1	2	3	4	5	6	7	8	9
1									
SR	0	0	0	0	0	0	0	0	0
R	.0223811	.153055	-6.28707E-03	.153055	.0220128	.0960075	.0220128	.221973	.221973
AE-5	.90815	.905538	.910256	.90538	.910256	.90538	.910256	.90538	.90538
BP	0	0	0	0	0	0	0	.08	0
SB	0	0	0	0	0	0	0	5E-06	0
F1	1.29312	1.4897	1.10764	1.29853	1.0573	1.02751	.891232	.869739	.660967
F2	.700241	.826134	.680106	.864717	.812388	.978177	1.10367	1.43987	1.07187
B	9299.1	10878.2	8529.39	10499.5	9190.6	9992.51	9910.46	11346.4	9011.93
BB	0	0	0	0	0	0	0	0	0
P1	0	0	0	0	0	0	0	0	0
P2	0	0	0	0	0	0	0	0	0
FU	0	0	0	0	0	0	0	0	0
2									
SR	0	0	0	0	0	0	0	0	0
R	.153055	.0428304	.129688	-.0108201	.142816	1.90525E-03	.221973	-6.1966E-03	.221973
AE-5	.905538	.910256	.90538	.910256	.90538	.90538	.90538	.910256	.90538
BP	0	0	0	0	0	0	.08	0	0
SB	0	0	0	0	0	0	5E-06	0	0
F1	1.4888	1.26261	1.28672	1.04519	1.25444	.984294	1.09043	.729084	.483805
F2	.826291	.725133	.795628	.708073	.943803	.912965	1.40666	.993079	.814121
B	10877	9400.88	9997.07	8542.87	10873.7	9475.08	12362.1	8755.56	6738.77
BB	0	0	0	0	0	0	0	0	0
P1	0	0	0	0	0	0	0	0	0
P2	0	0	0	0	0	0	0	0	0
FU	0	0	0	0	0	0	0	0	0
3									
SR	0	0	0	0	0	0	0	0	
R	-6.28707E-03	.129688	9.9155E-03	.10976	.0482828	.155491	.11244	.221973	
AE-5	.910256	.90538	.910256	.90538	.910226	.90538	.90538	.90538	
BP	0	0	0	0	0	0	0	0	
SB	0	0	0	0	0	0	0	0	
F1	1.10716	1.28784	1.08646	1.24208	1.16495	1.28339	1.12158	1.01957	
F2	.680218	.795483	.713132	.857905	.891725	1.12152	1.18091	1.20973	
B	8528.89	9997.46	8687.09	10267.1	10139.2	12009.9	11626.7	11585.6	
BB	0	0	0	0	0	0	0	0	
P1	0	0	0	0	0	0	0	0	
P2	0	0	0	0	0	0	0	0	
FU	0	0	0	0	0	0	0	0	
4									
SR	0	0	0	0	0	0	0	0	
R	.153055	-.0108201	.10976	.100552	.132068	.0360762	.0389345	.221973	
AE-5	.90538	.910256	.90538	.90538	.90538	.910256	.910256	.90538	
BP	0	0	0	0	0	0	0	0	
SB	0	0	0	0	0	0	0	0	
F1	1.29774	1.0446	1.24162	1.31526	1.28141	.999391	.842215	.821689	
F2	.865192	.707358	.857843	.924806	1.01829	.955859	1.01124	1.07111	
B	10502.5	8537.03	10270.9	10995.8	11403.6	9764.44	9331.32	9703.39	
BB	0	0	0	0	0	0	0	0	
P1	0	0	0	0	0	0	0	0	
P2	0	0	0	0	0	0	0	0	
FU	0	0	0	0	0	0	0	0	

TABLE D.3 (continued)

Typical Printout of the Final Results of the LRM-NODAL Code

```
 5
SR          0           0           0           0           0           0           0           0
R           .0220128    .142816     .0482828    .132068     .0520786    .0908015    .221973     .221973
AE-5        .910256     .90538      .910226     .90538      .910256     .90538      .90538      .90538
BP          0           0           0           0           0           0           .08         0
SB          0           0           0           0           0           0           5E-06       0
F1          1.05696     1.25372     1.16547     1.2823      1.05911     .97945      .842855     .523666
F2          .813253     .942677     .891543     1.01468     .991888     1.14142     1.37204     .882931
B           9200.59     10860.7     10146.8     11387.4     10103.8     10447.8     10477.6     7033.62
BB          0           0           0           0           0           0           0           0
P1          0           0           0           0           0           0           0           0
P2          0           0           0           0           0           0           0           0
FU          0           0           0           0           0           0           0           0

 6
SR          0           0           0           0           0           0           0
R           .0960075    1.90525E-03 .155491     .0360762    .0908015    .221973     .221973
AE-5        .90538      .90538      .90538      .910256     .90538      .90538      .90538
BP          0           0           0           0           0           .045        0
SB          0           0           0           0           0           2.8125E-06  0
F1          1.02705     .981526     1.28163     .998824     .977091     .99358      .583393
F2          .979452     .911793     1.12257     .951983     1.14648     1.37899     .969554
B           10012.1     9456.8      12025.6     9755.33     10472.1     11576       7680.39
BB          0           0           0           0           0           0           0
P1          0           0           0           0           0           0           0
P2          0           0           0           0           0           0           0
FU          0           0           0           0           0           0           0

 7
SR          0           0           0           0           0           0
R           .0220128    .221973     .11244      .0389345    .221973     .221973
AE-5        .910256     .90538      .90538      .910256     .90538      .90538
BP          0           .08         0           0           .08         0
SB          0           5E-06       0           0           5E-06       0
F1          .890993     1.08809     1.1196      .844021     .841431     .5837
F2          1.10397     1.406       1.18357     1.0048      1.37734     .966326
B           9930.41     12344.5     11642.6     9327.59     10504       7671.83
BB          0           0           0           0           0           0
P1          0           0           0           0           0           0
P2          0           0           0           0           0           0
FU          0           0           0           0           0           0

 8
SR          0           0           0           0           0
R           .221973     -6.1966E-03 .221973     .221973     .221973
AE-5        .90538      .910256     .90538      .90538      .90538
BP          .08         0           0           0           0
SB          5E-06       0           0           0           0
F1          .869688     .72626      1.01215     .822083     .521124
F2          1.43651     .992323     1.21579     1.06377     .8876
B           11359       8749.2      11581.6     9708.1      7050.42
BB          0           0           0           0           0
P1          0           0           0           0           0
P2          0           0           0           0           0
FU          0           0           0           0           0

 9
SR          0           0
R           .221973     .221973
AE-5        .90538      .90538
BP          0           0
SB          0           0
F1          .661522     .494503
F2          1.06462     .801024
B           9018.67     6767.94
BB          0           0
P1          0           0
P2          0           0
FU          0           0

CYCLE BURNUP: 9916.53
```

D.2 Code Listing

```
          ************  The LRM-NODAL program     ************

9 BS=2000
10 NB=10
11 NU=10
12 NE=1
13 ND=5
14 NM=1
15 NO=15
16 AC=.666
17 NV=10
20 NP=10
25 AQ=.5 : AP=.5
26 AB=.5
35 KR=0
40 ME=1.30 : MB=1.30
50 GP=1 : GS=0 :  O5=1
80 H=20:M=SQR(54) : RP=.0025 : MF=1
90 KL=0
100 DIM PR(10),CF(10,10),Y(10,10),RQ(9,9),W(10,10)
150 DIM R(9,9),A(9,9),BP(9,9),F(9,9),F1(9,9)
200 DIM F2(9,9),RX(9,9),FU(9,9),FA(9,9),FX(9,9)
250 DIM P1(9,9),P2(9,9),SB(9,9),B(9,9),S1(9,9),G(9,9)
300 DIM FB(9,9),BB(9,9),FE(9,9),SR(9,9),RW(9,9),FW(9,9)
350 DIM FJ(2),FI(2),SI(2),SJ(2),BJ(2),BI(2)
400 'PR=REF.POS;CF=CONFIG;Y=FRACTION 1/4;RQ=LEAKAGE;W=BORON
 WORTH;R=REACT.;A=SLOPE;BP=BP;F=AUX;F1=BOC POWER;F2=EOC;RX,
FU,FA,FX=AUX
405 'P1=PERT BOC;P2=EOC; SB=SLOPE BP;B=BUP,S1=PERT SP;FB=PE
RT BOC;BB=PERT BC;FE=PERT.EOC;SR=RESTRICTIONS
410 NT=27:DIM Q(NT),RI(NT),AI(NT),RB(NT),ZI(NT),RA(NT),TP(N
T),T(55),TR(55)
520 TS=1-HC2/(12*MC2)
530 TH=1+HC2/(6*MC2)
540 T1=1+HC2/(4*MC2)
550 T2=1+5*HC2/(12*MC2)
560 TL=HC2/(2*MC2)
570 T5=1+17*HC2/(84*MC2)
2000 CLS: PRINT "**********************************************
***"
2010  PRINT  " SELECT OPTIONS FOR THIS CASE :"
2020 PRINT "**********************************"
2030 PRINT "DATA ENTRY FORM     -     ENTER:     1 - FOR 1/4 C
ORE, WITH PRE-DEFINED  PATTERN INPUT; 2 - FOR FULL CORE DAT
A ;  3- FOR 1/4 CORE, WITH AUTOMATIC PATTERN GENERATION"
2035 INPUT O1
2040 PRINT "**********************************************
*
```

```
2050 IF O1=2 OR O1=3 THEN PRINT "SELECT INITIAL PATTERN GEN
ERATION OPTION (note:libraries for options 1,2,3 have to be
 specified at 6100,6300,6500): 1 - FOR LOW-LEAKAGE;  2- FOR
 OUT-IN;  3- FOR IN-OUT-IN; OR 4- FOR RANDOM PLACEMENT OF A
SSEMBLIES": INPUT O2
2070 PRINT "************************************************"
2080 PRINT "SELECT PROBLEM OBJECTIVE :   ENTER : 1) MAXIMUM
 BURNUP CONFIGURATION AND OPT. BURNABLE POISON;  2) MAXIMUM
 BURNUP CONFIGURAGTION; "
2085 PRINT " 3) OPTIMAL BURNABLE POISON ;    4) DEPLETION (
STEP-WISE) ;   5) DEPLETION  (SYNTHESIS);  6) DEPLETION (IN
TEGRATED METHOD);"
2090 INPUT O3
3000 REM DEFAULT REFLECTORS PLACEMENT - MAINE YANKEE REACTO
R
3020 PR(1)=10   : PR(2)=10 :     PR(3)=9   :  PR(4)=9 : PR(
5)=9
3040 PR(6)=8  :  PR(7)=7 :  PR(8)=6 : PR(9)=3  : PR(10)=0
3045 REM DEFINE CONFIGURATION OF ASSEMBLIES IN CORE
3050 FOR I=0 TO 10:CF(0,I)=12:CF(I,0)=12 : NEXT I
3120 FOR I=1 TO 8: FOR J=1 TO PR(I)-1: CF(I,J)=1: NEXT J: N
EXT I
3220 CF(8,2)=2  :   CF(2,8)=3   :  CF(8,3)=4   :   CF(3,8)=
5
3240 CF(9,1)=6  :   CF(1,9)=7   :  CF(8,4)=8   :   CF(4,8)=
8
3260 CF(9,2)=9  :   CF(2,9)=10  :  CF(8,5)=11  :   CF(5,8)=
11
3280 CF(7,6)=11:    CF(6,7)=11
3320 FOR I=1 TO 10: FOR J=PR(I) TO 10: CF(I,J)=0 : Y(I,J)=0
: NEXT J: NEXT I
3510 FOR I=2 TO 8:Y(1,I)=.5 : Y(I,1)=.5 : NEXT I
3550 Y(1,1)=.25    :  Y(9,1)=1    : Y(1,9)=1
3560 FOR I=2 TO 9: FOR J=2 TO PR(I)-1: Y(I,J)=1 : NEXT J: N
EXT I
3700 REM DEFINE LEAKAGE FRACTIONS FOR PERIPHERAL ASSEMBLIES
3720 FOR I=1 TO 9
3740 FOR J=1 TO PR(I)-1
3760 ON CF(I,J) GOTO 3800,3800,3800,3840,3840,3880,3880,388
0,3920,3920,3920
3780 GOTO 3940
3800 RQ(I,J)=0: GOTO 3940
3840 RQ(I,J)= .0650*MF: GOTO 3940
3880 RQ(I,J)=.130*MF: GOTO 3940
3920 RQ(I,J)=.26*MF
3940 NEXT J,I
4000 REM DEFINE BORON WORTH FRACTIONS FOR LOCATIONS
4020 FOR I=0  TO PR(1)-1
```

```
4040 FOR J=0 TO PR(I)-1
4060 W(I,J)=1
4080 NEXT J
4100 FOR K= PR(I) TO 10
4120 W(I,J)=0
4140 NEXT K
4160 NEXT I
4500 N4=0:FOR I=1 TO 9: FOR J=1 TO PR(I)-1: N4=N4+Y(I,J):NE
XT J,I
4700 PRINT "DATA ENTRY FOR RESTRICTED ASSEMBLIES"
4710 INPUT" ENTER NUMBER OF TYPES OF FUEL TO BE PLACED DIRE
CTLY AND RESTRICTED";NT
4720 IF NT=0 THEN GOTO 4900
4730 FOR I=1 TO NT
4740 PRINT "ENTER DATA FOR FUEL TYPE:";I
4750 INPUT "REACTIVITY AND NUMBER OF ASSEMBLIES"; RI(I),Q(I
)
4760 IF Q(I)=0 THEN Q(I)=1
4770 INPUT "ENTER SLOPE (A) AND INITIAL BP REACTIVITY"; AI(
I),RB(I)
4780 IF RB(I)><0 THEN "INPUT BP SLOPE - PRESS ENTER FOR ADJ
USTABLE SLOPE";ZI(I)
4790 NEXT I
4800 NK=0
4810 INPUT "ENTER POSITION I,J TO BE FUELED -  ENTER  0  TW
ICE TO EXIT";I,J
4820 IF I=0 THEN GOTO 4900
4825 IF I=1 AND(J>1 AND J<9) THEN PRINT "PLACE FUEL IN OTHE
R DIAGONAL, CHOOSE POSITION ";J,I : GOTO 4810
4830 PRINT "ENTER TYPE OF FUEL IN:"I,J
4840 INPUT K
4850 NK=NK+1
4860 SR(I,J)=1: R(I,J)=RI(K): A(I,J)=AI(K): BP(I,J)=RB(K):
SB(I,J)= ZI(K)
4870 GOTO 4810
4900 ON O1 GOTO 5010,5000,5010
5000 PRINT " DATA ENTRY FOR FULL CORE ": N9=4*N4-NK*4 +SR(1
,1)*3 : GOTO 5020
5010 PRINT " DATA ENTRY FOR QUARTER CORE" : N9=INT(N4+1)-NK
5020 PRINT " ENTER DATA FOR A TOTAL OF "; N9," ASSEMBLIES."
5030 INPUT" ENTER NUMBER OF TYPES OF ASSEMBLIES - ENTER 0 T
O READ DATA FROM TAPE";TN
5035 IF TN=0 THEN INPUT#-1,NT : ELSE NT=TN
5040 IF TN=0 THEN GOTO 5130
5050 FOR I=1 TO NT
5060 PRINT "ENTER DATA FOR FUEL TYPE:";I
5070 INPUT "REACTIVITY AND NUMBER OF ASSEMBLIES";RI(I),Q(I)
5080 IF Q(I)=0 THEN Q(I)=1
5090 INPUT " ENTER SLOPE (A)  AND INITIAL BP REACTIVITY"; A
I(I),RB(I)
```

```
5100 IF RB(I)<>0 THEN INPUT "BP SLOPE - PRESS  ENTER  FOR
ADJUSTABLE BP SLOPE"; ZI(I)
5120 NEXT I
5130 IF TN=0 THEN FOR I=1 TO NT: INPUT#-1,RI(I),Q(I),AI(I),
RB(I),ZI(I):NEXT I
5135 NA=0: FOR I=1 TO NT:NA=NA+Q(I):NEXT I
5140 IF NA>< N9 THEN PRINT " NUMBER OF ASSEMBLIES INPUT DOE
S NOT MATCH CORE CONFIGURATION - START OVER AGAIN": STOP
5150 FOR I=1 TO NT
5155 RA(I)=0
5160 FOR J=1 TO NT
5170 IF (RI(I)<RI(J)) OR (RI(I)=RI(J) AND J<=I) THEN RA(I)=
RA(I)+1
5180 NEXT J
5190 TP(RA(I))=I
5195 NEXT I
5200 ON O1 GOTO 5500, 5210, 5500
5205 PRINT "ERROR ON INPUT OPTION": STOP
5209 IF SR(1,1)=1 THEN GOTO 5250
5210 I=TP(NT)
5215 T(INT(N4+1))=I
5220 LT=NT-1
5230 Q(I)=Q(I)-1
5240 IF Q(I)>0 THEN LT=NT
5250 J=0 : NF=0 : RF=0 : NR=0 : RR=0
5260 FOR K=1 TO LT
5270 I=TP(K)
5280 FOR L=1 TO Q(I)
5290 IF (NF<INT(NR/3)) OR (RF<=RR/3 AND NF*3<(NR+3)) THEN N
F=NF+1: RF=RF+RI(I) : T(NF)=I : TR(NF)=I : ELSE NR=NR+1:RR=
RR+RI(I)
5300 NEXT L
5310 NEXT K
5320 GOTO 5565
5500 K=0
5510 FOR L=1 TO NT
5515 I=TP(L)
5520 FOR J=1 TO Q(I)
5530 K=K+1
5540 T(K)=I:TR(K)=I
5550 NEXT J
5560 NEXT L
5565 LPRINT  " RANK            TYPE                # ASSY
     REACTIVITY     SLOPE              BP          BP SLOPE
  "
5570 FOR L=1 TO NT : I=TP(L)
5580 LPRINT L, TP(L), Q(I), RI(I), AI(I), RB(I), ZI(I)
5590 NEXT L
5600 INPUT"ENTER 1 TO STORE DATA IN TAPE";ZT
```

```
5620 IF ZT=1  THEN PRINT#-1,NT: FOR I=1 TO NT:  PRINT#-1,RI
(I),Q(I),AI(I),RB(I),ZI(I):NEXT I
6000 REM INITIAL PATTERN GENERATION
6005 IF O1=1 THEN GOTO 10000
6010 ON O2 GOTO 6100, 6300, 6500, 7000
6100 PRINT " LOW-LEAKAGE PATTERN LIBRARY not available  (TO
 BE SPECIFIED)  - SELECT OTHER OPTION " :GOTO 2010
6300 PRINT "OUT-IN PATTERN LIBRARY not available (TO BE SPE
CIFIED) - SELECT OTHER OPTION": GOTO 2010
6500 PRINT " IN-OUT-IN PATTERN LIBRARY not available  - SEL
ECT OTHER OPTION":GOTO 2010
7000 REM  ROUTINE FOR RANDOM PLACEMENT OF ASSEMBLIES
7010  NA=INT(N4+1)-NK
7020 FOR I=1 TO 9
7030 FOR J=1 TO PR(I)-1
7035 IF SR(I,J)=1 THEN GOTO 7110
7040 IF I=1 AND J>1 AND J<9 THEN GOTO 7110
7050 X=RND(NA)
7055 K=T(X)
7060 R(I,J)=RI(K):A(I,J)=AI(K):BP(I,J)=RB(K):SB(I,J)=ZI(K)
7070 NA=NA-1
7080 FOR L=X  TO NA
7090 T(L)=T(L+1)
7095 NEXT L
7100 T(NA+1)=0
7110 NEXT J
7120 NEXT I
7130 FOR K=2 TO 8
7140 R(1,K)=R(K,1):A(1,K)=A(K,1):BP(1,K)=BP(K,1):SB(1,K)=SB
(K,1)
7150 NEXT K
7490 CLS
7500 FOR I=1 TO 9:PRINT @((I-0)*6+64*2),I;:NEXT I
7510 FOR I=1 TO 9:PRINT @((I+2)*64),I;:NEXT I
7520 FOR I=1 TO 9:FOR J=1 TO PR(I)-1:PRINT @((I+2)*64+J*6),
R(I,J);:NEXT J:NEXT I
7600 GOTO 10700
10000 INPUT" ENTER 1 TO READ DATA FROM TAPE";TA
10020 IF TA=1 THEN GOTO 10500
10030 INPUT "ENTER 1 TO STORE PATTERN DATA ON TAPE";ZT
10040 FOR I=1 TO 9
10060 FOR J=1 TO PR(I)-1
10070 IF SR(1,J)=1 THEN PRINT"POSITION";I,J,"IS RESTRICTED"
:GOTO 10200
10080 IF CF(I,J)=0 THEN GOTO 10200
10100 PRINT " ENTER TYPE OF ASSEMBLY AT :"; I,",";J
10120 INPUT K
10130 IF K=0 THEN K=1
10135 IF ZT=1 THEN PRINT#-1,K
10140 R(I,J)=RI(K) : A(I,J)=AI(K) : BP(I,J)=RB(K) : SB(I,J)
```

```
=ZI(K)
10200 NEXT J,I
10490 GOTO 10700
10500 FOR I=1 TO PR(1)-1
10510 FOR J=1 TO PR(I)-1
10520 IF SR(I,J)=1 THEN 10550
10530 INPUT#-1, K
10540 R(I,J)=RI(K) : A(I,J)=AI(K) : BP(I,J)=RB(K) : SB(I,J)
= ZI(K)
10550 NEXT J,I
10700 PRINT:PRINT "RESTRICTIONS ON BP LOADING PER LOCATION"
10710 FOR I=1 TO PR(1)-1:FOR J=1 TO PR(I)-1: G(I,J)=.0: NEX
T J,I
10720 INPUT "ENTER RESTRICTED POSITION: I,J - ENTER 0 TWICE
 TO EXIT";I,J
10730 IF I=0 THEN GOTO 10800
10740 PRINT "ENTER LIMIT OF BP IN:";I,J:INPUT G(I,J)
10750 GOTO 10720
10800 GOTO 12000
12000 GOSUB 15000
12100 ON O3 GOTO 12200,12200,13000,14500,14700,14600
12200 IF O5=1 THEN GOSUB 12600
12210 GOSUB 16000
12300 GOSUB 14800
12500 IF O3 =3 THEN GOTO 13000: ELSE STOP
12600 GOSUB 36000
12603 LPRINT "BC:";BC
12605 IF O5><1 THEN GOTO 12660
12610 FOR I=1 TO PR(1)-1:FOR J=1 TO PR(I)-1:BB(I,J)=(F2(I,J
)*(1-RQ(I,J))*((1-R(I,J))[GP)):NEXT J:NEXT I
12630 GOSUB 16500
12640 IF XY=1 THEN GOTO 12600
12650 IF XY=0 THEN LPRINT "PRELIMINARY RESULT CONVERGED"
12660 GOSUB 14800
12670 RETURN
13000 PRINT "CHANGE IN BP LIMITS "
13010 INPUT "ENTER 0 FOR NO CHANGE, ELSE POSITION I,J TO BE
 CHANGED";I,J
13020 IF I=0 THEN GOTO 13100
13030 PRINT" ENTER NEW LIMIT IN:";I,J : INPUT G(I,J)
13040 GOTO 13010
13100 IF O3=3 THEN GOSUB 36000
13490 UF=0:GOSUB 14800
13500 GOSUB 20000
13600 GOSUB 14800
13900 STOP
14500 GOSUB 36000
14550 GOSUB 14800
14590 STOP
14600 GOSUB 40000
```

```
14610 GOSUB 45000
14620 GOSUB 50000
14650 GOSUB 14800
14690 STOP
14700 GOSUB 38000
14750 GOSUB 14800
14790 STOP
14800 FOR I=1 TO PR(1)-1:LPRINT TAB(I*10) I;:NEXT I
14810 FOR I=1 TO PR(1)-1:LPRINT:LPRINT:LPRINT I
14820 LPRINT:LPRINT "SR";:FOR J=1 TO PR(I)-1:LPRINT TAB(J*1
0) SR(I,J);:NEXT J
14830 LPRINT:LPRINT "R";:FOR J=1 TO PR(I)-1:LPRINT TAB(J*10
) R(I,J);:NEXT J
14840 LPRINT:LPRINT "AE-5";:FOR J=1 TO PR(I)-1:LPRINT TAB(J
*10) A(I,J)/1E-5;:NEXT J
14850 LPRINT:LPRINT"BP";:FOR J=1 TO PR(I)-1:LPRINT TAB(J*10
) BP(I,J);:NEXT J
14860 LPRINT:LPRINT "SB";:FOR J=1 TO PR(I)-1:LPRINT TAB(J*1
0) SB(I,J);:NEXT J
14870 LPRINT:LPRINT "F1";:FOR J=1 TO PR(I)-1:LPRINT TAB(J*1
0) F1(I,J);:NEXT J
14880 LPRINT:LPRINT "F2";:FOR J=1 TO PR(I)-1:LPRINT TAB(J*1
0) F2(I,J);:NEXT J
14890 LPRINT: LPRINT"B";:FOR J=1 TO PR(I)-1:LPRINT TAB(J*10
) B(I,J);: NEXT J
14900 LPRINT:LPRINT "BB";:FOR J=1 TO PR(I)-1:LPRINT TAB(J*1
0) BB(I,J);: NEXT J
14904 LPRINT:LPRINT "P1";:FOR J=1 TO PR(I)-1:LPRINT TAB(10*
J) P1(I,J);:NEXT J
14906 LPRINT:LPRINT "P2";:FOR J=1 TO PR(I)-1:LPRINT TAB(J*1
0) P2(I,J);:NEXT J
14907 'LPRINT:LPRINT "FB";:FOR J=1 TO PR(I)-1:LPRINT TAB(J*
10) FB(I,J);:NEXT J
14908 'LPRINT:LPRINT "FE";:FOR J=1 TO PR(I)-1:LPRINT TAB(J*
10) FE(I,J);:NEXT J
14909 LPRINT:LPRINT "FU";:FOR J=1 TO PR(I)-1:LPRINT TAB(J*1
0) FU(I,J);:NEXT J
14910 NEXT I
14920 LPRINT:LPRINT:LPRINT "CYCLE BURNUP:";BC
14930 LPRINT "LIMITS ON PEAKS: BOC";MB,"EOC";ME:LPRINT
14950 RETURN
15000 REM PREPARE FOR POWER ITERATION AT BOC
15020  AA=0  : CR=0  : RL=0
15040 FOR I=1 TO 9
15060 FOR J=1 TO PR(I)-1
15100 AA=AA+A(I,J)*Y(I,J):CR=CR+(R(I,J)-BP(I,J))*Y(I,J) :RL
=RL+RQ(I,J)*Y(I,J)
15110 NEXT J,I
15120 AA=AA/N4 : CR=CR/N4 : RL=RL/N4 : SP=CR-RL
15250 FOR I=1 TO PR(1)-1
```

```
15255 FOR J=1 TO PR(I)-1
15260 ON CF(I,J)GOTO 15270,15270,15270,15275,15275,15280,15
280,    15280,15285,15285,15285
15265 GOTO 15290
15270 F(I,J)=1/(1-TH*(R(I,J)-BP(I,J)-SP))
15273 GOTO 15290
15275 F(I,J)=1/(1-T5*(R(I,J)-BP(I,J)-SP)+2*TL*RQ(I,J)/3.5)
15277 GOTO 15290
15280 F(I,J)=1/(1-T1*(R(I,J)-BP(I,J)-SP)+2*TL*RQ(I,J)/3)
15283 GOTO 15290
15285 F(I,J)=1/(1-T2*(R(I,J)-BP(I,J)-SP)+TL*RQ(I,J))
15290 NEXT J,I
15300 RETURN
16000 REM SHUFFLING TO MAXIMIZE CYCLE BURNUP
16010 GOSUB 36000
16012 LPRINT "BC=";BC
16015 GOTO 16160
16020 V=-1 : VE=-RP      ' LIMITS
16025 FOR NI=1 TO 2
16028 TT=0 : DB=0
16030 FOR I=1 TO PR(1)-1
16040 FOR J=1 TO PR(I)-1
16050 IF (I=1 AND J>1 AND J<9) OR G(I,J)=0 THEN GOTO 16130
16060 IF F1(I,J)<=MB AND F2(I,J)<=ME THEN GOTO 16130
16070 GOSUB 55000
16080 GOSUB 30000
16090 IF F1(I,J)>=MB AND F2(I,J)>=ME THEN GOSUB 17700
16100 IF F1(I,J)>=MB AND F2(I,J)<ME THEN GOSUB 17600
16110 IF F1(I,J)<MB AND F2(I,J)>=ME THEN GOSUB 17650
16115 IF DB+BP(I,J)>G(I,J) THEN DB=G(I,J)-BP(I,J)
16120 IF DB><0 THEN TT=1
16125 BP(I,J)=BP(I,J)+DB : SB(I,J)=BP(I,J)*(1-RP)/(B(I,J)+D
B*FU(I,J))
16130 NEXT J,I
16140 IF TT=1 THEN GOSUB 17750
16150 NEXT N1
16160 V=1 : VB=1 :VE=1 : DZ=0   '   COEFFICIENTS
16170 FOR I=1 TO PR(1)-1
16180 FOR J=1 TO PR(I)-1
16190 IF SR(I,J)=1 OR (I=1 AND J>1 AND J<9) THEN GOTO 16220
16200 GOSUB 55000
16210 GOSUB 30000
16220 NEXT J,I
16230 GOSUB 14800
16235 FOR K=1 TO PR(1)-1
16240 FOR L=1 TO PR(K)-1
16250 IF SR(K,L)=1 OR (K=1 AND L<1 AND L<9) THEN GOTO 16290
16260 BB(K,L)=BB(K,L)*((1-R(K,L))[GS)
16290 NEXT L,K
16300 FOR K=1 TO 8:BB(K,1)=BB(K,1)/Y(K,1):NEXT K
```

```
16400 GOSUB 16500
16450 IF XY=1 THEN GOTO 16000
16470 IF XY=0 THEN LPRINT "      CONVERGED   "
16480 RETURN
16500 REM RANKINGS OF BC COEFFICIENTS
16510 FOR I=1 TO PR(1)-1
16520 FOR J=1 TO PR(I)-1
16530 IF SR(I,J)=1 THEN GOTO 16700
16540 IF I=1 AND J>1 AND J<9 THEN GOTO 16700
16550 RX(I,J)=1
16560 FOR K=1 TO PR(1)-1
16570 FOR L=1 TO PR(K)-1
16580 IF SR(K,L)=1 OR (K=1 AND L>1 AND L<9) THEN GOTO 16680
16590 IF BB(I,J)< BB(K,L) THEN RX(I,J)=RX(I,J)+1
16600 IF BB(I,J)=BB(K,L) AND (I<K OR (I=1 AND J<K)) THEN R
X(I,J)=RX(I,J)+1
16680 NEXT L,K
16700 NEXT J,I
17000 REM  SHUFFLING
17010 BD=0 : XY=0
17030 FOR I=1 TO PR(1)-1
17040 FOR J=1 TO PR(I)-1
17050 IF SR(I,J)=1 OR (I=1 AND J>1 AND J<9) THEN GOTO 17100
17060 K=TR(RX(I,J))  : Z= RI(K)- R(I,J)
17080 IF R(I,J)><RI(K) THEN LPRINT "CHANGE";I,J ": FROM ";R
(I,J),"TO";RI(K),"TYPE";K : R(I,J)=RI(K): A(I,J)=AI(K) : BP
(I,J)=RB(K) : SB(I,J)=ZI(K) : XY=1
17100 F(I,J)=F1(I,J)
17300 NEXT J,I
17350 FOR K=2 TO 8: R(1,K)=R(K,1) : A(1,K)=A(K,1): BP(1,K)=
BP(K,1) : SB(1,K)=SB(K,1): NEXT K
17500 RETURN
17600 DB=(MB-F1(I,J))/P1(I,J)
17610 IF DB*P2(I,J)+F2(I,J)>ME THEN 17700
17620 RETURN
17650 DB=(ME-F2(I,J))/P2(I,J)
17660 IF DB*P1(I,J)+F1(I,J)>MB THEN 17700
17670 RETURN
17700 DB=(F1(I,J)-F2(I,J)-MB+ME)/(P2(I,J)-P1(I,J))
17710 RETURN
17750 FOR I=1 TO PR(1)-1:FOR J=1 TO PR(I)-1:F(I,J)=F1(I,J)+
BP(I,J)*P1(I,J):NEXT J,I
17760 GOSUB 36000
17770 RETURN
20000 REM BURNABLE POISON DISTRIBUTION
20010 V=-1 : VE=-RP : VB=(1-RP)/2: HS=.95
20020 FOR I=1 TO PR(1)-1
20030 FOR J=1 TO PR(I)-1
20035 IF I=1 AND J>1 AND J<9 THEN GOTO 20100
20040 IF G(I,J)=0 OR R(I,J)<0 THEN GOTO 20100
```

```
 20050 GOSUB 55000
20060 GOSUB 30000
20100 NEXT J,I
20105 FOR K=1 TO 8:BB(K,1)=BB(K,1)/Y(K,1):NEXT K
20110   XR=.01: ZU=0 : ZB=0 : ZN=0
20300 FOR I=1 TO PR(1)-1
20310 FOR J=1 TO PR(I)-1
20315 IF I=1 AND J>1 AND J<1 THEN GOTO 20400
20320 IF G(I,J)=0 OR R(I,J)<0 THEN GOTO20400
20340 IF  BP(I,J)=G(I,J) THEN GOTO 20400
20350 ZU=ZU+BB(I,J)  : ZB=ZB+S1(I,J)*BB(I,J) : ZN=ZN+ 1
20400 NEXT J,I
20500 X=XR*ZN/ZU : IF  06 =1 THEN X=-SC*N4/ZB
20510 FOR I=1 TO PR(1)-1
20520 FOR J=1 TO PR(I)-1
20530 1F G(I,J)=0 OR R(I,J)<0 OR (I=1 AND J>1 AND J<9) THEN
20630
20540 DP=X*BB(I,J)
20550 IF F1(I,J)<=MB AND F2(I,J)<=ME AND (BP(I,J)+DP)<=G(I,J
) THEN 20630
20560 PB=P1(I,J)*DP'*(1+DP/(1-R(I,J)+BP(I,J)))
20570 PE=P2(I,J)*DP'*(1+DP/(1-R(I,J)+BP(I,J)))
20580 IF F1(I,J)>=MB AND F2(I,J)>=ME THEN GOSUB 21700
20590 IF F1(I,J)>=MB AND F2(I,J)<ME THEN GOSUB 21500
20600 IF F1(I,J)<MB AND F2(I,J)>=ME THEN GOSUB 21600
20610 IF DB+BP(I,J)>G(I,J) THEN DB=G(I,J)-BP(I,J)
20620 BP(I,J)=BP(I,J)+DB  : SB(I,J)=BP(I,J)*(1-RP)/(B(I,J)+D
B*FU(I,J))
20625 IF BP(I,J)<0 THEN BP(I,J)=0: SB(I,J)=0
20630 NEXT J,I
21010 FOR I=1 TO PR(1)-1
21020 FOR J=1 TO PR(I)-1
21030 IF G(I,J)=0 OR BP(I,J)=G(I,J) OR R(I,J)<0 OR F1(I,J)>M
B OR F2(I,J)>ME OR (I=1 AND J>1 AND J<9) THEN 21200
21040 DP=X*BB(I,J): IF BP(I,J)+DP > G(I,J) THEN DP=G(I,J)-BP
(I,J)
21050 BP(I,J)=BP(I,J)+DP : SB(I,J)=BP(I,J)*(1-RP)/(B(I,J)+DP
*FU(I,J))
21080 IF BP(I,J)<0 THEN BP(I,J)=0: SB(I,J)=0
21200 NEXT J,I
21250 FOR K=2 TO 8: BP(1,K)=BP(K,1):SB(1,K)=SB(K,1):NEXT K
21260 FOR I=1 TO PR(1)-1:FOR J=1 TO PR(I)-1:F(I,J)=F1(I,J):N
EXT J,I
21270 GOSUB 36000
21280 GOSUB 14800
21300 07=0 : 08=0
21310 FOR I=1 TO PR(1)-1
21320 FOR J=1 TO PR(I)-1
```

```
21330 IF G(I,J)=0 OR BP(I,J)>=G(I,J) OR R(I,J)<0 OR (I=1 AND
 J>1 AND J<9) THEN 21400
21340 IF ((F1(I,J)>MB+.005 AND F2(I,J)> ME+.005) AND (ABS(F1
(I,J)-F2(I,J))>(ABS(MB-ME)+.005))) OR(F2(I,J)>ME+.005 AND F1
(I,J)<MB)OR (F1(I,J)>MB+.005 AND F2(I,J)<ME) THEN 08=1:GOTO
21400
21350 IF BB(I,J)>10  THEN 07=1
21400 NEXT J,I
21410 IF HG/(SC+HG)>=HS THEN LPRINT:LPRINT "BP CONTROL LIMIT
 ACHIEVED=";HG/(SC+HG):RETURN
21420 IF 07>0 OR 08>0 THEN GOTO 20000: ELSE  LPRINT "BP ALLO
CATION FINISHED": RETURN
21500 DB=(-F1(I,J)+MB)/P1(I,J)
21510 IF DB*P2(I,J)+F2(I,J)>ME THEN GOTO 21700
21520 IF DB<DP AND PE+F2(I,J)>ME THEN DB=(-F2(I,J)+ME)/P2(I,
J)
21530 IF DB<DP AND PE+F2(I,J)<=ME THEN DB=DP
21550 RETURN
21600 DB=(-F2(I,J)+ME)/P2(I,J)
21610 IF F1(I,J) +DB*P1(I,J)>MB THEN GOTO 21700
21620 IF DB>DP AND PB+F1(I,J)<=MB THEN DB=DP
21630 'IF DB>DP AND PB+F1(I,J)>MB THEN DB=(F1(I,J)-MB)/P1(I,
J)
21650 RETURN
21700 DB=(F1(I,J)-F2(I,J)-MB+ME)/(-P1(I,J)+P2(I,J))
21710 IF DB+BP(I,J)> G(I,J) THEN DB=G(I,J)-BP(I,J)
21720 RETURN
30000 REM EOC & BUP SENSITIVITY / SYNTHESIS DEPLETION
30010 FOR K=1 TO (PR(1)-1)
30020 FOR L=1 TO (PR(K)-1)
30030 RX(K,L)=R(K,L)-A(K,L)*(B(K,L)+BC*F2(K,L)/2)-BP(K,L)*RP
+KR
30040 NEXT L,K
30050 FOR K=1 TO 8
30060 F1(K,0)=F1(K,2) : F1(0,K)=F1(2,K)
30070 RX(K,0)=RX(K,2) : RX(0,K)=RX(2,K)
30080 FB(K,0)=FB(K,2) : FB(0,K)=FB(2,K)
30090 B(K,0)=B(K,2)   : B(0,K)=B(2,K)
30100 A(K,0)=A(K,2)   : A(0,K)=A(2,K)
30110 F2(K,0)=F2(K,2) : F2(0,K)=F2(2,K)
30120 NEXT K
30130 F1(9,0)=F1(9,1) : F1(0,9)=F1(1,9)
30140 RX(9,0)=RX(9,1) : RX(0,9)=RX(1,9)
30150 FB(9,0)=FB(9,1) : FB(0,9)=FB(1,9)
30160 B(9,0)=B(9,1)   : B(0,9)=B(1,9)
30170 F2(9,0)=F2(9,1) : F2(0,9)=F2(1,9)
30180 A(9,0)=A(9,1)   : A(0,9)=A(1,9)
30200 FOR K=1 TO PR(1)-1
30210 FOR L=1 TO PR(K)-1
30220 IF CF(K,L)=0 OR CF(K,L)=12 THEN GOTO 30850
30230 GOSUB 31300
```

```
30240 ON CF(K,L)GOTO 30350,30260,30310,30400, 30450,30550,3
0600,30650,30700,30750,30800
30260 X=K+1 : Z=L-1
30280 FJ(2)=(FJ(2)+A(X,Z)*F2(X,Z)*FB(X,Z))/2
30290 SJ(2)=(SJ(2)+A(X,Z)*F2(X,Z)*B(X,Z))/2
30300 GOTO 30350
30310 X=K-1 : Z=L+1
30330 FI(2)=(FI(2)+A(X,Z)*F2(X,Z)*FB(X,Z))/2
30340 SI(2)=(SI(2)+A(X,Z)*F2(X,Z)*B(X,Z))/2
30350 GOSUB 31500
30360 SF=SF/4 : SS=SS/4
30370 FX(K,L)=(-TH*A(K,L)*F2(K,L)*FB(K,L)+SF)*BC/2
30380 FA(K,L)=(-TH*A(K,L)*F2(K,L)*B(K,L)  +SS)/BC
30390 F(K,L)=FX(K,L)/(1-TH*RX(K,L))
30400 X=K+1 : Z=L-1
30420 FJ(2)=A(X,Z)*F2(X,Z)*FB(X,Z)/2
30430 SJ(2)=A(X,Z)*F2(X,Z)*B(X,Z)/2
30440 GOTO 30500
30450 X=K-1 : Z=L+1
30460 FI(2)=A(X,Z)*F2(X,Z)*FB(X,Z)/2
30470 SI(2)=A(X,Z)*F2(X,Z)*B(X,Z)/2
30500 GOSUB 31500
30510 SF=SF/3.5 : SS=SS/3.5
30520 FX(K,L)=(-T5*A(K,L)*F2(K,L)*FB(K,L)+SF)*BC/2
30530 FA(K,L)=(-T5*A(K,L)*F2(K,L)*B(K,L) + SS)/BC
30540 F(K,L)=FX(K,L)/(1-T5*RX(K,L)+2*TL*RQ(K,L)/3.5)
30545 GOTO 30850
30550 X=K-1 : Z=L+1
30560 FJ(1)=(FJ(1)+A(X,Z)*F2(X,Z)*FB(X,Z))/2
30570 SJ(1)=(SJ(1)+A(X,Z)*F2(X,Z)*B(X,Z))/2
30590 GOTO 30650
30600 X=K+1 : Z=L-1
30610 FI(1)=(FI(1)+A(X,Z)*F2(X,Z)*FB(X,Z))/2
30620 SI(1)=(SI(1)+A(X,Z)*F2(X,Z)*B(X,Z))/2
30650 GOSUB 31500
30660 SF=SF/3 : SS=SS/3
30670 FX(K,L)=(-T1*A(K,L)*F2(K,L)*FB(K,L)+SF)*BC/2
30680 FA(K,L)=(-T1*A(K,L)*F2(K,L)*B(K,L) +SS)/BC
30690 F(K,L)=FX(K,L)/(1-T1*RX(K,L)+2*TL*RQ(K,L)/3)
30695 GOTO 30850
30700 X=K-1 : Z=L+1
30710 FJ(1)=(FJ(1)+A(X,Z)*F2(X,Z)*FB(X,Z))/2
30720 SJ(1)=(SJ(1)+A(X,Z)*F2(X,Z)*B(X,Z))/2
30740 GOTO 30800
30750 X=K+1 : Z=L-1
30770 FI(1)=(FI(1)+A(X,Z)*F2(X,Z)*FB(X,Z))/2
30780 SI(1)=(SI(1)+A(X,Z)*F2(X,Z)*B(X,Z))/2
30800 GOSUB 31500
30810 SF=SF/2 : SS=SS/2
30820 FX(K,L)=(-T2*A(K,L)*F2(K,L)*FB(K,L)+SF)*BC/2
```

```
30830 FA(K,L)=(-T2*A(K,L)*F2(K,L)*B(K,L)+SS)/BC
30840 F(K,L)=FX(K,L)/(1-T2*RX(K,L)+TL*RQ(K,L))
30850 NEXT L
30860 NEXT K
30870 GOSUB 30900
30880 GOTO 31600  '    ITERATION BRANCH
30900 L=J
30910 FOR K=I-1 TO I+1 STEP 2
30920 GOSUB 31100
30930 NEXT K
30940 K=I
30950 FOR L=J-1 TO J+1 STEP 2
30960 GOSUB 31100
30970 NEXT L
30980 FOR K=I-1 TO I+1 STEP 2
30990 FOR L=J-1 TO J+1 STEP 2
31000 GOSUB 31200
31010 NEXT L
31020 NEXT K
31030 ON CF(I,J) GOTO 31040,31040,31040,31050,31050,31060,3
1060,31060,31060,31070,31070,31070,31080
31040 T=TH:GOTO 31080
31050 T=T5:GOTO 31080
31060 T=T1:GOTO 31080
31070 T=T2:GOTO 31080
31080 DY=FX(I,J)/F(I,J)
31084 FX(I,J)=FX(I,J)+T*F2(I,J)*VE
31086 F(I,J)=FX(I,J)/DY
31090 RETURN
31100 IF CF(K,L)=0 OR CF(K,L)=12 THEN RETURN
31110 GOSUB 58000
31120 ON CF(K,L) GOTO 31130,31130,31130,31140,31140,31150,3
1150,31150,31160,31160,31160
31130 NS=4:GOTO 31170
31140 NS=3.5:GOTO 31170
31150 NS=3:GOTO 31170
31160 NS=2:GOTO 31170
31170 DY=FX(K,L)/F(K,L)
31174 FX(K,L)=FX(K,L)-TS*F2(K,L)*FC*VE/NS
31176 F(K,L)=FX(K,L)/DY
31180 RETURN
31200 IF CF(K,L)=0 OR CF(K,L)=12 THEN RETURN
31210 GOSUB 58200
31220 ON CF(K,L) GOTO 31230,31230,31230,31240,31240,31250,3
1250,31250,31260,31260,31260
31230 NS=4:GOTO 31270
31240 NS=3.5:GOTO31270
31250 NS=3:GOTO 31270
31260 NS=2:GOTO 31270
```

```
31270 DY=FX(K,L)/F(K,L)
31280 FX(K,L)=FX(K,L)-TS*F2(K,L)*FC*VE/NS
31285 F(K,L)=FX(K,L)/DY
31290 RETURN
31300 FOR X=1 TO 2
31310 FJ(X)=0:FI(X)=0:SJ(X)=0:SI(X)=0
31320 NEXT X
31330 U=0
31340 FOR X=K-1 TO K+1 STEP 2
31350 U=U+1
31360 IF CF(X,L)=0 THEN GOTO 31400
31370 FJ(U)=A(X,L)*F2(X,L)*FB(X,L)
31380 SJ(U)=A(X,L)*F2(X,L)*B(X,L)
31400 NEXT X
31410 U=0
31420 FOR Z=L-1 TO L+1 STEP 2
31430 U=U+1
31440 IF CF(K,Z)=0 THEN GOTO 31480
31450 FI(U)=A(K,Z)*F2(K,Z)*FB(K,Z)
31460 SI(U)=A(K,Z)*F2(K,Z)*B(K,Z)
31480 NEXT Z
31490 RETURN
31500 SF=0 : SS=0
31510 FOR U=1 TO 2
31520 SF=SF+FI(U)+FJ(U)
31530 SS=SS+SI(U)+SJ(U)
31540 NEXT U
31550 SS=SS*TS : SF=SF*TS
31560 RETURN
31600 CI=0 : CA=0
31610 FOR X=1 TO PR(1)-1
31620 FOR Z=1 TO PR(X)-1
31630 CI=CI+A(X,Z)*F2(X,Z)*B(X,Z)*Y(X,Z)
31640 CA=CA+A(X,Z)*F2(X,Z)*FB(X,Z)*Y(X,Z)
31650 NEXT Z,X
31660 CA=-CA*BC/2+(F2(I,J)-ZD)*Y(I,J)*VE : CI=CI/BC
31670 FOR NI=1 TO NU
31680  CR=0 : FT=0
31690 FOR X=1 TO PR(1)-1
31700 FOR Z=1 TO PR(X)-1
31720 CR=CR+(RX(X,Z)-RQ(X,Z))*F(X,Z)*Y(X,Z)
31725 FT=FT+F(X,Z)*Y(X,Z)
31730 NEXT Z,X
31750 DC=(CA+CR)/CI
31760 GOSUB 61000
31765 NN=FT/N4:FOR X=1 TO PR(1)-1:FOR Z=1 TO PR(X)-1:F(X,Z)
=F(X,Z)-NN:NEXT Z,X
31768 PRINT "NORMALIZATION";NN
31770 NEXT NI
31780 CR=0
```

```
31790 FOR X=1 TO PR(1)-1
31800 FOR Z=1 TO PR(X)-1
31820 CR=CR+(RX(X,Z)-RQ(X,Z))*F(X,Z)*Y(X,Z)
31830 NEXT Z,X
31850 DC=(CA+CR)/CI
31860 FOR X=1 TO PR(1)-1
31870 FOR Z=1 TO PR(X)-1
31880 FE(X,Z)=F(X,Z)
31890 F(X,Z)=((F1(X,Z)+F2(X,Z))*DC+BC*(FB(X,Z)+FE(X,Z)))/2
31895 'FU(X,Z)=F(X,Z)
31900 NEXT Z,X
31940 CLS:PRINT "EOC BUP SENSITIVITY";DC
31960 GOSUB 65400
31970 BB(I,J)=DC : P2(I,J)=FE(I,J) : FU(I,J)=F(I,J)
32000 RETURN
36000 REM STEP-WISE DEPLETION
36010 BC=0:NB=NO
36020 FOR I=1 TO 9
36030 FOR J=1 TO PR(I)-1
36040 B(I,J)=0:RX(I,J)=R(I,J)-BP(I,J)': G(I,J)=0
36050 NEXT J,I
36070 GOSUB 40000

36100 FOR I=1 TO PR(1)-1:FOR J=1 TO PR(I)-1:F1(I,J)=F(I,J):
FA(I,J)=F(I,J):NEXT J,I
36110 SC=SP: SX=SP : NB=NM : HG=RB
36130 FOR IT=1 TO ND
36140 FOR I=1 TO 9
36150 FOR J=1 TO PR(I)-1
36155 DZ=1: IF (B(I,J)+BS*(FA(I,J)+F(I,J))/2)*SB(I,J) >=BP(
I,J)*(1-RP) THEN DZ=0
36160 RX(I,J)=R(I,J)-(A(I,J)-DZ*SB(I,J))*(B(I,J)+BS*(FA(I,J
)+F(I,J))/2)-BP(I,J)*(DZ*(1-RP)+RP)
36170 NEXT J
36180 NEXT I
36190 GOSUB 40400
36195 PRINT "UPDATE #";IT
36200 NEXT IT

36240 FOR I=1 TO 9
36250 FOR J=1 TO PR(I)-1
36260 B(I,J)=B(I,J)+BS*(FA(I,J)+F(I,J))/2
36265 'G(I,J)=G(I,J)+(SX*FA(I,J)+SP*F(I,J))*BS/2
36270 FA(I,J)=F(I,J)
36275 SX=SP
36280 NEXT J
36290 NEXT I
36295 BC=BC+BS
36298 CLS
```

```
36300 FOR I=1 TO 9:PRINT @((I-0)*6+64*2),I;:NEXT I
36303 FOR I=1 TO 9:PRINT @((I+2)*64),I;:NEXT I
36306 FOR I=1 TO 9:FOR J=1 TO PR(I)-1:PRINT @((I+2)*64+J*6)
,B(I,J);:NEXT J:NEXT I
36308 PRINT:PRINT "BC";BC,"STEP #";INT(BC/BS)
36310 IF(SP+RB)/AA>2*BS THEN GOTO 36130
36315 DN=0 : DD=0
36320 FOR I=1 TO 9
36330 FOR J=1 TO PR(I)-1
36340 DN=DN+(R(I,J)-A(I,J)*B(I,J)-RP*BP(I,J))*F(I,J)*Y(I,J)
36350 DD=DD+(A(I,J)*Y(I,J)*F(I,J)[2)
36360 NEXT J
36370 NEXT I
36380 BR=(DN/N4-RL)/(DD/N4)
36390 IF BR>BS THEN GOTO 36130
36400 FOR I=1 TO 9
36410 FOR J=1 TO PR(I)-1
36420 RX(I,J)=R(I,J)-A(I,J)*(B(I,J)+BR*(F(I,J)+FA(I,J))/2)-
RP*BP(I,J)
36430 NEXT J
36440 NEXT I
36450 NE=NM
36460 FOR IT=1 TO ND
36470 GOSUB 50400
36473 PRINT "UPDATE #";IT
36475 DN=0   :   DD=0
36480 FOR I=1 TO 9
36490 FOR J=1 TO PR(I)-1
36500 RX(I,J)=R(I,J)-(B(I,J)+BR*(F(I,J)+FA(I,J))/2)*A(I,J)-
BP(I,J)*RP+KR
36510 DN=DN+F(I,J)*Y(I,J)*(R(I,J)-A(I,J)*B(I,J)-RP*BP(I,J)+
KR)
36520 DD=DD+A(I,J)*Y(I,J)*F(I,J)*(FA(I,J)+F(I,J))/2
36530 NEXT J
36540 NEXT I
36550 BR=(DN/N4-RL)/(DD/N4)
36560 NEXT IT
36570 FOR I=1 TO PR(1)-1
36580 FOR J=1 TO PR(I)-1
36590 B(I,J)=B(I,J)+BR*(F(I,J)+FA(I,J))/2
36595 'G(I,J)=G(I,J)+(FA(I,J)*SX+SP*F(I,J))*BR/2
36600 F2(I,J)=F(I,J)
36610 NEXT J,I
36630 BC=BC+BR
36660 CLS:FOR I=1 TO 9:PRINT @((I-0)*6+64*2),I;:NEXT I
36670 FOR I=1 TO 9:PRINT @((I+2)*64),I;:NEXT I
36680 FOR I=1 TO 9:FOR J=1 TO PR(I)-1:PRINT @((I+2)*64+J*6)
,B(I,J);:NEXT J:NEXT I
36690 PRINT :PRINT "BC";BC
36700 PRINT "LAST STEP OF DEPLETION IS OVER, #"; INT(BC/BS+
```

```
1)
36730 'FOR I=1 TO PR(1)-1:FOR J=1 TO PR(I)-1:G(I,J)=G(I,J)/
(SC*(B(I,J)/3+F1(I,J)*BC/6)):NEXT J,I
36760 RETURN
38000 REM ONE-STEP DEPLETION
38020 NB=NM: GOSUB 40000
38030 BO=(RC-RL)/AA
38035 SC=SP
38040 FOR I=1 TO 9
38050 FOR J=1 TO PR(I)-1
38060 RX(I,J)=R(I,J)- BO*A(I,J)*F(I,J)-BP(I,J)*RP+KR:F1(I,J
)=F(I,J)
38080 NEXT J,I
38100 FOR NY=1 TO NO
38110 GOSUB 50400
38120 RC=0 : CO=0
38130 FOR I=1 TO 9
38140 FOR J=1 TO PR(I)-1
38150 RC=RC+F(I,J)*(R(I,J)-RP*BP(I,J)+KR)*Y(I,J)
38160 CO=CO+Y(I,J)*A(I,J)*F(I,J)*(F1(I,J)+F(I,J))/2
38170 NEXT J,I
38190 CO=CO/N4:RC=RC/N4:BO=(RC-RL)/CO
38220 FOR I=1 TO 9
38230 FOR J=1 TO PR(I)-1
38240 B(I,J)=BO*(F(I,J)+F1(I,J))/2
38250 RX(I,J)=R(I,J)-RP*BP(I,J)-A(I,J)*B(I,J)+KR
38260 NEXT J,I
38360 CLS:FOR I=1 TO 9:PRINT @((I-0)*6+64*2),I;:NEXT I
38370 FOR I=1 TO 9: PRINT @((I+2)*64),I;:NEXT I
38380 FOR I=1 TO 9: FOR J=1 TO PR(I)-1:PRINT @((I+2)*64+J*6
),B(I,J);:NEXT J:NEXT I
38390 PRINT:PRINT "ITERATION # ";NY, " BURNUP ";BO, "RC  ";
RC,"  RL  ";RL
38400 NEXT NY
38450 FOR X=1 TO PR(1)-1:FOR Z=1 TO PR(X)-1:F2(X,Z)=F(X,Z):
F(X,Z)=0:NEXT Z,X ' G(X,Z)=1
38500 RETURN
40000  REM  BOC POWER SUBROUTINE
40010 CR=0  :  RL=0  :  WS=0  : RC=0
40020 FOR I=1 TO 9
40030 FOR J=1 TO PR(I)-1
40040 IF CF(I,J)=0 THEN GOTO 40140
40050 RX(I,J)=R(I,J)-BP(I,J)
40060 CR=CR+F(I,J)*RX(I,J)*Y(I,J)
40070 WS=WS+F(I,J)*W(I,J)*Y(I,J)
40080 RL=RL+F(I,J)*Y(I,J)*RQ(I,J)
40140 NEXT J,I
40160 SP=(CR-RL)/WS
40400 REM PLACE MIRRORS
40410 FOR K=1 TO 8
```

```
40420 R(0,K)=R(2,K) :  R(K,0)=R(K,2)
40430 BP(0,K)=BP(2,K): BP(K,0)=BP(K,2)
40440 RX(0,K)=RX(2,K): RX(K,0)=RX(K,2)
40450 NEXT K
40460 R(0,0)=R(2,2)   :  BP(0,0)=BP(2,2)   :  RX(0,0)=RX(2,2
)
40470 R(0,9)=R(1,9)   :  BP(0,9)=BP(1,9)   :  RX(0,9)=RX(1,9
)
40480 R(9,0)=R(9,1)   :  BP(9,0)=BP(9,1)   :  RX(9,0)=RX(9,1
)
40490 REM POWER ITERATIONS
40500 FOR NI=1 TO NB
40510 FOR I=1 TO PR(1)-1:FOR J=1 TO PR(I)-1: RX(I,J)=RX(I,J
)-SP*W(I,J):NEXT J,I
40520 FT=0 : CR=0 : WS=0 : RL=0 : RB=0
40530 FOR K=1 TO 8
40540 F(0,K)=F(2,K):   F(K,0)=F(K,2)
40545 RX(0,K)=RX(2,K) : RX(K,0)=RX(K,2)
40550 NEXT K
40560 F(0,0)=F(2,2) :  F(0,9)=F(1,9)   :  F(9,0)=F(9,1)
40570 RX(0,9)=RX(1,9) : RX(9,0)=RX(9,1)
40580 'FOR I=1 TO 9
40581 FOR I=9 TO 1 STEP -1
40590 'FOR J=1 TO PR(I)-1
40591 FOR J=PR(I)-1 TO 1 STEP -1
40600 IF CF(I,J)=0 THEN GOTO 44600
40650 GOSUB 51000
44500 CR=CR+RX(I,J)*F(I,J)*Y(I,J)
44510 FT=FT+F(I,J)*Y(I,J)
44515 RC=RC+F(I,J)*Y(I,J)*(R(I,J)-RP*BP(I,J))
44520 WS=WS+W(I,J)*F(I,J)*Y(I,J)
44530 RB=RB+F(I,J)*(BP(I,J)-SB(I,J)*B(I,J))*Y(I,J)
44600 NEXT J
44610 NEXT I
44620 NF=FT/N4
44630 CR=CR+WS*SP
44640 WS=WS/FT : RL=RL/FT : CR=CR/FT : RB=RB/FT
44700 REM   NORMALIZATION OF POWERS
44710 FOR I=1 TO PR(1)-1
44720 FOR J=1 TO PR(I)-1
44730 IF CF(I,J)=0 THEN GOTO 44810
44740 F(I,J)=F(I,J)/NF
44800 RX(I,J)=RX(I,J)+SP*W(I,J)
44810 NEXT J,I
44820 SP=(CR-RL)/WS
44900 RC=RC/FT
44910 CLS: IF SP<0 THEN PRINT "OUT OF REACTIVITY"
44920 GOSUB 65400
44935 PRINT :PRINT "ITERATION NUMBER";NI,"RL",;RL,"CR";CR,"
SP";SP,"NORMALIZATION";NF
44937 PRINT "POWER CALCULATION"
44940 NEXT NI
44950 RETURN
```

```
45000  REM  BURNUP/DEPLETION  CALCULATIONS
45010 CR=0 :  RL=0
45020 FOR I=1 TO 9
45030 FOR J=1 TO PR(I)-1
45040 IF CF(I,J)=0 THEN GOTO 45100
45050 RX(I,J)= R(I,J)- BP(I,J)*(1+RP)/2 -W(I,J)*SP/3
45060 CR=CR+(R(I,J)-RP*BP(I,J))*Y(I,J)
45070 AA=AA + A(I,J)*Y(I,J)
45080 RL=RL+(RQ(I,J)*(1+KL*SP/2))*Y(I,J)
45090 REM
45100 NEXT J
45110 NEXT I
45120 BC=(CR-RL)/AA
45130 FOR I=1 TO 9
45140 FOR J=1 TO PR(I)-1
45150 IF CF(I,J)=0 THEN GOTO 45170
45160 B(I,J)= BC
45170 NEXT J
45180 NEXT I
45400 REM PLACE MIRRORS
45410 FOR K=1 TO 8
45420 R(0,K)= R(2,K)    :  R(K,0)=R(K,2)
45430 BP(0,K)=BP(2,K)   : BP(K,0)=BP(K,2)
45440 F1(0,K)=F1(2,K)   : F1(K,0)=F1(K,2)
45450 RX(0,K)=RX(2,K)   : RX(K,0)=RX(K,2)
45455 A(0,K)=A(2,K)    : A(K,0)=A(K,2)
45460 NEXT K
45470 R(0,9)=R(1,9) : R(9,0)=R(9,1)
45480 BP(0,9)=BP(1,9)   : BP(9,0)=BP(9,1)
45490 F1(0,9)=F1(1,9)   : F1(9,0)=F1(9,1)
45500 RX(0,9)=RX(1,9)   : RX(9,0)=RX(9,1)
45505 A(0,9)=A(1,9)    : A(9,0)=A(9,1)
45510 REM  BEGIN ITERATIONS
45520 FOR NI=1 TO NU
45530 BT=0 : CR=0 : RL=0
45540 REM UPDATE MIRRORS
45550 FOR K=1 TO 8
45560 B(0,K)=B(2,K)   :  B(K,0)=B(K,2)
45570 NEXT K
45580 B(0,9)=B(1,9)   :   B(9,0)=B(9,1)
45590 REM TARGET ASSEMBLY CALCULATIONS
45600 'FOR I=1 TO 9
45601 FOR I=9 TO 1 STEP -1
45610 'FOR J=1 TO PR(I)-1
45611 FOR J=PR(I)-1 TO 1 STEP -1
45620 IF CF(I,J)=0 THEN GOTO 49600
46000  REM CALCULATE SURROUNDING'S CONTRIBUITION
46010 BJ(1)=0   :  BJ(2)=0    : L=0
46020 FOR K=I-1 TO I+1 STEP 2
46030 L=L+1
```

```
46040 IF CF(K,J)=0 THEN GOTO 46090
46050 BJ(L)=B(K,J)*(1-TS*(RX(K,J)-A(K,J)*B(K,J)/2))+TS*BC*S
P*F1(K,J)/6
46090 NEXT K
46100 BI(1)=0  :  BI(2)=0  : L=0
46110 FOR K=J-1 TO J+1 STEP 2
46120 L=L+1
46130 IF CF(I,K)=0 THEN GOTO 46160
46140 BI(L)=B(I,K)*(1-TS*(RX(I,K)-A(I,K)*B(I,K)/2))+TS*BC*S
P*F1(I,K)/6
46160 NEXT K
47000 REM -  CORRECT SURROUNDINGS' FOR ODD ASSEMBLIES,POWER
47010 ON CF(I,J) GOTO 47500,47100,47300,47700,47800,48000,4
8200,48400,48600,48800,49000
47020 GOTO 49600
47100  REM CF=2
47110 K=I+1  : L=J-1
47120 SS= B(K,L)*(1-TS*(RX(K,L)-A(K,L)*B(K,L)/2))+TS*BC*SP*
F1(K,L)/6
47130 BJ(2)=(BJ(2)+SS)/2
47140 GOTO 47500
47300 REM CF=3
47310 K=I-1  :  L=J+1
47320 SS=B(K,L)*(1-TS*(RX(K,L)-A(K,L)*B(K,L)/2))+TS*BC*SP*F
1(K,L)/6
47330 BI(2)=(BI(2)+SS)/2
47340 GOTO 47500
47500 REM CF=1,2,3
47510 SY=TH*SP*BC*F1(I,J)/6
47520 CS=0
47530 FOR K=1 TO 2
47540 CS=CS+BI(K)+BJ(K)
47550 NEXT K
47560 CY=SY-CS/4
47570 BY=1-TH*RX(I,J)
47580 AY=TH*A(I,J)/2
47590 B(I,J)=(-BY+SQR(BY[2-4*AY*CY))/(2*AY)
47600 GOTO 49500
47700 REM CF=4
47710 K=I+1 : L=J-1
47720 GOTO 47820
47800 REM CF=5
47810 K=I-1  : L=J+1
47820 SS=B(K,L)*(1-TS*(RX(K,L)-A(K,L)*B(K,L)/2))+TS*BC*SP*F
1(K,L)/6
47830 LR=RQ(I,J)*(1+KL*SP/2)
47840 CS=0
47850 FOR K=1 TO 2
47860 CS=CS+BJ(K)+BI(K)
47870 NEXT K
```

```
47880 CS=CS+SS/2
47890 SY=T5*SP*BC*F1(I,J)/6
47900 CY=SY-CS/3.5
47910 BY=1-T5*RX(I,J)+TL*LR*2/3.5
47920 AY=T5*A(I,J)/2
47930 B(I,J)=(-BY+SQR(BY[2-4*AY*CY))/(2*AY)
47940 RL=RL+B(I,J)*LR*Y(I,J)
47950 GOTO 49500
48000 REM CF=6
48010 K=I-1 : L=J+1
48020 SS=B(K,L)*(1-TS*(RX(K,L)-A(K,L)*B(K,L)/2))+TS*BC*SP*F
1(K,L)/6
48030 BJ(1)=(BJ(1)+SS)/2
48040 GOTO 48400
48200 REM CF=7
48210 K=I+1 : L=J-1
48220 SS=B(K,L)*(1-TS*(RX(K,L)-A(K,L)*B(K,L)/2))+TS*BC*SP*F
1(K,L)/6
48230 BI(1)=(BI(1)+SS)/2
48240 GOTO 48400
48400 REM CF=6,7,8
48410 LR=RQ(I,J)*(1+KL*SP/2)
48420 SY=T1*SP*BC*F1(I,J)/6
48430 CS=0
48440 FOR K=1 TO 2
48450 CS=CS+BI(K)+BJ(K)
48460 NEXT K
48470 CY=SY-CS/3
48480 BY=1-T1*RX(I,J)+TL*LR*2/3
48490 AY=T1*A(I,J)/2
48500 B(I,J)=(-BY+SQR(BY[2-4*AY*CY))/(2*AY)
48510 RL=RL+B(I,J)*LR*Y(I,J)
48520 GOTO 49500
48600 REM CF=9
48610 K=I-1  :  L=J+1
48620 SS=B(K,L)*(1-TS*(RX(K,L)-A(K,L)*B(K,L)/2))+TS*BC*SP*F
1(K,L)/6
48630 BJ(1)=(BJ(1)+SS)/2
48640 GOTO 49000
48800 REM CF=10
48810 K=I+1  : L=J-1
48820 SS=B(K,L)*(1-TS*(RX(K,L)-A(K,L)*B(K,L)/2))+TS*BC*SP*F
1(K,L)/6
48830 BI(1)=(BI(1)+SS)/2
48840 GOTO 49000
49000 REM CF=9,10,11
49010 LR=RQ(I,J)*(1+KL*SP/2)
49020 SY=T2*SP*BC*F1(I,J)/6
49030 CS=0
49040 FOR K=1 TO 2
```

```
49050 CS=CS+BJ(K)+BI(K)
49060 NEXT K
49070 CY=SY-CS/2
49080 BY=1-T2*RX(I,J)+TL*LR
49090 AY=T2*A(I,J)/2
49100 B(I,J)=(-BY+SQR(BY[2-4*AY*CY))/(2*AY)
49110 RL=RL+B(I,J)*LR*Y(I,J)
49120 GOTO 49500
49500 CR=CR+((RX(I,J)-A(I,J)*B(I,J)/2)*B(I,J)-SP*BC*F1(I,J)
/6)*Y(I,J)
49510 BT=BT+B(I,J)*Y(I,J)
49600 NEXT J
49610 NEXT I
49620 BC=BT/N4
49640 CR=CR/BT  : RL=RL/BT  :PP=CR-RL
49900 CLS
49910 FOR I=1 TO 9: PRINT @((I-0)*6+64*2),I;:NEXT I
49920 FOR I=1 TO 9: PRINT @((I+2)*64),I;:NEXT I
49930 FOR I=1 TO 9: FOR J=1 TO PR(I)-1 : PRINT @((I+2)*64+J
*6),B(I,J);:NEXT J: NEXT I
49940 PRINT
49950 PRINT "ITERATION NUMBER";NI:PRINT"BC";BC,"CR";CR,"RL"
;RL,"PP";PP
49960 NEXT NI
49970 RETURN
```

```
50000 REM EOC SUBROUTINE
50010 FOR I=1 TO 9
50020 FOR J=1 TO PR(I)-1
50030 IF CF(I,J)=0 THE GOTO 50100
50040 RX(I,J)=R(I,J)-A(I,J)*B(I,J)-BP(I,J)*RP+KR
50100 NEXT J
50120 NEXT I
50400 REM PLACE MIRROS
50410 FOR K=1 TO 8
50420 R(0,K)=R(2,K) : R(K,0)=R(K,2)
50430 BP(0,K)=BP(2,K) : BP(K,0)=BP(K,2)
50440 RX(0,K)=RX(2,K)  : RX(K,0)=RX(K,2)
50450 NEXT K
50470 R(0,9)=R(1,9)     :RX(0,9)=RX(1,9)    : BP(0,9)=BP(1,9)
50480 R(9,0)=R(9,1)     :RX(9,0)=RX(9,1)   : BP(9,0)=BP(9,1)
50500  FOR NI=1 TO NE
50510 FT=0 : CR=0  :  WS=0  :  RL=0
50520 FOR K=1 TO 8
50530 F(0,K)=F(2,K) : F(K,0)=F(K,2)
50535 RX(0,K)=RX(2,K) : RX(K,0)=RX(K,2)
50540 NEXT K
50550 F(0,9)=F(1,9) : F(9,0)=F(9,1)
50560 RX(0,9)=RX(1,9) : RX(9,0)=RX(9,1)
50580 'FOR I=1 TO 9
50581 FOR I=9 TO 1 STEP -1
50590 'FOR J=1 TO PR(I)-1
50591 FOR J=PR(I)-1 TO 1 STEP -1
50600 IF CF(I,J)=0 THEN GOTO 50700
50650 GOSUB 51000
50670 CR=CR+RX(I,J)*F(I,J)*Y(I,J)
50680 FT=FT+F(I,J)*Y(I,J)
50700 NEXT J,I
50800 NF=FT/N4 : CR=CR/FT : RL=RL/FT
50810 FOR I=1 TO PR(1)-1
50820 FOR J=1 TO PR(I)-1
50830 IF CF(I,J)=0 THEN GOTO 50880
50840 F(I,J)=F(I,J)/NF
50880 NEXT J,I
50900 CLS:GOSUB 65400
50930 PRINT:PRINT "ITERATION #";NI,"NORMALIZATION";NF,"CR";
CR,"RL";RL
50940 PRINT "EOC POWER CALCULATION"
50950 NEXT NI
50960 RETURN
51000 REM POWER ITERATION ROUTINE
51500 BJ(1)=0  : BJ(2)=0  : L=0
51510 FOR K=I-1 TO I+1 STEP 2
51520 L=L+1
51530 IF CF(K,J)=0 THEN GOTO 51550
51540 BJ(L)=F(K,J)*(1-TS*RX(K,J))
```

```
51550 NEXT K
51560 BI(1)=0 : BI(2)=0 : L=0
51570 FOR K=J-1 TO J+1 STEP 2
51580 L=L+1
51590 IF CF(I,K)=0 THEN GOTO 51610
51600 BI(L)=F(I,K)*(1-TS*RX(I,K))
51610 NEXT K
51650 DX=F(I,J)
52000 REM CALCULATE SURROUNGING'S INFLUENCE FOR ODD ASSEMBL
IES,THEN CALCULATE POWER
52010 ON CF(I,J) GOTO 52500,52100,52300,52700,52800,53000,5
3200,53400,53600,53800,54000
52020 GOTO 54500
52100 K=I+1  :  L=J-1
52110 BJ(2)=(BJ(2) + F(K,L)*(1-TS*RX(K,L)))/2
52130 GOTO 52500
52300 K=I-1 : L=J+1
52320 BI(2)=(BI(2)+F(K,L)*(1-TS*RX(K,L)))/2
52340 GOTO 52500
52500 GOSUB 54800
52550 F(I,J)=CS/(4*(1-TH*RX(I,J)))
52565 F(I,J)=F(I,J)/(1+AC*(DX-F(I,J))/F(I,J))
52580 GOTO 54500
52700 K=I+1 : L=J-1
52720 BJ(2)=F(K,L)*(1-TS*RX(K,L))/2
52730 GOTO 52850
52800 K=I-1 : L=J+1
52820 BI(2)=F(K,L)*(1-TS*RX(K,L))/2
52850 LR=RQ(I,J)*(1+KL*SP)
52860 GOSUB 54800
52930 F(I,J)=CS/((1-T5*RX(I,J)+2*TL*LR/3.5)*3.5)
52945 F(I,J)=F(I,J)/(1+AC*(DX-F(I,J))/F(I,J))
52950 RL=RL+F(I,J)*Y(I,J)*LR
52960 GOTO 54500
53000 K=I-1 : L=J+1
53020 BJ(1)= (BJ(1)+F(K,L)*(1-TS*RX(K,L)))/2
53030 GOTO 53400
53200 K=I+1 : L=J-1
53220 BI(1)=(BI(1)+F(K,L)*(1-TS*RX(K,L)))/2
53230 GOTO 53400
53400 LR=RQ(I,J)*(1+KL*SP)
53410 GOSUB 54800
53420 F(I,J)=CS/(3*(1-T1*RX(I,J)+2*TL*LR/3))
53475 F(I,J)=F(I,J)/(1+AC*(DX-F(I,J))/F(I,J))
53480 RL=RL+F(I,J)*LR*Y(I,J)
53500 GOTO 54500
53600 K=I-1  : L=J+1
53620 BJ(1)=(BJ(1)+F(K,L)*(1-TS*RX(K,L)))/2
53630 GOTO 54000
53800 K=I+1  : L=J-1
53820 BI(1)=(BI(1)+F(K,L)*(1-TS*RX(K,L)))/2
53830 GOTO 54000
```

```
54000 GOSUB 54800
54020 LR=RQ(I,J)*(1+KL*SP)
54030 F(I,J)=CS/(2*(1-T2*RX(I,J)+TL*LR))
54045 F(I,J)=F(I,J)/(1+AC*(DX-F(I,J))/F(I,J))
54050 RL=RL+F(I,J)*LR*Y(I,J)
54500 RETURN
54800 CS=0
54810 FOR X=1 TO 2
54820 CS=CS+BI(X)+BJ(X)
54830 NEXT X
54840 RETURN
55000 REM  - BOC  SENSITIVITY - USE V=1 FOR REACT. V=1P FOR
 BP
55010 FT=0:RC=0:RL=0:DS=0
55020 FOR K=1 TO 9
55030 FOR L=1 TO PR(K)-1
55035 F(K,L)=0
55040 RX(K,L)=R(K,L)-BP(K,L)-SC*W(K,L)
55050 NEXT L
55060 NEXT K
55070 FOR K=1 TO 8
55080 F1(K,0)=F1(K,2)   :  F1(0,K)=F1(2,K)
55090 RX(K,0)=RX(K,2)   :  RX(0,K)=RX(2,K)
55100 NEXT K
55110 F1(9,0)=F1(9,1) :   F1(0,9)=F1(1,9)
55120 RX(9,0)=RX(9,1) :   RX(0,9)=RX(1,9)
55170 DS=F1(I,J)*V*(1+TH*(RX(I,J)-RQ(I,J)))/N4
55200 FOR NI=1 TO NP
55205 IF NI=1 THEN AP=0:ELSE AP=AQ
55210 FOR K=1 TO 8
55220 F(K,0)=F(K,2)     :   F(0,K)=F(2,K)
55230 NEXT K
55240 F(9,0)=F(9,1)    :   F(0,9)=F(1,9)
55250 REM START COMPUTING
55260 K=I    :   L=J
55270 GOSUB 56000
55280 REM
55290 REM
55300 FOR N=I-1 TO I+1 STEP 2
55310 IF CF(N,J)=0 OR CF(N,J)=12 GOTO 55340
55320 K=N : L=J
55330 GOSUB 56100
55340 NEXT N
55350 FOR N=J-1 TO J+1 STEP 2
55360 IF CF(I,N)=0 OR CF(I,N)=12 GOTO 55390
55370 K=I :  L=N
55380 GOSUB 56100
55390 NEXT N
55400 FOR K=I-1 TO I+1 STEP 2
55410 FOR L=J-1 TO J+1 STEP 2
55420 IF CF(K,L)=0 OR CF(K,L)=12 THEN GOTO 55440
```

```
55430 GOSUB 56300
55440 NEXT L
55450 NEXT K
55500  REM SWEEP  REST OF CORE
55510 FOR D=2 TO 8
55520 FOR SN=-1 TO 1 STEP 2
55530 K=I+D*SN
55540 IF K<1 OR K>9 THEN GOTO 55640
55550 L=J
55560 IF CF(K,L)><0 THEN GOSUB 56550
55570 FOR SM=-1 TO 1 STEP 2
55580 FOR D1=1 TO D-1
55590 L=J+D1*SM
55600 IF L<1 OR L>9 GOTO 55630
55610 IF CF(K,L)><0 THEN GOSUB 56550
55620 NEXT D1
55630 NEXT SM
55640 NEXT SN
55650 FOR SN=-1 TO 1 STEP 2
55660 L=J+D*SN
55670 IF L<1 OR L>9 THEN GOTO 55770
55680 K=I
55690 IF CF(K,L)><0 THEN GOSUB 56550
55700 FOR SM=-1 TO +1 STEP 2
55710 FOR D1=1 TO D
55720 K=I+SM*D1
55730 IF K<1 OR K>9 THEN GOTO 55760
55740 IF CF(K,L)><0 THEN GOSUB 56550
55750 NEXT D1
55760 NEXT SM
55770 NEXT SN
55780 NEXT D
55790 'FOR U=1 TO 9:FOR P=1 TO PR(U)-1:F(U,P)=(N4*F(U,P)-F1
(U,P)*FT)/(N4+FT):NEXT P:NEXT U
55800 NN=FT/N4: RL=0 : RC=(F1(I,J)-ZD)*V*Y(I,J)
55810 FOR X=1 TO PR(1)-1
55820 FOR Z=1 TO PR(X)-1
55830 F(X,Z)=F(X,Z)-NN
55840 RC=RC+F(X,Z)*Y(X,Z)*(RX(X,Z)+SC) : RL=RL+F(X,Z)*Y(X,Z
)*RQ(X,Z)*(1+KL*SC)
55850 NEXT Z,X
55855 DS=(RC-RL)/N4
55860 CLS:FOR U=1 TO 9:PRINT @((U-0)*6+64*2),U;:NEXT U
55870 FOR U=1 TO 9:PRINT @((U+2)*64),U;:NEXT U
55880 FOR U=1 TO 9:FOR P=1 TO PR(U)-1:PRINT @((U+2)*64+P*6)
,F(U,P);:NEXT P:NEXT U
55890 PRINT : PRINT "NORMALIZATION";NN, "FT";FT,"DS";DS,"RL
";RL,"RC";RC,"ITERATION#";NI
55900 FT=0 : RL=0 :RC=0
55910 NEXT NI
```

```
55920 FOR U=1 TO PR(1)-1  :FOR P=1 TO PR(U)-1:FB(U,P)=F(U,P
): F(U,P)=0:NEXT P:NEXT U
55930 S1(I,J)=DS : P1(I,J)=FB(I,J)
55970 RETURN
56000 REM SUB  TARGET ASSEMBLY
56010 ON CF(K,L) GOSUB 56900,56700,56800,57000,57050,57200,
57250,57300,57400,57450,57500
56030 F(K,L)=((SF*TS-T*F1(K,L))*DS+SD+T*F1(K,L)*V)/DN
56035 F(K,L)=F(K,L)+AP*(F(K,L)-DX)
56040 FT=FT+F(K,L)*Y(K,L)
56090 RETURN
56100 REM SUB  SURROUNDINGS
56110 ON CF(K,L) GOSUB 56900,56700,56800,57000,57050,57200,
57250,57300,57400,57450,57500
56120 GOSUB 58000
56250 F(K,L)=((SF*TS-T*F1(K,L))*DS+SD-FC*F1(I,J)*TS*V/NS)/D
N
56255 F(K,L)=F(K,L)+AP*(F(K,L)-DX)
56260 FT=FT+F(K,L)*Y(K,L)
56290 RETURN
56300 REM SUB CORNERS
56310 ON CF(K,L) GOSUB 56900,56700,56800,57000,57050,57200,
57250,57300,57400,57450,57500
56320 GOSUB 58200
56500 F(K,L)=((SF*TS-T*F1(K,L))*DS+SD-FC*F1(I,J)*TS*V/NS)/D
N
56505 F(K,L)=F(K,L)+AP*(F(K,L)-DX)
56510 FT=FT+F(K,L)*Y(K,L)
56545 RETURN
56550 REM SUB ALL REMANINING CORE
56560 ON CF(K,L) GOSUB 56900,56700,56800,57000,57050,57200,
57250,57300,57400,57450,57500
56580 F(K,L)=((SF*TS-T*F1(K,L))*DS+SD)/DN
56585 F(K,L)=F(K,L)+AP*(F(K,L)-DX)
56590 FT=FT+F(K,L)*Y(K,L)
56650 RETURN
56700 GOSUB 57600
56710 K1=K+1 : L1=L-1
56720 FJ(2)=(FJ(2)+F1(K1,L1))/2
56730 BJ(2)=(BJ(2)+F(K1,L1)*(1-TS*RX(K1,L1)))/2
56740 GOTO 56910
56800 GOSUB 57600
56810 K1=K-1  : L1=L+1
56820 FI(2)=(FI(2)+F1(K1,L1))/2
56830 BI(2)=(BI(2)+F(K1,L1)*(1-TS*RX(K1,L1)))/2
56840 GOTO 56910
56900 GOSUB 57600
56910 NS=4
56920 T=TH
```

```
56930 SF=(FI(1)+FI(2)+FJ(1)+FJ(2))/NS
56940 SD=(BI(1)+BI(2)+BJ(1)+BJ(2))/NS
56950 DN=1-TH*RX(K,L)
56960 LR=0
56980 RETURN
57000 GOSUB 57600
57010 K1=K+1   : L1=L-1
57020 BJ(2)=(F(K1,L1)*(1-TS*RX(K1,L1)))/2
57030 FJ(2)=F1(K1,L1)/2
57040 GOTO 57100
57050 GOSUB 57600
57060 K1=K-1  : L1=L+1
57070 BI(2)=(F(K1,L1)*(1-TS*RX(K1,L1)))/2
57080 FI(2)=F1(K1,L1)/2
57100 T=T5
57110 NS=3.5
57120 SF=(FI(1)+FI(2)+FJ(1)+FJ(2))/3.5
57130 SD=(BI(1)+BI(2)+BJ(1)+BJ(2))/3.5
57140 LR=RQ(K,L)*(1+KL*SC)
57150 DN=1-T5*RX(K,L) +TL*2*LR/3.5
57160 RETURN
57200 GOSUB 57600
57210 K1=K-1   : L1=L+1
57220 BJ(1)=(BJ(1)+F(K1,L1)*(1-TS*RX(K1,L1)))/2
57230 FJ(1)=(FJ(1)+F1(K1,L1))/2
57240 GOTO 57310
57250 GOSUB 57600
57260 K1=K+1  : L1=L-1
57270 BI(1)=(BI(1)+F(K1,L1)*(1-TS*RX(K1,L1)))/2
57280 FI(1)=(FI(1)+F1(K1,L1))/2
57290 GOTO 57310
57300 GOSUB 57600
57310 T=T1
57320 NS=3
57330 SF=(FI(1)+FI(2)+FJ(1)+FJ(2))/3
57340 SD=(BI(1)+BI(2)+BJ(1)+BJ(2))/3
57350 LR=RQ(K,L)*(1+KL*SC)
57360 DN=1-T1*RX(K,L)+TL*LR*2/3
57370 RETURN
57400 GOSUB 57600
57410 K1=K-1    :  L1=L+1
57420 BJ(1)=(BJ(1)+F(K1,L1)*(1-TS*RX(K1,L1)))/2
57430 FJ(1)=(FJ(1)+F1(K1,L1))/2
57440 GOTO 57510
57450 GOSUB 57600
57460 K1=K+1   : L1=L-1
57470 BI(1)=(BI(1)+F(K1,L1)*(1-TS*RX(K1,L1)))/2
57480 FI(1)=(FI(1)+F1(K1,L1))/2
57490 GOTO 57510
57500 GOSUB 57600
```

```
57510 T=T2
57520 SF=(FI(1)+FJ(1))/2
57530 SD=(BI(1)+BJ(1))/2
57540 LR=RQ(K,L)*(1+KL*SC)
57550 DN=1-T2*RX(K,L)+TL*LR
57570 RETURN
57600 DX=F(K,L) 'REM SUBROUTINE  SUM
57610 FJ(1)=0  : FJ(2)=0    : BJ(1)=0      : BJ(2)=0    : K1=
0
57620 FOR I1=K-1 TO K+1 STEP 2
57630 K1=K1+1
57640 IF CF(I1,L)=0 THEN GOTO 57670
57650 BJ(K1)=F(I1,L)*(1-TS*RX(I1,L))
57660 FJ(K1)=F1(I1,L)
57670 NEXT I1
57680 FI(1)=0  : FI(2)=0    : BI(1)=0      : BI(2)=0   : K1=0
57690 FOR I1=L-1 TO L+1 STEP 2
57700 K1=K1+1
57710 IF CF(K,I1)=0 THEN GOTO 57740
57720 BI(K1)=F(K,I1)*(1-TS*RX(K,I1))
57730 FI(K1)=F1(K,I1)
57740 NEXT I1
57750 RETURN
58000 REM SUB FC SURR/NEIGHBOUR
58020 FC=1
58030 ON CF(K,L) GOTO 58150,58050,58070,58150,58150,58090,5
8090,58150,58110,58130,58150
58040 RETURN
58050 IF CF(I,J)=9 THEN FC=.5 : RETURN
58070 IF CF(I,J)=10 THEN FC=.5 : RETURN
58090 IF CF(I,J)=1 THEN FC=.5:RETURN
58110 IF CF(I,J)=2 THEN FC=.5:RETURN
58130 IF CF(I,J)=3 THEN FC=.5
58150 RETURN
58200 REM SUB FC SURR/CORNERS
58210 FC=0
58230 ON CF(K,L) GOTO 58400,58250,58270,58290,58310,58330,5
8350,58400,58370,58390,58400
58240 RETURN
58250 IF CF(I,J)=6 THEN FC=.5 : RETURN
58270 IF CF(I,J)=7 THEN FC=.5 : RETURN
58290 IF CF(I,J)=9 THEN FC=.5 : RETURN
58310 IF CF(I,J)=10 THEN FC=.5 : RETURN
58330 IF CF(I,J)=2 THEN FC=.5 : RETURN
58350 IF CF(I,J)=3 THEN FC=.5 : RETURN
58370 IF CF(I,J)=4 THEN FC=.5:RETURN
58390 IF CF(I,J)=5 THEN FC=.5
58400 RETURN
61000 REM ITERATION PROCESS
61030 IF NI>1 THEN GOTO 61110
61040 FOR X=1 TO 8
```

```
61050 FX(0,X)=FX(2,X) : FX(X,0)=FX(X,2)
61060 FA(0,X)=FA(2,X) : FA(X,0)=FA(X,2)
61065 NEXT X
61070 FX(0,9)=FX(1,9) : FX(9,0)=FX(9,1)
61080 FA(0,9)=FA(1,9) : FA(9,0)=FA(9,1)
61110 FOR X=1 TO 8
61120 F(0,X)=F(2,X):F(X,0)=F(X,2)
61130 NEXT X
61140 F(0,9)=F(1,9):F(9,0)=F(9,1)
61170 K=I : L=J
61180 GOSUB 61700
61200 FOR D=1 TO 8
61210 FOR SN=-1 TO 1 STEP 2
61220 K=I+D*SN
61230 IF K<1 OR K>9 THEN GOTO 61340
61240 L=J
61250 IF CF(K,L)><0 THEN GOSUB 61700
61260 IF D=1 THEN GOTO 61340
61270 FOR SM=-1 TO 1 STEP 2
61280 FOR D1=1 TO D-1
61290 L=J+D1*SM
61300 IF L<1 OR L>9 THEN GOTO 61330
61310 IF CF(K,L)><0 THEN GOSUB 61700
61320 NEXT D1
61330 NEXT SM
61340 NEXT SN
61350 FOR SN=-1 TO 1 STEP 2
61360 L=J+D*SN
61370 IF L<1 OR L>9 THEN GOTO 61470
61380 K=I
61390 IF CF(K,L)><0 THEN GOSUB 61700
61400 FOR SM=-1 TO 1 STEP 2
61410 FOR D1=1 TO D
61420 K=I+SM*D1
61430 IF K<1 OR K>9 THEN GOTO 61460
61440 IF CF(K,L)><0 THEN GOSUB 61700
61450 NEXT D1
61460 NEXT SM
61470 NEXT SN
61480 NEXT D
61510 CLS:FOR U=1 TO 9:PRINT @((U-0)*6+64*2),U;:NEXT U
61520 FOR U=1 TO 9:PRINT @((U+2)*64),U;:NEXT U
61530 FOR U=1 TO 9:FOR P=1 TO PR(U)-1:PRINT @((U+2)*64+P*6)
,F(U,P);:NEXT P:NEXT U
61540 PRINT : PRINT "BUP SENSITIVITY AT";I,J,"IS";DC,"ITERA
TION";NI
61550 PRINT "FT";FT
61600 RETURN
```

```
61700 REM POWER SUB FOR BUP SENSITIVITY ITERATION
61705 DX=F(K,L)
61710 GOSUB 62150
61720 ON CF(K,L) GOTO 61800,61750,61780,61850,61880,61950,6
1980,62000,62050,62080,62100
61750 X=K+1 : Z=L-1
61760 FJ(2)=(FJ(2)+F(X,Z)*(1-TS*RX(X,Z)))/2
61770 GOTO 61800
61780 X=K-1 : Z=L+1
61790 FI(2)=(FI(2)+F(X,Z)*(1-TS*RX(X,Z)))/2
61800 SF=(FI(1)+FI(2)+FJ(1)+FJ(2))/4
61810 DN=1-TH*RX(K,L)
61820 F(K,L)=(FX(K,L)+FA(K,L)*DC+SF)/DN
61825 F(K,L)=F(K,L)+AB*(F(K,L)-DX)
61840 RETURN
61850 X=K+1 : Z=L-1
61860 FJ(2)=F(X,Z)*(1-TS*RX(X,Z))/2
61870 GOTO 61900
61880 X=K-1 : Z=L+1
61890 FI(2)=F(X,Z)*(1-TS*RX(X,Z))/2
61900 SF=(FI(1)+FI(2)+FJ(1)+FJ(2))/3.5
61910 DN=1-T5*RX(K,L)+2*TL*RQ(K,L)/3.5
61920 F(K,L)=(FX(K,L)+FA(K,L)*DC+SF)/DN
61925 F(K,L)=F(K,L)+AB*(F(K,L)-DX)
61940 RETURN
61950 X=K-1:Z=L+1
61960 FJ(1)=(FJ(1)+F(X,Z)*(1-TS*RX(X,Z)))/2
61970 GOTO 62000
61980 X=K+1 : Z=L-1
61990 FI(1)=(FI(1)+F(X,Z)*(1-TS*RX(X,Z)))/2
62000 SF=(FI(1)+FI(2)+FJ(1)+FJ(2))/3
62010 DN=1-T1*RX(K,L)+2*TL*RQ(K,L)/3
62020 F(K,L)=(FX(K,L)+FA(K,L)*DC+SF)/DN
62025 F(K,L)=F(K,L)+AB*(F(K,L)-DX)
62040 RETURN
62050 X=K-1 :Z=L+1
62060 FJ(1)=(FJ(1)+F(X,Z)*(1-TS*RX(X,Z)))/2
62070 GOTO 62100
62080 X=K+1 : Z=L-1
62090 FI(1)=(FI(1)+F(X,Z)*(1-TS*RX(X,Z)))/2
62100 SF=(FI(1)+FJ(1))/2
62110 DN=1-T2*RX(K,L)+TL*RQ(K,L)
62120 F(K,L)=(FX(K,L)+FA(K,L)*DC+SF)/DN
62125 F(K,L)=F(K,L)+AB*(F(K,L)-DX)
62140 RETURN
62150 FI(1)=0:FI(2)=0:FJ(1)=0:FJ(2)=0
62160 U=0
62165 Z=L
```

```
62170 FOR X=K-1 TO K+1 STEP 2
62180 U=U+1
62190 IF CF(X,Z)=0 THEN GOTO 62210
62200 FJ(U)=F(X,Z)*(1-TS*RX(X,Z))
62210 NEXT X
62220 U=0
62225 X=K
62230 FOR Z=L-1 TO L+1 STEP 2
62240 U=U+1
62250 IF CF(X,Z)=0 THEN GOTO 62270
62260 FI(U)=F(X,Z)*(1-TS*RX(X,Z))
62270 NEXT Z
62280 RETURN
65400 CLS:FOR X=1 TO PR(1)-1:PRINT @ ((X-0)*6+64*2),X;:NEXT
 X
65410 FOR X=1 TO PR(1)-1:PRINT @ ((X+2)*64),X;: NEXT X
65420 FOR X=1 TO PR(1)-1:FOR Z=1 TO PR(X)-1:PRINT @((X+2)*6
4+Z*6),F(X,Z);:NEXT Z:NEXT X
65430 RETURN
```

REFERENCES

A1 Abadie, J. (ed.), Non-Linear Programming, North Holland Publishing Company, Amsterdam, (1967).

A2 Amster, H. and Suarez, R., "The Calculation of Thermal Constants Averaged over a Wigner-Wilkins Flux Spectrum: Description of the SOFOCATE Code," WAPD-TM-39, January 1957.

A3 Ahn, D.H. and Levine, S.H., "Direct Placement of Fuel Assemblies Using the Gradient Projection Method," Trans.Am.Nucl.Soc., 46, 123 (1984).

B1 Barry, R.F., "LEOPARD - A Spectrum Dependent Non-Spatial Depletion Code," WCAP-3269-26, September 1963.

B2 Bohl, H., Gelbard, E., and Ryan, G., "MUFT-4-Fast Neutron Spectrum Code for the IBM-704, " WAPD-TM-72, July 1957.

B3 Becker, M., "Incorporation of Spectral Effects Into One-Group Nodal Simulators," Nucl.Sci.Eng., 59, 276 (1976).

B4 Box, M.J., Davies, D., and Swann, W.H., "Monograph No. 5: Non-Linear Optimization Techniques," Oliver & Boyd, Edinburgh, (1969).

C1 Cienchanowiecz, W., "A Multilevel Approach to Nuclear Fuel Burnup Optimization," Nucl.Sci.Eng., 57, 39 (1975).

C2 Chitkara, K. and Weisman, J., "An Equilibrium Approach to Optimal In-Core Fuel Management for Pressurized Water Reactors," Nuclear Technology, 24, 33 (1974).

C3 Colletti, J.P., Levine, S.H., and Lewis, J.B., "Iterative Solution to the Optimal Poison Management Problem in Pressurized Water Reactors," Nuclear Technology, 63, 415 (1983).

C4 Chang, D. and Levine, S.H., "Optimal Placement and Poison Control Depletion of Individual Assemblies Using the Gradient Projection Method," Trans.Am.Nucl.Soc., 43, 164 (1982).

C5 Correa, F., Driscoll, M.J., and Lanning, D.D., "An Evaluation of Tight-Pitch PWR Cores," MIT Energy Laboratory Report No. MIT-EL-79-022, August 1979.

C6 Cadwell, W.R., "PDQ-7 Reference Manual," WAPD-TM-678, January 1967.

D-1 Driscoll, M.J. et al., The Linear Reactivity Model for Nuclear Reactor Fuel Management. To be published. (Also: MIT Class Notes, Subject 22.35: Nuclear Fuel Management).

D2 Downar, T.J., "An Integrated Method for Mid-Range In-Core PWR Fuel Management and Core Design," Ph.D. Thesis, Dept. of Nucl. Eng., MIT, April 1984.

D3 Dwight, H.B., Tables of Integrals and Other Mathematical Data, The Macmillan Company, New York, (1961).

D4 Downar, T.J., VerPlanck, D. and Edenius, M., "A Two-Dimensional Nodal Model for Fuel Management Analysis," Trans.Am.Nucl.Soc., 47, 122 (1984).

D5 Dreyfus, S.E., Dynamic Programming and the Calculus of Variations, Academic Press, New York, (1965).

D6 Dantzig, G.B., Linear Programming and Extensions, Prentice-Hall, Englewood Cliffs, N.J., (1961).

D7 Delp, D.L. et al., "FLARE a Three-Dimensional Boiling Water Reactor Simulator," GEAP-4598, July 1964.

E1 Edenius, M., "CASMO-2: A Fuel Assembly Burnup Program," Studsvik/NR-8113, March 1981.

F1 Fagan, J.R. and Sesonske, A., "Optimal Fuel Replacement in Reactivity Limited Systems," Journal of Nuclear Energy, 23, 683, (1969).

G1 Goertzel, G., "Minimum Critical Mass and Flat Flux," J. Nuclear Energy, 2, 193 (1956).

G2 Goldschmidt, P., "Minimum Critical Mass in Intermediate Reactors Subject to Constraints on Power Density and Fuel Enrichment," Nucl.Sci.Eng., 49, 263, (1972).

G3 Graves, H.W., Nuclear Fuel Management, John Wiley & Sons, Inc., New York, (1970).

G4 Garel, K.C. and Driscoll, M.J., "Fuel Cycle Optimization of Thorium and Uranium Fueled PWR Systems," MIT Energy Laboratory Report No. MIT-EL-77-018, October 1977.

G5 Gass, S.I., Linear Programming, McGraw-Hill, New York, 1964.

G6 Griffith, R.E., and Stewart, R.A., "A Non-Linear Programming Technique for Optimization of Continuous Processing Systems," Management Science, 7, 379 (1961).

H1 Hoshino, T., "In-Core Fuel Management Optimization by Heuristic Learning Technique," Nucl.Sci.Eng., 49, 59 (1972).

H2 Ho, A and Sesonske, A., "Extended Burnup Fuel Cycle Optimization for Pressurized Water Reactors," Nuclear Technology, 58, 422 (1982).

H3 Ho, L.W. and Rohach, A.F., "Perturbation Theory in Nuclear Fuel Management Optimization," Nucl.Sci.Eng., 82, 151 (1982).

H4 Huang, H.Y. and Levine, S.H., "A New Method for Optimizing Core Reloads," Trans.Am.Nucl.Soc., 30, 339 (1978).

H5 Henry, A.F., Nuclear-Reactor Analysis, The MIT Press, Cambridge, Massachusetts, (1980).

H6 Holl, R.J. and Zweifel, "Highly Self Shielded Burnable Poisons," Trans.Am.Nucl.Soc., Vol. 3, No. 2, December 1960.

H7 Hukai, Y., Rasmussen, N.C. and Driscoll, M.J., "Some Applications of Ge(Li) Gamma-Ray Spectroscopy to Fuel Element Assay," MIT Nucl. Eng. Dept. Report No. MITNE-113, April 1970.

H8 Handshuh, J.A., DiGiovine, A.S., and Lucien, R.D., "Maine Yankee Cycle 6 Design Report," YAEC-1269, July 1981.

I-1 Izenson, M.G., "Automated PWR Reload Design Optimization," SM Thesis, Dept. of Nucl. Eng., MIT, June 1983.

J-1 Johnson, A., et al., "Verification of a Fuel Assembly Spectrum Code Based on Integral Transport Theory," CE/TIS-5818, and Trans.Am. Nucl.Soc., 28, 778 (1978).

K-1 Kamal, A., Driscoll, M.J. and Lanning, D.D., "The Selective Use of Thorium and Heterogeneity in Uranium-Efficient Pressurized Water Reactors," MIT Energy Laboratory Report No. MIT-EL-82-033, August 1982.

K2 Kamal, A., "The Effect of Axial Power Shaping on Ore Utilization in Pressurized Water Reactors," SM Thesis, Dept. of Nucl. Eng., MIT, January 1980.

K3 Kang, C.S., Rasmussen, N.C. and Driscoll, M.J., "Use of Gamma Spectroscopy for Neutronic Analysis of LMFBR Blankets," MIT Nucl. Eng. Dept. Report No. MITNE-130, November 1971.

K4 Kalra, M.S. and Driscoll, M.J., "Gamma Heating in LMFBR Media," MIT Nucl. Eng. Dept. Report No. MITNE-179, February 1976.

K5 Khalil, H.S., "The Application of Nodal Methods to PWR Analysis," Ph.D. Thesis, Dept. of Nucl. Eng., MIT, December 1982.

K6 Kuhn, H.W. and Tucker, A.W., "Nonlinear Programming," in: Proc. 2nd Berkeley Symp on Math. Stat. and Prob., Vol. 5, University of California Press, Berkeley, 1952.

L1 Lin, B.I., Zolotar, B. and Weisman, J., "An Automated Procedure for Selection of Optimal Refueling Policies for Light Water Reactors," Nuclear Technology, 44, 258 (1979).

L2 Loh, W.T., Driscoll, M.J. and Lanning, D.D., "The Use of Burnable Poison to Improve Uranium Utilization in PWRs," MIT Energy Laboratory Report No. MIT-EL-82-014, May 1982.

L3 Lan, J.S., "Assessment of the Prevailing Physics Codes: LEOPARD, LASER and EPRI-CELL," Trans.Am.Nucl.Soc., 38, 685, June 1981.

L4 Lewins, J. and Becker, M. (ed.), "Advances in Nuclear Science and Technology," Vol. 14, Plenum Publishing Corporation, (1982).

M1 Malik, M.A. and Driscoll, M.J., "A Long Term Perspective on the LWR Fuel Cycle," MIT Nucl. Eng. Dept. Report No. MITNE-263, December 1984.

M2 Melice, M., "Pressurized Water Reactor Optimal Core Management and Reactivity Profiles," Nucl.Sci.Eng., 37, 451 (1969).

M3 Motoda, H., Herczeg, J. and Sesonske, A., "Optimization of Refueling Schedule for Light-Water Reactors," Nuclear Technology, 25, 477 (1975).

M4 Mingle, J. O., "In-Core Fuel Management Via Perturbation Theory," Nuclear Technology, 27, 248 (1975)

M5 Motoda, H. and Yokomizo, O., "Method to Minimize Power Peaking in Refueling Schedule of Boiling Water Reactor," J.Nucl.Sci.Tech., 14, 108 (1977).

M6 Montaldo-Volachec, E.M., "Computation of Sequential Batch Interactions in Nuclear Fuel Management," NE Thesis, Dept. of Nucl. Eng., MIT, February 1984.

M7 Malik, M.A., et al., "Optimization of the Axial Power Shape in Pressurized Water Reactors," MIT Energy Laboratory Report MIT-EL-81-037, November 1981.

N1 Naft, B.N. and Sesonske, A., "Pressurized Water Reactor Optimal Fuel Management," Nuclear Technology, 14, 123 (1972).

O1 Oblow, E.M., "Sensitivity Theory for General Non-Linear Algebraic Equations with Constraints," ORNL/TM-5815, April 1977.

O2 Oblow, E.M., "Sensitivity Theory for Reactor Thermal-Hydraulics," ORNL/TM-6303, July 1978.

R1 Rieck, T.A., et al., "The Effect of Refueling Decisions and Engineering Constraints on the Fuel Management for a Pressurized Water Reactor," MIT Nuclear Eng. Dept. Report No. MITNE-158, January 1974.

R2 Reeve, H.R. and Gailar, O.H., "Cell Depletion and Spectrum Recalculations," Trans.Am.Nucl.Soc., Vol. 13, No. 1, June 1970.

R3 Roberts, S.M. and Lyers, H.I., "The Gradient Method in Process Control," Ind.Eng.Chem., 53, 877 (1961).

R4 Rosen, J.B., "The Gradient Projection Method for Non-Linear Programming. Part I. Linear Constraints," J.Soc.Ind.App.Math., 8, 181 (1960).

S1 Sefcik, J.A., Driscoll, M.J. and Lanning, D.D., "Analysis of Strategies for Improving Uranium Utilization in Pressurized Water Reactors," MIT Energy Laboratory Report No. MIT-EL-80-032, January 1981.

S2 Suzuki, A. and Kiyose, R., "Application of Linear Programming to Refueling Optimization for Light Water Moderated Power Reactors," Nucl.Sci.Eng., 46, 112 (1971).

S3 Sauar, T.O., "Application of Linear Programming to In-Core Fuel Management Optimization in Light Water Reactors," Nucl.Sci.Eng., 46, 274 (1971).

S4 Stout, R.B. and Robinson, A.H., "Determination of Optimum Fuel Loading in Pressurized Water Reactors Using Dynamic Programming," Nuclear Technology, 20, 86 (1973).

S5 Stamm'ler, R.J.J. and Abbate, M.J., Methods of Steady-State Reactor Physics in Nuclear Design, Academic Press, London, (1983).

S6 Smith, K.S., "An Analytic Nodal Method for Solving the Two-Group, Multidimensional, Static and Transient Neutron Diffusion Equations," NE Thesis, Dept. of Nucl. Eng., MIT, March 1979.

S7 Sher, R., and Beck, C., "Fission Energy Release for 16 Fissioning Nuclides," EPRI NP-1771, March 1981.

S8 Suzuki, A. and Kiyose, R., "Maximizing the Average Fuel Burnup Over Entire Cycle: A Poison Management Optimization Problem for Multizone Light-Water Reactor," Nucl.Sci.Eng., 44, 121 (1971).

T1 Terney, W.B. and Williamson, Jr., E.A., "The Design of Reload Cores Using Optimal Control Theory," Nucl.Sci.Eng., 82, 260 (1982).

T2 Todreas, N.E., Lecture Notes, Subject 22.313: Advanced Engineering of Nuclear Reactors, Dept. of Nucl. Eng., MIT, (1981).

U1 Unik, J.P. and Gindler, J.E., "A Critical Review of the Energy Released in Nuclear Fission," ANL-7748, March 1971.

V1 VerPlanck, D.M., "SIMULATE-2: A Nodal Core Analysis Program for LWRs," EPRI Research Project 710-1, July 1982.

W1 Wall, I. and Fenech, H., "The Application of Dynamic Programming to Fuel Management Optimization," Nucl.Sci.Eng., 22, 285 (1965).

W2 Wade, D.C. and Terney, W.B., "Optimal Control of Nuclear Reactor Depletion," Nucl.Sci.Eng., 45, 199 (1971).

W3 Walsh, G.R., Methods of Optimization, John Wiley & Sons, Inc., New York, (1975).

W4 Wilde, D.J., Optimum Seeking Methods, Prentice-Hall, Inc., Englewood Cliffs, N.J., (1964).

W5 Williams, M.L., "Development of Depletion Perturbation Theory for Coupled Neutron/Nuclide Fields," Nucl.Sci.Eng., 70, 20 (1979).

W6 Williams, M.L., Greenspan, E and Marable, J.H., "Time-Dependent Generalized Perturbation Theory for Coupled Neutron-Nuclide Problems," Nucl.Sci.Eng., 73, 210 (1980).